Upscaling of Reactive Flows

Upscaling of Reactive Flows

PROEFSCHRIFT

ter verkrijging van de graad van doctor aan de
Technische Universiteit Eindhoven, op gezag van de
rector magnificus, prof.dr.ir. C.J. van Duijn, voor een
commissie aangewezen door het College
voor Promoties in het openbaar te verdedigen
op dinsdag 18 september 2012 om 14.00 uur

door

Kundan Kumar

geboren te Patna, India

Dit proefschrift is goedgekeurd door de promotoren:

prof.dr. I.S. Pop
en
prof.dr. M.A. Peletier

Contents

Chapter 1

Introduction

This thesis deals with the mathematical models which involve more than one spatial scale. In nature, many complex processes involve hierarchically organized structures exhibiting different scales. For instance, in material science, biology and the environmental sciences, we encounter this hierarchy with the scales ranging from molecular ones (biological applications) to field scales (reservoir simulations for oil extraction). To understand the modeled real-life processes, we need to perform computations at the larger scale (macroscale). Two related issues are encountered in this:

- To perform macroscale computations starting from full scale smaller scale (microscale) calculations is often very complex and out of reach.

- A certain form of the macroscopic law is presumed involving certain material specific parameters to be determined from experiments.

The first issue outlines the limitations of a direct numerical approach starting from the microscale. The second issue bypasses the first issue but raises another problem: how do we justify or preferably, derive the macroscopic laws? The upscaling approach answers this question by making transition from one scale to the next. This linkage of observable macroscale parameters with the microscopic description provides a way to derive the law as well as determine the dependence of these parameters on the microscopic processes. Apart from the computational advantage accrued from using macroscopic models, one may also obtain the error estimates through the upscaling procedure. The latter provides information about the quality of upscaling. Moreover, depending upon the requirements, one may also improve the averaged equations albeit at some computational costs.

The class of problems involving *bridging scales* is incredibly large and we address an

important subclass of problems here. We will deal with the situations when both the scales involve continuum equations. Even within this smaller set, we restrict ourselves to physical processes dealing with flow and transport. The connection between the two continuum processes involving flow is best exemplified by taking soil as an example. The Darcy equation gives velocity field as proportional to the pressure gradient with the proportionality constant named as permeability. At the same time, the flow is given by Stokes equation or Navier-Stokes equation for a given geometry at the microscale. In forming this link between these two equations, we obtain not only the derivation of the macroscale equation but also the information about the permeability constant and its dependence on the geometry of the microstructure [18].

We mention some of the relevant applications that are at the heart of our considerations.

1.0.1   3D all-solid-state batteries

One of the central applications of this work is in the manufacturing of a 3D solid state battery. As indicated by its name, the constituents of this battery (anode, cathode and electrodes) are all solid. The intended practical implementation is in the manufacturing of autonomous devices. These devices have very promising and futuristic applications. For instance, an autonomous medical pill, after ingested, will release the intended drug at a certain rate on its own. Naturally, these kinds of applications should minimize any chance of leakage of the constituent material which explains the choice of solid electrolytes instead of more common liquid counterparts. Now we explain what stands for 3D in this battery. The idea was first mooted in [110] and is motivated by high capacity design of energy storage devices such as capacitors. The energy capacity of the capacitor is dependent, among other characteristics, on the surface area. To enhance the surface area, instead of using planar surface, trenches are made. A similar strategy for the batteries yields (estimated) three orders of magnitude higher than the capacitors. A proof of concept for the successful implementation was discussed in the PhD thesis of Jos Oudenhoven [112] (see also [113, 114]). A schematic picture is shown in Figure 1.1.

Important challenges however remain in the deposition process. The deposition of the different layers should be uniform across the battery (e.g., to avoid short-circuit). For the trenches with high aspect ratio (desirable for higher energy capacity as the effective area increases) the uniform deposition problem may be aggravated (see Figure 1.2). Next, the size (2D cross-section) of the trenches is typically $10\mu\text{m} \times 30\mu\text{m}$ and the substrate (the base material on which deposition takes place) size of the order of 10cm $\times$ 10cm, hence a direct numerical simulation is computationally very demanding as the mesh size should be small enough to resolve the trench scale. Furthermore, the layers deposited successively may have thickness comparable to that of the trench itself leading to the clogging of the trench.
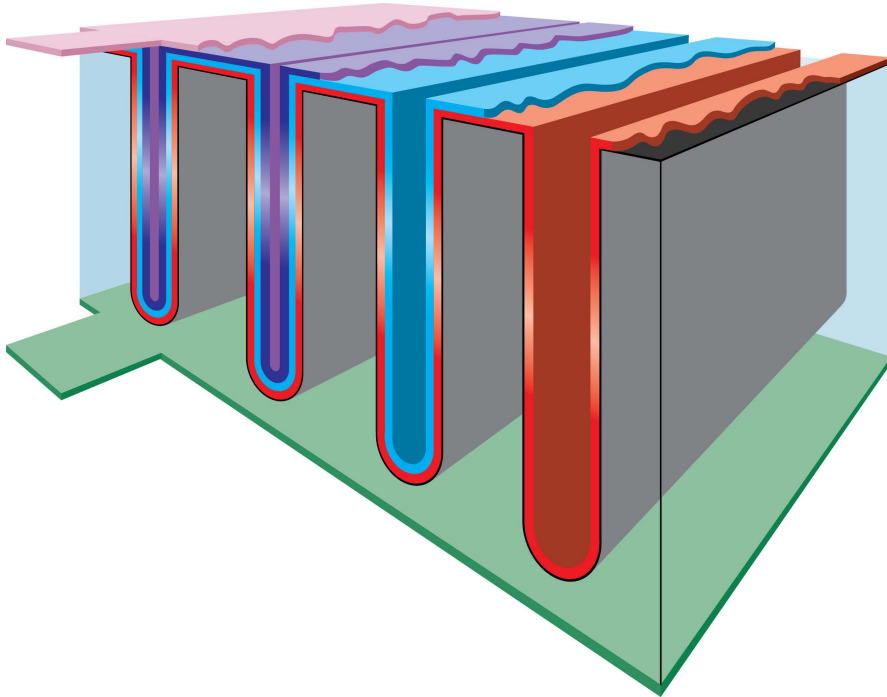
Figure 1.1: *A schematic of the 3D battery: trenches in a silicon substrate are etched to enhance the effective surface area. The different colors of deposition represent variety of layers corresponding to different constituents such as cathode, anode or electrode. The effective surface area enhancement leads to higher energy capacity compared to the planar counterpart. The copyright of the picture remains with [110] (Advanced Materials, 19(24):4564-4567, 2007).*

Mathematics can play important roles in dealing with the above challenges. The modeling and the numerical computations of the deposition process can predict the deposition profile in the trench. To tackle the problem of direct numerical approach, alternative ways can be found to compute the solutions efficiently. The modeling of this process can take into account the geometry changes since one can no longer ignore these changes. To take into account the changes in the geometry, we should model the processes by so-called free boundary problems because the change in the geometry itself is part of the solution. Having information about the deposition profile for a given geometry then would lead us to investigate the design question: what should be an optimal configuration of the microstructure?

In this work, we will discuss the modeling issues, a model that predicts the deposition profile, both including and excluding the geometry changes. Also, we will use the upscaling arguments to provide a simplified way of computing approximate solutions. Specifically, the chapters 2, 3, and 4 focus on these issues.
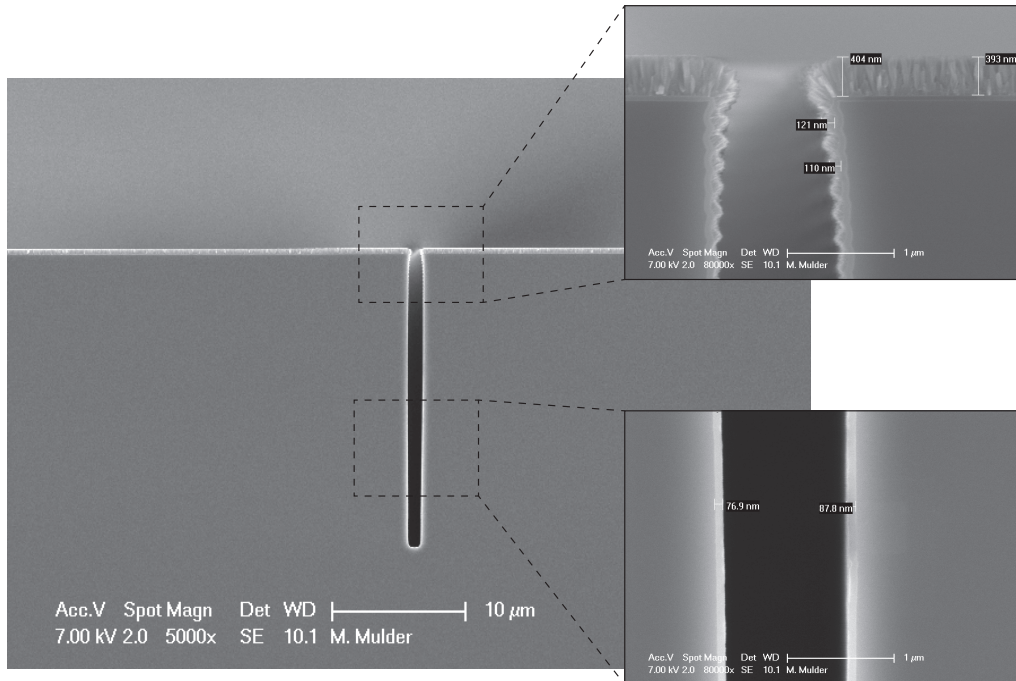
Figure 1.2: *Experimental results for deposition in thin trenches: the deposition is quite non-uniform; at the top the thickness is approximately 400 nm while at the bottom there is negligible deposition. Uniform deposition of the layer thicknesses yields better battery performance.*

1.0.2 Reactive flows in porous media

In a porous medium (soil being a familiar example), solid grains are surrounded by void spaces (the pores). The totality of the grains form the solid matrix (porous skeleton). Fluids (like water and oil) or gasses may flow through the pores of the medium transporting solutes and ions. By reactions, we mean the process of these ions combining among each other in the pore space or reacting on the grain boundaries. For example, consider the flow of common salt which consists of sodium and chloride ions. These ions combine to form the precipitate (crystals) on the grain boundaries. The nature abounds with the applications of reactive flows in porous media. The spreading of contaminants in the ground water flow, biological applications such as tissue and bone formation, pharmaceutical applications or the operation of the solid state batteries are all examples where the concepts from porous media are used to understand the properties.

Generally, the porous media consist of heterogeneities with a wide variation in the properties of porosity (void/solid matrix ratio) and the connectivity of the void spaces. Due to the high number of grains, the resulting medium is extremely complex. The solu-

tion in such situations, if it takes into account the detailed microstructure of the pore space, is usually prohibitive from the computational point of view and quite often unnecessary. Therefore, one tries to study the average properties, for example the effective permeability or the average concentration of solute or ions. These average properties are understood at a so-called Darcy scale where one does not distinguish between the grains and the pore space. However, we need to make this transition from the pore scale model to the Darcy scale (also called macroscale). This is achieved by employing homogenization or upscaling techniques. Naturally, these average properties depend on the microstructure and these techniques establish this linkage. More detailed discussions on the properties of porous media are outside the scope of this work and there are excellent textbooks dealing with this vast subject. We refer to [17] for more details on the porous media and the various topics associated with these.

In this thesis, we show how the upscaling approach is used to derive macroscopic model for a specific model describing a particular class of reactions, namely the precipitation and dissolution processes. In doing so, we make drastic simplifications regarding the geometry. It is often assumed that the geometry consists of periodic array of solid grains with surrounding connected pore space. Moreover, in another problem that will be considered in this thesis, the representative pore space is taken to be a thin strip. These simplifications, however drastic they are, bring out many useful insights having practical applications. These have been treated in chapters 5, 6, 7, and 8.

This chapter is organized as follows. In Section 1.1, we describe a general framework for the reactive flow model and the relevant issues. Subsequently, in Section 1.2, we state the upscaling problems that have been treated in this thesis. The analysis of the numerical schemes considered here are introduced in Section 1.3. We conclude by outlining this thesis in Section 1.4.

1.1   General framework of reactive flows in complex media

In this section we provide a general framework that all the problems treated in this thesis fit into. The reactive flow model has equations for: the flow part and the transport with reactions. The flow is usually described using the Navier-Stokes equation or for simplicity, Stokes equation. The transport part is often modeled by the convection-diffusion equation with reactions at the boundary. Let us consider a flow carrying the ions or solutes which are dissolved in the fluid. When the concentration of these dissolved species is low enough, the flow remains unaffected by the changes in the concentration of the solutes. This allows us to decouple the flow from the transport problem. Thus, one solves the flow equations first and then uses this flow term (in the convection term) in the convection-diffusion equation modeling transport.

There is another interesting aspect of the reactive flow modeling. The reactions may lead to changes in the geometry itself, for example the deposition process in the manufacturing of the battery. As a general guideline, the resulting free boundary problems involving the geometry changes are difficult to tackle using rigorous mathematical arguments. The simpler counterpart, where one ignores these geometry changes and takes a simplified description of the reactions by a variable defined on the boundary, is more convenient to deal with. In the general framework that we present, we will demonstrate how different choices for the reaction term lead to different models each one tailored to specific applications.

1.1.1   Fixed geometry versus variable geometry

To explain the two concepts, we consider a smooth and bounded domain $\Omega \subset \mathbb{R}^2$ with boundary $\partial\Omega$. For the discussion here, let us assume that the flow is given (even for the situation when the flow is time dependent). For any reactions (except for self-reactions such as aggregation), one needs at least two types of ions, however, under certain compatibility conditions [44,45], it suffices to consider only one type of ions. Let $(0, T)$ be the time of observation and u denote the concentration of the ions. The transport equation reads as follows

$$\partial_t u - D\Delta u + \nabla \cdot (\mathbf{q}u) = 0 \quad \text{in} \quad \Omega \times (0, T). \tag{1.1.1}$$

Here, D denotes the diffusion coefficient, $\mathbf{q}$ is the flow field assumed to be known. Let us assume that the initial conditions are given and smooth. In the equation above, to focus on the issue of fixed versus variable geometry, we have assumed that there are no reactions taking place in Ω.

To complete the model above, we need boundary conditions. Let $\Gamma \subset \partial\Omega$ be the part of the boundary where the reactions take place. On $\partial\Omega \setminus \Gamma$ we assume u to be prescribed. It is at Γ that we have two modeling choices which are illustrated in Figure 1.3:

Fixed geometry case: The geometry remains fixed and the precipitate concentration v is described by an equation defined on Γ (Figure 1.3, left).

Variable geometry case: The geometry changes are explicitly taken into account; the deposition thickness is denoted by d and we prescribe the movement of Γ as well as the equation describing d (Figure 1.3, right). The deposition thickness d is the signed distance function from initial boundary ($\Gamma(t = 0)$) and for the reaction rates that are considered here, we ensure that $d \geq 0$.

Fixed geometry

On $\Gamma \times (0, T)$, the following boundary condition and equation hold:

$$-\boldsymbol{\nu} \cdot \nabla u = \partial_t v, \tag{1.1.2}$$

$$\partial_t v = f(u, v), \tag{1.1.3}$$

where v is the precipitate concentration, $\boldsymbol{\nu}$ denotes the outward normal to Γ and f stands for the reaction term. The first equation (1.1.2) is simply mass balance while (1.1.3) describes the reaction term. This together with (1.1.1) completes the system and when solved together gives the solution pair (u, v).

Variable geometry

In the variable geometry case, the density of ions in the solid is different from the bulk. Let ρ be the density of ions in the solid phase (the deposition or the precipitate). The corresponding boundary condition and equations in this case are:

$$-\boldsymbol{\nu} \cdot \nabla u = v_n(\rho - u) \quad \text{on} \quad \Gamma(t) \times (0, T), \tag{1.1.4}$$

$$\rho \partial_t d = f(u, \rho d) \quad \text{on} \quad \Gamma(t) \times (0, T), \tag{1.1.5}$$

$$v_n = f(u, \rho d), \tag{1.1.6}$$

where v_n stands for the normal velocity of Γ and f represents the reaction term. The time-dependence of Γ has been explicitly shown. Consequently, Ω is also a function of time.

The forms for the equations suggest that v may be identified with ρd. Indeed, formal arguments suggest that the results for the fixed geometry case are a special case of variable geometry case and may be obtained as a formal limit of $\rho \nearrow \infty$ with $\rho d \to v$.

What are the respective advantages of these two modeling choices? First, the fixed geometry model yields a simpler description. One does not have to track these geometry changes and computing the solutions is less complex. Secondly, the fixed geometry cases are more amenable to rigorous mathematical arguments. Having said this, the fixed geometry case is a simplification and may not always be the appropriate choice. For instance, if the reaction rates are also functions of geometric features such as curvature, the fixed geometry case fails to model the phenomenon while it is easily handled by the variable geometry case. For the reaction rates considered in this thesis, the rigorous mathematical arguments are still open for the variable geometry case. One has to resort to formal justifications to derive equations in this case. We will, therefore, resort to the simpler description (fixed case) whenever we present rigorous mathematical
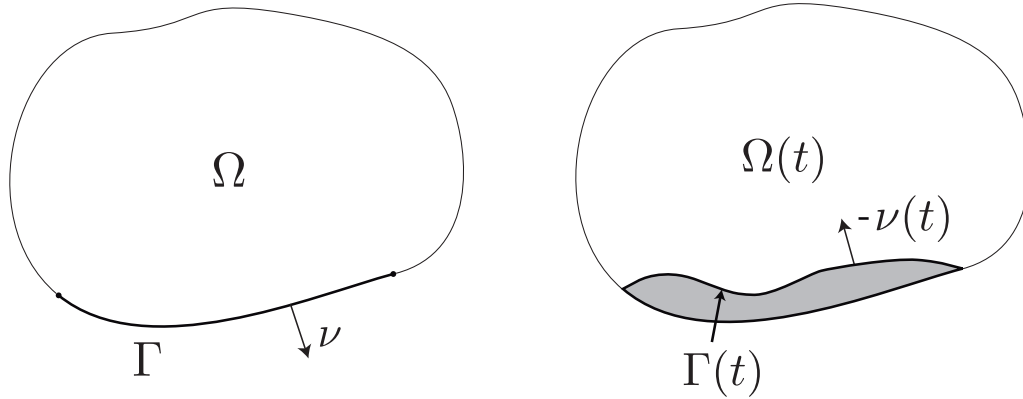
Figure 1.3: *The fixed (left) and the variable geometry (right) descriptions for the reactive flow in a domain Ω. For the variable geometry, the time dependence of $\Omega(t)$ and $\Gamma(t)$ are emphasized. For the fixed geometry case, variables are defined on Γ which describe the reaction product.*

proofs while we handle the variable geometry situation by formal arguments. As we will see in Chapter 5, depending on the value of ρ, one may incur significant errors by considering fixed models instead of the more appropriate variable geometry case.

1.1.2   Examples of reaction rates

The term f, representing the reaction rate, may have different forms. We present some examples relevant to the present work.

First order kinetics

Naturally, one of the simplest choices for the reaction rates is linear, that is,

$$f(u,v) = ku. \tag{1.1.7}$$

This assumption is, for example, used in chemical vapor deposition (CVD) processes. Often the reaction mechanisms for non-elementary reactions are not known for a complicated process such as CVD and one resorts to simplest description in order to minimize the number of parameters to fit.

Nonlinear but Lipschitz rates

One of the frequently used reaction rates is of the following type:

$$f(u,v) = r(u) - g(v), \tag{1.1.8}$$

where r and g are locally Lipschitz functions and take positive values. These reaction rates are considered, for example, in modeling the reactive flows in porous media [62]. Also, similar models are used in biological contexts in the diffusion of receptors in a cell [89] or in the description of sulphate attack for sewer pipes [53].

Other choices such as Langmuir types are also used to model the chemical reaction rates. For this type, the right hand side of (1.1.8) is replaced by $\frac{u}{C+u}$ where C is a given constant.

Non-Lipschitz and multi-valued reaction rates

For the most part of the thesis, we are concerned with the reaction rates which model the precipitation-dissolution process. Under certain conditions, the ions precipitate at the grain boundaries and form the crystal and hence become immobile. The reverse reaction of dissolution is also possible. The rate laws for these reactions have a certain non-linear and multi-valued structure. We consider the following reactions:

$$f(u,v) = r(u) - w, \tag{1.1.9}$$
$$w \in H(v), \tag{1.1.10}$$

where r denotes the precipitation process and w models the dissolution process. The precipitation rate r is locally Lipschitz. The interesting aspect is the description of the dissolution rate. It is assumed constant (1, by scaling) at some $(x,t) \in \Gamma \times (0,T)$ where the precipitate is present, i.e. if $v(x,t) > 0$. In the absence of the precipitate, the overall rate (precipitate minus dissolution) is either zero, if the solute present there is insufficient to produce a net precipitation gain, or positive. This can be summarized as

$$w \in H(v), \quad \text{where} \quad H(v) = \begin{cases} 0 & \text{if} \quad v < 0, \\ [0,1] & \text{if} \quad v = 0, \\ 1 & \text{if} \quad v > 0. \end{cases} \tag{1.1.11}$$

In a related context, [23] discusses the following precipitation dissolution model used in the context of nuclear waste disposal,

$$f(u,v) = r(u)(1 - \text{sign}^+(v)) \tag{1.1.12}$$

where $\text{sign}^+(v)$ is defined as

$$\text{sign}^+(v) = \left\{ \begin{array}{ll} 1 & \text{if} \quad v > 0, \\ 0 & \text{if} \quad v \leq 0. \end{array} \right. \qquad (1.1.13)$$

The detailed discussions on issues such as existence and uniqueness concerning this rate are given in this thesis (also see [41, 47, 117]).

Other applications of diffusive-reactive processes in different contexts include, for instance, in concrete formation [131], in biological applications [70]. Other examples dealing with similar processes are dealt with in algae modeling, [77] and image processing [78].

1.2   Upscaling problems

In this section, we state the type of problems that will be treated in this thesis. These problems relate to upscaling and usually contain two or more scales. For instance, in the discussion above, we referred to the deposition problem related to the formation of battery or the different scales in porous media. For the deposition problem, the trench size (microscale) and the substrate size (macroscale) give rise to these scales. One tries to obtain an effective equation by averaging over the smaller scale thus defining equations only on the macroscale with some information carried over from the microscale. We classify this averaging process depending upon the geometries that are considered. Again, we emphasize that the description of the problem on the smaller scale (microscale) may involve fixed geometry description or the variable geometry description. We will come back to these choices in the discussions below.

1.2.1   Boundary homogenization

In this class of problems, the original problem is defined in a domain with oscillating boundary. Figure 1.4 illustrates this situation where the domain is denoted by Ω^ε and the oscillating boundary by Γ^ε. The boundary Γ^ε consists of oscillations with both period and amplitude ε. Let us consider the transport problem defined in the domain Ω^ε with reactive boundary conditions on Γ^ε. We denote the $\varepsilon-$dependent problem by $\mathcal{P}^\varepsilon$ with the solution pair represented by $(u^\varepsilon, v^\varepsilon)$. An intuitive definition of the relevant upscaling problem is as follows:

Problem 1.2.1 *Derive a Problem $\mathcal{P}$ in a simple domain Ω with flat boundary or more generally smooth boundary Γ so that the solution (u, v) approximates the original solution pair $(u^\varepsilon, v^\varepsilon)$.*

Of course, we need to make the various notions precise: defining an appropriate norm to express the approximation; defining a suitable Ω and Γ. Figure 1.4 provides a pictorial representation for such Ω and Γ.

Imagine that we are able to obtain such a good approximation. How does this help us? Let us say, we would like to solve the problem numerically. To solve the problem in the original domain, one needs to resolve the oscillations in the boundary. This implies that the mesh size should be smaller than the size of oscillations. This makes the problem computationally quite expensive. The upscaling process provides an approximation to the original solution by defining the approximate problem in a domain with flat boundaries. This means that one needs to take into account the corrections due to this simplification, which is incorporated in modified boundary conditions. For the reactive boundary conditions at the oscillating boundaries, the flux needs to be corrected if we are to simplify the boundary to a flat one. Also, the upscaling process should use some information from the original geometry. We justify this upscaling process in a rigorous manner.

As remarked before, the oscillating boundary may change with time due to deposition processes. This implies that the geometry may change with time and since the change in the geometry is unknown, we have a free (evolving) boundary problem. The problem is to find an upscaled equation defined in a simple domain with flat boundaries for this free boundary problem posed in a complex domain with oscillatory boundaries. Figure 1.5 is a schematic for this free and moving boundary problem.

For the flow problem, the ideas from boundary homogenization have been applied to find the coupling conditions between the porous medium and the free flow region [66–68]. For the transport problem, [3, 29, 55, 56, 100] deal with the boundary homogenization.

Our contributions in this respect are following: In the fixed geometry case, we consider a model for reactions described by a non-linear, non-Lipschitz ODE at the oscillating boundary coupled with a parabolic PDE in domain; and we use periodic unfolding techniques for deriving effective boundary conditions. The derivation sustains the mathematical rigor and has been presented in Chapter 3. Next, in Chapter 4 we treat the moving geometry case using formal asymptotic techniques. We have considered both the flow and the transport problems simultaneously and the derivation has been done for the non-linear reaction terms. There is novelty both in the derivation part and the upscaled model which exhibits new aspects arising out of geometry changes.
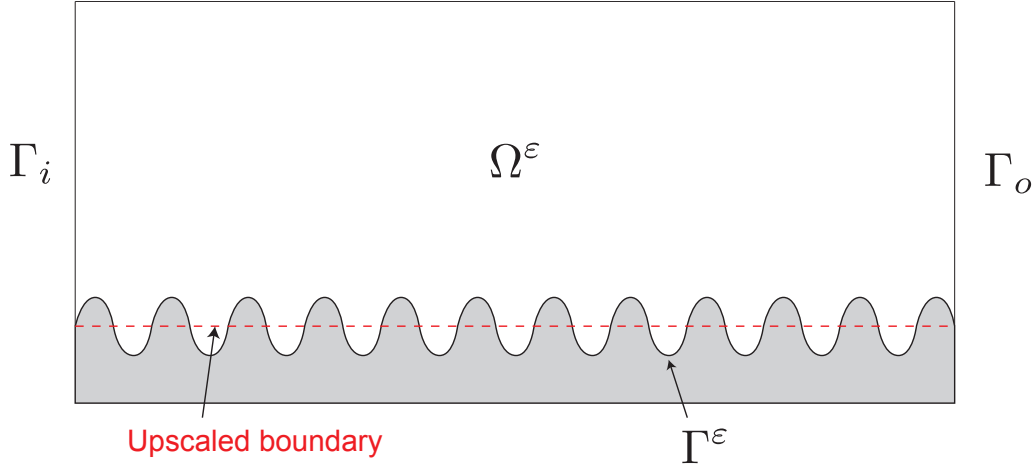
Figure 1.4: Ω^ε *is the domain considered here. The inlet boundary* Γ_i*, the outlet boundary* Γ_o *and the reactive boundary* Γ^ε *are part of the boundary* $\partial\Omega^\varepsilon$*. The boundary* Γ^ε *consists of a periodic function. Note that the geometry remains fixed in time for a given* ε*.*
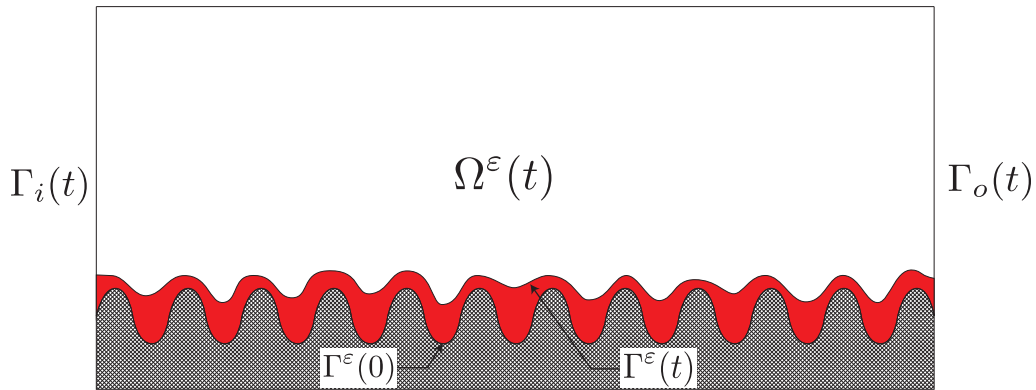
Figure 1.5: *Schematic for the domain* Ω^ε : *channel with rough boundary* Γ^ε*. Initially, the boundary* $\Gamma^\varepsilon \subset \partial\Omega^\varepsilon$ *consists of a periodic function of period and amplitude* ε*. Note that the geometry may change in time due to reactions taking place.*

1.2.2   Thin strip homogenization

A 2D thin strip, as has already been stated before, may be considered as a simplified representation of the pore scale geometry. Also, the rectangular trenches with high aspect ratio may be also considered as a thin strip. Let us again consider a fluid flowing through this thin strip and transporting dissolved ions. Reactions can take place at the pore walls, with the resulting component being attached to or detached from the pore walls. As before, two situations can be identified in this case: the reaction product forming a very thin layer that does not influence the pore space (fixed geometry); al-
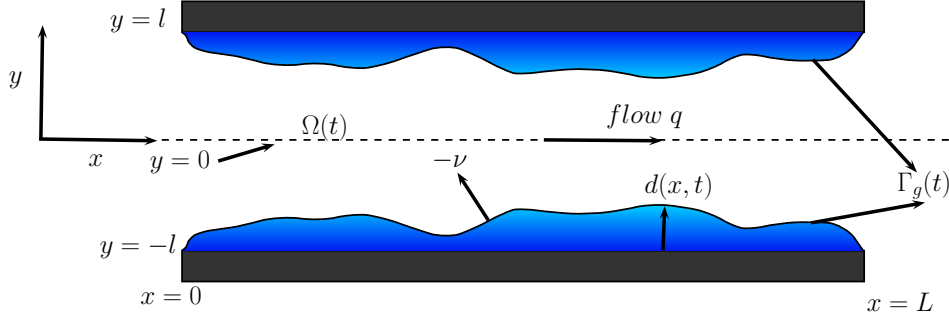
Figure 1.6: $\Omega(t)$ *is the domain (thin strip) considered here. The boundary* Γ_g *as well as the domain* Ω *are functions of time. The flow profile is also time dependent. Schematic for the geometry for the upscaling of reactive flow in a thin strip.*

ternatively, the thickness of the deposited layer is not negligible when compared to the pore thickness. In the second case, the reactions can lead to variations in the pore space, and hence in the flow domain. The interface separating this domain from the the solid part is a free boundary having an unknown, time dependent location. The schematic for the processes involving variable geometry is shown in Figure 1.6.

The ratio of thickness to length of the strip defines a small quantity ε. Let us denote the thin strip solution by $(u^\varepsilon, d^\varepsilon, \mathbf{q}^\varepsilon)$ with ε emphasizing the dependence of the solutions on the parameter ε. The upscaling problem has the following informal objective:

Problem 1.2.2 *Define a 1D problem so that the solutions* $(u, d, \mathbf{q})$ *approximate the original solution pair* $(u^\varepsilon, d^\varepsilon, \mathbf{q}^\varepsilon)$ *solving the transport and flow problems in 2D thin strip.*

The details of the solution for the thin strip are computationally expensive, especially when there are many of such thin strips e.g. in pore-network modeling of porous medium [124, 125]. The attempt is then to find an average equation. However, to approximate the average of 2D strip, the upscaled equations should be very good to reduce the cumulative error. The simplest way to obtain such a dimensional reduction is simply integrating along y axis, nonetheless in the given case, there is a product term $\mathbf{q}^\varepsilon \nabla u^\varepsilon$ for which the average is not the product of average. Moreover, the strength of convective strength to diffusion is characterized by a non-dimensional Péclet number. When the Péclet number is low or moderate, that is, the diffusion is dominant or of equal strength to convection, one expects a non-significant variation of concentration along y axis. However, for high Péclet number, implying relatively stronger strength of convection, a curious phenomenon takes place where the net spreading of solutes is enhanced by the convective strength. This is known as Taylor dispersion, first observed by British fluid mechanist Sir G. I. Taylor [132] (see [4, 31, 46, 93–95] for both formal and rigorous derivation of this effect and [105] for the case when the Péclet number is of moderate order).

For the case when Péclet number is in Taylor dispersion regime, with the geometry changing due to reactions, the derivation of the upscaled equation has not been studied so far. In Chapter 5, we study this phenomenon and derive similar effects for the case when the geometry changes are taken into account. Since the geometry changes are involved, we resort to formal arguments to derive the effective equations. The upscaled equations have novel terms containing effects of geometry changes and the numerical experiments show the effectiveness of our upscaled model compared to the simpler, intuitive models.

1.2.3   Periodic media homogenization

We proceed to discuss the geometric setting where the complex media is supposed to be periodic. This may be considered as a simplified representation of porous media. Figure 1.7 shows how one visualizes this complex medium as a tessellation of periodic cell. For simplicity, assume that there are two scales involved in the problem. The microscale problem pertains to the one defined in the unit cell. The macroscale consists of the domain formed by the scaling and translation of this unit cell. The scaling factor is referred to as ε.
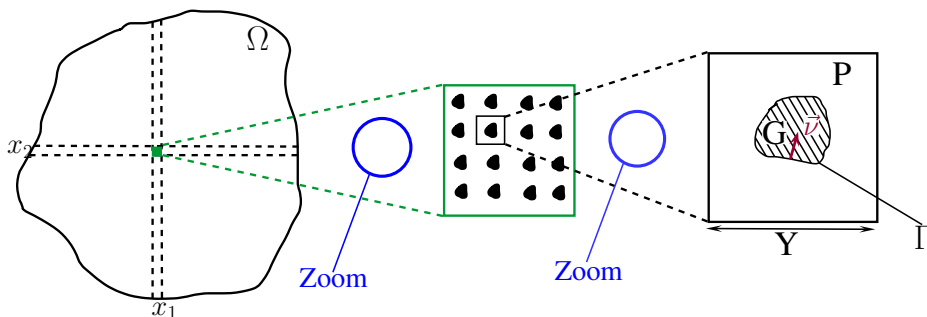
Figure 1.7: *The schematic showing the macroscale. The magnification of a small part of this macroscale yields a periodic structure. One period of this structure is taken as the unit cell.*

A general problem is to derive rigorously macroscopic laws from the microscopic equations describing the reactive flows. To this aim, homogenization procedure is applied to rigorously derive upscaled equation from well-posed microscopic (pore-scale) models. For instance, [36,60–62] deal with the homogenization of fluid flows involving reactions and diffusion of solutes. There is a vast literature on the homogenization technique and we mention in particular 2-scale convergence approach developed in [2] and further extended in [101].

In terms of applications, reactive flows in a porous medium have a wide range ranging from spreading of polluting chemicals leading to ground water contamination (see [128]

and references therein) to biological applications such as tissue and bone formation, or pharmaceutical applications [91] or technological applications such as operation of solid batteries.

In this thesis, we restrict to a specific model. This model describes the transport of ions by fluid flow in a porous medium while undergoing precipitation and dissolution reactions. At the solid grain boundaries, the ions attach themselves to the crystal grains, however, the reverse process of dissolution may also take place in which the ions detach themselves from the crystal grains and get dissolved in the fluid. For the present work we assume that the reactions taking place do not lead to the change in the geometry at the pore-scale. This is justified for the case when the layer where the attachment-detachment reactions take place is negligible.

The problem that we deal with in this work is then stated as:

Problem 1.2.3 *For the specific model describing the precipitation-dissolution process, rigorously derive the effective macroscopic equations.*

From the application perspective, the homogenization of this model closes the issue of rigorous transition from the pore scale model [47] to the macroscale model proposed in [73]. Furthermore, the techniques used here are applicable to a larger class of problems dealing with reactions at the boundary. From the mathematical perspective, there are two key challenges: overcoming the low regularity of the microscale solutions and the multi-valued description of the dissolution term. This has been treated in Chapter 6.

1.3   Numerical schemes

As we have already emphasized, a direct numerical approach for the problems involving multiple scales is computationally expensive. However, in situations when we need the full solution or to compare the upscaled equations, we are required to solve the full problem. Referring to the deposition problem in the battery, to understand the process (e.g. the layer conformality) at the trench scale (*microscale*), we need solutions at both the trench and reactor scales (*macroscale*). However, due to the huge difference in the sizes of these scales, straightforward numerical computations are very challenging. To overcome this difficulty, we consider a multiscale approach by introducing an intermediate scale (*mesoscale*). Using the ideas of domain decomposition, we provide an iterative coupling conditions for these three different scales. A direct numerical computation has allowed us to compare the simulations with the experimental results. The fitting of the profiles have led to the determination of physical parameters such as diffusion and reaction rate. For more details on this work, we refer to [112], Ch. 9.

In Chapter 2, we have provided a numerical algorithm that treats the question of convergence of domain decomposition based techniques applied to the deposition on a patterned surface. We have performed the time-discretization of the continuum equations and provided an iterative method at each time-step.
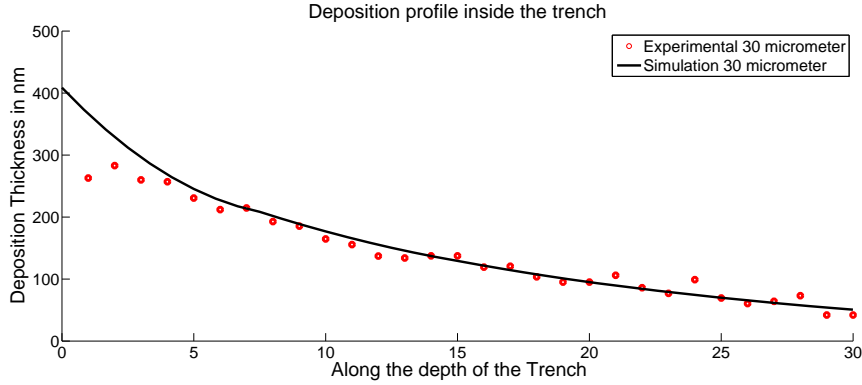
Figure 1.8: *Comparison of experimental deposition profile with the simulation for the trench of cross-sectional size* $30\mu m \times 30\mu m$.

1.3.1 Numerical schemes for upscaled system

Solving the upscaled equations requires appropriate numerical methods. We are motivated by analyzing such methods for solving the reactive flows for an upscaled model. In this respect, two widely used schemes are conformal and the non-conformal (mixed variational) formulations. The former is simpler but suffers from the lack of local conservation of mass property as opposed to the latter which preserves the same in addition to providing an explicit calculation for the flux. Again for the reaction rates, the precipitation-dissolution processes are considered. As it can be recalled, the physics of these processes dictates that the reaction terms are non-linear, non-Lipschitz and possibly multi-valued.

To deal with the multi-valued term, we consider a regularization of this term and consider the sequence of regularized equations. The compactness arguments are used for obtaining convergence. The a priori estimates required for such arguments need to be independent of the discretization parameters as well as the regularization parameter. Even then, these a priori estimates fail to provide the strong convergence for obtaining the limit. To solve the above issues, we let the regularization parameter δ depend on the time discretization parameter τ in such a way that as $\tau \searrow 0$, it is ensured that $\delta \searrow 0$. Thus, obtaining the limit of discretized scheme automatically yields, by virtue of the regularization parameter also vanishing, the original equation. Moreover, the transla-

tion estimates are employed to retrieve stronger convergence.

Our contributions in the numerical analysis of the upscaled equations include considering a non-linear, non-Lipschitz ODE coupled with parabolic PDE. We consider both the semi-discrete and the fully discrete cases. The usual problem of lack of stronger compactness has been tackled by the translation estimates. The application of such estimates has to be tuned to the numerical discretization and by dealing with different kinds such as time-discrete and fully discrete situations; we have exhibited a variety of ways to use these estimates. The numerical analysis also yields the alternative proof of existence for different formulations of the upscaled model. The convergence analysis of appropriate numerical schemes for the problem considered here is a stepping stone towards the pursuit for an eventual plan of coupled flow and transport problems (for example, Richards' equation coupled with precipitation-dissolution reaction models) [13, 96].

1.4   Outline of the thesis

Having given a brief description of the kind of problems that have been considered in this thesis, we proceed to provide a chapter wise description.

In **Chapter 2**, we provide a numerical scheme for multiscale computations for the model describing the chemical vapor deposition process on a trenched Si substrate. To understand the process (e.g. the layer conformality) at the trench scale (microscale), we need solutions at both the trench and reactor scales (macroscale). The multiscale approach considered here introduces an intermediate scale to deal with the huge difference in the sizes of the scales involved. We start with time-continuous model describing the transport processes and then perform time discretization. At each time step, using the ideas of domain decomposition inspired from [87], we provide iterative coupling conditions for these three different scales. Using weak formulation for the time-discrete equations, we prove the convergence of this iterative scheme at each time-step. The approach also provides an alternative proof for the existence of the solutions for the time-discrete formulation [21].

In **Chapter 3** we consider reactive flows in a channel which has oscillating horizontal bed with period ε (see Figure 1.4). The ions/solutes are being transported by the convection and diffusion processes and react at the oscillating boundaries. The reactions rates are assumed to be non-linear. We define the upscaled problem in a domain with flat boundaries, thus greatly simplifying the geometry. Assuming that the reaction rates are defined on a fixed geometry, we provide a rigorous derivation of this upscaling process. The framework is quite general and provides us a way of performing upscaling for different description of reaction rates.

Chapter 4 focusses on the flow and transport of chemically reactive substances (pre-

cursors) in a channel over substrates having complex geometry (see Figure 1.5). In particular, these substrates are in the form of trenches forming oscillating boundaries. The precursors react at the boundaries and get deposited. The deposited layers lead to changes in the geometry and are explicitly taken into account. Consequently, the system forms a free boundary problem. Using formal asymptotic techniques, we obtain the upscaled equations for the system where these equations are defined on a domain with flat boundaries. Numerical experiments show the effectiveness of the upscaling process [76].

Chapter 5 considers a pore-scale model for reactive flow in a thin 2D strip, where the convective transport dominates the diffusion (refer to Figure 1.6). Reactions take place at the lateral boundaries of the strip (the walls), where the reaction product can deposit in a layer with a non-negligible thickness compared to the width of the strip. This leads to a free boundary problem, in which the moving interface between the fluid and the deposited (solid) layer is explicitly taken into account. Using asymptotic expansion methods, we derive an upscaled, one-dimensional model by averaging in the transversal direction. This chapter derives Taylor dispersion type models for the variable geometry case. Numerical computations are presented to compare the outcome of the effective (upscaled) model with the transversally averaged, two-dimensional solution.

Chapter 6 discusses the homogenization approach to derive the upscaled equations for reactive flows in a periodic medium (refer to Figure 1.7). We define a sequence of microscopic solutions u^ε and obtain the upscaled equations as the limit of $\varepsilon \searrow 0$. We adopt the 2-scale framework to achieve this. The challenges are in dealing with the low regularity of microscopic solutions and particular non-linearities in the reaction term. This chapter closes the gap of the rigorous transition from the pore scale model given in [47] to the heuristically proposed macroscopic model in [73].

Chapter 7 contains the numerical analysis of an upscaled (core scale) model describing the transport, precipitation and dissolution of solutes in a porous medium. We consider the weak formulation for the upscaled equation and provide rigorous stability and convergence results for both the semi-discrete (time discretization) and the fully discrete scheme. In doing so, compactness arguments are employed.

In **Chapter 8** we deal with the numerical analysis of an upscaled model describing the transport, precipitation and dissolution of solutes in a porous medium. We consider the mixed variational formulation for the model and provide the numerical discretizations for both the time-discrete form and fully discrete form. We analyse the numerical schemes and prove the convergence to the continuous formulation. Apart from the proof for the convergence, this also yields an existence proof for the mixed variational formulation. Numerical experiments are performed to study the convergence behavior [81].

Chapter 2

Numerical scheme for multiscale computations

We consider the chemical vapor deposition process on a trenched Si-substrate. To understand the process (e.g. the layer conformality) at the trench scale (*microscale*), we need solutions at both the trench and reactor scales (*macroscale*). Due to huge difference in the sizes of these scales, straightforward numerical computations are very challenging. To overcome this difficulty, we consider a multiscale approach by introducing an intermediate scale (*mesoscale*). We start with time-continuous model describing the transport processes and then perform time discretization. At each time step, using the ideas of domain decomposition inspired from [87], we provide an iterative coupling conditions for these three different scales. Using weak formulation for the time-discrete equations, we prove the convergence of this iterative scheme at each time-step. The approach also provides an alternative proof for the existence of the solutions for the time-discrete formulation.

2.1   The motivation

This work is motivated by the chemical vapor deposition (CVD) processes involved in the manufacturing of the 3-D all-solid-state batteries. In this process, a carrier gas flows through a tube with rectangular cross-section (the reactor). A Silicon (Si) substrate is placed at the bottom of the reactor. The carrier gas transports a small amount of reac-

tive substances, the precursors. These precursors react at the substrate, which becomes the lower part of the reactor boundary, where a solid layer is produced [110, 113, 114]. This leads to an overall transport process with reactions at the boundary. The details on the mathematical models are provided in Section 2.3.

To increase the energy storage capacity of the batteries, the geometries of the Si substrate is made complex. To increase the surface area, trenches are etched in the Si-substrate, which has therefore a rough surface instead of being flat. The typical size of a trench is in the order of micrometers ($\sim 10 \ \mu m$), whereas the substrate size is in the order $\sim 30 \ cm$. This evidently indicates the existence of two distinct scales in the problem, the trench scale (referred as the *microscale*) and the reactor scale (the *macroscale*).

For a thorough understanding of the CVD process, in particular the conformality of the deposited layers, one needs an accurate computation of the solution at the trench scale. However, this requires computing the solution at the reactor scale as well. The scale difference (an order of $\sim 10^4$) makes a direct numerical simulation computationally demanding because of the very fine mesh required for resolving the trench scale. Alternatively, we zoom-in a small region of the reactor near the region of interest, the substrate. This introduces an intermediate scale, henceforth referred to as *mesoscale*. Next we zoom-in a small region of the mesoscale where the trenches (the microscale) can be identified. These three domains are thus formed as a result of successive zooming-in so that the trenches are resolved only at the microscale, and the mesoscale is used only for exchanging the information from the macroscale to the microscale. To compute the solution at each scale, coupling conditions between the different scales are needed. In doing so, we use ideas from the domain decomposition method.

Our aim here is providing a numerical scheme allowing to compute the detailed solutions at each scale. The focus being on the numerics for the transport equations, we consider a simple flow model, allowing a complete decoupling from the transport equations. Moreover, the flow is computed only at the macroscale and projected further at the mesoscale. However, the transport equations describing the concentration of the reactants (precursor) are defined in all the three scales. The coupling between different scales is through the boundary conditions providing the continuity of the concentration and of the normal fluxes. To achieve this we first perform the time discretization of the model. Then, at each time-step, an iterative non-overlapping domain decomposition algorithm [87] is considered. The iteration involves a linear combination of the normal fluxes and the concentrations at the separating boundaries, allowing a decoupling of the models at the different scales. For the iterative scheme, rigorous convergence results are obtained by compactness arguments. This approach allows a comparison of the numerical results with the experimental results, and to identify parameters such as the diffusion coefficient and the reaction rate constants for the deposition process. This can hence be used to predict the deposition at alternative conditions and also for different geometries.

Below we briefly describe the geometry in Section 2.2 and provide the mathematical model in Section 2.3. In Section 2.4, we give the definitions of the weak solutions for both the time-continuous and the time-discrete equations. Next, the iterative non-overlapping domain decomposition algorithm is considered. This is followed by the proof of convergence of this iterative numerical method.

2.2 The mathematical model

In this section we give a simplified mathematical model for the motivating application. This model describes the reactive flow inside a reactor, with reactions taking place on the substrate being a part of the boundary. Before giving the equations we give some details regarding the geometry of the system, justifying the multi-scale approach. The scales introduced above (macro-, meso- and microscale) are involving three domains, Ω_1, Ω_2 and Ω_3. Their boundaries are denoted by respectively $\partial\Omega_j$, $j = 1, 2, 3$. Each boundary $\partial\Omega_j$, includes a part Γ_{jR} where reactions (depositions) take place. For the other parts of boundaries, let us first consider the microscale. We define $\Gamma_2 = \partial\Omega_3 \setminus \Gamma_{3R}$, where the the variables in Ω_2 and Ω_3 are coupled. For the mesoscale, we define two parts of $\partial\Omega_2$, namely, Γ_1 and Γ_2. These provide the coupling with Ω_3, respectively Ω_1. In other words, $\Gamma_2 = \partial\Omega_3 \cap \partial\Omega_2$ (the interface between the micro- and the mesoscale), while $\Gamma_1 = \partial\Omega_1 \cap \partial\Omega_2$ (the interface between the macro- and the mesoscale). Figure 2.1 displays these regions and the nomenclatures.

2.3 The equations

The mathematical model consists of two components: the flow and the reactive transport. The reactive substance (precursor) is transported to the substrate through a combined effect of convective flow and the molecular diffusion. The flow velocity of the carrier gas is described by the Navier-Stokes system, while the reactive transport processes are described by the linear convection-diffusion equation.

2.3.1 The flow component

The focus here is on the numerics for the reactive transport component. For the flow we consider a simplified setting, allowing a decoupling from the transport part. For instance, thermal effects are disregarded. Next, as suggested by the numerical evidence, the flow is absent in the trenches and therefore the flow is considered only at the macro-
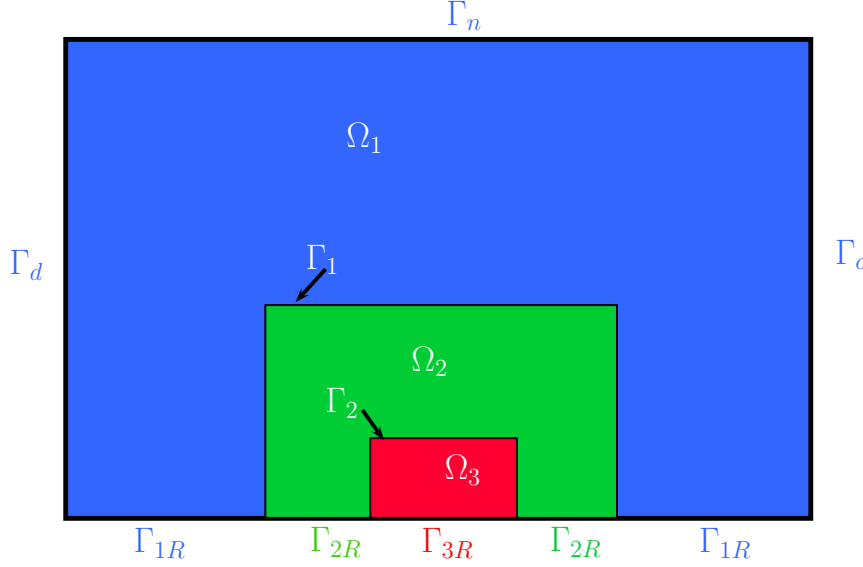
Figure 2.1: *Schematic for the multiscale computation method.*

and the mesoscale, where no roughness is encountered at the boundary. Further simplifications include that the flow is laminar and incompressible, and no gravity effects are taken into account. It is also assumed that the concentration of the precursor is much smaller than the one of the carrier gas and hence, therefore the flow is not affected by the adsorption of the precursors. Finally, we only consider a steady-state, hence the flow problem needs to be solved once (in the beginning). Under the above assumptions, the flow component of the model reads

$$
\begin{aligned}
\text{Continuity:} \quad & \nabla \cdot \mathbf{q} &=& \ 0, \\
\text{Momentum:} \quad & \rho \mathbf{q} \nabla \cdot \mathbf{q} &=& \ \nabla \cdot \left(\mu (\nabla \mathbf{q} + \nabla \mathbf{q}^T) - \tfrac{2}{3} \mu (\nabla \cdot \mathbf{q}) I \right) - \nabla P,
\end{aligned} \qquad (2.3.1)
$$

in the simple domain $\Omega_1 \cup \Omega_2 \cup \Gamma_1$, where $\mathbf{q}$ is the gas velocity and P its pressure. For the boundary conditions, we provide a parabolic inlet for the velocity (at Γ_i) and use no-slip boundary conditions at the side walls. We prescribe pressure at the outlet Γ_o).

$$
\mathbf{q} = \mathbf{q}_d \quad \text{on} \quad \Gamma_d; \quad P = P_0 \quad \text{on} \quad \Gamma_o; \quad \text{and} \quad \mathbf{q} = 0 \quad \text{on} \quad \Gamma_2 \cup \Gamma_{1R} \cup \Gamma_{2R} \cup \Gamma_n,
$$

for instance, in 2D, the choice of parabolic inlet profile gives $\mathbf{q}_d = Q(\ell^2 - y^2)\mathbf{e}_1$, where Q is a positive constant and $\mathbf{e}_1$ is a unit vector along $x-$ direction.

2.3.2 The reactive transport/deposition equations

For the CVD model we restrict to the basic equations, including the convective transport and the molecular diffusion, neglect the reactions taking place in the gas phase and consider the situation when the precursor has only one species. Inside the domain Ω_i its concentration is denoted by u_i, where $i = 1, 2, 3$ is indexing the scale. For the boundary conditions we assume that the deposition takes place only on the bottom plate (the substrate). For simplicity, we assume a first order kinetics.

The macroscale equations

With $T > 0$ standing for the maximal time, at the reactor scale the precursor is modeled by the linear convection-diffusion equation

$$\partial_t u_1 - \Delta u_1 + \mathbf{q} \cdot \nabla u_1 = 0 \quad \text{in} \quad \Omega_1 \times (0, T] \tag{2.3.2}$$

coupled with the reactive boundary conditions

$$- \boldsymbol{\nu} \cdot \nabla u_1 = C_R u_1 \quad \text{on} \quad \Gamma_{1R} \times (0, T], \tag{2.3.3}$$

where C_R is the (positive) reaction constant. The macroscale equations are coupled with the micro scale ones at $\Gamma_1 \subset \partial \Omega_1$. The boundary $\partial \Omega_1 = \Gamma_d \cup \Gamma_n \cup \Gamma_o \cup \Gamma_{1R} \cup \Gamma_1$ and the boundary part Γ_d has non-zero measure where Dirichlet boundary conditions are prescribed, and for $\Gamma_n \in \Gamma_o$ homogeneous Neuman boundary conditions $(-\boldsymbol{\nu} \cdot \nabla u_3 = 0)$ are taken.

The mesoscale equations

At the mesoscale we use the same equation for the precursor

$$\partial_t u_2 - \Delta u_2 + \mathbf{q} \cdot \nabla u_2 = 0 \quad \text{in} \quad \Omega_2 \times (0, T] \tag{2.3.4}$$

and the reactive boundary conditions

$$- \boldsymbol{\nu} \cdot \nabla u_2 = C_R u_2 \quad \text{on} \quad \Gamma_{2R} \times (0, T]. \tag{2.3.5}$$

Coupling conditions are imposed along $\Gamma_2 \cup \Gamma_1$, as explained in the next section.

The microscale equations

The geometrical dimensions of the microscale are comparable to the mean free path length of the gas particles. This means that the diffusion is no longer Fickian, but involves the Knudsen diffusion coefficient, a parameter that can be determined by comparing with experimental results. Further, we ignore the convective term for the transport in the trench as the velocity is negligible. Also, the flux at the mesoscale automatically takes into account the flux due to convection. The deposition process inside the trench is described by the following equations:

$$\partial_t u_3 = D_T \Delta u_3 \quad \text{in} \quad \Omega_3 \times (0, T] \tag{2.3.6}$$

where D_T is the diffusion coefficient, outside the trench we use the Fickian diffusion while inside the trench we use different diffusion coefficient. For the boundary conditions we prescribe

$$- \boldsymbol{\nu} \cdot \nabla u_3 = C_R u_3 \quad \text{on} \quad \Gamma_{3R} \times (0, T] \tag{2.3.7}$$

where Γ_{3R} is the surface on which reactions take place. The remaining boundary part $\partial \Omega_3 \setminus \Gamma_{3R}$ is involved in the coupling with the mesoscale, as explained below.

Note that we have the same structure for the equations defined in the macroscale as well as the mesoscale. Moreover, the ratio of microscale to macroscale is of the order 10^4 and a two step domain decomposition algorithm would require very small discretization to allow coupling with the microscale boundaries. To overcome this discretization restriction, we propose a three-stage numerical scheme to compute the solution.

The coupling conditions

The different scales are coupled by the boundary conditions at non-reactive surfaces. We provide coupling conditions that are natural for this setting of the problem, namely, the flux continuity and the continuity of the concentrations. Specifically, after having fixed the normal $\boldsymbol{\nu}$ to Γ_1 and into Ω_1 we have the following coupling conditions:

$$\boldsymbol{\nu} \cdot \left(- \nabla u_2 + \mathbf{q} u_2 \right) = \boldsymbol{\nu} \cdot \left(- \nabla u_1 + \mathbf{q} u_1 \right) \quad \text{on} \quad \Gamma_1 \tag{2.3.8}$$

and

$$u_1 = u_2 \quad \text{on} \quad \Gamma_1. \tag{2.3.9}$$

Similar coupling conditions are imposed at the interface Γ_2 between the microscale and mesoscale.

$$u_2 = u_3 \quad \text{and} \quad \boldsymbol{\nu} \cdot \left(- \nabla u_2 + \mathbf{q} u_2 \right) = -D_T \boldsymbol{\nu} \cdot \nabla u_3 \quad \text{on} \quad \Gamma_2. \tag{2.3.10}$$

Having specified the boundary conditions, the model is closed by the initial conditions:

$$u_1(0, \cdot) = u_1^0, \quad u_2(0, \cdot) = u_2^0, \quad u_3(0, \cdot) = u_3^0. \tag{2.3.11}$$

For more general coupling conditions (transmission problems), we refer to [27] and [65].

2.4 The numerical scheme

In this section we analyze the numerical scheme for solving the reactive transport model component, posed in the three sub-domains of the reactor. The scheme is based on the time Euler implicit time stepping. We start by defining the concept of weak solution for both the continuous and the time discrete cases. Then, for the resulting sequence of time discrete problems we give an iterative domain decomposition scheme, and prove its convergence based on compactness arguments.

2.4.1 The weak form

We start with the concept of weak solution for the coupled model in (2.3.2)-(2.3.11), involving standard notations in the functional analysis. In particular, $H^1(\Omega_i)$ is the Sobolev space of functions defined on Ω_i and having L^2 weak derivatives. By $H^1_{0,\Gamma_D}(\Omega_i)$ we mean the functions in $H^1(\Omega_i)$ having a vanishing trace on Γ_D, and $H^{-1}(\Omega_i)$ is its dual. Further, $L^2(0, T; X)$ is the Bochner space of functions valued in X, and $(\cdot, \cdot)_U$ denotes the inner product in $L^2(U)$ (with U a bounded domain) or the duality pairing between H^1_{0,Γ_D} and its dual. Finally we define the spaces

$$\mathcal{V}_i = \{u_i \in L^2(0, T; H^1_{0,\Gamma_D}(\Omega_i)) \mid \partial_t u_i \in L^2(0, T; H^{-1}(\Omega_i))\}, \qquad i = 1, 2, \text{ or } 3.$$

Also, let $\Omega_i^T := \Omega_i \times (0, T)$, $\Gamma_{iR}^T = \Gamma_{iR} \times (0, T)$ and assume that $u_i^0 \in H^1_{0,\Gamma_D}(\Omega_i)$ for all i. Furthermore, for $\mathbf{q}$ we assume that $\mathbf{q} \in H(div; \Omega_1 \cup \Omega_2) \bigcap L^\infty(\Omega_1 \cup \Omega_2)$. Adopting the standard definition of $H(div; \Omega)$, it consists of vector valued functions having divergence in $L^2(\Omega)$.

Definition 2.4.1 *A weak solution of (2.3.2)-(2.3.11) is a triple $(u_1, u_2, u_3) \in \mathcal{V}_1 \times \mathcal{V}_2 \times \mathcal{V}_3$ satisfying the initial conditions $u_i(0, \cdot) = u_i^0$ ($i = 1, 2$, or 3), the boundary conditions*

$$u_1 = u_2 \quad at \quad \Gamma_1, \qquad u_2 = u_3 \quad at \quad \Gamma_2,$$

and

$$(\partial_t u_1, \phi_1)_{\Omega_1^T} + (\nabla u_1, \nabla \phi_1)_{\Omega_1^T} + (q \nabla u_1, \phi_1)_{\Omega_1^T} + (C_R u_1, \phi_1)_{\Gamma_{1R}^T}$$

$$+ (\partial_t u_2, \phi_2)_{\Omega_2^T} + (\nabla u_2, \nabla \phi_2)_{\Omega_2^T} + (q \nabla u_2, \phi_2)_{\Omega_2^T} + (C_R u_2, \phi_2)_{\Gamma_{2R}^T} \qquad (2.4.1)$$

$$+ (\partial_t u_3, \phi_3)_{\Omega_3^T} + (D_T \nabla u_3, \nabla \phi_3)_{\Omega_3^T} + (C_R u_3, \phi_3)_{\Gamma_{3R}^T} = 0$$

for all $\phi_i \in L^2(0, T; H^1_{0,\Gamma_D}(\Omega_i))$ such that $\phi_1 = \phi_2$ at Γ_1 and $\phi_2 = \phi_3$ at Γ_2.

In this section the equalities at the non-reactive interfaces Γ_1 and Γ_2 should be interpreted in the sense of traces. Next we consider the Euler implicit time discretization of (2.4.1). To this aim we take $N \in \mathbb{N}$ and define $\triangle t = T/N$. With $t_k = k \triangle t$ and u_i^k approximating $u_i(t_k)$ ($i = 1, 2$, or $3; k = 1, \ldots, N$), the time discrete solution triple at $t = t_k$ is defined by

Definition 2.4.2 *Given $u_i^{k-1} \in H^1_{0,\Gamma_D}(\Omega_i)$ we seek for $u_i^k \in H^1_{0,\Gamma_D}(\Omega_i)$ satisfying*

$$u_1^k = u_2^k \quad at \quad \Gamma_1, \qquad u_2^k = u_3^k \quad at \quad \Gamma_2,$$

and

$$\frac{1}{\triangle t}(u_1^k - u_1^{k-1}, \phi_1) + (\nabla u_1^k, \nabla \phi_1) + (q \nabla u_1^{k-1}, \phi_1) + (C_R u_1^k, \phi_1)_{\Gamma_{1R}}$$

$$+ \frac{1}{\triangle t}(u_2^k - u_2^{k-1}, \phi_2) + (\nabla u_2^k, \nabla \phi_2) + (q \nabla u_2^{k-1}, \phi_2) + (C_R u_2^k, \phi_2)_{\Gamma_{2R}} \qquad (2.4.2)$$

$$+ \frac{1}{\triangle t}(u_3^k - u_3^{k-1}, \phi_3) + (D_T \nabla u_3^k, \nabla \phi_3) + (C_R u_3^k, \phi_3)_{\Gamma_{3R}} = 0$$

for all $\phi_i \in H^1_{0,\Gamma_D}(\Omega_i)$, such that that $\phi_1 = \phi_2$ on Γ_1 and $\phi_2 = \phi_3$ on Γ_2.

Note that in either the continuous case or the time discrete one, the equations posed in each subdomain are coupled by imposing explicitly the continuity of the concentrations at the non-reactive surfaces $\Gamma_1 \cup \Gamma_2$. The flux continuity instead is a consequence of the fact that the test functions ϕ_i are also equal along these surfaces. In this way, the boundary terms along $\Gamma_1 \cup \Gamma_2$ can only vanish if the outwards normal components of the fluxes cancel each other.

The equations (2.4.2) form a system of linear elliptic partial differential equations. Standard elliptic theory tells us that for a given $u_i^{k-1} \in H^1_{0,\Gamma_D}(\Omega_i)$, we obtain $u_i^k \in H^2_{0,\Gamma_D}(\Omega_i)$. We will use this fact below in the iterative scheme proposed here.
The numerical iterative scheme considered here also provides proof for the existence for the time-discrete formulation. Moreover, one can treat more complicated reaction rates (for example, Lipschitz reaction rates) by considering Euler explicit time stepping in the reaction term. For numerical reasons, we formulate the original problem in the three

(non-overlapping) domains. This allows separating the computations at the trench scale from those at the reactor scale without requiring any correlation between the meshes employed at the different scales. Having introduced the weak solutions above, we now consider a numerical scheme to compute the solution at each time step and investigate its convergence. To simplify the presentation we fix a time step t_k and define

$$v_i := u_i^k, \quad i = 1, 2, 3,$$

so that all the estimates are obtained in terms of v_i.

2.4.2 The iterative domain decomposition scheme

Here we describe the iterative scheme used for solving the time-discrete problem (2.4.2). The scheme is inspired from [87, 88]. To understand its background, we consider first consider the strong form of the equation and define the quantities ($\boldsymbol{\nu}_1$ is the normal to Γ_1 and into Ω_1 $\boldsymbol{\nu}_2$ is normal to Γ_2 and into Ω_2)

$$g_{21} := \boldsymbol{\nu}_1 \cdot (-\nabla v_2) + \lambda v_2 \quad \text{and} \quad g_{12} := \boldsymbol{\nu}_1 \cdot \nabla v_1 + \lambda v_1 \quad \text{on} \quad \Gamma_1, \tag{2.4.3}$$

$$g_{23} := \boldsymbol{\nu}_2 \cdot \nabla v_2 + \lambda v_2 \quad \text{and} \quad g_{32} := -\boldsymbol{\nu}_2 \cdot D_T \nabla v_3 + \lambda v_3 \quad \text{on} \quad \Gamma_2, \tag{2.4.4}$$

where $\lambda > 0$ is a positive constant. For the convergence proof, it suffices to have $\lambda > 0$ however, its value influences the speed of convergence [20]. Note that the g_{ij} terms depend on the time step k and define (decoupling) boundary conditions at the non-reacting interfaces. To ensure that the solving the decoupled problems are providing a solution of the originally coupled one, additional conditions will be given later.

Based on the above we let $n \in \mathbb{N}$ denote the iteration index and construct the nth as the solution of

Problem P^n: Given $v_i^{n-1} \in H_{0,\Gamma_D}^1(\Omega_i)$ and $g_{ji}^{n-1} \in H_{\Gamma_1/\Gamma_2}^{1/2}$ $(i, j = 1, 2, 3)$, find $v_i^n \in H_{0,\Gamma_D}^1(\Omega_i)$ and $g_{ij}^n(i, j = 1, 2, 3)$ such that

$$\frac{1}{\triangle t}(v_1^n, \phi_1)_{\Omega_1} + (\nabla v_1^n, \nabla \phi_1)_{\Omega_1} + (C_R v_1^n, \phi_1)_{\Gamma_{1R}} + (g_{12}^n, \phi_1)_{\Gamma_1}$$
$$= \frac{1}{\triangle t}(u_1^{k-1}, \phi_1)_{\Omega_1} - (\mathbf{q}\nabla u_1^{k-1}, \phi_1)_{\Omega_1}, \tag{2.4.5}$$

$$\frac{1}{\triangle t}(v_2^n, \phi_2)_{\Omega_2} + (\nabla v_2^n, \nabla \phi_2)_{\Omega_2} + (C_R v_2^n, \phi_2)_{\Gamma_{2R}} + (g_{21}^n, \phi_2)_{\Gamma_1} + (g_{23}^n, \phi_2)_{\Gamma_2}$$
$$= \frac{1}{\triangle t}(u_2^{k-1}, \phi_2)_{\Omega_2} - (\mathbf{q}\nabla u_2^{k-1}, \phi_2)_{\Omega_2}, \tag{2.4.6}$$

$$\frac{1}{\triangle t}(v_3^n, \phi_3)_{\Omega_3} + (D_T \nabla v_3^n, \nabla \phi_3)_{\Omega_3} + (C_R v_3^n, \phi_3)_{\Gamma_{3R}} + (g_{32}^n, \phi_3)_{\Gamma_2} = \frac{1}{\triangle t}(u_3^{k-1}, \phi_3)_{\Omega_3}.$$

(2.4.7)

for all $\phi_i \in H^1_{0,\Gamma_D}(\Omega_i)$, such that $\phi_1 = \phi_2$ on Γ_1 and $\phi_2 = \phi_3$ on Γ_2, and

$$g_{ij}^n := 2\lambda v_j^{n-1} - g_{ji}^{n-1}.$$

(2.4.8)

The iterative scheme requires a starting triple (v_1^0, v_2^0, v_3^0). Since the problem under consideration is, in fact, an evolution one, a good option is $v_i^0 = u_i^{k-1}$. However, this choice is not required for the convergence proof below. Further, $g_{ij}^0 = -\mathbf{v} \cdot \nabla v_i^0 + \lambda v_i^0$ for $i \neq 3$; and $g_{32}^0 = -\mathbf{v} \cdot D_T \nabla v_3^0 + \lambda v_3^0$. For the notation, we remind that k is the time-step and n stands for the iteration index. Thus v_i^n stands for $u_i^{k,n}$, the n-th iterate at time step $t = t_k$. Note that at each iterative step n, the equations are decoupled by the boundary conditions obtained from the previous iterative step.

Remark 2.1 As stated earlier, it is reasonable to assume that $u_i^{k-1} \in H^2_{0,\Gamma_D}(\Omega_i)$ which implies that for the starting triple, $v_i^0 = u_i^{k-1}$, we have $g_{ij}^0 \in H^{1/2}_{\Gamma_1/\Gamma_2}$. With the boundary conditions decoupled for the Problem $\mathbf{P}^n$, the standard elliptic theory provides existence and uniqueness of the solution triple v_i^n. The results below are obtained assuming that $u_i^{k-1} \in H^2_{0,\Gamma_D}(\Omega_i)$. □

Remark 2.2 Note that the explicit discretization of the convective term requires CFL condition to be satisfied for stability reasons. This may seem restrictive especially in view of spatial discretization of Ω_2 being much smaller compared to the macroscale discretization. However, note that with the parabolic inlet profile of the fluid velocity, $\mathbf{q}$ itself is much smaller in Ω_2, in fact of the order of $|\Omega_2|$. Thus, the CFL restriction is quite reasonable with

$$\triangle t \leq \max\{\frac{h_2}{Q|\Omega_2|}, \frac{h_1}{Q}\}$$

where h_1 and h_2 refer to the sizes of spatial discretization of Ω_1, respectively Ω_2. □
Before giving a rigorous convergence proof, we give a formal justification of the iterative scheme. Assuming that $v_i^n \to v_i$ and $g_{ij}^n \to g_{ij}$, passing to the limit in the updates (2.4.8) gives

$$g_{ij} = 2\lambda v_j - g_{ji}.$$

In other words, at Γ_1 we have

$$g_{12} = 2\lambda v_2 - g_{21}, \qquad \text{and} \qquad g_{21} = 2\lambda v_1 - g_{12},$$

implying $v_2 = v_1$. Once the continuity is established, the following simple calculation establishes the equality of normal component of diffusive fluxes at Γ_1

$$\mathbf{v}_1 \cdot \nabla v_1 - \mathbf{v}_1 \cdot \nabla v_2 + \lambda(v_1 + v_2) = g_{12} + g_{21} = 2\lambda v_1 = \lambda(v_1 + v_2).$$

The justification of the coupling conditions at Γ_2 is completely similar.

In the formal definition of g_{ij} above, we have only included the normal diffusive flux. This is because equality of normal component of diffusive flux together with the continuity of concentration also implies the equality of normal flux. Clearly,

$$\boldsymbol{\nu}_1 \cdot (-\nabla u_2 + \mathbf{q} u_2) = \boldsymbol{\nu}_1 \cdot (-\nabla u_1 + \mathbf{q} u_1) \quad \text{on} \quad \Gamma_1$$

and similarly for Γ_2.

2.4.3 The convergence proof

We follow the ideas in [87] and the main ideas of the proof are obtaining a priori estimates for v_i^n and using compactness arguments to show the H^1 convergence in space. Application of compact embeddings and trace inequalities lead to establishing convergence on the boundaries. It is afterwards of no particular difficulty to prove that the limits satisfy the time-discrete formulation (2.4.2).

We have the following theorem:

Theorem 2.4.1 *As $n \to \infty$, the solutions v_i^n satisfying (2.4.5)-(2.4.7) converge weakly to v_i in $H^1(\Omega_i)$ norm satisfying (2.4.2).*

A priori estimates

To prepare the proof of Theorem 2.4.1, we define the following

$$e_i^n := v_i^n - v_i^{n-1} \quad (i = 1, 2, 3), \tag{2.4.9}$$

$$e_{1,\Gamma_1}^n := g_{12}^n - g_{12}^{n-1}, \quad e_{2,\Gamma_1}^n = g_{21}^n - g_{21}^{n-1}, \tag{2.4.10}$$

$$e_{3,\Gamma_2}^n := g_{32}^n - g_{32}^{n-1}, \quad e_{4,\Gamma_2}^n = g_{23}^n - g_{32}^{n-1}, \tag{2.4.11}$$

$$e_{\Gamma_1}^n := \left[(e_{1,\Gamma_1}^n)^2 + (e_{2,\Gamma_2}^n)^2 \right]^{1/2}, \quad e_{\Gamma_2}^n := \left[(e_{3,\Gamma_2}^n)^2 + (e_{4,\Gamma_2}^n)^2 \right]^{1/2}. \tag{2.4.12}$$

With these definitions in mind, we have the following Lemma.

Lemma 2.3 *A constant $C > 0$ depending on the starting triple (v_1^0, v_2^0, v_3^0) exists such that the boundary errors introduced in (2.4.9) satisfy:*

$$\sum_{n=1}^N \left(\|e_1^n\|_{\Gamma_1}^2 + \|e_2^n\|_{\Gamma_1}^2 + \|e_2^n\|_{\Gamma_2}^2 + \|e_3^n\|_{\Gamma_2}^2 \right) \le C. \tag{2.4.13}$$

Proof. Subtracting (2.4.5) for v_1^{n-1} from the one for v_1^n gives

$$\frac{1}{\triangle t}(v_1^n - v_1^{n-1}, \phi_1)_{\Omega_1} + (\nabla v_1^n - \nabla v_1^{n-1}, \nabla \phi_1)_{\Omega_1} + C_R(v_1^n - v_1^{n-1}, \phi_1)_{\Gamma_{1R}}$$
$$+ \lambda(v_1^n - v_1^{n-1}, \phi_1)_{\Gamma_1} - (g_{12}^n - g_{12}^{n-1}, \phi_1)_{\Gamma_1} = 0. \qquad (2.4.14)$$

Taking in the above $\phi_1 = e_1^n$ leads to

$$\frac{1}{\triangle t}\|e_1^n\|_{\Omega_1}^2 + \|\nabla e_1^n\|_{\Omega_1}^2 + C_R\|e_1^n\|_{\Gamma_{1R}}^2 + \lambda(e_1^n, e_1^n)_{\Gamma_1} = (e_{1,\Gamma_1}^n, e_1^n)_{\Gamma_1}. \qquad (2.4.15)$$

In a similar manner one gets

$$\frac{1}{\triangle t}\|e_2^n\|_{\Omega_2}^2 + \|\nabla e_2^n\|_{\Omega_2}^2 + C_R\|e_2^n\|_{\Gamma_{2R}}^2 + \lambda(e_2^n, e_2^n)_{\Gamma_1} + \lambda(e_2^n, e_2^n)_{\Gamma_2} = (e_{2,\Gamma_1}^n, e_2^n)_{\Gamma_1} + (e_{3,\Gamma_2}^n, e_3^n)_{\Gamma_2},$$
$$(2.4.16)$$

and

$$\frac{1}{\triangle t}\|e_3^n\|_{\Omega_3}^2 + \|D_T \nabla e_3^n\|_{\Omega_3}^2 + C_R\|e_3^n\|_{\Gamma_{3R}}^2 + \lambda(e_3^n, e_3^n)_{\Gamma_2} = (e_{4,\Gamma_2}^n, e_3^n)_{\Gamma_2}. \qquad (2.4.17)$$

Recalling the notations in (2.4.10)-(2.4.12), we have

$$\begin{aligned}(e_{\Gamma_1}^{n+1})^2 &= (g_{12}^{n+1} - g_{12}^n)^2 + (g_{21}^{n+1} - g_{21}^n)^2 \\
&= (2\lambda(v_2^n - v_2^{n-1}) - g_{21}^n + g_{21}^{n-1})^2 + (2\lambda(v_1^n - v_1^{n-1}) - g_{12}^n + g_{12}^{n-1})^2 \\
&= (2\lambda(v_2^n - v_2^{n-1}) - e_{2,\Gamma_1}^n)^2 + (2\lambda(v_1^n - v_1^{n-1}) - e_{1,\Gamma_1}^n) \\
&= (e_{1,\Gamma_1}^n)^2 + (e_{2,\Gamma_1}^n)^2 + 4\lambda(\lambda(v_1^n - v_1^{n-1}) - e_{1,\Gamma_1}^n)(v_1^n - v_1^{n-1}) \\
&\quad + 4\lambda(\lambda(v_2^n - v_2^{n-1}) - e_{2,\Gamma_1}^n)(v_2^n - v_2^{n-1}).\end{aligned}$$

By (2.4.12) this gives

$$(e_{\Gamma_1}^{n+1})^2 - (e_{\Gamma_1}^n)^2 = 4\lambda(\lambda e_1^n - e_{1,\Gamma_1}^n, e_1^n)_{\Gamma_1} + 4\lambda(\lambda e_2^n - e_{2,\Gamma_1}^n, e_2^n)_{\Gamma_1}.$$

Similarly,

$$(e_{\Gamma_2}^{n+1})^2 - (e_{\Gamma_2}^n)^2 = 4\lambda(\lambda e_2^n - e_{3,\Gamma_2}^n, e_2^n)_{\Gamma_2} + 4\lambda(\lambda e_3^n - e_{4,\Gamma_2}^n, e_3^n)_{\Gamma_2}.$$

With the above, adding (2.4.15) - (2.4.17) gives

$$\frac{1}{\triangle t}\|e_1^n\|_{\Omega_1}^2 + \|\nabla e_1^n\|_{\Omega_1}^2 + C_R(\|e_1^n\|_{\Gamma_{1R}}^2 + \|e_2^n\|_{\Gamma_{2R}}^2 + \|e_3^n\|_{\Gamma_{3R}}^2) + \frac{1}{\triangle t}\|e_2^n\|_{\Omega_2}^2 + \|\nabla e_2^n\|_{\Omega_2}^2$$
$$+ \frac{1}{\triangle t}\|e_3^n\|_{\Omega_3}^2 + \|\nabla e_3^n\|_{\Omega_3}^2 + \frac{1}{4\lambda}\left(\|e_{\Gamma_1}^{n+1}\|_{\Gamma_1}^2 - \|e_{\Gamma_1}^n\|_{\Gamma_1}^2\right) + \frac{1}{4\lambda}\left(\|e_{\Gamma_2}^{n+1}\|_{\Gamma_2}^2 - \|e_{\Gamma_2}^n\|_{\Gamma_2}^2\right) = 0.$$

Summing the above over $n = 1 \cdots N$ leads to

$$\|e_{\Gamma_1}^{N+1}\|^2 + \|e_{\Gamma_2}^{N+1}\|^2 + 4\lambda \sum_{n=1}^{N} \left(\|\nabla e_1^n\|^2 + \|\nabla e_2^n\|^2 + \|\nabla e_3^n\|^2 \right)$$

$$+ \frac{4\lambda}{\triangle t} \sum_{n=1}^{N} \left(\|e_1^n\|_{\Omega_1}^2 + \|e_2^n\|_{\Omega_2}^2 + \|e_3^n\|_{\Omega_3}^2 \right) \tag{2.4.18}$$

$$+ C_R(\|e_1^n\|_{\Gamma_{1R}}^2 + \|e_2^n\|_{\Gamma_{2R}}^2 + \|e_3^n\|_{\Gamma_{3R}}^2) = \|e_{\Gamma_1}^0\|_{\Gamma_1}^2 + \|e_{\Gamma_2}^0\|_{\Gamma_2}^2.$$

By the trace theorem, one has $\|e_{\Gamma_1}^0\|_{\Gamma_1} + \|e_{\Gamma_2}^0\|_{\Gamma_2}^2 \le C \sum_{i=1}^{3} \|v_i^0\|_{H^2(\Omega_1)}$ (C depends only on the domain). Another application of trace theorem in view of the above inequality gives

$$\sum_{n=1}^{N} \left(\|e_1^n\|_{\Gamma_1}^2 + \|e_2^n\|_{\Gamma_1}^2 + \|e_2^n\|_{\Gamma_2}^2 + \|e_3^n\|_{\Gamma_2}^2 \right) \le C, \tag{2.4.19}$$

which concludes the proof. $\qquad\square$

Lemma 2.3 implies that the series on the left of (2.4.13) is finite, therefore the (error) terms are converging to 0. However, this is not sufficient to prove the desired convergence result.

Lemma 2.4 *With the solution triple (v_1^n, v_2^n, v_3^n) solving Problem $\mathbf{P}^n$ ($n \ge 1$), one has*

$$\sum_{i=1}^{3} \|v_i^N\|_{H^1(\Omega_i)}^2 + \sum_{n=1}^{N} \left(\|v_1^{n+1} - v_2^n\|_{\Gamma_1}^2 + \|v_2^{n+1} - v_1^n\|_{\Gamma_1}^2 + \|v_1^{n+1} - v_3^n\|_{\Gamma_2}^2 + \|v_3^{n+1} - v_2^n\|_{\Gamma_2}^2 \right) \le C$$

$$\tag{2.4.20}$$

with C independent of N and depends on the initial data.

Proof. We start by observing that

$$g_{12}^{n+1} - g_{12}^{n-1} = 2\lambda v_2^n - 2\lambda v_1^{n-1}, \qquad g_{21}^{n+1} - g_{21}^{n-1} = 2\lambda v_1^n - 2\lambda v_2^{n-1},$$

$$g_{23}^{n+1} - g_{23}^{n-1} = 2\lambda v_3^n - 2\lambda v_2^{n-1}, \qquad g_{32}^{n+1} - g_{32}^{n-1} = 2\lambda v_2^n - 2\lambda v_3^{n-1}.$$

Further, we have the elementary identities

$$(v_i^{n+1} - v_i^{n-1}, v_i^{n+1}) = \tfrac{1}{2}\|v_i^{n+1}\|^2 + \tfrac{1}{2}\|v_i^{n+1} - v_i^{n-1}\|^2 - \tfrac{1}{2}\|v_i^{n-1}\|^2,$$

$$(\nabla(v_i^{n+1} - v_i^{n-1}), \nabla v_i^{n+1}) = \tfrac{1}{2}\|\nabla v_i^{n+1}\|^2 + \tfrac{1}{2}\|\nabla(v_i^{n+1} - v_i^{n-1})\|^2 - \tfrac{1}{2}\|\nabla v_i^{n-1}\|^2,$$

$$(v_i^{n+1} + v_i^{n-1} - 2v_j^n, v_i^{n+1}) = \tfrac{1}{2}\|v_i^{n+1}\|^2 + \tfrac{1}{2}\|v_i^{n-1}\|^2 - \|v_j^n\|^2$$
$$+ \|v_i^{n+1} - v_j^n\|^2 - \tfrac{1}{2}\|v_i^{n+1} - v_i^{n-1}\|^2.$$

We now proceed as in Lemma 2.3 and subtract (2.4.5)-(2.4.7) for v_i^{n-1} from the one for v_i^{n+1}, test the resulting with $\phi = v_i^{n+1}$, and double the resulting and summing it over

$n = 1, \cdots, N$ to obtain

$$\frac{1}{\triangle t} \sum_{i=1}^{3} \left(\|v_i^{N+1}\|_{\Omega_1}^2 + \|v_i^n\|_{\Omega_1}^2 \right) + \sum_{i=1}^{3} \left(\|\nabla v_i^{N+1}\|_{\Omega_1}^2 + \|\nabla v_i^n\|_{\Omega_1}^2 \right)$$

$$+ \frac{1}{\triangle t} \sum_{n=1}^{N} \sum_{i=1}^{3} \|v_i^{n+1} - v_i^{n-1}\|_{\Omega_i}^2 + \sum_{n=1}^{N} \sum_{i=1}^{3} \|\nabla v_i^{n+1} - \nabla v_i^{n-1}\|_{\Omega_i}^2 + \sum_{i=1}^{3} \left(\|v_i^{n+1}\|_{\Gamma_{iR}}^2 + \|v_i^n\|_{\Gamma_{iR}}^2 \right)$$

$$+ 2 \sum_{n=1}^{N} \left(\|v_1^{n+1} - v_2^n\|_{\Gamma_1}^2 + \|v_2^{n+1} - v_1^n\|_{\Gamma_1}^2 + \|v_2^{n+1} - v_3^n\|_{\Gamma_2}^2 + \|v_3^{n+1} - v_2^n\|_{\Gamma_2}^2 \right)$$

$$\leq C + \sum_{n=1}^{N} \left(\|v_1^{n+1} - v_1^{n-1}\|_{\Gamma_1} + \|v_2^{n+1} - v_2^{n-1}\|_{\Gamma_1} + \|v_2^{n+1} - v_2^{n-1}\|_{\Gamma_2} + \|v_3^{n+1} - v_3^{n-1}\|_{\Gamma_2} \right).$$

Using (2.4.19) in the above yields

$$\sum_{i=1}^{3} \left(\|v_i^N\|_{\Omega_i}^2 + \|\nabla v_i^N\|_{\Omega_i}^2 \right)$$
$$+ \sum_{n=1}^{N} \left(\|v_1^{n+1} - v_2^n\|_{\Gamma_1}^2 + \|v_2^{n+1} - v_1^n\|_{\Gamma_1}^2 + \|v_1^{n+1} - v_3^n\|_{\Gamma_2}^2 + \|v_3^{n+1} - v_2^n\|_{\Gamma_2}^2 \right) \leq C$$

$$(2.4.21)$$

with C independent of N and depending only on the initial data. $\qquad \square$

Proof of Theorem 2.4.1

Proof. Lemma 2.4 provides enough compactness to pass to the limit. Note that (2.4.21) implies that there exists a subsequence again denoted by v_i^n such that

$$v_i^n \to v_i \quad \text{weakly in} \quad H^1(\Omega_i)$$

and hence, strongly in $L^2(\Omega_i)$. Further, to establish the continuity of the concentration at the boundaries, let us take for instance,

$$\|v_1 - v_2\|_{\Gamma_1} \leq \|v_1 - v_1^{n+1}\|_{\Gamma_1} + \|v_2^{n+1} - v_2\|_{\Gamma_1} + \|v_1^{n+1} - v_2^{n+1}\|_{\Gamma_1}$$

whereby the last term on the right hand side vanishes because of estimate (2.4.21). The vanishing of the first two terms are consequence of weak convergence in H^1 leading to L^2 strong convergence at the boundaries. Similarly, $v_2 = v_3$ at the boundary Γ_2.
From the preceding discussions, we conclude that the triple $(v_1, v_2, v_3) \equiv (u_1^k, u_2^k, u_3^k)$ satisfies

$$\frac{1}{\triangle t}(u_1^k - u_1^{k-1}, \phi_1)_{\Omega_1} + (\nabla u_1^k, \nabla \phi_1)_{\Omega_1} - (\mathbf{q} \nabla u_1^{k-1}, \phi_1)_{\Omega_1} \qquad (2.4.22)$$

$$+ (C_R u_1^k, \phi_1)_{\Gamma_{1R}} + \frac{1}{\triangle t}(u_2^k - u_2^{k-1}, \phi_2)_{\Omega_2} + (\nabla u_2^k, \nabla \phi_2)_{\Omega_2} - (\mathbf{q} \nabla u_2^{k-1}, \phi_2)_{\Omega_2}$$

$$+ (C_R u_2^k, \phi_2)_{\Gamma_{2R}} + \frac{1}{\triangle t}(u_3^k - u_3^{k-1}, \phi_3)_{\Omega_3} + (D_T \nabla u_3^k, \nabla \phi_3)_{\Omega_3} + (C_R u_3^k, \phi_3)_{\Gamma_{3R}} = 0$$

for all $\phi_i \in H^1(\Omega_i)$ such that $\phi_1 = \phi_2$ at Γ_1 and $\phi_2 = \phi_3$ at Γ_2. $\qquad \square$

Chapter 3

Rigorous upscaling of rough boundaries

We consider a reactive flow in a channel which has a periodically oscillating boundary with both period and amplitude ε. The ions are being transported by the convection and diffusion processes. These ions can react at the oscillating boundaries and get attached to form the crystal (precipitation) and become immobile. The reverse process of dissolution is also possible. The model involves non-linear and multi-valued rates. We provide a rigorous justification for the upscaling process in which we define an upscaled problem defined in a simpler domain with flat boundaries. To this aim, we use periodic unfolding techniques combined with translation estimates. Numerical experiments confirm the theoretical predictions and illustrate a practical application of this upscaling process.

3.1 Introduction

We consider the reactive flow through a channel having oscillating boundaries. The flow carries the ions/solutes which are transported through the channel by a combined process of diffusion and convection. The modeling of the process therefore consists of transport and flow problems. The ions in the bulk react at the oscillating surfaces and form crystals (hence become immobile). The opposite process of dissolution, the ions dissolving in the bulk phase is also possible. We assume that the thickness of the crystal deposited is small enough so that we ignore the change in the geometry that is due to

the chemistry.

As the original problem is defined in a domain with oscillating boundary, solving it numerically requires resolving these oscillations at sufficient resolution. This implies that the mesh size should be much smaller than the size of oscillations. This makes the problem computationally expensive. Alternatively, one can consider an upscaled model providing an approximation to the original model in a domain with flat boundaries. Of course, this requires taking into account some corrections due to this simplification, which are incorporated in modified boundary conditions. In particular, the flux at the oscillating boundaries needs to be corrected if we are to simplify the boundary to a flat one. Also, the upscaling process should contain some information from the original geometry. In this work, we justify this upscaling process in a rigorous manner.

We make a specific choice for the reaction rate in this work, describing the crystal precipitation and dissolution processes. The rate description is defined at the boundary and hence on a lower dimensional manifold. Moreover, this rate is the net result of two opposing processes: precipitation and dissolution. The precipitation term is described by a non-linear term while the dissolution term is described by the Heaviside graph resulting in a multi-valued character. These kind of models are well established in literature; for details we refer to [44, 45, 47, 104, 105]. This specific choice of the reaction rate poses mathematical difficulties and in particular the multi-valued nature of the dissolution term defined at the boundary limits the regularity of the solution.

Homogenization techniques are widely applied for reactive flows. Compactness and 2-scale convergence arguments are successfully employed for perforated domains like porous media, see [2, 60–62, 89, 101–103]. Upscaling of rough boundaries however require slightly different approaches and extensive work has been done in this respect. The elliptic equations defined in domains with rough boundaries have been treated in [3, 9–11, 29, 54, 100]. Also, we refer to [55] for upscaling when geometry changes are taken into account.

Our contributions in this respect are two-fold: first, we consider a model for reactions described by a non-linear, non-Lipschitz ODE at the oscillating boundary coupled with a parabolic PDE in domain; and secondly, we use periodic unfolding techniques for deriving effective boundary conditions. This technique has been systematically introduced by [35] (see also [24] for similar ideas) and has been applied for homogenization problems, in particular for periodic homogenization. A relevant reference to this work is [37] where homogeneous boundary conditions are treated for a related but different geometry. The use of periodic unfolding provides a natural framework to deal with upscaling problems by mapping the integrals from $\varepsilon-$dependent geometries to fixed geometries thereby making the use of compactness properties in a fairly evident manner. In this work, we use the periodic unfolding technique to obtain the upscaled problem for the oscillating boundary case. Specifically, we consider the boundary, oscillating with amplitude and period ε. We consider the limit of the problem as $\varepsilon \searrow 0$ and define

this limit to be the upscaled problem. As a technical note, the idea is as follows: the system of equations provides a priori estimates in the original domain and at the oscillating boundary. The latter estimates are used to obtain those for the unfolded sequences of the traces. In addition to this, the non-linearities in the reaction rate requires stronger compactness which is achieved by considering translation estimates.

This chapter is structured as follows. We present a brief introduction of the model in Section 3.2 followed by the definition of upscaled problem in Section 3.3. The a priori estimates are stated in Section 3.4 and the derivation of the upscaled equations is completed in Section 3.5. Note that even though the details of the proof are presented for a particular rate, the techniques presented in this work can be used to treat other cases. We comment on this in Section 3.6. The numerical computations are discussed in Section 3.7.

3.2 Geometry and modeling

First we describe the setting of the geometry in which the physical processes are observed. This will be followed by a brief recall of the model describing the convective and diffusive transport of solutes in the fluid. The present context falls into the general framework of reactive flows in porous media. For the particular description of dissolution and precipitation, we refer to [43–45] for an upscaled (core scale) model. Here we adopt the pore scale counterpart discussed in [47]. The rigorous homogenization procedure from the pore scale model to the core scale model one is proved in [74] (see Chapter 6).

3.2.1 Basic geometry

Let $\Omega := (0, 1) \times (0, 1)$ be the homogenized domain with flat boundaries. The domain with $\varepsilon-$dependent oscillating boundary is defined as follows. Let $h : \mathbb{R} \mapsto [-1, 0]$ be a given smooth $1-$ periodic function and define

$$h^\varepsilon(x) = \varepsilon h \left(\frac{x}{\varepsilon} \right).$$

Then $\Omega^\varepsilon \subset \mathbb{R}^2$ with Ω^ε is the open, bounded set

$$\Omega^\varepsilon := \left\{ (x, y) \in \mathbb{R}^2 : x \in (0, 1) \quad y \in (h^\varepsilon(x), 1) \right\}.$$
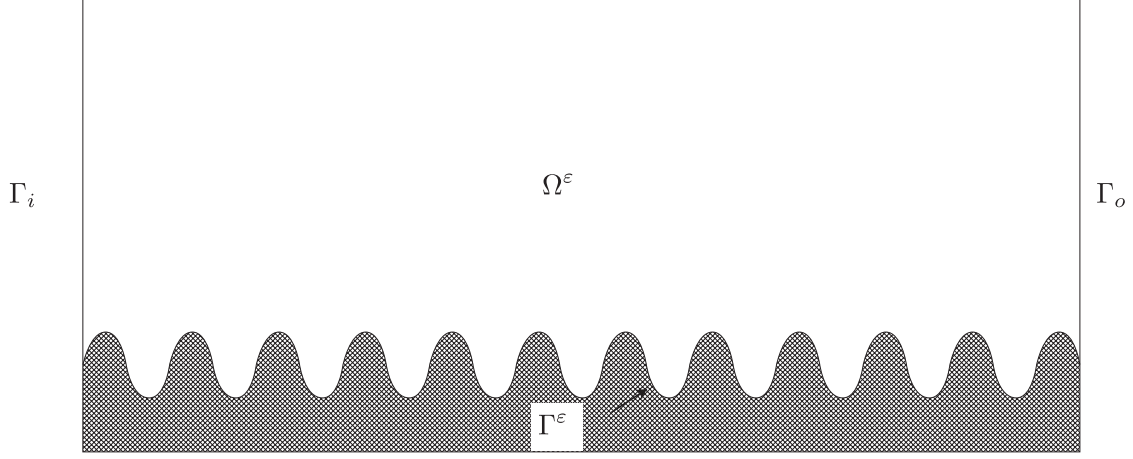
Figure 3.1: Ω^ε *is the domain considered here. The boundary Γ^ε consists of a periodic function. Note that the geometry remains fixed in time for a given ε. Schematic for the geometry for the homogenization of crystal precipitation-dissolution model in a channel with rough boundary.*

With $\partial\Omega^\varepsilon$ being the boundary of Ω^ε, the oscillating boundary $\Gamma^\varepsilon (\subset \partial\Omega^\varepsilon)$ is defined as:

$$\Gamma^\varepsilon := \left\{ (x,y) : x \in (0,1), \quad y = \varepsilon h \left(\frac{x}{\varepsilon} \right) \right\}.$$

Since Γ^ε is periodic, we scale one period and define Γ

$$\Gamma := \left\{ (z,y) : z \in (0,1), \quad y = h(z) \right\}.$$

The inlet and outlet boundaries of Ω^ε are defined as

$$\Gamma_i := \{ (x,y) : x = 0, \ h^\varepsilon(0) \leq y \leq 1 \}$$
$$\Gamma_o := \{ (x,y) : x = 1, \ h^\varepsilon(0) \leq y \leq 1 \}.$$

This particular scaling for Γ^ε ensures that its $\mathcal{H}^1$ Lebesgue measure remains bounded and is of order $O(1)$. Note that, by construction, we have $\Omega \subset \Omega^\varepsilon$ since $h^\varepsilon \leq 0$. We take $\Omega \subset \Omega^\varepsilon$ to avoid extension arguments. See Figure 3.1 for a sketch of the geometry.

Let T be a given time; we define

$$\Omega^T := \Omega \times (0,T), \quad \Omega^{\varepsilon T} := \Omega^\varepsilon \times (0,T), \quad \Gamma^{\varepsilon T} := \Gamma^\varepsilon \times (0,T).$$

 As announced before, the solutes in the channel diffuse, are transported by the flow, and react at the oscillating boundary. To fix the ideas, we assume that the flow is mod-

eled by the Stokes system, where $\mathbf{q}^\varepsilon$ denotes the flow velocity and P^ε its pressure,

$$\begin{cases} \Delta \mathbf{q}^\varepsilon = \nabla P^\varepsilon & \text{in} \quad \Omega^{\varepsilon T}, \\ \nabla \cdot \mathbf{q}^\varepsilon = 0 & \text{in} \quad \Omega^{\varepsilon T}. \end{cases} \tag{3.2.1}$$

Without loss of generality, we have normalized the dynamic viscosity to be 1. For the boundary conditions, we pose a parabolic profile at the inlet,

$$\mathbf{q}^\varepsilon(y) = Q(y - h^\varepsilon(0))(1 - y)\mathbf{e}_1 \quad \text{at} \quad \Gamma_i,$$

where $Q > 0$ is a positive constant and $\mathbf{e}_1$ is the unit vector in $x-$direction. For the outlet, we prescribe the pressure. For the other boundaries, including Γ^ε, we impose no-slip boundary conditions. The specific model for $\mathbf{q}^\varepsilon$ considered here is not essential and the results remain valid for other situations.

Next, we consider the model for the transport of solutes which is described by the linear convection-diffusion equation. Under assumed compatibility conditions [44,45,73] (e.g. electrical neutrality) it is sufficient to consider only one type of ions. Let u^ε denote the concentration of the ions and v^ε the crystal concentration, the transport equation reads

$$\partial_t u^\varepsilon + \nabla \cdot (\mathbf{q}^\varepsilon u^\varepsilon - \nabla u^\varepsilon) = 0, \quad \text{in} \quad \Omega^{\varepsilon T}, \tag{3.2.2}$$

and for the reactive boundary condition, we have by the conservation of mass,

$$-\boldsymbol{\nu} \cdot \nabla u^\varepsilon = \partial_t v^\varepsilon \quad \text{on} \quad \Gamma^{\varepsilon T}. \tag{3.2.3}$$

For the crystal concentration, the rate of change is the net result of two opposing processes, precipitation and dissolution. This is given by

$$\partial_t v^\varepsilon = (r(u^\varepsilon) - w^\varepsilon) \quad \text{on} \quad \Gamma^{\varepsilon T}, \tag{3.2.4}$$

where $r(\cdot)$ is the precipitation rate while w denotes the rate of dissolution. We assume the following structure for the precipitation rate $r(u^\varepsilon)$

A1. $r : \mathbb{R} \to [0, \infty)$ is locally Lipschitz .

A2. There exists a unique $u_* \geq 0$, such that
$$r(u^\varepsilon) = \begin{cases} 0 & \text{for} \quad u^\varepsilon \leq u_*, \\ \text{strictly increasing for} & u^\varepsilon \geq u_* \quad \text{with} \quad r(\infty) = \infty. \end{cases}$$

All the equations are considered in dimensionless form. The diffusion constant has been scaled to 1, with the extension to positive definite tensor being straightforward. The dissolution process takes place only when the crystal precipitate is present (i.e. if $v(t, x) > 0$) and it is a surface process hence proceeds with a constant rate. We normalize

this rate to 1. In the absence of precipitate, the overall rate (precipitation minus dissolution) is either zero or positive depending upon the amount of solute present. Further, the absence of net gain in the crystal concentration under insufficient amount of solutes is related to the time-scale of observation. The derivation of the precipitation-dissolution is based on chemical kinetics and the ideas of solubility product for the crystals. For further discussions and derivation of this model, we refer to [45, 73]. A similar model leading to the dissolution fronts is given in [23].

To summarize the discussion above, the dissolution rate is

$$w \in H(v), \quad \text{where} \quad H(v) = \begin{cases} 0, & \text{if} \quad v < 0, \\ [0,1] & \text{if} \quad v = 0, \\ 1 & \text{if} \quad v > 0. \end{cases} \tag{3.2.5}$$

Remark 3.1 Since the precipitation rate r is monotonically increasing, under the setting above, a unique u^* exists for which $r(u^*) = 1$. If $u = u^*$ for all t and x, then the system is in equilibrium: no precipitation or dissolution occurs, since the precipitation rate is balanced by the dissolution rate regardless of the presence of absence of crystals. $\qquad\square$

The system (3.2.2) is complemented by the following initial and boundary conditions,

$$\begin{cases} u^\varepsilon(0,\cdot) &= u_I, \quad \text{in} \quad \Omega^\varepsilon, \\ v^\varepsilon(0,\cdot) &= v_I, \quad \text{on} \quad \Gamma^\varepsilon, \\ u^\varepsilon &= 0 \quad \text{on} \quad \Gamma_D^T. \end{cases} \tag{3.2.6}$$

Note that (3.2.4) describes reaction of ions under both equilibrium and non-equilibrium conditions. The model (3.2.2) is a simplified setting for the model considered in [41, 44, 45, 47] and we refer to the cited literatures for more details.

We emphasize here the fact that no changes in the Ω^ε are encountered due to the dissolution or precipitation. In other words, the precipitate layer is very thin, so it does not change the boundary Γ^ε. Alternatively, where such changes are taken into account are discussed in [104] (see also [75]).

3.2.2   Weak formulation

Since the reaction term has a multi-valued description, we do not expect sufficient regularity for the existence of strong solutions except for in particular instances. To rectify this, we define appropriate weak solutions for the system of equations considered here.

Let $(\cdot, \cdot)$ denote the L^2 inner product or duality pairing of H^1, H^{-1}. Also, we define $H_0^1(\Omega^\varepsilon)$ the space with $w \in H^1$ with homogeneous Dirichlet boundary condition on $\partial \Omega^\varepsilon \setminus \Gamma^\varepsilon$. The dual of $H_0^1(\Omega^\varepsilon)$ is the function space $H^{-1}(\Omega^\varepsilon)$.

We consider the following function spaces, where we follow the usual notations from functional analysis.

$$\mathcal{U}^\varepsilon := \{ u \in L^2(0, T; H_0^1(\Omega^\varepsilon)) : \partial_t u \in L^2(0, T; H^{-1}(\Omega^\varepsilon)) \},$$
$$\mathcal{V}^\varepsilon := H^1(0, T; L^2(\Gamma_G^\varepsilon)),$$
$$\mathcal{W}^\varepsilon := \{ w \in L^\infty(\Gamma^{\varepsilon T}) : 0 \le w \le 1 \}.$$

We assume that the initial conditions $(u_I, v_I) \in (H_0^1(\Omega^\varepsilon), H^1(\Gamma^\varepsilon))$. The definition of a weak solution is given as follows.

Definition 3.2.1 *A triple $(u^\varepsilon, v^\varepsilon, w^\varepsilon) \in \mathcal{U}^\varepsilon \times \mathcal{V}^\varepsilon \times \mathcal{W}^\varepsilon$ is called a weak solution of (3.2.2)-(3.2.6) if $u^\varepsilon(0, \cdot) = u_I, v^\varepsilon(0, \cdot) = v_I$ and*

$$(\partial_t u^\varepsilon, \phi)_{\Omega^{\varepsilon T}} + (\nabla u^\varepsilon, \nabla \phi)_{\Omega^{\varepsilon T}} - (q^\varepsilon u^\varepsilon, \nabla \phi)_{\Omega^{\varepsilon T}} = -(\partial_t v^\varepsilon, \phi)_{\Gamma^{\varepsilon T}},$$
$$(\partial_t v^\varepsilon, \theta)_{\Gamma^{\varepsilon T}} = (r(u^\varepsilon) - w^\varepsilon, \theta)_{\Gamma^{\varepsilon T}}, \qquad (3.2.7)$$
$$w^\varepsilon \in H(v^\varepsilon) \quad a.e. \ in \quad \Gamma^{\varepsilon T},$$

for all $(\phi, \theta) \in L^2(0, T; H_0^1(\Omega^\varepsilon)) \times L^2(\Gamma^{\varepsilon T})$.

Remark 3.2 The existence of weak solutions of (3.2.2)-(3.2.6) has been proved in [47] by approximation arguments. The approximating solutions were constructed by regularizing the Heaviside function which models the dissolution process. For solutions $(u^\varepsilon, v^\varepsilon, w^\varepsilon)$ constructed in this way, the dissolution rate w^ε satisfies

$$w^\varepsilon = \begin{cases} 1 & \text{if} \quad v^\varepsilon > 0, \\ \min(r(u^\varepsilon), 1) & \text{if} \quad v^\varepsilon = 0, \\ 0 & \text{if} \quad v^\varepsilon < 0. \end{cases} \qquad (3.2.8)$$

$\square$

3.2.3   Known results

The results derived for the pore scale model in [41, 47] remain valid in the present context. Below we cite some of the results that will be used later.

Theorem 3.2.1 *Under assumptions (A.1) and (A.2) on the reaction rates $r(u^\varepsilon)$, there exists a*

weak solution in the sense of Definition 3.2.1. In addition, the solution satisfies

$$0 \leq u^\varepsilon, v^\varepsilon \leq M, \tag{3.2.9}$$

$$\|u^\varepsilon\|^2_{L^\infty(0,T;L^2(\Omega^\varepsilon))} + \|\nabla u^\varepsilon\|^2_{L^2(\Omega^{\varepsilon T})} + \|\partial_t u^\varepsilon\|^2_{L^2(0,T;H^{-1}(\Omega^\varepsilon))}$$
$$+ \|v^\varepsilon\|^2_{L^\infty(0,T;L^2(\Gamma^\varepsilon))} + \|\partial_t v^\varepsilon\|^2_{L^2(\Gamma^{\varepsilon T})} \leq C, \tag{3.2.10}$$

where M is a given constant depending on the initial conditions and the constant $C > 0$ is independent of $u^\varepsilon, v^\varepsilon, w^\varepsilon$ and ε.

To continue with the analysis, the above estimates are not enough to guarantee uniqueness. In the wake of nonlinearities and discontinuities present in the reaction rate defined on a lower dimensional manifold, the L^2 stability with respect to initial data is out of reach, however, a L^1 contraction is achieved. Indeed, in [108] the following contraction result with respect to the initial values has been proven.

Theorem 3.2.2 *Assume (A.1) and (A.2) and consider two weak solutions $(u^{(i)\varepsilon}, v^{(i)\varepsilon}, w^{(i)\varepsilon}) \in \mathcal{U}^\varepsilon, \mathcal{V}^\varepsilon, \mathcal{W}^\varepsilon, i = 1, 2$ of (3.2.7) with initial values $(u_I^{(i)}, v_I^{(i)}, i = 1, 2)$ respectively. Then for any $t \in (0, T]$ we have*

$$\int_{\Omega^\varepsilon} |u^{(1)\varepsilon}(t,x) - u^{(2)\varepsilon}(t,x)| dx + \int_{\Gamma^\varepsilon} |v^{(1)\varepsilon}(t,x) - v^{(2)\varepsilon}(t,x)| dx$$
$$\leq \int_{\Omega^\varepsilon} |u_I^{(1)}(x) - u_I^{(2)}(x)| dx + \int_{\Gamma^\varepsilon} |v_I^{(1)}(x) - v_I^{(2)}(x)| dx.$$

Note that Theorem 6.3.1 provides, in particular, the uniqueness of the solution.

In addition to the analysis of the model presented above, numerical treatment of this model has also been carried out. For example, in [41], a semi-discrete numerical scheme is presented for the pore scale model and the convergence is proved. For the core scale model, both the semi-discrete and fully discrete numerical schemes have been analyzed [80].

The rigorous derivation of the macro scale model from the pore scale model in the classical homogenization context is carried out in [74]. There the domain is considered to be covered by a translation of a scaled unit cell (with scaling parameter ε, see [2,60–62,101]) and homogenization techniques are employed to derive upscaled equations as the limit of $\varepsilon \searrow 0$. For the simpler geometry of a thin strip, the 1D upscaled model is rigorously justified in [47]. The present context is different as the only oscillating part is the boundary of domain Ω^ε.

3.3 Upscaled equations

The flow equations are decoupled from the transport equation for ions. Hence, we can homogenize the velocity field separately. Here we assume that the velocity field $\mathbf{q}^\varepsilon$ is given, satisfies L^∞ bounds and

$$\|\mathbf{q}^\varepsilon - \mathbf{q}\|_{L^2(\Omega)} \searrow 0 \text{ as } \varepsilon \searrow 0. \tag{3.3.1}$$

For the specific case of Stokes equation, in [66–68] it is proved that the homogenized equation is the Stokes equation with Dirichlet boundary condition for the leading order term.

$$\nabla \cdot \mathbf{q} = 0, \quad \text{in } \Omega \times (0, T), \tag{3.3.2}$$
$$\Delta \mathbf{q} = \nabla P \quad \text{in } \Omega \times (0, T),$$
$$\mathbf{q} = 0 \quad \text{on } \{y = 0\} \cup \{y = 1\},$$
$$\mathbf{q} = Qy(1 - y)\mathbf{e}_1 \quad \text{on } \{x = 0\}.$$

In fact, the cited references go beyond leading order terms. For the first order term, slip boundary conditions are derived. However, for our present purposes, the Dirichlet boundary condition suffices since for the concentration term we restrict only to the leading order approximation. With the simple geometry Ω considered here, and under the parabolic inlet boundary conditions, we can solve the above equations exactly. It is straightforward to check that the unique solution of the above equations is

$$\mathbf{q} = Qy(1 - y)\mathbf{e}_1.$$

The interesting aspect here is the derivation of the upscaled equation for the reaction terms. Indeed, the main result of this chapter is the derivation of the following result. The homogenized variables u, v, w satisfy the following system of equations.

$$\partial_t u - \Delta u + \mathbf{q}\nabla u = 0 \qquad \qquad \text{in} \quad \Omega \times (0, T) \tag{3.3.3}$$

$$-\boldsymbol{\nu} \cdot \nabla u = \int_\Gamma \partial_t v ds \qquad \qquad \text{on} \quad (0, 1) \times (0, T) \tag{3.3.4}$$

$$\partial_t v = r(u) - w \qquad \qquad \text{on} \quad (0, 1) \times \Gamma \times (0, T) \tag{3.3.5}$$

$$w \in H(v). \tag{3.3.6}$$

Note that the above equations are defined in domains where the boundaries are flat. Further, the information about the geometry of the oscillating boundary Γ^ε in the original domain is incorporated through terms defined on Γ— which is scaled from a unit period of Γ^ε. Performing computations on domains with flat boundaries is much cheaper compared to smaller mesh sizes required for resolving the oscillations at Γ^ε. This is the essential advantage of this upscaling. The results are also consistent with intuitive ar-

guments. For the rough boundary to be replaced by the flat one, we need to correct for the flux. The above upscaling results show that this flux correction, in the leading order, is obtained by simply accounting for the entire length of the rough boundary.

Our aim is proving the convergence of the upscaling procedure. We start by defining the concept for solution for (3.3.3)-(3.3.6).

Definition 3.3.1 *A triple* $(u, v, w) \in L^2(0, T; L^2(\Omega)) \times L^2(0, T; L^2((0, 1) \times \Gamma)) \times L^\infty((0, T) \times (0, 1) \times \Gamma)$ *is called a weak solution of* (3.3.3)-(3.3.6) *if* $u(0, \cdot) = u_I, v(0, \cdot) = v_I$ *and*

$$-(u, \partial_t \phi)_{\Omega^T} + (\nabla u, \nabla \phi)_{\Omega^T} - (qu, \nabla \phi)_{\Omega^T} + (\partial_t v, \phi)_{(0,1) \times \Gamma \times (0,T)} = (u_I, \phi(0, x))_\Omega,$$

$$(\partial_t v, \theta)_{(0,1) \times \Gamma} - (r(u) - w, \theta)_{(0,1) \times \Gamma \times (0,T)} = 0, \qquad (3.3.7)$$

$$w \in H(v) \quad a.e.,$$

for all $\phi \in H^1((0, T) \times \Omega), \phi(T, x) = 0; \phi = 0$ *on* Γ_D *and* $\theta \in L^2(0, T; L^2((0, 1) \times \Gamma))$.

The main result of this paper is:

Theorem 3.3.1 *Along any sequence* $\varepsilon \searrow 0$, *the solution triple* $(u^\varepsilon, v^\varepsilon, w^\varepsilon)$ *in the sense of Definition 3.2.1 converges to* (u, v, w), *the solution introduced in Definition 3.3.1.*

In what follows, we prove the above Theorem 3.3.1. We have taken a restricted class of test function for ϕ (compare this with ϕ in Definition 3.2.1) which helps in dealing with the low regularity of $\partial_t u^\varepsilon$. The estimates for Ω^ε are easily carried over to the estimates for Ω and the trace theorem also provides a compactness for the traces defined at the boundary Γ^ε. However, Γ^ε depends on ε and therefore the estimates are defined in a $\varepsilon-$dependent domain. We use the unfolding operator to map the estimates and integrals from $\varepsilon-$dependent domains to a fixed domain. Also, the non-linearities need strong convergence for which we use translation estimates. Further, we connect the limits from the unfolded sequence defined at the boundary to the limits obtained from the estimates in Ω.

3.4 A priori estimates

In this section, we begin with estimate dealing with translation in time. Next, we deal with the periodic unfolding operator defined for the boundaries. This is followed by the a priori estimates both for the domain and the boundary. Let us begin with the following lemma.

Lemma 3.3 *Let $t \in [0, T]$, $\eta > 0$, and $(u^\varepsilon, v^\varepsilon, w^\varepsilon)$ be a weak solution of (3.2.7) in the sense of Definition 3.2.1. Then the following estimate is uniform in η,*

$$\int_0^{T-\eta} \int_{\Omega^\varepsilon} |u^\varepsilon(t+\eta, x) - u^\varepsilon(t, x)|^2 dx dt \leq C\eta^{\frac{1}{2}}. \tag{3.4.1}$$

Proof. Consider $(3.2.7)_1$ and by a shift in time co-ordinate we obtain

$$\int_0^{T-\eta} \left(\partial_t(u^\varepsilon(t+\eta, x) - u^\varepsilon(t, x)), \phi\right) dt + \int_0^{T-\eta} \int_{\Omega^\varepsilon} (\nabla u^\varepsilon(t+\eta, x) - \nabla u^\varepsilon(t, x))\nabla\phi \, dx dt$$

$$-\int_0^{T-\eta} \int_{\Omega^\varepsilon} \mathbf{q}^\varepsilon(u^\varepsilon(t+\eta, x) - u^\varepsilon(t, x))\nabla\phi \, dx dt = -\int_0^{T-\eta} \int_{\Gamma^\varepsilon} \partial_t(v^\varepsilon(t+\eta, x) - v^\varepsilon(t, x))\phi \, dx dt$$

and choose for $\phi = \int_t^{t+\eta} u^\varepsilon(s, x) ds \in H^1(0, T; H_0^1(\Omega^\varepsilon))$ to obtain

$$\int_0^{T-\eta} \int_{\Omega^\varepsilon} |u^\varepsilon(t+\eta, x) - u^\varepsilon(t, x)|^2 dx dt = -\int_{\Omega^\varepsilon} (u^\varepsilon(\eta, x) - u^\varepsilon(0, x)) \left(\int_0^\eta u^\varepsilon(s, x) ds\right) dx$$

$$+ \int_{\Omega^\varepsilon} (u^\varepsilon(T, x) - u^\varepsilon(T-\eta, x)) \left(\int_{T-\eta}^T u^\varepsilon(s, x) ds\right) dx$$

$$+ \int_{\Omega^\varepsilon} \left|\int_{T-\eta}^T \nabla u^\varepsilon(s, x) ds\right|^2 dx dt - \int_{\Omega^\varepsilon} \left|\int_0^\eta \nabla u^\varepsilon(s, x) ds\right|^2 dx dt$$

$$- \int_0^{T-\eta} \int_{\Omega^\varepsilon} \mathbf{q}^\varepsilon(u^\varepsilon(t+\eta, x) - u^\varepsilon(t, x)) \left(\nabla \int_t^{t+\eta} u^\varepsilon(s, x) ds\right) dx dt$$

$$+ \int_0^{T-\eta} \int_{\Gamma^\varepsilon} \partial_t(v^\varepsilon(t+\eta, x) - v^\varepsilon(t, x)) \left(\int_t^{t+\eta} u^\varepsilon(s, x) ds\right) dx dt.$$

We treat each term on the right separately. Let us denote the successive terms by $\mathcal{I}_i, i = 1, \ldots, 6$. Using L^∞ estimate for u^ε we have for both $\mathcal{I}_1$ and $\mathcal{I}_2$

$$|\mathcal{I}_1| \leq C\eta, \qquad |\mathcal{I}_2| \leq C\eta.$$

For $\mathcal{I}_3$, we use Cauchy Schwarz and the estimates on the gradient in Theorem 3.2.1 to obtain

$$|\mathcal{I}_3| \leq C\eta.$$

Because of its sign, $\mathcal{I}_4$ need not be treated. Next, for $\mathcal{I}_5$ we have using L^∞ estimates for $u^\varepsilon, \mathbf{q}^\varepsilon$ and Cauchy Schwarz for the gradient term,

$$|\mathcal{I}_5| \leq C\eta^{\frac{1}{2}}.$$

Furthermore, by triangle inequality and the $L^2(0, T; L^2(\Gamma^\varepsilon))$ estimates of $\partial_t v^\varepsilon$, we have

$$|\mathcal{I}_6| \leq C\|\partial_t v^\varepsilon\|_{L^2(\Gamma^{\varepsilon T})}\eta \leq C\eta$$

where we have again used the L^∞ estimate for u^ε. Collecting the above computations leads to the assertion. $\qquad\square$

3.4.1 The boundary unfolding operator

We start with introducing the unfolding operator and describe some of its properties. For more details for the properties and the proofs, we refer to [35] for unfolding operators in general, and to [37] for the boundary unfolding operator.

Following [37], we define the boundary unfolding operator as:

Definition 3.4.1 *Let $\phi^\varepsilon : (0, 1) \times \Gamma \mapsto \Gamma^\varepsilon$ be defined as $(x, (z, h(z))) \mapsto \left(\varepsilon \left\lfloor \frac{x}{\varepsilon} \right\rfloor + \varepsilon z, \varepsilon h(z)\right)$. The unfolding operator T^ε maps a function $u : \Gamma^\varepsilon \to \mathbb{R}$ to the function $u \circ \phi^\varepsilon : (0, 1) \times \Gamma \to \mathbb{R}$.*

Note that the unfolding operator is defined here only for the boundary and not for the whole domain. For the unfolding operator defined in the fully periodic context (classical homogenization), we refer to [24, 35] and to [89] for an application of this technique relevant to the present context . Below, we list some simple but useful propositions.

Proposition 3.4.1 *T^ε is linear.*

Proposition 3.4.2 *Let u,v be functions $\Gamma^\varepsilon \to \mathbb{R}$. Then $T^\varepsilon(uv) = T^\varepsilon u T^\varepsilon v$.*

The proofs for Proposition 3.4.1 and Proposition 3.4.2 are straightforward and therefore omitted.

Proposition 3.4.3 *For $u \in L^1(\Gamma^\varepsilon)$, it holds that*

$$\int\limits_{(0,1)\times\Gamma} T^\varepsilon u(x, (z, h(z)))dxds = \int\limits_{\Gamma^\varepsilon} u(x)\, dx.$$

Proof. A straightforward computation, which is similar in ideas for both fully periodic and the boundary periodic contexts, provides the result:

$$
\int\limits_{(0,1)\times\Gamma} T^\varepsilon u(x,z,h(z))dxds = \int\limits_{(0,1)\times\Gamma} u\left(\varepsilon\left(\left\lfloor\frac{x}{\varepsilon}\right\rfloor+z\right),\varepsilon h(z)\right)dxds
$$

$$
=\varepsilon\sum_{k=0}^{\frac{1}{\varepsilon}-1}\int\limits_\Gamma u\left(\varepsilon k+\varepsilon z,\varepsilon h(z)\right)ds
$$

$$
=\sum_{k=0}^{\frac{1}{\varepsilon}-1}\int\limits_{k\varepsilon}^{(k+1)\varepsilon} u\left(x,\varepsilon h\left(\frac{x}{\varepsilon}\right)\right)ds \quad \text{(by periodicity of } h\text{)}
$$

$$
=\int\limits_{\Gamma^\varepsilon} u\,ds^\varepsilon,
$$

where ds is the differential along the curve Γ and ds^ε the differential along Γ^ε. $\qquad\square$
Based on the above result, we obtain the following:

Proposition 3.4.4 *Let* $u\in L^2\left(\Gamma^\varepsilon\right)$. *Then* $T^\varepsilon u\in L^2\left((0,1)\times\Gamma\right)$ *and* T^ε *is a linear isometry between* $L^2\left(\Gamma^\varepsilon\right)$ *and* $L^2\left((0,1)\times\Gamma\right)$.

Proof. Suppose that $u\in L^2\left(\Gamma^\varepsilon\right)$. Then $|u|^2\in L^1\left(\Gamma^\varepsilon\right)$. Using propositions 3.4.2 and 3.4.3 we find

$$
\int\limits_{(0,1)\times\Gamma}|T^\varepsilon u|^2\,dx = \int\limits_{(0,1)\times\Gamma} T^\varepsilon\,|u|^2\,dx = \int\limits_{\Gamma^\varepsilon}|u|^2dx < \infty.
$$

Also $\|T^\varepsilon u\|_{L^2((0,1)\times\Gamma)} = \|u\|_{L^2(\Gamma^\varepsilon)}$ and together with Proposition 3.4.1, this implies that T^ε is a linear isometry between $L^2\left(\Gamma^\varepsilon\right)$ and $L^2\left((0,1)\times\Gamma\right)$. $\qquad\square$

The above linear isometry is an important result as it provides a way to connect the unfolded sequence defined on a fixed domain with the original variables defined on an $\varepsilon-$dependent domain. This makes it possible to use the estimates obtained for Γ^ε for the unfolded sequence directly.

3.4.2 Estimates in the domain

We proceed with the a priori estimates both for Ω and Γ^ε. Since we have taken $\Omega\subset\Omega^\varepsilon$, the estimate gets carried over and we obtain the following estimate from Theorem 3.2.1:

$$
\|\nabla u^\varepsilon\|^2_{L^2\left(0,T;L^2(\Omega)\right)} + \|\partial_t v^\varepsilon\|^2_{L^2\left(0,T;L^2(\Gamma^\varepsilon)\right)} + \|v^\varepsilon\|^2_{L^2\left(0,T;L^2(\Gamma^\varepsilon)\right)} \leq C. \tag{3.4.2}
$$

The above estimate is valid in fact for the restriction of u^ε to Ω, which is also further denoted by u^ε to simplify the writing. We have:

Lemma 3.4 *As $\varepsilon \searrow 0$,*

$$\nabla u^\varepsilon \rightharpoonup \nabla u_0 \text{ weakly in } L^2(0, T; \Omega). \tag{3.4.3}$$

$$u^\varepsilon \to u_0 \text{ strongly in } L^2(0, T; \partial\Omega). \tag{3.4.4}$$

Proof.   The first part of the lemma follows from the uniform bounds of ∇u^ε as in (3.4.2). To prove (3.4.4), we note that $\partial_t u^\varepsilon \in L^2(0, T; H^*(\Omega))$ where H^* is the dual of $H^1_{0,\partial\Omega}(\Omega)$ with $H^1_{0,\partial\Omega}(\Omega)$ referring to the space of H^1 functions with homogeneous Dirichlet boundary conditions on $\partial\Omega$. Note the difference with previously introduced $H^1_0(\Omega^\varepsilon)$ or $H^1_0(\Omega)$ where homogeneous Dirichlet boundary conditions are taken only on $\partial\Omega^\varepsilon \setminus \Gamma^\varepsilon$ respectively $\partial\Omega \setminus \Gamma$. With $u^\varepsilon \in L^2(0, T; H^1_0(\Omega))$ and $\partial_t u^\varepsilon \in L^2(0, T; H^*(\Omega))$, we conclude that u^ε converges strongly in $L^2(0, T; L^2(\Omega))$.

Now consider the integral $\mathcal{I}^\varepsilon$

$$\mathcal{I}^\varepsilon := \int_0^T \|u^\varepsilon(t) - u_0(t)\|^2_{L^2(\partial\Omega)} dt. \tag{3.4.5}$$

Following the proof of the trace theorem (see [50], chapter 5.5), we have

$$\mathcal{I}^\varepsilon \leq \int_0^T C\|u^\varepsilon - u_0\|_{L^2(\Omega)} \left(\|u^\varepsilon - u_0\|_{L^2(\Omega)} + \|\nabla(u^\varepsilon - u_0)\|_{L^2(\Omega)} \right) dt.$$

Using Cauchy Schwarz, the bounds on the gradients, and the semi-continuity of the norms, we obtain

$$\mathcal{I}^\varepsilon \leq C\|u^\varepsilon - u_0\|_{L^2(\Omega^T)}$$

from which the assertion follows.   □

The original equations are defined in Ω^ε and by construction also in Ω as $\Omega \subset \Omega^\varepsilon$. We now prove that the contributions for the integrals in $\Omega^\varepsilon \setminus \Omega$ are negligible as $\varepsilon \searrow 0$. We achieve this by decomposing the integrals defined on Ω^ε. Note that by decomposing the integrals in domains Ω and $\Omega^\varepsilon \setminus \Omega$ we have the property that the measure of $\Omega^\varepsilon \setminus \Omega$ becomes negligible as $\varepsilon \to 0$. Also, the test functions are defined independent of ε, which we will use here. We start with the following direct consequence of the dominated convergence theorem.

Proposition 3.4.5 *For any function $f \in L^1(\Omega)$, with $E \subset \Omega$, it holds that $\displaystyle\int_E |f| \searrow 0$ as*

$meas(E) \searrow 0$.

The following lemma shows that the contributions of the integrals in the set $\Omega^\varepsilon \setminus \Omega$ are negligible.

Lemma 3.5 *For $\phi \in H^1((0,T) \times \Omega)$, the following result holds*

$$
\lim_{\varepsilon \searrow 0} \left\{ \int_0^T \int_{\Omega^\varepsilon \setminus \Omega} (-u^\varepsilon \partial_t \phi + \nabla u^\varepsilon \nabla \phi + q^\varepsilon u^\varepsilon \nabla \phi) \, dx dt \right\} = 0
$$

Proof. Let us denote the integrals by $\mathcal{I}_i$, $i = 1,2,3$ respectively and we proceed by estimating them separately:

$$
\begin{aligned}
|\mathcal{I}_1| &\leq \|u^\varepsilon\|_{L^2(0,T;L^2(\Omega^\varepsilon \setminus \Omega))} \|\partial_t \phi\|_{L^2(0,T;L^2(\Omega^\varepsilon \setminus \Omega))} \\
&\leq \|u^\varepsilon\|_{L^2(0,T;L^2(\Omega^\varepsilon))} \|\partial_t \phi\|_{L^2(0,T;L^2(\Omega^\varepsilon \setminus \Omega))} \leq C \|\partial_t \phi\|_{L^2(0,T;L^2(\Omega^\varepsilon \setminus \Omega))}
\end{aligned}
$$

and with $\partial_t \phi \in L^2(0,T;L^2(\Omega^\varepsilon))$ we have $|\partial_t \phi|^2 \in L^2(0,T;L^1(\Omega^\varepsilon))$ and thus, by above Proposition 3.4.5 we conclude $\mathcal{I}_1 \searrow 0$ as $\varepsilon \searrow 0$. Similarly,

$$
\begin{aligned}
|\mathcal{I}_2| &\leq \|\nabla u^\varepsilon\|_{L^2(0,T;L^2(\Omega^\varepsilon \setminus \Omega))} \|\nabla \phi\|_{L^2(0,T;L^2(\Omega^\varepsilon \setminus \Omega))} \\
&\leq \|\nabla u^\varepsilon\|_{L^2(0,T;L^2(\Omega^\varepsilon))} \|\phi\|_{L^2(0,T;L^2(\Omega^\varepsilon \setminus \Omega))} \leq C \|\phi\|_{L^2(0,T;L^2(\Omega^\varepsilon \setminus \Omega))}
\end{aligned}
$$

and again using above Proposition 3.4.5, we conclude $\mathcal{I}_2$ vanishes in the limit $\varepsilon \searrow 0$. The calculations for $\mathcal{I}_3$ are completely similar. $\qquad \square$

3.4.3 The boundary estimates

The estimates in Theorem 3.2.1 provide estimates for $(u^\varepsilon, v^\varepsilon, w^\varepsilon)$ at Γ^ε:

$$
\|v^\varepsilon\|^2_{L^\infty(0,T;L^2(\Gamma^\varepsilon))} + \|\partial_t v^\varepsilon\|^2_{L^2(\Gamma^{\varepsilon T})} + \|w^\varepsilon\|^2_{L^2(\Gamma^{\varepsilon T})} \leq C.
$$

The unfolding operator defined at the boundary maps these estimates to a domain that does not depend on ε. In terms of the unfolded sequence and using the L^2 isometry, we rewrite the estimate above.

$$
\|T^\varepsilon v^\varepsilon\|^2_{L^\infty(0,T;L^2((0,1) \times \Gamma))} + \|\partial_t T^\varepsilon v^\varepsilon\|^2_{L^2((0,1) \times \Gamma \times (0,T))} + \|T^\varepsilon w^\varepsilon\|^2_{L^2((0,1) \times \Gamma \times (0,T))} \leq C. \quad (3.4.6)
$$

The bounds above immediately imply the following convergence result:

Lemma 3.6 *There exists $(u,v,w) \in L^2(0,T;L^2((0,1) \times \Gamma))$ such that*

$\partial_t v \in L^2(0, T; L^2((0,1) \times \Gamma))$ *and it holds*

$$T^\varepsilon v^\varepsilon \rightharpoonup v \text{ weakly in } L^2(0, T; L^2((0,1) \times \Gamma))$$
$$T^\varepsilon w^\varepsilon \rightharpoonup w \text{ weakly in } L^2(0, T; L^2((0,1) \times \Gamma))$$
$$T^\varepsilon u^\varepsilon \rightharpoonup u \text{ weakly in } L^2(0, T; L^2((0,1) \times \Gamma))$$
$$T^\varepsilon \partial_t v^\varepsilon \rightharpoonup \partial_t v \text{ weakly in } L^2(0, T; L^2((0,1) \times \Gamma)).$$

The domain of definition of limit objects is $(0,1) \times \Gamma$ in space. The unfolded sequences $T^\varepsilon u^\varepsilon$, $T^\varepsilon v^\varepsilon$, etc. are all defined on $(0,1) \times \Gamma$.

Note that we have only weak convergence for $T^\varepsilon v^\varepsilon$ and $T^\varepsilon u^\varepsilon$ and for passing to the limit in the non-linear terms, this is not sufficient. We therefore need to improve the convergence. We start with the following:

Proposition 3.4.6 *It holds that*

$$\|u^\varepsilon\|^2_{L^2(0,T;H^{\frac{1}{2}}(\Gamma^\varepsilon))} \leq C. \tag{3.4.7}$$

Proof. In view of (3.2.6)$_3$, the Poincaré inequality and the trace estimate give

$$\|u^\varepsilon\|^2_{L^2(0,T;H^{\frac{1}{2}}(\Gamma^\varepsilon))} \leq C\|\nabla u^\varepsilon\|^2_{L^2(0,T;L^2(\Omega^\varepsilon))}.$$

Also, it is to be noted that the boundary is uniformly Lipschitz continuous, as

$$|h^\varepsilon(x) - h^\varepsilon(y)| \leq \varepsilon|h(\frac{x}{\varepsilon}) - h(\frac{y}{\varepsilon})| \leq L_h|x - y|,$$

where L_h is the Lipschitz constant of h. Further, note that C is independent of ε (see [22] for a discussion on this issue and also [86] P.121). Combining this with the estimates in Theorem 3.2.1 gives the assertion. $\qquad\square$

We will use translation estimates to improve the convergence of $T^\varepsilon v^\varepsilon$ and $T^\varepsilon u^\varepsilon$ from weak to strong. Accordingly we make some preparations which will be used in the following.

Let I_C be a bounded interval in $\mathbb{R}$ and $h_C : I_C \mapsto \mathbb{R}$; h_C is a Lipschitz function. Consider $\widetilde{h}_C : \mathbb{R} \mapsto \mathbb{R}$ a smooth extension of h_C such that $\widetilde{h}_C$ has compact support. We define the corresponding curves Γ_C and $\widetilde{\Gamma}_C$

$$\Gamma_C := \{(z, h_C(z)) \mid z \in I_C\},$$
$$\widetilde{\Gamma}_C := \{(z, \widetilde{h}_C(z)) \mid z \in \mathbb{R}\}.$$

The above setting facilitates in defining the smooth extension $\widetilde{f} : \widetilde{\Gamma}_C \mapsto \mathbb{R}$ for any given function $f : \Gamma_C \mapsto \mathbb{R}$, $f \in H^{\frac{1}{2}}(\Gamma_C)$. Let us assume that the extension $\widetilde{f}$ has compact

support. Next, let $\bar{f} : \mathbb{R} \mapsto \mathbb{R}$ be defined as

$$\bar{f}(z) := \widetilde{f}(z, \widetilde{h}_C(z)).$$

Now for any given real number $\eta > 0$, we define the translation

$$\triangle_\eta \bar{f}(\cdot) := \bar{f}(\cdot + \eta) - \bar{f}(\cdot).$$

By an abuse of notation, we will often use $\triangle_\eta f$ in the above sense.
For a given function $f \in H^{\frac{1}{2}}(\Gamma_C)$, we have the following lemma.

Lemma 3.7 *Given $f \in H^{\frac{1}{2}}(\Gamma_C)$ the following translation estimate holds*

$$\|\triangle_\eta f\|_{L^2(\widetilde{\Gamma}_C)} \leq C|\eta|^{\frac{1}{2}}.$$

Proof. The proof is straightforward in the Fourier space. Let $\widetilde{f}$ be the extension of f as above with compact support. For any $f \in H^{\frac{1}{2}}(\Gamma_C)$ we have

$$\|f\|_{H^{\frac{1}{2}}(\widetilde{\Gamma}_C)} \leq C\|\widetilde{f}\|_{H^{\frac{1}{2}}(\mathbb{R})} \leq C.$$

Let $\hat{f}$ denote the Fourier transform of $\widetilde{f}$. For the $H^{\frac{1}{2}}(\mathbb{R})$ semi-norm, we have the following equivalent characterization in Fourier space

$$\|\widetilde{f}\|_{H^{\frac{1}{2}}(\mathbb{R})} = \int_{\mathbb{R}} |\omega||\hat{f}|^2 d\omega < C, \tag{3.4.8}$$

for any $\widetilde{f} \in H^{\frac{1}{2}}(\mathbb{R})$ with its $H^{\frac{1}{2}}$ norm uniformly bounded. Using the L^2 isometry of the Fourier transform

$$\int_{\widetilde{\Gamma}_C} |\triangle_\eta f|^2 ds \leq C \int_{\mathbb{R}} |\triangle_\eta \widetilde{f}|^2 dx = C \int_{\mathbb{R}} |(1 - e^{i\omega\eta})^2 \hat{f}(\omega)|^2 d\omega.$$

The right hand side can be re-written as

$$\int_{\mathbb{R}} (1 - e^{i\omega h})^2 |\hat{f}(\omega)|^2 d\omega = \int_{\mathbb{R}} \frac{(1 - e^{i\omega\eta})^2}{|\eta\omega|} |\eta\omega||\hat{f}(\omega)|^2 d\omega \leq C|\eta| \int_{\mathbb{R}} |\omega||\hat{f}(\omega)|^2 d\omega \tag{3.4.9}$$

and as noted above, the last term on the right hand side is bounded because $\widetilde{f} \in H^{\frac{1}{2}}(\mathbb{R})$. It is straightforward to check that

$$\frac{(1 - e^{i\omega\eta})^2}{|\omega\eta|} \leq C.$$

This leads to

$$\int_{\widetilde{\Gamma}_C} |\triangle_\eta f|^2 ds \le C|\eta| \tag{3.4.10}$$

where C depends on the $H^{\frac{1}{2}}$ norm.   □
Before using the translation estimate, we prove the following.

Proposition 3.4.7 *Given $u^\varepsilon : \Gamma^\varepsilon \mapsto \mathbb{R}$. The translation with respect to x commutes with the unfolding operator:*

$$\triangle_{\eta_x}(T^\varepsilon u^\varepsilon)(x, (z, h(z))) = T^\varepsilon(\triangle_{\eta_x} u^\varepsilon)(x, (z, h(z))). \tag{3.4.11}$$

Proof.   Note that,

$$\triangle_{\eta_x} T^\varepsilon u^\varepsilon := T^\varepsilon u^\varepsilon(x + \eta_x, (z, h(z))) - T^\varepsilon u^\varepsilon(x, (z, h(z))) \tag{3.4.12}$$

$$= u^\varepsilon\left(\varepsilon\left\lfloor\frac{x}{\varepsilon}\right\rfloor + k\varepsilon + \varepsilon z, \varepsilon h(z)\right) - u^\varepsilon\left(\varepsilon\left\lfloor\frac{x}{\varepsilon}\right\rfloor + \varepsilon z, \varepsilon h(z)\right) \quad \text{(by definition)} \tag{3.4.13}$$

where $k = \left\lfloor\frac{\eta_x + x}{\varepsilon}\right\rfloor - \left\lfloor\frac{\eta_x}{\varepsilon}\right\rfloor$. For the right hand side,

$$\begin{aligned}
T^\varepsilon \triangle_{\eta_x} u^\varepsilon &= T^\varepsilon\left(u^\varepsilon(x + \eta_x, h^\varepsilon(x + \eta_x)) - u^\varepsilon(x, h^\varepsilon(x))\right) \\
&= T^\varepsilon u^\varepsilon(x + \eta_x, h^\varepsilon(x + \eta_x)) - T^\varepsilon u^\varepsilon(x, h^\varepsilon(x)) \\
&= u^\varepsilon\left(\varepsilon\left\lfloor\frac{x + \eta_x}{\varepsilon}\right\rfloor + \varepsilon z, \varepsilon h(z)\right) - u^\varepsilon\left(\varepsilon\left\lfloor\frac{x}{\varepsilon}\right\rfloor + \varepsilon z, \varepsilon h(z)\right) \\
&= u^\varepsilon\left(\varepsilon\left\lfloor\frac{x}{\varepsilon}\right\rfloor + k\varepsilon + \varepsilon z, \varepsilon h(z)\right) - u^\varepsilon\left(\varepsilon\left\lfloor\frac{x}{\varepsilon}\right\rfloor + \varepsilon z, \varepsilon h(z)\right).
\end{aligned}$$

Using (3.4.13) proves the proposition.   □
From Proposition 3.4.7 we obtain the estimate

$$\|\triangle_{\eta_x} T^\varepsilon u^\varepsilon\|_{L^2((0,T)\times(0,1)\times\Gamma)} = \|T^\varepsilon(\triangle_{\eta_x} u^\varepsilon)\|_{L^2((0,T)\times(0,1)\times\Gamma)} = \|\triangle_{\eta_x} u^\varepsilon\|_{L^2(\Gamma^{\varepsilon T})}. \tag{3.4.14}$$

We use (3.4.14) to obtain the result below.

Lemma 3.8 *Along a sequence $\varepsilon \searrow 0$, there exists $u \in L^2((0,T) \times (0,1) \times \Gamma)$ such that*

$$T^\varepsilon u^\varepsilon \to u \text{ strongly in } L^2\left((0,T) \times (0,1) \times \Gamma\right).$$

Proof.   For a.e. $t \in (0,T)$,

$$\begin{aligned}
\triangle_{\eta_z} T^\varepsilon u^\varepsilon &= T^\varepsilon u^\varepsilon(x, (z + \eta_z, h(z + \eta_z))) - T^\varepsilon u^\varepsilon(x, (z, h(z))) \\
&= u^\varepsilon(\varepsilon\lfloor\tfrac{x}{\varepsilon}\rfloor + \varepsilon z + \varepsilon\eta_z, \varepsilon h(z + \eta_z)) - u^\varepsilon(\varepsilon\lfloor\tfrac{x}{\varepsilon}\rfloor + \varepsilon z, \varepsilon h(z))
\end{aligned} \tag{3.4.15}$$

in terms of translation for u^ε. Denote the right hand side by $\mathcal{I}_{\eta_z}$. Note that this is nothing but a translation along the curve Γ and hence, we can use Lemma 3.7 to obtain

$$\|\mathcal{I}_{\eta_z}\|_{L^2((0,T)\times(0,1)\times\Gamma)} \leq C|\eta_z|^{\frac{1}{2}}.$$

Next, we consider the translation along x. We note that

$$\|\triangle_{\eta_x} T^\varepsilon u^\varepsilon\| = \|\triangle_{\eta_x} T^\varepsilon u^\varepsilon\| = \|\triangle_{\eta_x} u^\varepsilon\|_{L^2(\Gamma^\varepsilon)}.$$

We use (3.4.14) together with the Lemma 3.7 to obtain

$$\|\triangle_{\eta_x} u^\varepsilon\|_{L^2(\Gamma^{\varepsilon T})} \leq C|\eta_x|^{\frac{1}{2}}.$$

Hence, we have the translations in x and z directions controlled which implies

$$(\|\triangle_{\eta_x}\|, \|\triangle_{\eta_z}\|) \searrow (0,0), \text{ along a sequence } (|\eta_x|, |\eta_z|) \searrow (0,0).$$

To obtain the strong convergence, one has to deal with time. Let $\eta_t > 0$ be a real number with $\eta_t \in (0,T)$. We have by the L^2-isometry of the boundary unfolding operator

$$\int_0^{T-\eta_t} \int_{\Gamma\times(0,1)} |T^\varepsilon u^\varepsilon(t+\eta_t, x, (z, h(z))) - T^\varepsilon u^\varepsilon(t, x, (z, h(z)))|^2 \, ds dx dt$$

$$= \int_0^{T-\eta_t} \int_{\Gamma^\varepsilon} |u^\varepsilon(t+\eta_t, x) - u^\varepsilon(t, x)|^2 \, dx dt.$$

Denote the left side by $\mathcal{I}$ and the translation operator by $\triangle_{\eta_t}$. The trace theorem (see [50], chapter 5.5) gives

$$\mathcal{I} \leq C \int_0^{T-\eta_t} \|\triangle_{\eta_t} u^\varepsilon(t, \cdot)\|_{L^2(\Omega^\varepsilon)} \left(\|\triangle_{\eta_t} u^\varepsilon(t, \cdot)\|_{L^2(\Omega^\varepsilon)} + \|\triangle_{\eta_t} (\nabla u^\varepsilon(t, \cdot))\|_{L^2(\Omega^\varepsilon)} \right) dt,$$

where the right side can be estimated by using Cauchy Schwarz inequality

$$\mathcal{I} \leq C \left(\int_0^{T-\eta_t} \|\triangle_{\eta_t} u^\varepsilon(t, \cdot)\|^2_{L^2(\Omega^\varepsilon)} dt \right)^{\frac{1}{2}} \left(\int_0^{T-\eta_t} \|\triangle_{\eta_t} (\nabla u^\varepsilon(t, \cdot))\|^2_{L^2(\Omega^\varepsilon)} dt \right)^{\frac{1}{2}}$$

$$+ C \int_0^{T-\eta_t} \|\triangle_{\eta_t} u^\varepsilon(t, \cdot)\|^2_{L^2(\Omega^\varepsilon)} dt.$$

Using the $L^2(0, T; L^2(\Omega^\varepsilon))$ bounds on the gradient, the above inequality reduces to

$$\mathcal{I} \leq C \left(\int_0^{T-\eta_t} \|\triangle_{\eta_t} u^\varepsilon(t, \cdot)\|_{L^2(\Omega^\varepsilon)}^2 dt \right)^{\frac{1}{2}} + C \int_0^{T-\eta_t} \|\triangle_{\eta_t} u^\varepsilon(t, \cdot)\|_{L^2(\Omega^\varepsilon)}^2 dt.$$

Now we use Lemma 3.3 to obtain

$$\mathcal{I} \leq C \left(\eta_t^{\frac{1}{4}} + \eta_t^{\frac{1}{2}} \right)$$

and with $\eta_t \searrow 0$, we conclude that the translations in time are controlled.

By Riesz-Kolmogorov compactness criterion, we conclude that $T^\varepsilon u^\varepsilon$ converges strongly in $L^2((0, T) \times (0, 1) \times \Gamma)$. $\square$

With the strong convergence of $T^\varepsilon u^\varepsilon$ established, we proceed to treat the non-linear terms on the boundary.

Lemma 3.9 *The following convergence result holds:*

$$T^\varepsilon r\left(u^\varepsilon\right) \to r(u) \text{ strongly in } L^2\left((0, T) \times (0, 1) \times \Gamma\right).$$

Proof.   Since r is Lipschitz, Proposition 3.4.4 gives

$$\|T^\varepsilon r\left(u^\varepsilon\right)\|_{L^2((0,T) \times (0,1) \times \Gamma)}^2 \quad = \|r\left(u^\varepsilon\right)\|_{L^2(\Gamma^{\varepsilon T})}^2 \leq C\|u^\varepsilon\|_{L^2(\Gamma^{\varepsilon T})}^2 \leq C.$$

Now because of Lemma 3.8

$$\begin{aligned}
\|T^\varepsilon r\left(u^\varepsilon\right) - r(u)\|_{L^2((0,T) \times (0,1) \times \Gamma)} &= \|r\left(T^\varepsilon u^\varepsilon\right) - r(u)\|_{L^2((0,T) \times (0,1) \times \Gamma)} \\
&\leq L_r \|T^\varepsilon u^\varepsilon - u\|_{L^2((0,T) \times (0,1) \times \Gamma)},
\end{aligned}$$

again vanishing as $\varepsilon \searrow 0$. $\square$

Next, we improve the convergence of $T^\varepsilon v^\varepsilon$.

Lemma 3.10 *It holds that*

$$T^\varepsilon v^\varepsilon \to v \text{ strongly in } L^2\left((0, T) \times (0, 1) \times \Gamma\right).$$

Proof.   The idea is again based on translation. First, we note that $w^\varepsilon \in H(v^\varepsilon)$ satisfies

$$w^\varepsilon = \begin{cases} 1 & \text{if } v^\varepsilon > 0, \\ \min(r(u^\varepsilon), 1) & \text{if } v^\varepsilon = 0, \\ 0 & \text{if } v^\varepsilon < 0. \end{cases}$$

and with this we conclude that w^ε is monotonically increasing with respect to v^ε. We re-write the equation $(3.2.7)_2$ by a change of co-ordinates,

$$\partial_t T^\varepsilon v^\varepsilon = T^\varepsilon r(u^\varepsilon) - T^\varepsilon w^\varepsilon \text{ in the sense of distributions.}$$

Our approach is close to that used in [102]. Since, $\partial_t v^\varepsilon$ is in L^2, the translation of $T^\varepsilon v^\varepsilon$ in time is controlled. To obtain equi-continuity with respect to translations in space, one needs to compare solutions from different cells and also within one cell which means we need to control these translations with respect to x and z. The strong convergence of $r(u^\varepsilon)$ to $r(u)$ in $L^2(0, T; L^2(\Gamma \times (0, 1)))$ and the monotonicity of w^ε are essentially used to achieve this.

First, we consider the translation in x. To this aim, let η_x be a positive real number and

$$Q_{\eta_x} := \{(x, z) \in (0, 1) \times (0, 1) \mid \text{dist}((x, z), \partial((0, 1) \times (0, 1))) < \eta_x\}.$$

Then,

$$\tfrac{1}{2} \tfrac{d}{dt} \|\triangle_{\eta_x} T^\varepsilon v^\varepsilon\|^2_{L^2(Q_{\eta_x})} = \int_{Q_{\eta_x}} \left(\triangle_{\eta_x} T^\varepsilon v^\varepsilon\right) \left(\triangle_{\eta_x} T^\varepsilon r(u^\varepsilon) - \triangle_{\eta_x} T^\varepsilon w^\varepsilon\right) dx dz.$$

Using the monotonicity of $T^\varepsilon w^\varepsilon$ with respect to $T^\varepsilon v^\varepsilon$, one has

$$\left(\triangle_{\eta_x} T^\varepsilon v^\varepsilon\right) \left(\triangle_{\eta_x} T^\varepsilon w^\varepsilon\right) \geq 0, \tag{3.4.16}$$

implying

$$\begin{aligned}
\tfrac{1}{2} \tfrac{d}{dt} \|\triangle_{\eta_x} T^\varepsilon v^\varepsilon\|^2_{L^2(\Gamma \times \Omega_{\eta_x})} &\leq \int_{\Gamma \times \Omega_{\eta_x}} \left(\triangle_{\eta_x} T^\varepsilon v^\varepsilon\right) \left(\triangle_{\eta_x} T^\varepsilon r(u^\varepsilon)\right) dx dz \\
&\leq \tfrac{1}{2} \|\triangle_{\eta_x} T^\varepsilon v^\varepsilon\|^2_{L^2(\Omega_{\eta_x})} + \tfrac{1}{2} \|\triangle_{\eta_x} T^\varepsilon r(u^\varepsilon)\|^2_{L^2(\Omega_{\eta_x})}
\end{aligned}$$

by using Young's inequality for the last step. As $|\eta_x| \searrow 0$, due to strong convergence of $T^\varepsilon r(u^\varepsilon)$, the second term goes to 0 uniformly with respect to η_x (IV.26 in [25]). Using Gronwall's lemma we conclude that

$$\|\triangle_{\eta_x} T^\varepsilon v^\varepsilon\|^2_{L^2(\Omega_{\eta_x})} \to 0 \text{ as } |\eta_x| \to 0$$

uniformly. For the translation with respect to z, we can proceed in a similar manner. We omit the details and observe that both these translations vanish uniformly; yielding the strong convergence of $T^\varepsilon v^\varepsilon$ and hence for $T^\varepsilon v^\varepsilon$ in $L^2(0, T; L^2(\Gamma \times (0, 1)))$. $\qquad \square$

The only term that remains to be considered is w^ε. Specifically, we have to identify its limit w with $H(v)$. For this, we have the following result.

Lemma 3.11 *For $w = \lim_{\varepsilon \searrow 0} T^\varepsilon w^\varepsilon$ we have $w \in H(v)$ where $v = \lim_{\varepsilon \searrow 0} T^\varepsilon v^\varepsilon$.*

Proof. We use the arguments from [47]. Since $T^\varepsilon v^\varepsilon \to v$ strongly in $L^2(0, T; L^2((0, 1) \times \Gamma))$ we have $T^\varepsilon v^\varepsilon \to v$ pointwise a.e. We have only two situations, either $v(t, x, z) > 0$ or $v(t, x, z) = 0$. In the first case and with $\mu := v(t, x, z)/2 > 0$, the pointwise convergence implies the existence of a $\varepsilon_\mu > 0$ such that $T^\varepsilon v^\varepsilon > \mu$ for all $\varepsilon \leq \varepsilon_\mu$. Then for any $\varepsilon \leq \varepsilon_\mu$ we have $T^\varepsilon w^\varepsilon = 1$ implying $w = 1$.
For the case when $v = 0$; consider the set $S = \{(t, x, z) : v(t, x, z) = 0\}$. Now in the interior of the set S, $\partial_t v = 0$. Next, from the weak convergence of $\partial_t v^\varepsilon, w^\varepsilon, r(u^\varepsilon)$, we have the following limit equation

$$(\partial_t v, \theta)_{\Omega^T \times \Gamma} = \int_{\Omega^T \times \Gamma} (r(u) - w)\, \theta \qquad \forall \qquad \theta \in C^\infty((0, T); (0, 1) \times (\Gamma)).$$

Hence, for the interior of the set S, we obtain $w = r(u)$. Furthermore, the bounds $0 \leq T^\varepsilon w^\varepsilon \leq 1$ with weak- convergence of $T^\varepsilon w^\varepsilon$ to w imply the same bounds on w and hence $w = r(u)$ with $0 \leq r(u) \leq 1$. $\square$

3.4.4   Connecting the limits

In Lemma 3.4 we have obtained u_0 as the limit of u^ε restricted to Ω. Since $u_0 \in L^2(0, T; H^1(\Omega))$, we have the trace of u_0 defined at $\partial \Omega$. Next, we considered trace of u^ε defined on Γ^ε and constructed the periodically unfolding sequence $T^\varepsilon u^\varepsilon$ defined at $(0, T) \times \Gamma \times (0, 1)$. We also proved in Lemma 3.8 that $T^\varepsilon u^\varepsilon$ converges strongly to u in $L^2((0, T) \times (0, 1) \times \Gamma)$. Naturally, we would like to connect these two limits and show that the trace of u_0 coincides with u. We prove this in the following Lemma.

Lemma 3.12 *It holds that*

$$\left\| u\left(t, x, (z, h(z))\right) - u_0\left(t, x, y = 0\right) \right\|_{L^1\left(0, T; L^1((0,1) \times \Gamma)\right)} = 0, \qquad (3.4.17)$$

implying that the trace of u_0 and u (obtained as limit of $T^\varepsilon u^\varepsilon$) coincide a.e..

Proof. The choice of L^1 norm simplifies the computations. Let

$$\mathcal{I} := \int_0^T \int_0^1 \int_\Gamma \left| u\left(t, x, z\right) - u_0\left(t, x, y = 0\right) \right| ds\, dx\, dt.$$

By using the triangle inequality we obtain

$$
\begin{aligned}
\mathcal{I} \;\leq\; & \int_0^T \int_0^1 \int_\Gamma \left| u\left(t, x, (z, h(z))\right) - T^\varepsilon u^\varepsilon\left(t, x, (z, h(z))\right) \right| ds\,dx\,dt \\
& + \int_0^T \int_0^1 \int_\Gamma \left| u^\varepsilon\left(t, \varepsilon \left\lfloor \frac{x}{\varepsilon} \right\rfloor + \varepsilon z, \varepsilon h(z)\right) - u^\varepsilon\left(t, \varepsilon \left\lfloor \frac{x}{\varepsilon} \right\rfloor + \varepsilon z, 0\right) \right| ds\,dx\,dt \\
& + \int_0^T \int_0^1 \int_\Gamma \left| u^\varepsilon\left(t, \varepsilon \left\lfloor \frac{x}{\varepsilon} \right\rfloor + \varepsilon z, 0\right) - u^\varepsilon\left(t, x, 0\right) \right| ds\,dx\,dt \\
& + \int_0^T \int_0^1 \int_\Gamma \left| u^\varepsilon\left(t, x, y = 0\right) - u_0\left(t, x, y = 0\right) \right| ds\,dx\,dt.
\end{aligned}
$$

Now we will show that each of the term on the right hand side tends to zero. Let us denote the corresponding terms on the right hand side by $\mathcal{I}_i, i = 1, \dots, 4$. For the first term, $\mathcal{I}_1$, we have

$$
\mathcal{I}_1 = \left\| u\left(t, x, (z, h(z))\right) - T^\varepsilon u^\varepsilon\left(t, x, h(z)\right) \right\|_{L^1((0,T) \times (0,1) \times \Gamma)} \to 0
$$

since $T^\varepsilon u^\varepsilon \to u$ in $L^2\left((0,T) \times (0,1) \times \Gamma\right)$.

For $\mathcal{I}_2$, using Cauchy-Schwarz inequality gives

$$
\mathcal{I}_2 = \int_0^T \int_0^1 \int_\Gamma \left| \int_0^{\varepsilon h(z)} \partial_\xi u^\varepsilon \right| \leq \int_0^T \int_0^1 \int_\Gamma \left(\varepsilon |h|^{\frac{1}{2}} \int_0^{\varepsilon h} |\partial_z u^\varepsilon|^2 \right)^{\frac{1}{2}} \leq C \varepsilon^{\frac{1}{2}} \| \partial_z u^\varepsilon \|_{L^2(\Omega^{\varepsilon T})} \leq C \sqrt{\varepsilon} \| \nabla u^\varepsilon \|_{L^2(\Omega^{\varepsilon T})}.
$$

The last term is bounded by $C \varepsilon^{\frac{1}{2}}$ because u^ε in $L^2(0, T; H^1(\Omega^\varepsilon))$. This implies that $\mathcal{I}_2 \searrow 0$ as $\varepsilon \searrow 0$.

The next term, $\mathcal{I}_3$, is a translation for u^ε in the x direction and the translation is bounded by ε and hence using Lemma 3.7, we obtain $\mathcal{I}_3 \leq C|\varepsilon|^{\frac{1}{2}}$ which tends to 0 as $\varepsilon \searrow 0$.

For the last term $\mathcal{I}_4$, we find

$$
\begin{aligned}
\mathcal{I}_4 &= \left\| u^\varepsilon\left(t, x, y = 0\right) - u_0\left(t, x, y = 0\right) \right\|_{L^1((0,T) \times (0,1) \times \Gamma)} \\
&= |\Gamma| \left\| u^\varepsilon\left(t, x, y = 0\right) - u_0\left(t, x, y = 0\right) \right\|_{L^1((0,T) \times (0,1))}
\end{aligned}
$$

and the last term goes to 0 since, as proved in Lemma 3.4, $u^\varepsilon \to u_0$ strongly in $L^2((0,T) \times \partial\Omega)$. This concludes the proof. $\qquad\square$

3.5   Limit equations: proof of Theorem 3.3.1

In this section, we establish the limit equations and hence prove Theorem 3.3.1. Since we have already established that the trace of u_0 is equal to u, the limit of $T^\varepsilon u^\varepsilon$, for notational convenience we denote both the limits u_0 and u by u. From the weak formulation, $(3.2.7)_1$, choose for $\phi \in H^1((0,T) \times \Omega)$, s.t. $\phi(T,x) = 0$ to rewrite

$$-\int_0^T \int_\Omega u^\varepsilon(\partial_t\phi)dxdt + \int_0^T \int_\Omega \nabla u^\varepsilon \nabla\phi dxdt + \int_0^T \int_\Omega \mathbf{q}^\varepsilon u^\varepsilon \nabla\phi dxdt + \int_0^T \int_{\Gamma^\varepsilon}(\partial_t v^\varepsilon)\phi dxdt$$

$$= -\int_0^T \int_{\Omega^\varepsilon\setminus\Omega} u^\varepsilon(\partial_t\phi)dxdt + \int_\Omega u_I\phi(x,0)dxdt + \int_{\Omega^\varepsilon\setminus\Omega} u_I\phi(x,0)dxdt$$

$$- \int_0^T \int_{\Omega^\varepsilon\setminus\Omega} \left(\nabla u^\varepsilon \nabla\phi + \mathbf{q}^\varepsilon u^\varepsilon \nabla\phi\right)dxdt.$$

On the left side, the first three terms go to desired limit; the limits of the first two terms follow from Lemma 3.4. For the third term, use (3.3.1) and the strong convergence of u^ε to get the limit. For the boundary term, we obtain

$$\lim_{\varepsilon\searrow 0}\int_0^T \int_{\Gamma^\varepsilon}(\partial_t v^\varepsilon)\phi dxdt = \int_0^T \int_{(0,1)\times\Gamma}(\partial_t v)\phi dxdsdt$$

using the weak convergence of $T^\varepsilon\partial_t v^\varepsilon$ as shown in Lemma 3.6. In the right hand side, all the integrals on $\Omega^\varepsilon \setminus \Omega$ vanish in the limit thanks to Lemma 3.5 giving us the desired limiting equation.

Next, we consider the equation $(3.2.7)_2$

$$\int_0^T \int_{\Gamma^\varepsilon}(\partial_t v^\varepsilon)\theta dxdt = \int_0^T \int_{\Gamma^\varepsilon}\left(r(u^\varepsilon) - w^\varepsilon\right)\theta dxdt$$

for all $\theta \in L^2(0,T;\Gamma^\varepsilon)$. A change of co-ordinates provides

$$\int_0^T \int_{(0,1)\times\Gamma}(\partial_t T^\varepsilon v^\varepsilon)(T^\varepsilon\theta)dxdsdt = \int_0^T \int_{(0,1)\times\Gamma}\left(T^\varepsilon r(u^\varepsilon) - T^\varepsilon w^\varepsilon\right)(T^\varepsilon\theta)dxdsdt.$$

Lemma 3.9 provides the strong convergence of $T^\varepsilon r^\varepsilon$; the weak convergence of $T^\varepsilon w^\varepsilon$ follows from Lemma 3.6 leading to

$$\int_0^T \int_{(0,1)\times\Gamma}(\partial_t v)\theta dxdsdt = \int_0^T \int_{(0,1)\times\Gamma}\left(r(u) - w\right)\theta dxdsdt$$

for all $\theta \in L^2(0, T; L^2((0, 1) \times \Gamma))$. Finally, thanks to Lemma 3.11, we have $w \in H(v)$ which completes the proof of Theorem 3.3.1.

3.6 Extensions to different rates

In this work, we have focussed on the proof for the crystal precipitation dissolution model involving a non-Lipschitz, possibly multi-valued rate. However, the techniques can be used to treat different reaction rates. In what follows, we provide two more examples of non-linear rates and comment upon the scheme of the proof. We spare the full details.

3.6.1 Model 1

We consider the following model

$$\partial_t u^\varepsilon - \Delta u^\varepsilon + \mathbf{q}^\varepsilon \nabla u^\varepsilon = 0, \quad \text{in} \quad \Omega^{\varepsilon T} \tag{3.6.1}$$

$$\partial_t v^\varepsilon = r(u^\varepsilon) - g(v^\varepsilon), \quad \text{on} \quad \Gamma^{\varepsilon T} \tag{3.6.2}$$

and let us assume that r has the same structure given earlier. For g, we assume Lipschitz continuity and that it takes positive values. Such rates are considered for example in modeling the reactive flows in porous medium [62], in biological contexts in the diffusion of receptors in a cell [89], or in the description of sulphate attack for sewer pipes [53]. The extension to more number of species living on the boundary or inside the domain is analogous. For the model, the derivation of a priori estimates follows standard techniques. Since the reaction terms are Lipschitz, we obtain for $\partial_t u^\varepsilon \in L^2(0, T; L^2(\Omega^\varepsilon))$ (see e.g. [89]). We directly give the results and comment upon the particularities.

Theorem 3.6.1 *As $\varepsilon \searrow 0$, the pair $(u^\varepsilon, v^\varepsilon)$ converges to (u, v) and the limits satisfy the following equation defined in Ω^T*

$$(\partial_t u, \phi)_{\Omega^T} + (\nabla u, \nabla \phi)_{\Omega^T} - (qu, \nabla \phi)_{\Omega^T} = -(\partial_t v, \phi)_{(0,1) \times \Gamma \times (0,T)},$$

$$(\partial_t v, \theta)_{(0,T) \times (0,1) \times \Gamma} = (r(u) - g(v), \theta)_{(0,1) \times \Gamma \times (0,T)} \tag{3.6.3}$$

for all $(\phi, \theta) \in L^2(0, T; H^1_{0, \Gamma_D}(\Omega)) \times L^2(0, T \times (0, 1) \times \Gamma)$.

Remark 3.13 Compared to the proof of Theorem 3.3.1, the only difference is in obtaining the strong convergence of $T^\varepsilon v^\varepsilon$. We sketch briefly the steps involved in the proof for this strong convergence. We adopt the same framework as in the proof for Lemma 3.10 and re-do some of the steps of the proof for the translation in x. Let η_x be a positive real

number and Q_{η_x} be an arbitrary compact subset of $(0,1) \times (0,1)$ as defined before. We have,

$$\frac{1}{2}\frac{d}{dt}\|\triangle_{\eta_x}(T^\varepsilon v^\varepsilon)\|^2_{L^2(Q_{\eta_x})} = \int\limits_{Q_{\eta_x}} \triangle_{\eta_x}(T^\varepsilon v^\varepsilon) \left(\triangle_{\eta_x}(T^\varepsilon r(u^\varepsilon)) - \triangle_{\eta_x}(T^\varepsilon g(v^\varepsilon))\right) dxdz$$

which leads to using Cauchy Schwarz and Young's inequality,

$$\frac{1}{2}\frac{d}{dt}\|\triangle_{\eta_x}T^\varepsilon v^\varepsilon\|^2_{L^2(\Gamma \times \Omega_{\eta_x})} \leq (\tfrac{1}{2} + L_g)\|\triangle_{\eta_x}T^\varepsilon v^\varepsilon(x)\|^2_{L^2(\Omega_{\eta_x})} + \tfrac{1}{2}\|\triangle_{\eta_x}T^\varepsilon r(u^\varepsilon)\|^2_{L^2(\Omega_{\eta_x})}$$

where L_g is the Lipschitz constant of g. For the rest, the arguments remain the same. Note that as $|\eta_x| \searrow 0$, the strong convergence of $T^\varepsilon r(u^\varepsilon)$, implies that the second term goes to 0 uniformly with respect to η_x (IV.26 in [25]). Using Gronwall's lemma we conclude that the translations go to 0 as $|\eta_x| \searrow 0$. Similarly, the translation with respect to z is similarly treated which together establish the strong convergence of $T^\varepsilon v^\varepsilon$ in $L^2(0,T; L^2(\Gamma \times (0,1)))$. $\qquad\square$

Remark 3.14 For the 2-scale convergence framework of periodic homogenization, the Lipschitz rate at the boundary is treated by the periodic unfolding techniques in [89]. There it is proved that $T^\varepsilon v^\varepsilon$ is a Cauchy sequence. Further, it is to be noted that the above proof also works if g is not Lipschitz but is only monotonic and bounded as is the case for the precipitation dissolution model considered here. $\qquad\square$

3.6.2 Model 2

We discuss another model with non-linear reaction rates that can be treated analogously.

$$\partial_t u^\varepsilon - \Delta u^\varepsilon + \mathbf{q}^\varepsilon \nabla u^\varepsilon = 0, \tag{3.6.4}$$
$$\partial_t v^\varepsilon = r(u^\varepsilon)(1 - sign^+(v^\varepsilon)) \tag{3.6.5}$$

where $sign^+(v^\varepsilon)$ is defined as

$$sign^+(v^\varepsilon) = \begin{cases} 1 & v^\varepsilon > 0, \\ 0 & v^\varepsilon \leq 0. \end{cases} \tag{3.6.6}$$

and let us assume that r has the same structure given earlier. The model is considered in [23] describing the stiff dissolution rates in the context of the safe disposal of nuclear waste. In the cited reference, this problem is posed on core scale in a porous medium and analyzed numerically using the finite volume method. Here, we assume that the reactions take place at the rough boundaries and we are concerned with the upscaling of these rough boundary. The a priori estimates are again derived from standard techniques and we simply state the final result.

Theorem 3.6.2 *As $\varepsilon \searrow 0$, the pair $(u^\varepsilon, v^\varepsilon)$ converges to (u, v) and the limits satisfy the following equation defined in Ω^T*

$$(\partial_t u, \phi)_{\Omega^T} + (\nabla u, \nabla \phi)_{\Omega^T} - (qu, \nabla \phi)_{\Omega^T} = -(\partial_t v, \phi)_{(0,1) \times \Gamma \times (0,T)},$$
$$(\partial_t v, \theta)_{(0,T) \times (0,1) \times \Gamma} = (r(u) - sign^+(v)r(u), \theta)_{(0,1) \times \Gamma \times (0,T)} \qquad (3.6.7)$$

for all $(\phi, \theta) \in L^2(0, T; H^1_{0,\Gamma_D}(\Omega)) \times L^2((0, T) \times (0, 1) \times \Gamma)$.

Remark 3.15 Once again the steps in the proof are analogous and we skip them. Note that once we have proved the strong convergence of $T^\varepsilon r^\varepsilon$ and $T^\varepsilon v^\varepsilon$, we are able to pass to the limit as this implies, $T^\varepsilon v^\varepsilon \to v$ pointwise a.e. with v bounded. The proof for strong convergence of $T^\varepsilon r^\varepsilon$ is same as in the above case. We remark on the difference in the proof for the strong convergence of $T^\varepsilon v^\varepsilon$. Adopting the same framework as in the proof for Lemma 3.10. Let Q_{η_x} be an arbitrary compact subset of $(0, 1) \times (0, 1)$ and let $\eta_x \in (0, dist(Q_{\eta_x}, \partial((0, 1) \times (0, 1))))$. We have,

$$\tfrac{1}{2} \tfrac{d}{dt} \| \triangle_{\eta_x} T^\varepsilon v^\varepsilon \|^2_{L^2(Q_{\eta_x})} = \int_{Q_{\eta_x}} \left(\triangle_{\eta_x} T^\varepsilon v^\varepsilon \right) \triangle_{\eta_x} \left(T^\varepsilon r^\varepsilon (1 - T^\varepsilon sign^+(v^\varepsilon)) \right) dx dz.$$

Note that the right hand side can be rewritten as

$$\triangle_{\eta_x} \left(T^\varepsilon r^\varepsilon (1 - T^\varepsilon sign^+(v^\varepsilon)) \right) = \triangle_{\eta_x} T^\varepsilon (r^\varepsilon)(1 - T^\varepsilon sign^+(v^\varepsilon))$$
$$+ T^\varepsilon r(u^\varepsilon) \triangle_{\eta_x} (1 - T^\varepsilon sign^+(v^\varepsilon))$$

and by the monotonicity (monotonically decreasing) of $1 - T^\varepsilon sign^+(v^\varepsilon)$ and positivity of r, we have

$$T^\varepsilon r(u^\varepsilon) \triangle_{\eta_x} (1 - T^\varepsilon sign^+(v^\varepsilon)) \triangle_{\eta_x} T^\varepsilon v^\varepsilon \leq 0.$$

Using Cauchy Schwarz and Young's inequality, this gives

$$\tfrac{d}{dt} \| \triangle_{\eta_x} T^\varepsilon v^\varepsilon \|^2_{L^2(\Gamma \times \Omega_{\eta_x})} \leq \| \triangle_{\eta_x} T^\varepsilon v^\varepsilon \|^2_{L^2(\Omega_{\eta_x})} + \| \triangle_{\eta_x} T^\varepsilon r(u^\varepsilon) \|^2_{L^2(\Omega_{\eta_x})}.$$

Following the argument that as $|\eta_x| \searrow 0$, the strong convergence of $T^\varepsilon r(u^\varepsilon)$ implies that the second term goes to 0 uniformly with respect to η_x (IV.26 in [25]). Using Gronwall's lemma then concludes the proof. $\qquad \square$

3.7 Numerical simulations

To study the approximation of the upscaled equations to the original equations, we make the following choices for the geometry. To construct Ω^ε, we make the following

choice for Γ^ε:

$$\Gamma^\varepsilon = \{(x, y) : x \in (0, 1) \; y = -1.1\varepsilon + \varepsilon \sin(\pi/2 + 2\pi\frac{x}{\varepsilon})\}$$

which makes sure that $\Omega \subset \Omega^\varepsilon$ and we conduct the numerical experiments for different ε. For the flow, we solve the Stokes equation for Ω^ε domain with parabolic inlet profile and for Ω we have the exact solution $\mathbf{q} = 6y(1 - y)\mathbf{e}_1$. For the choice of reaction rates, we choose for precipitation, $r(u) = [u]_+$, and for dissolution rate, we choose the regularized Heaviside function

$$H_\delta(v^\varepsilon) := \begin{cases} 1, & v^\varepsilon > \delta, \\ \frac{v^\varepsilon}{\delta}, & 0 \le v^\varepsilon \le \delta, \\ 0, & v^\varepsilon < 0 \end{cases} \qquad (3.7.1)$$

and we choose for $\delta = 0.01$. The choice of this regularized Heaviside function has been already investigated for numerical analysis and we refer to [41] for the details.

For the computations, we use finite element method with BDF time stepping for solving the equations as implemented in the COMSOL Multiphysics package [64].

We choose the following initial conditions:

$$u^\varepsilon(x, y, t = 0) = 1, \quad \text{in} \quad \Omega^\varepsilon, \quad v^\varepsilon(x, t = 0) = 0.2 \quad \text{on} \quad \Gamma^\varepsilon;$$

and for u, v also we choose

$$u(x, y, t = 0) = 1, \quad \text{in} \quad \Omega, \quad v(x, t = 0) = 0.2 \quad \text{on} \quad y = 0, \; x \in (0, 1).$$

Note that for this choice of v^ε, v we have $r(u^\varepsilon) - H_\delta(v^\varepsilon) = r(u) - H_\delta(v) = 0$ and hence $\partial_t v^\varepsilon = \partial_t v = 0$ leading to the equilibrium situation. According to different boundary conditions imposed at $x = 0$, we consider the following situations.

3.7.1 Dissolution fronts

We perturb the equilibrium at $x = 0$ by imposing the boundary condition $u^\varepsilon = u = 0$. Due to this the dissolution starts taking place as $\partial_t v^\varepsilon, \partial_t v < 0$ at $x = 0$. This gives rise to the dissolution fronts and these fronts proceed to the right as time progresses. We study this case for different choices of ε.

Concentration at the boundary

We compute the full solution for different ε and plot u^ε and u at the boundary Γ^ε and $y = 0$ boundary of Ω respectively at $t = 0.5$. The plot is shown in Figure 3.2. Due to the oscillations in the boundary the maximum error takes place at the boundary itself.

We compute the concentration at the oscillating boundary for given ε and then plot it against the upscaled concentration u at $y = 0$. Because of the oscillating boundary, the concentration has an oscillating profile while the upscaled concentration has a monotonic profile; however, as ε decreases, u^ε converges to u.

For v^ε, the corresponding plot is shown in Figure 3.3. For small ε we see that the upscaled profile provides a good approximation for the full solution. Further, as ε decreases, the v^ε converges to v.

Error at the boundary

Next, we consider the $L^2(\Gamma_1), \Gamma_1 := \{(x,0)|x \in (0,1)\}$ error at the boundary at $t = 0.5$. Specifically, we assume that the error is of order ε^{α_u},

$$E^u_\varepsilon := \|u^\varepsilon - u\|_{L^2(\Gamma_1)} \leq C\varepsilon^{\alpha_u}.$$

To estimate α_u, we compute the error for various values of ε and determine the ratio

$$\alpha_u(i) = \frac{\log(\text{error}(i)) - \log(\text{error}(i-1))}{\log(\varepsilon(i)) - \log(\varepsilon(i-1))}, \quad i = 2, \ldots, 6.$$

In Table 3.1 we give the values of the error as well as the convergence rate α_u computed from the preceding formula. The convergence order is close to 1.
Similarly, for v^ε we assume the convergence order α_v and compute

$$E^v_\varepsilon := \|v^\varepsilon - v\|_{L^2(\Gamma_1)} \leq C\varepsilon^{\alpha_v}.$$

The results are tabulated in Table 3.2. As it is seen below, the convergence order is better than 1.

We now compare the average concentration at the boundary. We define

$$\bar{u}(x) := \frac{1}{\varepsilon} \int_{\varepsilon\lfloor \frac{x}{\varepsilon} \rfloor - \frac{\varepsilon}{2}}^{\varepsilon\lfloor \frac{x}{\varepsilon} \rfloor + \frac{\varepsilon}{2}} u^\varepsilon ds$$

Observe that $\bar{u}$ provides information regarding the average concentration into one periodic unit for ε model. We compare this with the upscaled equation in Figure 3.4. The agreement is very good for small ε which indicates the quality of upscaling.
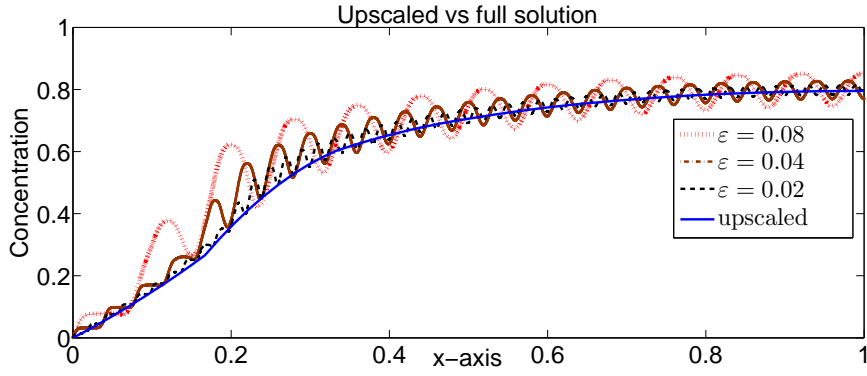
Figure 3.2: *Concentration profiles for dissolution process at the boundary for different ε at $t = 0.5$.*
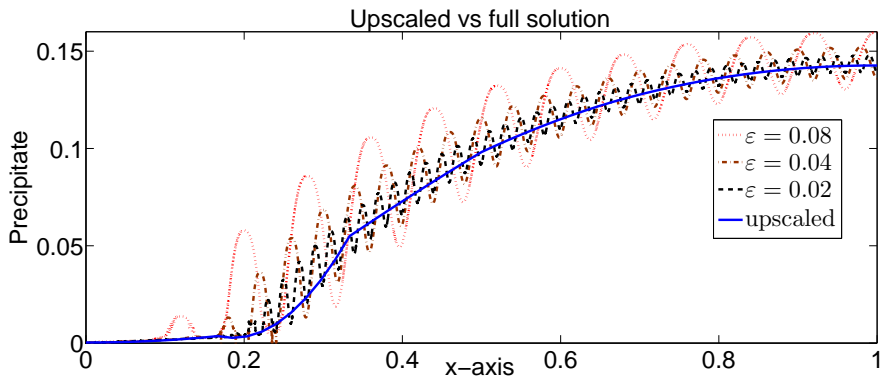
Figure 3.3: *Precipitate concentration profiles for dissolution process at the boundary for different ε at $t = 0.5$.*

ε	0.1000	0.0800	0.0500	0.0400	0.0200	0.0100
error	0.1118	0.0844	0.0516	0.0453	0.0218	0.0106
α_u		0.9195	0.9746	1.1003	0.9588	0.9754

Table 3.1: *Table for L^2 error for the concentrations.*

ε	0.1000	0.0800	0.0500	0.0400	0.0200	0.0100
error	0.0268	0.0206	0.0125	0.0114	0.0061	0.0030
α_v		1.3000	1.3725	1.4783	1.3403	1.2582

Table 3.2: *Table for L^2 error for the precipitate concentration.*

3.7.2 Precipitation process

Next, we again choose the same initial condition as above and we study the precipitation process by imposing the boundary condition

$$u^\varepsilon = u = 2, \quad \text{at} \quad x = 0$$

and with this choice, note that $\partial_t v^\varepsilon, \partial_t v > 0$ and hence the precipitation process starts taking place. This leads to an increase in v^ε, v as time progresses and for u^ε, u a steady state is achieved. We show the solutions for different ε and we compute the full solution for $\varepsilon = 0.1, 0.02$ and plot u^ε and u at the boundary Γ^ε and $y = 0$ boundary of Ω respectively at $t = 1$. The corresponding plots for u^ε and v^ε are shown in Figure 3.5, respectively in 3.6. Again, due to the oscillations in the boundary, we have the boundary layer and the maximum error takes place at the boundary itself. We compute the concentration at the oscillating boundary for given ε and then plot it against the upscaled concentration u at $y = 0$. Because of the oscillating boundary, the concentration has an oscillating profile while the upscaled concentration has a monotonic profile; however, as ε decreases, $u^\varepsilon, v^\varepsilon$ converges to u, v.

3.8 Conclusions

We have rigorously derived the upscaled model for the crystal precipitation dissolution model defined in a domain with oscillating boundary characterized by period and amplitude ε. The upscaled model is obtained as the limit of sequence $\varepsilon \searrow 0$. The derivation uses the homogenization arguments where we use the periodic unfolding techniques to use the desired compactness arguments. The non-linear reaction rates in particular the multi-valued dissolution rates require stronger convergence properties for passing to the limit which is achieved by considering translation estimates. Even though the derivation here has been specific to the precipitation-dissolution model, similar techniques may be used for a different kinds of reaction rates. We have given some specific examples of such rates. Moreover, we have provided numerical computations to show the convergence. We see that the upscaled solutions approximate the full solution very well and hence provide a convincing argument for the usefulness of upscaling techniques.
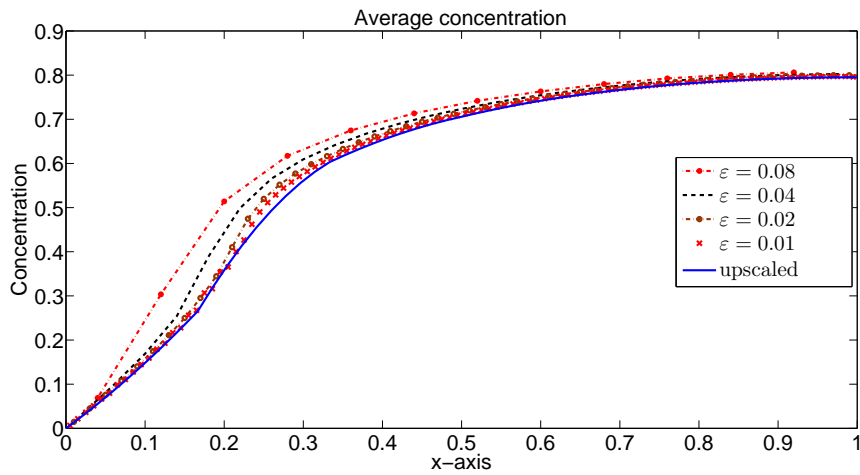
Figure 3.4: *Average concentration $\bar{u}$ for dissolution process for different ε at $t = 0.5$.*
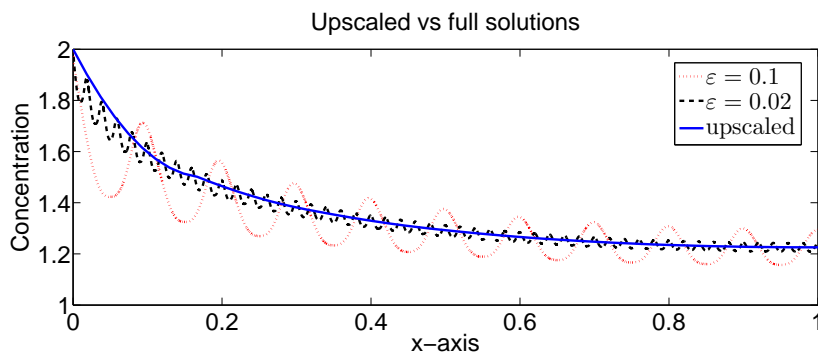
Figure 3.5: *Concentration profiles at the boundary for different ε at $t = 1$ (precipitation).*
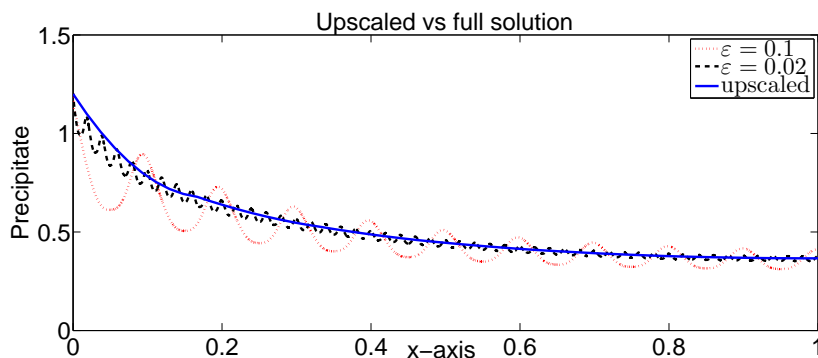
Figure 3.6: *Precipitate concentration at the boundary for different ε at $t = 1$ (precipitation).*

Chapter 4

Upscaling of moving rough boundaries

We consider the flow and transport of chemically reactive substances (precursors) in a channel over substrates having complex geometry. In particular, these substrates are in the form of trenches forming oscillating boundaries. The precursors react at the boundaries and get deposited. The deposited layers lead to changes in the geometry and are explicitly taken into account. Consequently, the system forms a free boundary problem. Using formal asymptotic techniques, we obtain the upscaled equations for the system where these equations are defined on a domain with flat boundaries. This provides a huge gain in computational time. Numerical experiments show the effectiveness of the upscaling process.

4.1 Introduction

This work deals with the upscaling of processes which are defined in a domain having oscillating (rough) boundaries. The aim is to approximate the model by one defined in a simpler domain with flat (non-oscillating) boundaries. The work presented here is motivated by reactive flow models where the reactive substances are transported by a carrier fluid (gas or liquid).

The reactions take place at the rough boundaries, and the reaction products are immobile species which get attached to or detached from the surface. Examples of these

processes are crystal precipitation and dissolution processes [105] and chemical vapor deposition processes [56]. The formation of reaction products at the boundary leads to changes in the thickness of the solid layer with time. There are two options: one is to ignore the geometry change and take a fixed geometry model and describe the deposition/dissolution process by an equation defined at the boundary and the other option is to take the changes in the geometry explicitly into account in which the thickness of the solid layer provides information about the amount of deposition/dissolution. We follow the second approach here. This implies that the geometry may change with time and since the change in the geometry is unknown, we have a free (evolving) boundary problem. The problem is to find an upscaled equation defined in a simple domain with flat boundaries for this free boundary problem posed in a complex domain with oscillatory boundaries.

A motivation for this work is the process of making 3-D batteries through the process of chemical vapor deposition (CVD) where a part of the domain consists of trenches (rough surface) instead of being flat to enhance the surface area hence increasing the capacity of the battery [110, 113, 114]. The sizes of these trenches may vary and are in the order of micrometers (typical size $\sim 10~\mu m$) and the substrate size is in the order of centimeters (typical size $\sim 30~cm$). In the trenches, the thickness of different layers of deposition (of electrodes/anode/cathode) may not be negligible compared to the size of trenches. In this situation, it is important to take into account the thickness of the deposited layer and consider a model for describing the deposition process for the time-dependent geometry.

We use upscaling arguments, in particular a formal (matched) asymptotic approach, to provide a rational derivation of this approximation. The presence of free boundary makes the rigorous arguments difficult and here we restrict to formal asymptotic arguments. One important aspect of this upscaling approach is that the system of equations defined inside the domain remains unchanged and only the boundary conditions are modified. Naturally, such an upscaling leads to computational efficiency as the fine scales need not be resolved. Further, for small enough oscillations, one takes advantage of the scale separation and obtains better approximation. Hence, the finer these oscillations are, the better approximation can be achieved. Also, the upscaled domain is fixed in time and the movement of the boundary of the original domain leads to a time-dependent boundary condition for the upscaled equations.

In this work we provide the upscaling for both the transport and the flow problems defined in a domain with moving and oscillating boundaries. As we apply only formal arguments, non-linear reactions rates have been considered. Further, in the work presented here, for the sake of exposition, we have considered only one species, however, an extension to multi-species and multi-component is straightforward. Also, more general diffusion terms may be dealt with the similar techniques considered here.

There exists extensive amounts of work dealing with both the formal and the rigor-

ous upscaling of rough boundaries. Most of the work however refers to the situation when the geometry remains fixed. Relevant to the work presented here are [56] for the transport problem and [66–68] for flow problem respectively. In the former, the formal approach is used for diffusion equation while the latter papers deal with rigorous treatment to the upscaling of Stokes equation in the fixed geometry situation. The difference with [56] is that the cited work deals with the fixed geometry situation and also the flow is absent. Although our techniques are inspired from [56], however, there are some differences in the way of our derivation. In an another related work, [54], rigorous treatment for the upscaling in the absence of flow and linear reaction rates when the geometry changes are explicitly taken into account. Our results are consistent with the results in the mentioned literature. Because of the formal approach employed here, we are able to take into account both the flow and the transport problem together and also much more general reaction rates are considered. For other related work on upscaling of reactive flows/transport involving oscillating boundaries we refer to [3, 9, 11, 29, 55, 75, 100]. These kind of problems find applications in making 3-D solid state batteries, flow in rough pipes, semiconductor industries, bio-film growth in porous medium and describing the evaporation processes in plants or through soil [13, 45–47, 57, 96, 104, 107].

The article is organized as follows. We start with the description of the geometry and the formulation of the problem in Section 4.2. In Sections 4.3 and 4.4 we treat the flow problem and transport problem. In Section 4.5, we provide numerical computations where we compare the upscaled equations with the original equations.

4.2   Modeling equations

We describe the setting of the problem and start with the precise description of the geometry considered here. To define the model, we consider the flow carrying reactive substances (precursors). The flow passes over the substrate and the precursor is deposited on the substrate making it a transport process with reactions at the boundary. To take into account the thickness of the deposited layer, we provide a model that describes the deposition process for the time-dependent geometry. The model consists of two components, one the flow component and the other the transport component. For the flow, we take for simplicity of computations, the Stokes equation and the transport part is described by a linear convection-diffusion equation. The boundary conditions for both the transport and flow equations are posed on a time-dependent boundary and we also prescribe a law for describing the movement of the geometry.
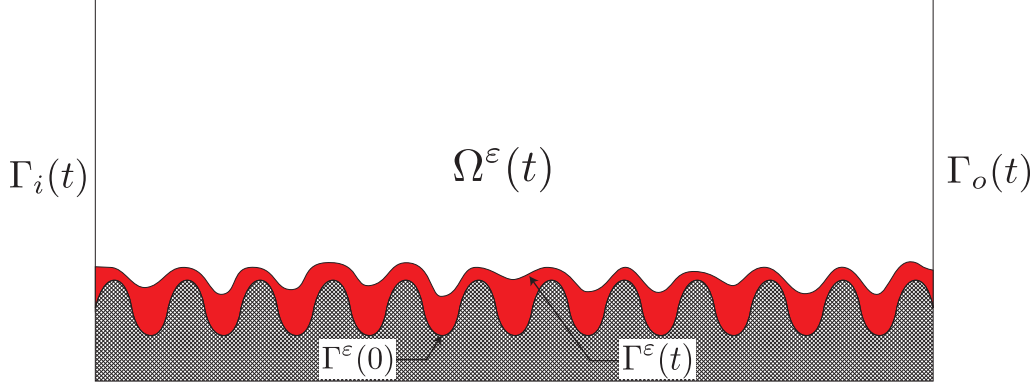
Figure 4.1: *Schematic for the domain Ω^ε : channel with rough boundary Γ^ε. Initially, the boundary $\Gamma^\varepsilon \subset \partial\Omega^\varepsilon$ consists of a periodic function $\varepsilon h(\frac{x}{\varepsilon})$. Note that the geometry may change in time due to reactions taking place.*

4.2.1 Geometry

Let Ω^ε denote the domain having rough boundaries denoted by Γ^ε. We define a system of equations describing the flow and transport processes in Ω^ε with reactive boundary conditions defined on Γ^ε. The question that we are concerned with is defining the appropriate system of equations in the simpler domain Ω with flat (non-oscillating) boundary such that the solutions in a simpler domain Ω approximate those in Ω^ε. We proceed to give the precise definitions of these geometries. A schematic of the geometry is presented in Figure 4.1.

First, the homogenized domain with flat boundaries is denoted by $\Omega := (0,1)^2$. Let h be a given smooth function that is 1- periodic. Let us define $h^\varepsilon(x,t)$ using the periodicity of h such that

$$h^\varepsilon(x,0) := \varepsilon h(\frac{x}{\varepsilon}).$$

We use the above to define Ω^ε

$$\Omega^\varepsilon(t) := \left\{ (x,y) \in \mathbb{R}^2 \mid x \in (0,1) \quad y \in (h^\varepsilon(x,t), 1) \right\}$$

where $h^\varepsilon(x,0)$ is as defined above and hence is a smooth function. Let $\partial\Omega^\varepsilon$ denote the boundary of Ω^ε.
The oscillating boundary $\Gamma^\varepsilon(\subset \partial\Omega^\varepsilon)$ is defined as:

$$\Gamma^\varepsilon(t) := \{(x,y) \mid x \in (0,1), \quad y = h^\varepsilon(x,t)\}.$$

We remark that the h^ε is not a priori known except for $t = 0$ and depends on the unknown solution of the transport equation. Hence, this defines a free-boundary problem.

The inlet and the outlet boundaries are correspondingly defined as

$$\Gamma_i(t) := \{(x, y) \mid x = 0, \ y = h^\varepsilon(0, t)\}$$
$$\Gamma_o(t) := \{(x, y) \mid x = 1, \ y = h^\varepsilon(1, t)\}.$$

This particular scaling for the boundary ensures that the Lebesgue measure of Γ^ε remains bounded and of order $O(1)$. Notice that we emphasize the time-dependence of the definition of $\Omega^\varepsilon, \Gamma^\varepsilon$ as opposed to the homogenized domain Ω which is time-independent.

4.2.2   The model

We start with the modeling for the processes taking place in the geometry described above. For the sake of simplicity, we write all the equations in dimensionless form (see [105] for the dimensional model and non-dimensionalization). As described above, because of the reactions taking place at the boundaries, the thickness of the layer attached to the boundary may change with time. The thickness of this layer is $h^\varepsilon(x, t) - h^\varepsilon(x, 0)$. The growth of the layers lead to variation in the domain, and implicitly to a change in the flow, an effect that is taken into account.

For the reactants in the domain, the different processes are diffusion, transport by the fluid flow, and reactions taking place at the boundaries of the domain. The flow problem is modeled by the Stokes equations,

$$\mu \Delta \mathbf{q}^\varepsilon = \nabla p^\varepsilon \quad \text{in} \quad \Omega^\varepsilon(t), \tag{4.2.1}$$

$$\nabla \cdot \mathbf{q}^\varepsilon = 0 \quad \text{in} \quad \Omega^\varepsilon(t), \tag{4.2.2}$$

where p^ε is the pressure field, $\mathbf{q}^\varepsilon$ is the flow field and μ is the dynamic viscosity. At the inlet, we take a parabolic velocity profile normal to the inlet,

$$\mathbf{q}^\varepsilon(0, y, t) = Q(y - 1)(h(0, t) - y)\mathbf{e}_1,$$

where $Q > 0$ is a normalisation factor related to the total flow in the x-direction and e_1 is the unit vector along the x-axis. For the outlet we prescribe the pressure $p^\varepsilon = 0$. At other boundaries, we assume no-flow boundary conditions, in particular $\mathbf{q}^\varepsilon = 0$ at Γ^ε. For the ease of presentation, without loss of generality, let us assume $\mu = 1$.

For the transport equation, for the sake of presentation, we consider only one species here, with its concentration denoted by u^ε. The convection-diffusion equation and the

boundary conditions describing the transport process of the reactant are

$$\partial_t u^\varepsilon = \nabla \cdot (\nabla u^\varepsilon - \mathbf{q}^\varepsilon u^\varepsilon), \quad \text{in} \quad \Omega^\varepsilon(t)$$
$$u^\varepsilon = u_b, \quad \text{on } \Gamma_i(t), \qquad\qquad\qquad\qquad (4.2.3)$$
$$\partial_x u^\varepsilon = 0, \quad \text{on } \Gamma_o(t),$$

where u_b is a given non-negative concentration. The diffusion coefficient is taken as 1. For simplicity, we assume homogeneous Neumann boundary conditions on the remaining boundary, that is, on $\partial\Omega^\varepsilon \setminus (\Gamma^\varepsilon \cup \Gamma_i \cup \Gamma_o)$.

The reactions take place only at the interface between the fluid and the solid, that is, $\Gamma^\varepsilon(t)$. The corresponding mathematical model involves the outer normal $\boldsymbol{\nu}^\varepsilon(t)$ to $\Gamma^\varepsilon(t)$,

$$\boldsymbol{\nu}^\varepsilon(t) = (\partial_x h^\varepsilon, -1)^T / \sqrt{1 + (\partial_x h^\varepsilon)^2}. \qquad\qquad (4.2.4)$$

At $\Gamma^\varepsilon(t)$, mass conservation yields

$$\boldsymbol{\nu}^\varepsilon \cdot (\nabla u^\varepsilon - \mathbf{q}^\varepsilon u^\varepsilon) = v_n(\rho - u^\varepsilon), \qquad\qquad (4.2.5)$$

where ρ is the molar density of the reactant in the solid phase (the adsorbed substance, or the deposited layer) and v_n is the outward normal velocity of the interface. Furthermore, the normal velocity of the interface v_n is proportional to the reaction rate $f = f(u^\varepsilon, h^\varepsilon)$,

$$\rho v_n = -f(u^\varepsilon, h^\varepsilon). \qquad\qquad\qquad (4.2.6)$$

Here f is a given function assumed to be sufficiently smooth. Similar results can be derived formally even for non-Lipschitz rates like Freundlich isotherms or multi-valued reaction rates as encountered for dissolution processes [75].
The velocity of a point $G^\varepsilon(t) = (x(t), h^\varepsilon(x(t), t))$ on $\Gamma^\varepsilon(t)$ is given by

$$\partial_t G^\varepsilon(t) = (x'(t), \partial_x h^\varepsilon(x(t), t)x'(t) + \partial_t h^\varepsilon(x(t), t)).$$

Then the normal velocity v_n becomes

$$v_n = \boldsymbol{\nu}^\varepsilon \cdot \partial_t G^\varepsilon(t) = -\frac{\partial_t h^\varepsilon}{\sqrt{1 + (\partial_x h^\varepsilon)^2}}, \qquad\qquad (4.2.7)$$

and (4.2.6) transforms into

$$\rho \partial_t h^\varepsilon = f(u^\varepsilon, h^\varepsilon)\sqrt{1 + (\partial_x h^\varepsilon)^2}. \qquad\qquad (4.2.8)$$

Further, we assume ρ to be of $O(1/\varepsilon)$ so that the movement in the boundary is of order ε thereby retaining the roughness as the reactions change the geometry.

4.3 The flow problem

We use here formal matched asymptotics to derive the upscaled equations. The procedure consists of considering the solutions in different regions, one close to Γ^ε (the inner solution) and far from it (the outer solution). We later derive the matching conditions at an intermediate scale. Using the matching conditions, we obtain the upscaled boundary conditions.

4.3.1 The inner region

Close to Γ^ε we assume $\mathbf{q}^\varepsilon = \mathbf{q}^\varepsilon(x, y, t)$, $p^\varepsilon = p^\varepsilon(x, y, t)$ and for the expansions we assume

$$\mathbf{q}^\varepsilon = \mathbf{q}_0(x, \frac{x}{\varepsilon}, \frac{y}{\varepsilon}, t) + \varepsilon \mathbf{q}_1(x, \frac{x}{\varepsilon}, \frac{y}{\varepsilon}, t) + \cdots, \tag{4.3.1}$$

$$p^\varepsilon = p_0(x, \frac{x}{\varepsilon}, \frac{y}{\varepsilon}, t) + \varepsilon p_1(x, \frac{x}{\varepsilon}, \frac{y}{\varepsilon}, t) + \cdots, \tag{4.3.2}$$

$$h^\varepsilon = \varepsilon h_0(x, \frac{x}{\varepsilon}, t) + \varepsilon h_1(x, \frac{x}{\varepsilon}, t) + \cdots. \tag{4.3.3}$$

In the expansions we assume that the thickness of the deposition layer remains of the order $O(\varepsilon)$ to retain roughness. Define: $\xi := \frac{x}{\varepsilon}, \eta := \frac{y}{\varepsilon}$. Following the periodicity in the geometry of oscillations, we assume periodicity of the inner variables in the ξ coordinate. This implies

$$\mathbf{q}_i(x, \xi + 1, \eta, t) = \mathbf{q}_i(x, \xi, \eta, t),$$
$$p_i(x, \xi + 1, \eta, t) = p_i(x, \xi, \eta, t),$$
$$h_i(x, \xi + 1, t) = h_i(x, \xi, t).$$

Denoting by $\mathbf{e}_1$ and $\mathbf{e}_2$ the unit vectors in the x- and y-directions respectively, we start with the gradient terms. For $i = 1, 2$

$$\nabla q^{\varepsilon(i)} = (\partial_x + \frac{1}{\varepsilon}\partial_\xi)q^{\varepsilon(i)}\mathbf{e}_1 + \frac{1}{\varepsilon}\partial_\eta q^{\varepsilon(i)}\mathbf{e}_2$$
$$= (\partial_x q_0^{(i)} + \varepsilon\partial_x q_1^{(i)} + \frac{1}{\varepsilon}\partial_\xi q_0^{(i)} + \partial_\xi q_1^{(i)})\mathbf{e}_1 + (\frac{1}{\varepsilon}\partial_\eta q_0^{(i)} + \partial_\eta q_1^{(i)})\mathbf{e}_2 + O(\varepsilon).$$

This implies for $i = 1, 2$

$$\Delta q^{(i)} = \partial_{xx}q_0^{(i)} + 2\varepsilon^{-1}\partial_{x\xi}q_0^{(i)} + 2\partial_{x\xi}q_1^{(i)} + \partial_{\xi\xi}q_2^{(i)} + \partial_{\eta\eta}q_2^{(i)}$$
$$+ \varepsilon^{-2}\partial_{\xi\xi}q_0^{(i)} + \varepsilon^{-1}\partial_{\xi\xi}q_1^{(i)} + \varepsilon^{-2}\partial_{\eta\eta}q_0^{(i)} + \varepsilon^{-1}\partial_{\eta\eta}q_1^{(i)} + O(\varepsilon).$$

Similarly,

$$\nabla p^\varepsilon = (\partial_x + \varepsilon^{-1}\partial_\xi)p^\varepsilon \mathbf{e}_1 + \varepsilon^{-1}\partial_\eta p^\varepsilon \mathbf{e}_2$$
$$= \left(\partial_x p_0 + \varepsilon \partial_x p_1 + \varepsilon^{-1}\partial_\xi p_0 + \partial_\xi p_1\right)\mathbf{e}_1 + \left(\varepsilon^{-1}\partial_\eta p_0 + \partial_\eta p_1\right)\mathbf{e}_2 + O(\varepsilon). \quad (4.3.4)$$

We proceed by inserting these expansions in the equations. For the continuity equation, we have

$$(\partial_x + \varepsilon^{-1}\partial_\xi)q^{\varepsilon(1)} + \varepsilon^{-1}\partial_\eta q^{\varepsilon(2)} = 0,$$

implying

$$\partial_x q_0^{(1)} + \varepsilon\partial_x q_1^{(1)} + \varepsilon^{-1}\partial_\xi(q_0^{(1)} + \varepsilon q_1^{(1)}) + \varepsilon^{-1}\partial_\eta q_0^{(2)} + \partial_\eta q_1^{(2)} = O(\varepsilon).$$

Equating the terms of similar order, for ε^{-1} terms we get

$$\partial_\xi q_0^{(1)} + \partial_\eta q_0^{(2)} = 0, \qquad\qquad\qquad (4.3.5)$$

and for ε^0 terms we have

$$\partial_x q_0^{(1)} + \partial_\xi q_1^{(1)} + \partial_\eta q_1^{(2)} = 0. \qquad\qquad\qquad (4.3.6)$$

We proceed with the Stokes equation. Plugging in the expansions for $\Delta\mathbf{q}^\varepsilon$ and ∇p^ε, we obtain after cascading the different orders of ε

$$\partial_{\xi\xi} q_0^{(1)} + \partial_{\eta\eta} q_0^{(1)} = 0, \qquad\qquad\qquad (4.3.7)$$

$$\partial_{\xi\xi} q_0^{(2)} + \partial_{\eta\eta} q_0^{(2)} = 0, \qquad\qquad\qquad (4.3.8)$$

$$2\partial_{x\xi} q_0^{(1)} + \partial_{\xi\xi} q_1^{(1)} + \partial_{\eta\eta} q_1^{(1)} = \partial_\xi p_0, \qquad\qquad\qquad (4.3.9)$$

$$2\partial_{x\xi} q_0^{(2)} + \partial_{\xi\xi} q_1^{(2)} + \partial_{\eta\eta} q_1^{(2)} = \partial_\eta p_0. \qquad\qquad\qquad (4.3.10)$$

With the expansion for h^ε we have for the leading order term for the normal of $\Gamma^\varepsilon(t)$

$$\mathbf{v}_0(x,\xi,t) = \frac{1}{\sqrt{1 + \left(\partial_\xi h_0(x,\frac{x}{\varepsilon},t)\right)^2}}\begin{pmatrix} \partial_\xi h_0(x,\frac{x}{\varepsilon},t) \\ -1 \end{pmatrix}.$$

For the boundary conditions, the no-slip boundary condition leads to $\mathbf{q}_0 = \mathbf{q}_1 = 0$ on $\Gamma^\varepsilon(t)$. Since there is no forcing term combined with the periodicity in ξ and homogeneous Dirichlet data at a part of the boundary, we conclude $\mathbf{q}_0 = 0$.

4.3.2 The outer region

For the outer region, we assume

$$\mathbf{q}^\varepsilon := \mathbf{q}^\varepsilon(x, \frac{x}{\varepsilon}, y, t), p^\varepsilon := P^\varepsilon(x, \frac{x}{\varepsilon}, y, t).$$

The usual formal asymptotic expansions give,

$$\mathbf{q}^\varepsilon = \mathbf{Q}_0(x, \xi, y, t) + \varepsilon \mathbf{Q}_1(x, \xi, y, t) + \cdots,$$

$$P^\varepsilon = P_0(x, \xi, y, t) + \varepsilon P_1(x, \xi, y, t) + \cdots.$$

Furthermore, we assume that $\mathbf{Q}_i$ and P_i are periodic in ξ with period 1. For the continuity equation, we have

$$\partial_x Q_0^{(1)} + \varepsilon \partial_x Q_1^{(1)} + \varepsilon^{-1} \partial_\xi Q_0^{(1)} + \partial_\xi Q_1^{(1)} + \partial_y Q_0^{(2)} + \varepsilon \partial_y Q_1^{(2)} = O(\varepsilon). \tag{4.3.11}$$

Upon ordering with different orders of ε we obtain

$$\partial_\xi Q_0^{(1)} = 0, \tag{4.3.12}$$

$$\partial_x Q_0^{(1)} + \partial_y Q_0^{(2)} + \partial_\xi Q_1^{(1)} = 0. \tag{4.3.13}$$

From (4.3.12) we conclude,

$$Q_0^{(1)} = Q_0^{(1)}(x, y, t). \tag{4.3.14}$$

For the Stokes equation, we first write down separately $\Delta \mathbf{q}^\varepsilon, \nabla P^\varepsilon$ for convenience. For $i = 1, 2$, we have

$$\Delta Q^{\varepsilon(i)} = (\partial_x + \varepsilon^{-1} \partial_\xi)(\partial_x Q^{\varepsilon(i)} + \varepsilon^{-1} \partial_\xi Q^{\varepsilon(i)}) + \partial_{yy} Q^{\varepsilon(i)}$$

which upon expansion and rearrangement gives

$$\Delta Q^{\varepsilon(i)} = \varepsilon^{-2} \partial_{\xi\xi} Q_0^{(i)} + \varepsilon^{-1}(2\partial_{x\xi} Q_0^{(i)} + \partial_{\xi\xi} Q_1^{(i)}) + (\partial_{xx} Q_0^{(i)} + \partial_{yy} Q_0^{(i)} + \partial_{\xi\xi} Q_2^{(i)})$$
$$+ 2\partial_{x\xi} Q_1^i + O(\varepsilon).$$

Similarly,

$$\nabla P^\varepsilon = (\partial_x P_0 + \frac{1}{\varepsilon} \partial_\xi P_0 + \partial_\xi P_1)\mathbf{e}_1 + (\partial_y P_0)\mathbf{e}_2 + O(\varepsilon).$$

Plugging these expansions into the Stokes equation and separating the different orders of ε we obtain

$$\partial_{\xi\xi} Q_0^{(1)} = 0, \tag{4.3.15}$$

$$2\partial_{x\xi} Q_0^{(1)} + \partial_{\xi\xi} Q_1^{(1)} = \partial_\xi P_0, \tag{4.3.16}$$

$$2\partial_{x\xi} Q_1^1 + \partial_{xx} Q_0^{(1)} + \partial_{yy} Q_0^{(1)} + \partial_{\xi\xi} Q_2^{(1)} = \partial_x P_0 + \partial_\xi P_1 \tag{4.3.17}$$

For the $\mathbf{e}_2$ direction, for the Stokes equation the different terms of different orders of ε provide

$$\partial_{\xi\xi} Q_0^{(2)} = 0, \tag{4.3.18}$$

$$2\partial_{x\xi} Q_0^{(2)} + \partial_{\xi\xi} Q_1^{(2)} = 0, \tag{4.3.19}$$

$$2\partial_{x\xi} Q_1^2 + \partial_{xx} Q_0^{(2)} + \partial_{yy} Q_0^{(2)} + \partial_{\xi\xi} Q_2^{(2)} = \partial_y P_0. \tag{4.3.20}$$

From (4.3.18) and the periodicity in ξ we obtain that $Q_0^{(2)}$ is independent of ξ and using this in (4.3.19) we conclude

$$Q_1^{(2)} = Q_1^{(2)}(x, y, t).$$

Differentiating (4.3.13) w.r.t. ξ and using (4.3.14) we obtain

$$\partial_{\xi\xi} Q_1^{(1)} = 0$$

and using periodicity in ξ direction,

$$Q_1^{(1)} = Q_1^{(1)}(x, y, t). \tag{4.3.21}$$

Using above in (4.3.16) we get

$$\partial_\xi P_0 = 0 \quad \text{which means} \quad P_0 = P_0(x, y, t). \tag{4.3.22}$$

Integrating (4.3.17) over ξ and using periodicity result in

$$\partial_{xx} Q_0^{(1)} + \partial_{yy} Q_0^{(1)} = \partial_x P_0. \tag{4.3.23}$$

We integrate (4.3.20) over ξ from 0 to 1 and use the fact that $Q_0^{(2)}$ and P_0 are independent of ξ and we get

$$\partial_{xx} Q_0^{(2)} + \partial_{yy} Q_0^{(2)} = \partial_y P_0. \tag{4.3.24}$$

Note that $Q_0^{(1)}, Q_0^{(2)}, Q_1^{(1)}$, and $Q_1^{(2)}$ are ξ-independent. This means that they satisfy the original Stokes model.

4.3.3　Matching conditions

Here we couple the inner solutions and the outer solutions. We use the asymptotic expansion, for the flow vector,

$$\mathbf{q}^\varepsilon(x, \xi, y, t) = \mathbf{Q}_0(x, y, t) + \varepsilon \mathbf{Q}_1(x, y, t) + O(\varepsilon^2)$$

and Taylor's expansion at $y = \varepsilon\eta$ to obtain

$$\mathbf{q}^\varepsilon(x, \varepsilon\eta, t) = \mathbf{Q}_0(x, 0, t) + \varepsilon\eta\partial_y\mathbf{Q}_0(x, 0, t) + \varepsilon\mathbf{Q}_1(x, 0, t) + O(\varepsilon^2).$$

For the inner solution we have the asymptotic expansion

$$\mathbf{q}^\varepsilon(x, \xi, \eta, t) = \mathbf{q}_0(x, \xi, \eta, t) + \varepsilon\mathbf{q}_1(x, \xi, \eta, t) + O(\varepsilon^2).$$

Therefore, by matching, we conclude

$$\lim_{\eta\to\infty} \mathbf{q}_0(x, \xi, \eta, t) - \mathbf{Q}_0(x, 0, t) = 0$$

$$\lim_{\eta\to\infty} \mathbf{q}_1 - (\partial_y\mathbf{Q}_0)\eta - \mathbf{Q}_1 = 0$$

and further using the above,

$$\lim_{\eta\to\infty} \partial_\eta\mathbf{q}_1(x, \xi, \eta, t) - \partial_y\mathbf{Q}_0 = 0.$$

Now we are in a position to provide the leading order approximation and the first order approximation. For the leading order approximation $\mathbf{Q}_0$ we simply have

$$\mathbf{Q}_0 = 0 \text{ at } y = 0.$$

Remark 4.1 To obtain the next order approximation, let us define $\mathbf{Q}_e := \mathbf{Q}_0 + \varepsilon\mathbf{Q}_1$. From the matching condition we have

$$\mathbf{Q}_0 = 0, \ \varepsilon\mathbf{Q}_1 = \varepsilon\alpha\partial_y\mathbf{Q}_0,$$

where

$$\alpha^{(i)} := \lim_{\eta\to\infty} \frac{q_1^{(i)}}{\partial_y Q_0^{(i)}} - \eta.$$

This provides us the effective boundary condition

$$\mathbf{Q}_e = \varepsilon\alpha(t)\partial_y\mathbf{Q}_e \text{ at } y = 0.$$

Notice that the factor α depends on the geometry which changes with time. However, here time only acts as a parameter and the free boundary does not appear explicitly. The computation requires the information about the geometry and we need to provide the law for the movement of the boundary of the cell, which we describe in the next section.
□

4.4 The transport equation

We consider the convection-diffusion equation (4.2.3) with boundary conditions (4.2.5), (4.2.6) and the movement of the boundary defined in (4.2.8). As before, we decompose the solution in the two regions, one close to Γ^ε (the inner solution) and away from it (the outer solution). For the sake of brevity, $\Delta_{xy} := \partial_{xx} + \partial_{yy}$ and $\nabla_{xy} := \partial_x \mathbf{e}_1 + \partial_y \mathbf{e}_2$. Denote the inner and outer solutions respectively by u^ε and U^ε and assume for the variables

- Inner solution (close to Γ^ε): $\quad u^\varepsilon := u^\varepsilon(x, \frac{x}{\varepsilon}, \frac{y}{\varepsilon}, t)$

- Outer solution (away from Γ^ε): $\quad U^\varepsilon := U(x, \frac{x}{\varepsilon}, y, t)$.

We make the following asymptotic ansatz:

$$u^\varepsilon = u_0 + \varepsilon u_1 + \varepsilon^2 u_2 + \cdots,$$
$$U^\varepsilon = U_0 + \varepsilon U_1 + \varepsilon^2 U_2 + \cdots,$$
$$h^\varepsilon = \varepsilon h_0 + \varepsilon^2 h_1 + \cdots.$$

4.4.1 The outer solution

We start with the outer solution. For the different terms in (4.2.3) we have (as before with $\xi = x/\varepsilon$; $\eta = y/\varepsilon$)

$$\Delta U^\varepsilon = \varepsilon^{-2}\partial_{\xi\xi}U_0 + \varepsilon^{-1}\partial_{\xi\xi}U_1 + \Delta_{xy}U_0 + \partial_{\xi\xi}U_2 + 2\varepsilon^{-1}\partial_{x\xi}U_0 + \cdots,$$
$$\mathbf{Q}^\varepsilon\nabla U^\varepsilon = \varepsilon^{-1}\mathbf{Q}_0^{(1)}\partial_\xi U_0 + \mathbf{Q}_0 \cdot \nabla_{x,y}U_0 + \cdots.$$

Inserting the asymptotic expansion in the transport equation (4.2.3), we obtain for the lowest order term, that is, the ε^{-2} term:

$$\partial_{\xi\xi}U_0 = 0$$

which combined with periodicity in ξ implies,

$$U_0 = U_0(x, y, t).$$

Similar treatment for ε^{-1} term gives,

$$\partial_{\xi\xi}U_1 = 0,$$

and imposing periodicity with respect to ξ makes it independent of ξ, that is,

$$U_1 = U_1(x, y, t).$$

The ε^0 term provides

$$\partial_t U_0 + \mathbf{Q}_0 \nabla_{xy} U_0 + Q_0^{(1)} \partial_\xi U_1 - \Delta_{xy} U_0 - 2\partial_{x\xi} U_1 - \partial_{\xi\xi} U_2 = 0. \tag{4.4.1}$$

Now integrate over ξ from 0 to 1 and noting that $U_0, \mathbf{Q}_0, U_1$ are independent of ξ and periodicity of U_2 with respect to ξ implies no contribution from that term, we obtain

$$\partial_t U_0 + \mathbf{Q}_0 \nabla_{xy} U_0 - \Delta_{xy} U_0 = 0. \tag{4.4.2}$$

4.4.2 The inner solution

Using the above asymptotic ansatz, we obtain

$$\Delta u^\varepsilon = \varepsilon^{-2} \Delta_{\xi\eta} u_0 + \varepsilon^{-1} \Delta_{\xi\eta} u_1 + 2\varepsilon^{-1} \partial_{x\xi} u_0 + 2\partial_{x\xi} u_1 + \partial_{xx} u_0 + \Delta_{\xi\eta} u_2 + \cdots,$$

$$\mathbf{q}^\varepsilon \cdot \nabla u^\varepsilon = \varepsilon^{-1} q_0^{(1)} \partial_\xi u_0 + q_0^{(1)} \partial_x u_0 + q_0^{(1)} \partial_\xi u_1 + q_1^{(2)} \partial_\eta u_0 + q_1^{(1)} \partial_\xi u_0 + \varepsilon^{-1} q_0^{(2)} \partial_\eta u_0 + q_0^{(2)} \partial_\eta u_1 + \cdots.$$

Using the above asymptotic expansions in the equation (4.2.3) for the inner region and rearranging the terms and using $\mathbf{q}_0 = 0$

$$\varepsilon^{-2} \Delta_{\xi\eta} u_0 + \varepsilon^{-1} \Delta_{\xi\eta} u_1 + \left(\partial_t u_0 - \partial_{xx} u_0 - \Delta_{\xi\eta} u_2 + q_1^{(1)} \partial_\xi u_0 + q_1^{(2)} \partial_\eta u_0 \right) = O(\varepsilon). \tag{4.4.3}$$

We separate the terms according to the different orders of ε; for the ε^{-2} term, we have

$$\Delta_{\xi\eta} u_0 = 0. \tag{4.4.4}$$

Proceeding further with ε^{-1} terms,

$$2\partial_{x\xi} u_1 + \Delta_{\xi\eta} u_1 = 0 \tag{4.4.5}$$

and the corresponding ε^0 terms provide

$$\partial_t u_0 - \partial_{xx} u_0 - \Delta_{\xi\eta} u_2 - 2\partial_{x\xi} u_1 + q_1^{(2)} \partial_\eta u_0 + q_1^{(1)} \partial_\xi u_0 = 0. \tag{4.4.6}$$

For the boundary condition (4.2.5) we get

$$-\boldsymbol{\nu}_0 \cdot \nabla_{\xi\eta} u_0 = 0, \tag{4.4.7}$$

and

$$- \boldsymbol{v}_0 \cdot \nabla_{\xi\eta} u_1 = f(u_0, h_0)(1 - \frac{u_0}{\rho}). \tag{4.4.8}$$

Using (4.4.4), the boundary condition (4.4.7), the periodicity in ξ and that U_0 does not depend on ξ, we conclude

$$u_0 = u_0(x, t).$$

For the leading order term of the normal of the oscillating boundary we have

$$\boldsymbol{v}_0(x, \xi, t) = \frac{1}{\sqrt{1 + \partial_\xi h_0(x, \xi, t)^2}} [\partial_\xi h_0(x, \xi, t), \, -1]^T.$$

Notice that the normal is dependent on time because of the change in geometry being taken into account. For any time t we denote by Γ_L and $\Gamma(T)$ respectively the lower and upper parts of the boundaries of the inner region,

$$\Gamma_L := \{(\xi, \eta) \mid 0 < \xi < 1, \, | \, , \eta = h_0(\xi)\}, \quad \Gamma(T) := \{(\xi, \eta) \mid 0 < \xi < 1, \eta = T\}. \tag{4.4.9}$$

Integrating (4.4.5) over the inner region, since by the periodicity with respect to ξ, the contributions from the u_0 term and the lateral terms cancel (corresponding to the sides $\xi = 0$ and $\xi = 1$) and we get

$$\int_{\Gamma_L} \boldsymbol{v}_0 \cdot \nabla u_1 = -\int_{\Gamma(T)} \boldsymbol{v}_0 \cdot \nabla u_1 \quad \text{for all } T > \max(h_0). \tag{4.4.10}$$

We will see that the above equation provides the effective boundary condition.

4.4.3 The matching conditions

As before, we couple the inner solutions and the outer solutions by deriving the matching conditions. We have for U^ε, the asymptotic expansion

$$U^\varepsilon(x, \xi, y, t) = U_0(x, y, t) + \varepsilon U_1(x, y, t) + O(\varepsilon^2)$$

and Taylor's expansion at $y = \varepsilon\eta$ to obtain

$$U^\varepsilon(x, \varepsilon\eta) = U_0(x, 0) + \varepsilon\eta\partial_y U_0(x, 0) + \varepsilon U_1(x, 0) + O(\varepsilon^2).$$

For the inner solution we have the asymptotic expansion

$$u^\varepsilon(x, \xi, \eta) = u_0(x, \xi, \eta) + \varepsilon u_1(x, \xi, \eta) + O(\varepsilon^2).$$

Therefore, by matching, we conclude

$$\lim_{\eta \to \infty} u_0 = U_0, \tag{4.4.11}$$

$$\lim_{\eta \to \infty} u_1 - \eta \partial_y U_0 + U_1 = 0. \tag{4.4.12}$$

and further using (4.4.12) above,

$$\lim_{\eta \to \infty} \partial_\eta u_1 = \partial_y U_0. \tag{4.4.13}$$

We use the matching conditions for deriving the effective boundary condition below.

4.4.4 The effective boundary condition

Using the matching condition (4.4.13), we obtain

$$\lim_{T \to \infty} \int_{\Gamma(T)} \boldsymbol{v}_0 \cdot \nabla u_1 = \frac{\partial U_0}{\partial y}. \tag{4.4.14}$$

Use the boundary condition at Γ_L to obtain

$$\int_{\Gamma_L} \boldsymbol{v}_0 \cdot \nabla u_1 = \int_{\Gamma_L} f(u_0, h_0)(1 - \frac{u_0}{\rho}) . \tag{4.4.15}$$

The fact that $u_0 = u_0(x, t)$ and the matching condition (4.4.11) imply $u_0 = U_0$. This leads to

$$\int_{\Gamma_L} \boldsymbol{v}_0 \cdot \nabla u_1 = \int_{\Gamma_L} f(U_0, h_0)(1 - \frac{U_0}{\rho}). \tag{4.4.16}$$

The equations (4.4.15) and (4.4.16) together with (4.4.10) provide us the effective boundary condition

$$\frac{\partial U_0}{\partial y} = \int_{\Gamma_L} f(U_0, h_0)(1 - \frac{U_0}{\rho}).$$

Note that Γ_L is a function of time t and using parametrization of the boundary, we have

$$\int_{\Gamma_L} f(U_0, h_0)(1 - \frac{U_0}{\rho}) = f(U_0, h_0)(1 - \frac{U_0}{\rho}) \int_0^1 \sqrt{1 + (\partial_\xi h_0)^2} d\xi.$$

For the movement of the boundary, using (4.2.8) for the leading order term h_0 and using the assumption that ρ is of order $O(1/\varepsilon)$, we have

$$\partial_t h_0 = f(U_0, h_0) \sqrt{1 + (\partial_\xi h_0)^2}.$$

Recalling that $\Omega = (0,1)^2$ and the definition of Γ_L in (4.4.9), the upscaled equations become,

$$\Delta Q_0 = \nabla P \quad \text{in} \quad \Omega, \tag{4.4.17}$$

$$\nabla \cdot Q_0 = 0 \quad \text{in} \quad \Omega, \tag{4.4.18}$$

$$\partial_t U_0 - \Delta U_0 + Q_0 \cdot \nabla U_0 = 0 \quad \text{in} \quad \Omega, \tag{4.4.19}$$

$$Q_0 = 0 \quad \text{at} \quad y = 0, \tag{4.4.20}$$

$$\frac{\partial U_0}{\partial y} = \int_0^1 f(U_0, h_0)(1 - \frac{U_0}{\rho})\sqrt{1 + (\partial_\xi h_0)^2} d\xi \quad \text{at} \quad y = 0, \tag{4.4.21}$$

$$\partial_t h_0 = f(U_0, h_0)\sqrt{1 + (\partial_\xi h_0)^2} \quad \text{for} \quad t > 0, x \in (0,1), \xi \in (0,1). \tag{4.4.22}$$

4.5   Numerical simulations

To study the approximation of the upscaled equations to the original equations, we make the following choices for the geometry. Initially, $\Gamma^\varepsilon(t = 0)$ is defined as follows:

$$\Gamma^\varepsilon = \{(x,y) : x \in (0,1) \; y = \varepsilon \sin(2\pi\frac{x}{\varepsilon})\}$$

and we conduct the numerical experiments for different ε. We choose a linear rate for the reaction, specifically,

$$f(u,h) = ku,$$

and choose $\rho = 50$ so that $\frac{1}{\rho}$ is of order ε. This ensures that the deposition profile retains the roughness of the boundary. Furthermore, for the equations, we choose the following parameters:

$$k = 0.5; \; \mathbf{q}(0,y,t) = 10(y - h(0,t))(1 - y)\mathbf{e}_1.$$

For the computations for (4.2.1)-(4.2.3), we use finite element method with BDF time stepping for solving the equations. Since, the geometry changes with time, we use the Arbitrary Lagrangian Eulerian (ALE) method to solve the problem on a moving domain. This method is a generalization of Eulerian and Lagrangian descriptions of the free boundaries. We use ALE method as implemented in the COMSOL Multiphysics package [64], with Laplacian smoothing [42]. For more details on ALE method we refer to [42].

For the upscaled equations (4.4.19) with the boundary condition (4.4.21), we use finite

difference with implicit in time for the diffusion and convection term and explicit time stepping for the reaction term. Note that for the upscaled geometry, we have an explicit solution for Stokes equation (4.4.17),(4.4.18) under the given conditions, namely, the parabolic inlet profile and no-slip boundary conditions on the lateral flat boundaries (4.4.20);

$$\mathbf{Q}_0 = 10y(1 - y)\mathbf{e}_1.$$

Also, for (4.4.22) we use time-explicit discretization. For the sake of convenience, as the geometry is simple, we implement the scheme in Matlab [90].

For the numerical simulations, we consider the following situations.

4.5.1 Concentration at the boundary

We compute the full solution for $\varepsilon = 0.1, 0.04, 0.02$ and plot u^ε and u at the boundary Γ^ε and $y = 0$ boundary of Ω respectively at $t = 0.5$. The plot is shown in Figure 4.2. Due to the oscillations in the boundary, we have the boundary layer and the maximum error takes place at the boundary itself. We compute the concentration at the oscillating boundary for given ε and then plot it against the upscaled concentration u at $y = 0$. Because of the oscillating boundary, the concentration has an oscillating profile while the upscaled concentration has a monotonic profile; however, as ε decreases, u^ε converges to u.

4.5.2 Error at the boundary

Next, we consider the $L^2(0, 1)$ error at the boundary at $t = 0.5$. Specifically, we propose the following convergence rate for the error

$$\|u^\varepsilon - u\|_{L^2(0,1)} \leq C\varepsilon^\alpha.$$

Numerical experiments show the following results:

Where we compute

$$\alpha(i) = \frac{\log(error(i)) - \log(error(i-1))}{\log(\varepsilon(i)) - \log(\varepsilon(i-1))}, \quad i = 2, \ldots, 5.$$

In Table 4.1 we give the values of the error as well as the convergence rate α computed from the preceding formula. The convergence rate is close to ε and this is expected as for linear reaction rates, H^1 convergence in Ω is of the order $\sqrt{\varepsilon}$ which suggests that we expect a better rate than $\sqrt{\varepsilon}$ for L^2 at the boundary.

4.5.3   Mass balance: full vs upscaled

Further, we compare the mass balance for the full model with the upscaled model. We define

$$\bar{u}(x) := \frac{1}{\varepsilon} \int_{\varepsilon \lfloor \frac{x}{\varepsilon} \rfloor - \frac{\varepsilon}{2}}^{\varepsilon \lfloor \frac{x}{\varepsilon} \rfloor + \frac{\varepsilon}{2}} u^\varepsilon ds$$

Observe that $\bar{u}$ provides information regarding the average concentration (and hence the flux) into one periodic unit for ε model. We compare this with the upscaled equation in Figure 4.3. We note that as ε decreases, the mass balance for the ε model tends to the upscaled one. The agreement is very good for small ε which indicates the quality of upscaling. Also, the mass balance suggests that in one periodic unit, the net amount of flux in the upscaled model approximates very well to the ε model which means that by defining a cell problem with this flux provides how to compute the deposition profile.

4.5.4   Deposition profile

The upscaled model also provides information about the deposition profile. The solution to (4.4.22) gives h_0 which after suitable rescaling is compared to h^ε. The deposition profile for the upscaled equation approximates that of the ε model and the error is of ε order. The corresponding plot is shown in Figure 4.4.

4.6   Conclusions

We have used formal asymptotic arguments to derive the upscaled equations. The model defined in a geometry with oscillating boundary is approximated by a model defined in a simpler geometry with flat boundaries. Also, the geometry changes due to the reactions taking place at the oscillating boundary have been incorporated. In the upscaled model, the geometry changes lead to time-dependent boundary condition. For
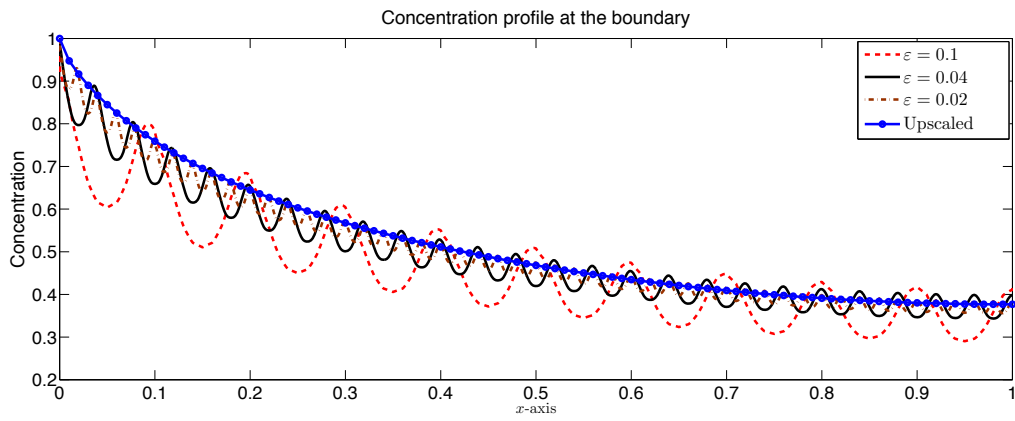
Figure 4.2: *Concentration profiles at the boundary for different ε at t = 0.5.*

ε	0.1000	0.0800	0.0600	0.0400	0.0200
error	0.0880	0.0770	0.0604	0.0415	0.0242
α		0.5984	0.8440	0.9256	0.7781

Table 4.1: *Table for L^2 error for the concentrations.*
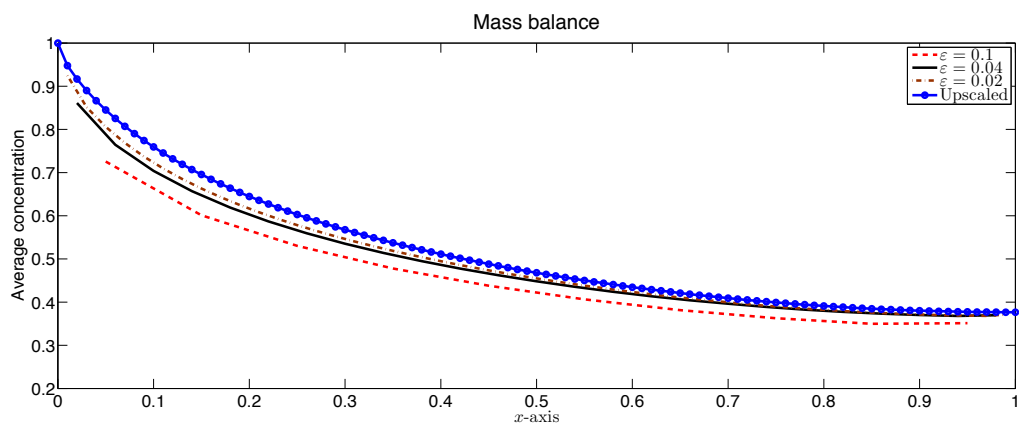
Figure 4.3: *Mass balance for different ε at t = 0.5. The average concentration is $\bar{u}$.*

Deposition profile for $\varepsilon = 0.02$
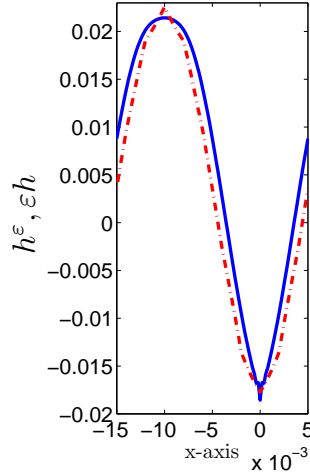
Figure 4.4: *The deposition profiles for both the upscaled model and the original ε model for ε = 0.02. In broken line is the original model while the solid represents the upscaled model.*

the flow problem, we derived upscaled equations for both the leading order and the next order approximations. For the leading order, the no-flow boundary condition at the oscillating boundary is approximated by homogeneous Dirichlet boundary condition; however, in the first order effect, the upscaled boundary condition is of slip-type with the slip parameter α implicitly dependent on time t because of the changes in geometry.

For the transport equation, the approximation model retains the equation inside the domain but with a modified boundary condition. This boundary condition takes into account the geometry of the $\varepsilon-$dependent model. For the numerical experiments, we compute the solutions for different ε and then compare the approximate solution. As ε decreases, we see that the upscaled model approximates the original model pretty well. For the concentration at the boundary, for the original problem, the profile is oscillating while for the upscaled model, the profile is monotonic. However, as ε decreases, the approximations for the concentrations at the boundary are excellent. Further, we have investigated the convergence of L^2 error for the concentrations at the boundary and we find that the order is ε. Also, the upscaling process provides a good approximation for the deposition profile.

The quality of upscaling as evidenced by the numerical experiments provides a convincing argument for using these upscaling techniques instead of solving the original problem in a complex geometry.

Chapter 5

Reactive flow in a thin strip

We consider a pore-scale model for reactive flow in a thin 2D strip, where the convective transport dominates the diffusion. Reactions take place at the lateral boundaries of the strip (the walls), where the reaction product can deposit in a layer with a non-negligible thickness compared to the width of the strip. This leads to a free boundary problem, in which the moving interface between the fluid and the deposited (solid) layer is explicitly taken into account. Using asymptotic expansion methods, we derive an upscaled, one-dimensional model by averaging in the transversal direction. The result is consistent with (Taylor dispersion) models obtained previously for a constant geometry. Finally, numerical computations are presented to compare the outcome of the effective (upscaled) model with the transversally averaged, two dimensional solution.

5.1   Introduction

We consider a pore-scale model for reactive flows in porous media. A fluid flowing through the void space of the medium (the pores) transports some dissolved ions. Reactions can take place at the pore walls, with the resulting component being attached to or detached from the pore walls. Two situations can be identified in this case. In the first situation, we assume that the reaction product forms a very thin layer that does not influence the pore space and the pore-scale models are written in a fixed geometry. Alternatively, one assumes that the thickness of the deposited layer is not negligible when compared to the pore thickness, particularly when thin pores are considered. Then the reactions can lead to variations in the pore space, and hence in the flow domain. The

---

interface separating this domain from the the solid part is a free boundary having an unknown, time dependent location. In this chapter, we consider the case with variable pore space.

The scenario described above is generic. It can be encountered, for example, in crystal precipitation and dissolution (see e.g. [45,47,104–106]), atomic layer deposition [84], chemical vapor deposition [75] and etching in a heterogenous surface [134,135], concrete carbonation [98,99] and cement hydration [30], or biological applications such as biofilm growth [107] and thrombosis [136].

In practice one is often not interested in the detailed solution on microscale, but only in the description of the average behavior of the system. In such situation, upscaled models are very useful as they describe average behavior with relatively low computational efforts. Considering the 2D strip as a representative pore-scale geometry, by the upscaled or effective model, we mean the set of equations defined in 1-D, the solution of which describes the average behavior of the thin strip. These effective equations clearly depend upon the choice of microscopic model. Moreover, the effective model also depends on the ratio of the time scales for the diffusion and the convective transport, referred to as Péclet number **Pe**. For the case of moderate or small **Pe**, when diffusion dominates or is in balance with the transport, the situation is well-understood in both fixed and variable geometry framework (see e.g. [36,45,47,48,58,61,63,101,104–106,125] and references therein). The present work builds on the the results in [105], where a model for crystal dissolution and precipitation involving free boundaries is considered in a thin strip, but for moderate **Pe**.

Here we consider the case of high Peclét number, **Pe** $>>$ 1. Then the convective transport dominates the diffusion and it is observed that the net diffusion is enhanced by the transport term itself, leading to Taylor dispersion [132]. In the fixed geometry case the Taylor dispersion mechanism is investigated in [12,19,129]. In the same context, reactive flow under dominating convective transport or reaction is studied in [4,31,32,46,93,95,126,137], presenting either a formal derivation of dispersion models, or rigorous convergence proofs for the upscaling procedure. In a similar context, in [94] an upscaled model of hyperbolic type is derived, sustained by rigorous mathematical arguments. In this chapter, we derive upscaled equations for the convection-diffusion-reaction system for the thin strip taking into account the changes in the geometry of the microscale in the transport dominated regime. Because of the changes in the geometry, the flow profile does not remain constant, which is in contrast to the Taylor dispersion models for the fixed geometry case [46]. As in [46,105], we employ the asymptotic expansion method to derive the upscaled flow and concentration equations, and in particular the Taylor dispersion terms. It is worth noting that restricting only to the leading order terms leads to an upscaled model of hyperbolic type, and dispersion terms are lost. Therefore we also take into account the first order correctors, and avoid making a specific choice of the integration constants, like in the anisotropic singular perturbation approach (see [129] and [46]). The advantage of such an upscaling is evidenced by the

numerical experiments. Figure 5.1 shows the comparison of the present upscaled model named 'Upscaled' with the other simpler macroscopic models and clearly the upscaled model derived here provides more accurate description of the average behavior given by the name **2-D Average**. We discuss the details of these numerical experiments and other macroscopic equations in Section 5.4.

The chapter is organized as follows. The modeling details are provided in Section 5.2,
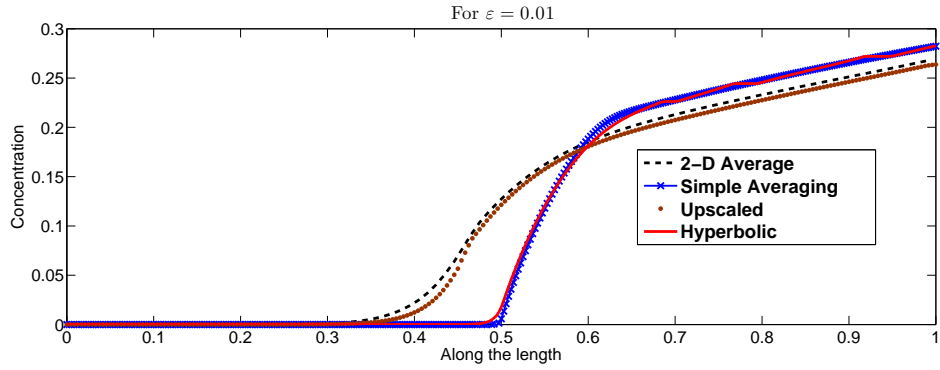
Figure 5.1: *Concentration profile using different upscaled models*

followed by the derivation of the effective model in the case of a variable geometry in Section 5.3. Section 5.4 provides numerical experiments including comparisons with other upscaled equations, whereas the Appendix A gives a derivation, using a different approach, of the upscaled model for the fixed geometry case.

5.2 The mathematical model

We start with the modeling for the two dimensional thin strip of length L [m] and width ℓ [m]. The thin strip is represented by

$$\mathcal{Y} := (0, L) \times (-\ell, \ell).$$

The boundary of the strip consists of three parts: the solid part defined by

$$\Gamma_s := (0, L) \times \{\pm\ell\},$$

the inflow part defined by

$$\Gamma_i := \{0\} \times (-\ell, \ell),$$

and the outflow defined by

$$\Gamma_o := \{L\} \times (-\ell, \ell).$$

As described above, because of the reactions (attachment/detachment) taking place at the solid boundaries of the strip, the thickness of the layer attached to the boundary may change with time. The thickness of this layer is denoted by $d(x, t)$ [m]. For simplicity, we assume that initially the layer thickness on both the upper and the lower part of Γ_s is equal. This implies symmetry with respect to the x- axis. note that for $d = \ell$, the thin strip will be blocked leading to clogging. Separate models are required to treat this case. Thus, throughout this chapter, to rule out clogging we assume that $d(x, t) < \ell$.

Because of the growth of the layers, the pore structure changes, leading to a change in the flow. We include this effect of change in flow due to the changes in geometry. The
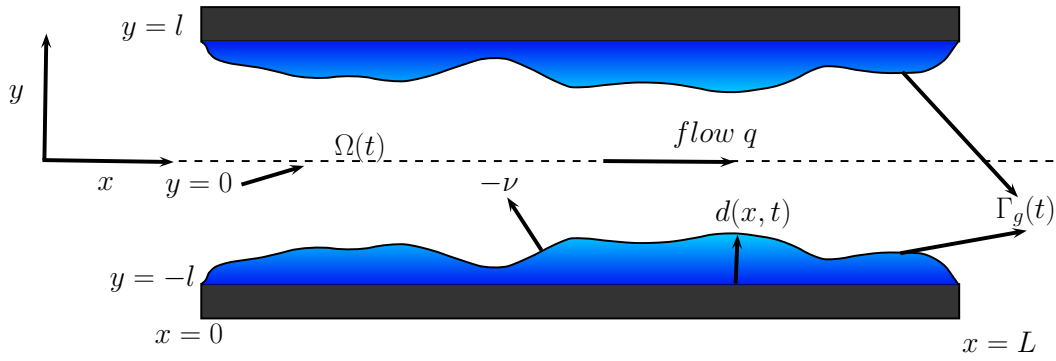
Figure 5.2: *Reactive flow in 2D thin strip (Pore Geometry), $y = 0$ is the line of symmetry.*

region occupied by the fluid is represented by

$$\Omega(t) := \{(x, y) \in \mathbb{R}^2 \mid 0 \leq x \leq L, \ -(\ell - d(x, t)) \leq y \leq (\ell - d(x, t))\}.$$

The boundary of $\Omega(t)$ contains three parts: the lateral boundary $\Gamma_g(t)$ denoting the interface between the fluid phase and the deposited layer, defined by

$$\Gamma_g(t) := \{(x, y) \in \mathbb{R}^2 \mid 0 \leq x \leq L, \ y \in \{-(\ell - d(x, t)), (\ell - d(x, t))\}\},$$

$\Gamma_{if}(t)$, the inflow boundary at $x = 0$ for the flow of the fluid phase ,

$$\Gamma_{if}(t) := \{(x, y) \in \mathbb{R}^2 \mid x = 0, \ -(\ell - d(0, t)) \leq y \leq (\ell - d(0, t))\},$$

and $\Gamma_{of}(t)$ the outflow boundary at $x = L$ for the fluid phase,

$$\Gamma_{of}(t) := \{(x, y) \in \mathbb{R}^2 \mid x = L, \ -(\ell - d(L, t)) \leq y \leq (\ell - d(L, t))\}.$$

note that $\Gamma_{if} \subset \Gamma_i$, $\Gamma_{of} \subset \Gamma_o$, but Γ_g and Γ_s need not to have common points. A sketch of the geometry is shown in Figure 5.2.

For the solutes in the thin strip, the different processes are diffusion, transport by the fluid flow, and reactions taking place at the boundaries of the strip. We denote the concentration of the solute by u $[\text{mol}/\text{m}^3]$. The convection-diffusion equation describing the transport process of the solute concentration is

$$\begin{aligned}
\partial_t u &= \nabla \cdot (D\nabla u - \mathbf{q}u), \\
u &= u_b, \quad \text{on } \Gamma_i(t), \\
\partial_x u &= 0, \quad \text{on } \Gamma_o(t),
\end{aligned} \tag{5.2.1}$$

where, u_b $[\text{mol}/\text{m}^3]$ is a non-negative constant. D $[\text{m}^2/\text{s}]$ is the diffusion coefficient and q $[\text{m}/\text{s}]$ is the flow field.

We assume that reactions such as precipitation and dissolution take place only at the interface between the fluid and the solid, that is, $\Gamma_g(t)$. The corresponding mathematical description involves the outer normal $\mathbf{v}$. At the lower part of $\Gamma_g(t)$ this is

$$\mathbf{v} = (\partial_x d, -1)^T / \sqrt{1 + (\partial_x d)^2}. \tag{5.2.2}$$

At the lower part of $\Gamma_g(t)$, mass conservation yields

$$\mathbf{v} \cdot (D\nabla u - \mathbf{q}u) = v_n(\rho - u), \tag{5.2.3}$$

where ρ $[\text{mol}/\text{m}^3]$ is the molar density of the solute in the solid phase (the adsorbed substance, or the precipitate) and v_n is the outward normal velocity of the interface. Furthermore, the normal velocity of the interface v_n $[\text{m}/\text{s}]$ is proportional to the reaction rate $f = f(u, \rho d)$,

$$\rho v_n = -f(u, \rho d). \tag{5.2.4}$$

Here f is a given function assumed to be sufficiently smooth. Similar results can be derived formally even for non-Lipschitz rates like Freundlich isotherms or multi-valued reaction rates as encountered for dissolution processes. Such rates are used in the numerical computations presented in Section 5.4.

The velocity of a point $G(t) = (x(t), -\ell + d(x(t), t))$ on the lower part of the boundary $\Gamma_g(t)$ is given by

$$G'(t) = (x'(t), \partial_x d(x(t), t)x'(t) + \partial_t d(x(t), t)).$$

Then the normal velocity v_n becomes

$$v_n = \mathbf{v} \cdot G'(t) = -\frac{\partial_t d}{\sqrt{1 + (\partial_x d)^2}}, \tag{5.2.5}$$

and (5.2.4) transforms into

$$\rho \partial_t d = f(u, \rho d) \sqrt{1 + (\partial_x d)^2}. \tag{5.2.6}$$

The flow problem is modeled by the Stokes equations,

$$\mu \Delta \mathbf{q} = \nabla p, \tag{5.2.7}$$
$$\nabla \cdot \mathbf{q} = 0, \tag{5.2.8}$$

where p [Pa] is the pressure field and μ [Pa-s] is the dynamic viscosity. At the inlet, we take a parabolic velocity profile normal to the inlet,

$$\mathbf{q}(0, y, t) = Q((\ell - d(0, t))^2 - y^2)\mathbf{e}_1,$$

where $Q > 0$ is a normalisation factor related to the total flow in the x-direction and e_1 is the unit vector along the x-axis. For the outlet we prescribe the pressure $p = 0$.

5.2.1 The dimensionless form

Before seeking for an effective model, we bring (5.2.1)-(5.2.8) to a non-dimensional form. We introduce therefore the reference time $t_{ref} := T$, coordinates $(x_{ref}, y_{ref}) := (L, \ell)$, velocity $q_{ref} := Q$, pressure p_{ref}, and concentration u_{ref}. The reference time is the characteristic convective transport time, satisfying

$$T = \frac{L}{Q}.$$

We consider the case of thin strips, characterized by the ratio of its width to the length, $\varepsilon := \ell/L$, and are interested in the limiting case $\varepsilon \searrow 0$. By an abuse of notation we define the dimensionless independent variables and parameters

$$x := x/L, \quad y := y/\ell, \quad t := t/T, \quad \rho = \rho/u_{ref},$$

and the ε-dependent dimensionless quantities

$$u^\varepsilon := u/u_{ref}, \quad d^\varepsilon := d/\ell, \quad \mathbf{q}^\varepsilon := \mathbf{q}/q_{ref},$$
$$P^\varepsilon := p/p_{ref}, \quad D := \frac{DT}{\varepsilon^{-\alpha}L^2}, \quad \mu := \frac{\mu L q_{ref}}{\ell^2 p_{ref}}.$$

Remark 5.1 To understand the particular scaling in the dimensionless D we note that the original diffusion coefficient D, and the length scale L define a diffusion time scale $T_D := L^2/D$. Here we are interested in the convection dominated regime, thus $T_D \gg T$. The ratio of these times is commonly defined as the *Péclet* number, for which we

assume

$$\mathbf{Pe} = \frac{T_D}{T} = \varepsilon^{-\alpha}$$

for some $\alpha > 0$. We only consider the case $0 < \alpha < 2$, which corresponds to the Taylor dispersion regime. note that applying this strategy for the experiments carried out by G.I. Taylor [132], the exponent α is close to 1.6 and to 1.9 (see also [46]). The case $\alpha < 0$ corresponds to a diffusion dominated flow, and there will be no gradient in the concentration in the vertical direction. The case $\alpha = 0$ has been treated in [105]. Whenever $\alpha \geq 2$, the gradient of the concentration along the width becomes too large and other upscaling approaches should be considered. $\qquad\square$

Remark 5.2 The chemical processes such as adsorption, desorption, deposition, or precipitation and dissolution, define a characteristic reaction time scale, T_R. This can be interpreted as the time needed to deposit a layer of thickness ℓ. Then one can define the Damköhler number as the ratio of T_R and T. Here we are interested in the regime of a moderate Damköhler number, thus when $T_R \approx T$. $\qquad\square$

In view of the scaling, the derivatives become

$$\partial_x \mapsto \frac{1}{L}\partial_x, \quad \partial_y \mapsto \frac{1}{\varepsilon L}\partial_y, \quad \partial_t \mapsto \frac{1}{T}\partial_t,$$

and the geometry is scaled as:

$$\Omega^\varepsilon(t) := \{(x,y) \in \mathbb{R}^2 \mid 0 \leq x \leq 1, \ -(1 - d^\varepsilon(x,t)) \leq y \leq (1 - d^\varepsilon(x,t))\}.$$

The boundaries of $\Omega^\varepsilon(t)$ are then defined by the lateral boundary $\Gamma_g^\varepsilon(t)$:

$$\Gamma_g^\varepsilon(t) := \{(x,y) \in \mathbb{R}^2 \mid 0 \leq x \leq 1, \ y \in \{-(1 - d^\varepsilon(x,t)), (1 - d^\varepsilon(x,t))\}\},$$

the inlet boundary $\Gamma_{if}^\varepsilon(t)$,

$$\Gamma_{if}^\varepsilon(t) := \{(x,y) \in \mathbb{R}^2 \mid x = 0, \ -(1 - d^\varepsilon(0,t)) \leq y \leq (1 - d^\varepsilon(0,t))\},$$

and the outflow boundary $\Gamma_{of}^\varepsilon(t)$,

$$\Gamma_{of}^\varepsilon(t) := \{(x,y) \in \mathbb{R}^2 \mid x = 1, \ -(1 - d^\varepsilon(1,t)) \leq y \leq (1 - d^\varepsilon(1,t))\}.$$

We use ε as a superscript to emphasize the dependence of the respective variable on ε. Following (5.2.2), the dimensionless unit normal $\boldsymbol{\nu}^\varepsilon$ becomes

$$\boldsymbol{\nu}^\varepsilon = (\varepsilon\partial_x d^\varepsilon, -1)^T / \sqrt{1 + (\varepsilon\partial_x d^\varepsilon)^2}.$$

By (5.2.3), (5.2.4) and (5.2.5), the boundary condition on the lower part of $\Gamma_g^\varepsilon(t)$ is transformed into

$$\varepsilon^\alpha D \left(-\varepsilon^2 \partial_x d^\varepsilon \partial_x u^\varepsilon + \partial_y u^\varepsilon \right) = \varepsilon^2 \partial_t d^\varepsilon (\rho - u^\varepsilon), \quad \text{on} \quad \Gamma_g^\varepsilon(t),$$

where we have used the no-slip boundary condition for the velocity field at $\Gamma_g^\varepsilon(t)$. In this way, the dimensionless system of equations take the form

$$\partial_t u^\varepsilon - \varepsilon^\alpha D \left(\partial_{xx} u^\varepsilon + \frac{1}{\varepsilon^2} \partial_{yy} u^\varepsilon \right) + \partial_x q^{(1)\varepsilon} u^\varepsilon + \varepsilon^{-1} \partial_y q^{(2)\varepsilon} u^\varepsilon = 0, \quad \text{in} \quad \Omega^\varepsilon(t), \qquad (5.2.9)$$

$$\partial_x q^{(1)\varepsilon} + \varepsilon^{-1} \partial_y q^{(2)\varepsilon} = 0, \quad \text{in} \quad \Omega^\varepsilon(t), \qquad (5.2.10)$$

$$\varepsilon^2 \mu \partial_{xx} \mathbf{q}^\varepsilon + \mu \partial_{yy} \mathbf{q}^\varepsilon = \left(\partial_x P^\varepsilon, \frac{1}{\varepsilon} \partial_y P^\varepsilon \right)^T, \quad \text{in} \quad \Omega^\varepsilon(t), \qquad (5.2.11)$$

$$\partial_t d^\varepsilon = \sqrt{1 + (\varepsilon \partial_x d^\varepsilon)^2} f(u^\varepsilon, \rho d^\varepsilon), \quad \text{on} \quad \Gamma_g^\varepsilon(t) \qquad (5.2.12)$$

$$\varepsilon^\alpha D \left(-\varepsilon^2 \partial_x d^\varepsilon \partial_x u^\varepsilon + \partial_y u^\varepsilon \right) = \varepsilon^2 \partial_t d^\varepsilon (\rho - u^\varepsilon), \quad \text{on} \quad \Gamma_g^\varepsilon(t), \qquad (5.2.13)$$

$$\mathbf{q}^\varepsilon = 0, \quad \text{on} \quad \Gamma_g^\varepsilon(t), \qquad (5.2.14)$$

$$u^\varepsilon(x, y, 0) = u_0, \quad \text{in} \quad \Omega^\varepsilon(0), \qquad (5.2.15)$$

$$d^\varepsilon(x, 0) = d_0(x) \quad \text{in} \quad (0, L). \qquad (5.2.16)$$

Remark 5.3 The well-posedness of the above model is in itself a non-trivial research subject. Nevertheless, this is beyond the scope of the present contribution. Here we note that the equations are based on physical laws such as the convection-diffusion equation, Stokes equation and the conservation of mass. This is a natural approach for the modeling of the advection-diffusion-reactive flows. For smooth reaction rates, assuming that initially the free boundary is smooth, one may expect sufficient regularity of the solution, including the free boundary. In this case one can prove the existence and uniqueness of solution. For a one-dimensional situation, this has been proved in [106]. The delicate part in the rigorous analysis of this model is the regularity of free boundary and remains open for future considerations. □

5.3   Upscaling

To obtain the upscaled equations, we use an asymptotic expansion for pressure, velocity, concentration and the location of the free boundary. We define the effective quantities to describe the average behavior of the concentration and the free boundary variable. As it will be seen below, the leading order terms of the expansion solve an upscaled equation of hyperbolic type. As the numerical experiments confirm, this hyperbolic model

does not describe the average behavior in a satisfactory manner, because of (Taylor) dispersion effects leading to an enhanced diffusion. To improve the hyperbolic model, we combine the leading order term and the first order term to define the effective quantities. Higher order terms are ignored in the expansion. The upscaled equation thereby obtained is of parabolic type and exhibits features of Taylor dispersion. The average of the flow profile satisfies a Darcy-type equation with an explicit dependence of the permeability on the width of the strip.

5.3.1 The case Pe = $O(\varepsilon^{-1})$

For the sake of presentation, the calculations below are performed for the case $\alpha = 1$. The general situation, when $0 < \alpha < 2$ is analogous and leads to similar results, provided at the end of Section 5.3.2.
We make the upscaling ansatz:

$$
\begin{aligned}
P^\varepsilon &= P_0 + \varepsilon P_1 + O(\varepsilon^2), \\
q^{\varepsilon(1)} &= q_0^{(1)} + \varepsilon q_1^{(1)} + O(\varepsilon^2), \\
q^{\varepsilon(2)} &= q_0^{(2)} + \varepsilon q_1^{(2)} + O(\varepsilon^2), \\
d^\varepsilon &= d_0 + \varepsilon d_1 + O(\varepsilon^2), \\
u^\varepsilon &= u_0 + \varepsilon u_1 + O(\varepsilon^2).
\end{aligned}
\tag{5.3.1}
$$

We start with the flow problem. Substituting into the Stokes law (5.2.10), (5.2.11) the expansion for $P^\varepsilon, q^{\varepsilon(i)}$ $i = 1, 2$; where $q^{\varepsilon(i)} = (q^{\varepsilon(1)}, q^{\varepsilon(2)})^T$, we obtain

$$
\begin{aligned}
\partial_x(q_0^{(1)} + \varepsilon q_1^{(1)}) + \varepsilon^{-1}\partial_y(q_0^{(2)} + \varepsilon q_1^{(2)}) &= O(\varepsilon^2), \\
\varepsilon^2 \mu \partial_{xx}(q_0^{(1)} + \varepsilon q_1^{(1)}) + \partial_{yy}(q_0^{(1)} + \varepsilon q_1^{(1)}) &= \partial_x(P_0 + \varepsilon P_1) + O(\varepsilon^2), \\
\varepsilon^2 \mu \partial_{xx}(q_0^{(2)} + \varepsilon q_1^{(2)}) + \partial_{yy}(q_0^{(2)} + \varepsilon q_1^{(2)}) &= \varepsilon^{-1}\partial_y(P_0 + \varepsilon P_1) + O(\varepsilon^2),
\end{aligned}
$$

We proceed by equating terms of similar order in the equations above. For the ε^{-1} order term in $\Omega^\varepsilon(t)$, we get

- ε^{-1} terms

$$
\partial_y q_0^{(2)} = 0, \tag{5.3.2}
$$
$$
\partial_y P_0 = 0. \tag{5.3.3}
$$

At $y = d^\varepsilon - 1$,

$$\mathbf{q}^\varepsilon = 0,$$

and together with (5.3.2)

$$q_0^{(2)} \equiv 0. \tag{5.3.4}$$

Also (5.3.3) implies

$$P_0 = P_0(x, t). \tag{5.3.5}$$

Further, in $\Omega^\varepsilon(t)$ we have

- ε^0 terms

$$\partial_x q_0^{(1)} + \partial_y q_1^{(2)} = 0 \tag{5.3.6}$$
$$\mu \partial_{yy} q_0^{(2)} = \partial_y P_1, \tag{5.3.7}$$
$$\mu \partial_{yy} q_0^{(1)} = \partial_x P_0. \tag{5.3.8}$$

- ε^1 terms

$$\mu \partial_{yy} q_1^{(1)} = \partial_x P_1. \tag{5.3.9}$$

Using (5.3.4) and (5.3.7), we conclude $P_1 = P_1(x, t)$. Combining (5.3.8) and (5.3.9), we obtain

$$\mu \partial_{yy}(q_0^{(1)} + \varepsilon q_1^{(1)}) = \partial_x(P_0 + \varepsilon P_1). \tag{5.3.10}$$

However, the boundary conditions need a careful treatment. To take into account the terms up to first order, we start with defining the effective quantity describing the free boundary variable d_e with

$$d_e = d_0 + \varepsilon d_1. \tag{5.3.11}$$

Note that with this definition $d^\varepsilon = d_e + O(\varepsilon^2)$. Other effective quantities are defined below (see (5.3.14)).

Since we are primarily interested in effects that are up to first order in ε, we define the boundary conditions at $y = d_e - 1$. Note that rewriting the boundary conditions at

$d_e - 1$ introduces an error of the order $O(\varepsilon^2)$. Using the ansatz expansion (5.3.1) and Taylor expansion around $d_e - 1$ provides

$$\begin{aligned}
0 = \mathbf{q}^\varepsilon(x, d^\varepsilon - 1, t) &= q_0(x, d^\varepsilon - 1, t) + \varepsilon q_1(x, d^\varepsilon - 1, t) + O(\varepsilon^2), \\
&= q_0(x, d_0 + \varepsilon d_1 - 1, t) + \varepsilon q_1(x, d_0 + \varepsilon d_1 - 1, t) + O(\varepsilon^2), \\
&= q_0(x, d_e - 1, t) + \varepsilon q_1(x, d_e - 1, t) + O(\varepsilon^2). \quad (5.3.12)
\end{aligned}$$

Using the boundary condition (5.3.12) at $d_e - 1$ and the symmetry condition at $y = 0$, (5.3.10) gives

$$q_0^{(1)} + \varepsilon q_1^{(1)} = (y^2 - (1 - d_e)^2)\frac{\partial_x(P_0 + \varepsilon P_1)}{2\mu} + O(\varepsilon^2). \quad (5.3.13)$$

The $O(\varepsilon^2)$ terms are due to the approximation of the boundary condition (5.3.12). Similar to d_e, we define the effective quantities

$$\begin{aligned}
u_e(x, t) &:= u_0 + \varepsilon \bar{u}_1, \\
\bar{q}_e(x, t) &:= \int_{d_e - 1}^{0} q_e^{(1)}(x, y, t)dy, \quad (5.3.14) \\
P_e(x, t) &:= P_0 + \varepsilon P_1,
\end{aligned}$$

where

$$\mathbf{q}_e := \mathbf{q}_0 + \varepsilon \mathbf{q}_1 \quad \text{and} \quad \bar{u}_1 := \frac{1}{1 - d_e}\int_{d_e - 1}^{0} u_1(x, y, t)dy.$$

The definition of u_e assumes that $u_0 = u_0(x, t)$, which will be justified below. Moreover, as will be shown below $q_e^{(2)}$ does not play any role in the upscaled equations, therefore we define $\bar{q}_e$ in terms of $q_e^{(1)}$ only. Neglecting higher order terms, (5.3.13) and (5.3.14) give

$$q_e^{(1)} = (y^2 - (1 - d_e)^2)\frac{\partial_x P_e}{2\mu}.$$

Integrating $q_e^{(1)}$ from the above expression for y over $(d_e - 1, 0)$ provides,

$$\bar{q}_e := \int_{d_e - 1}^{0} q_e^{(1)}dy = -(1 - d_e)^3\frac{\partial_x P_e}{3\mu}, \quad (5.3.15)$$

which may be interpreted as Darcy law for the thin strip case with variable geometry. Note that the permeability reported in literature [17] is proportional to $(1 - d_e)^2$ but since we integrate the velocity over the thickness of the strip, here we get it proportional to $(1 - d_e)^3$.

We consider the convection diffusion equation and first average it along the transverse

direction, and substitute the expansion for variables. Averaging (5.2.9) along the transverse direction gives

$$\int_{d^\varepsilon-1}^{0} \partial_t u^\varepsilon - \varepsilon D(\partial_{xx} u^\varepsilon + \frac{1}{\varepsilon^2}\partial_{yy} u^\varepsilon) + \partial_x(q^{(1)\varepsilon} u^\varepsilon) + \partial_y(q^{(2)\varepsilon} u^\varepsilon) = 0. \qquad (5.3.16)$$

Exchanging the derivative and the integral in the first two terms gives

$$\partial_t \int_{d^\varepsilon-1}^{0} u^\varepsilon dy + \partial_t d^\varepsilon u^\varepsilon|_{(y=d^\varepsilon-1)} - \varepsilon D \partial_x \int_{d^\varepsilon-1}^{0} \partial_x u^\varepsilon dy - (\varepsilon D \partial_x d^\varepsilon \partial_x u^\varepsilon + \frac{D}{\varepsilon}\partial_y u^\varepsilon)|_{(y=d^\varepsilon-1)}$$

$$+ \partial_x \int_{d^\varepsilon-1}^{0} q^{(1)\varepsilon} u^\varepsilon dy$$

$$+ (\partial_x d^\varepsilon q^{(1)\varepsilon} u^\varepsilon)|_{(y=d^\varepsilon-1)} + q^{(2)\varepsilon} u^\varepsilon|_{(y=d^\varepsilon-1)}^{0} = 0. \qquad (5.3.17)$$

To simplify the expression above, we use the boundary condition (5.2.13) for the third term. The last two terms vanish; the last but one term does not contribute due to no-slip boundary condition whereas the last term is 0 due to both the symmetry condition at $y = 0$ and the no-slip boundary condition at $y = d^\varepsilon - 1$. This leads to

$$\partial_t \int_{d^\varepsilon-1}^{0} u^\varepsilon dy + \partial_t d^\varepsilon \rho - \varepsilon D \partial_x \int_{d^\varepsilon-1}^{0} \partial_x u^\varepsilon dy + \partial_x \int_{d^\varepsilon-1}^{0} q^{(1)\varepsilon} u^\varepsilon dy = 0. \qquad (5.3.18)$$

Substituting the ansatz (5.3.1) in (5.3.18), and retaining the terms up to $O(\varepsilon)$, we obtain

$$\partial_t \int_{d_e-1}^{0} (u_0 + \varepsilon u_1) dy + \partial_t(d_0 + \varepsilon d_1)\rho - \varepsilon D \partial_x \int_{d_e-1}^{0} (\partial_x u_0 + \varepsilon \partial_x u_1) dy$$

$$+ \partial_x \int_{d_e-1}^{0} q_0^{(1)} u_0 + \varepsilon(q_0^{(1)} u_1 + q_1^{(1)} u_0) dy = O(\varepsilon^2). \qquad (5.3.19)$$

Observe that by retaining only two terms of the expansion, in each term of the expression (5.3.18), the remainder introduces an error of the order $O(\varepsilon^2)$. Also, changing the domain of integration from $d^\varepsilon - 1$ to $d_e - 1$ introduces an error of the order $O(\varepsilon^2)$. Adding $\varepsilon^2 q_1^{(1)} u_1$ term in the (5.3.19) we obtain up to $O(\varepsilon^2)$

$$\partial_x \int_{d_e-1}^{0} \left(q_0^{(1)} + \varepsilon q_1^{(1)}\right) u_0 + \varepsilon \left(q_0^{(1)} + \varepsilon q_1^{(1)}\right) u_1 dy = \partial_x \int_{d_e-1}^{0} (q_e^{(1)} u_0 + \varepsilon q_e u_1) dy$$

$$= \partial_x \left\{ u_e \bar{q}_e - \varepsilon \bar{u}_1 \bar{q}_e + \varepsilon \int_{d_e-1}^{0} q_e u_1 dy \right\} \qquad (5.3.20)$$

The above equation contains the unknown term u_1. For computing it, the leading order term u_0 is needed. The ε^{-1} and ε^0 terms for the convection diffusion equation using the

ansatz expansion (5.3.1) provide

$$\partial_{yy}u_0 = \partial_y q_0^{(2)} u_0, \tag{5.3.21}$$

$$\partial_t u_0 - D\partial_{yy}u_1 + \partial_x(q_0^{(1)}u_0) + \partial_y(q_1^{(2)}u_0) = 0, \tag{5.3.22}$$

and using (5.3.21) together with symmetry condition at $y = 0$, we conclude $u_0 \equiv u_0(x,t)$. Simplifying (5.3.22) using (5.3.6), we obtain

$$\partial_t u_0 - D\partial_{yy}u_1 + q_0^{(1)}\partial_x u_0 = 0. \tag{5.3.23}$$

As for the flow, we now treat the boundary condition for the convection diffusion equation. Using (5.2.13) and a Taylor expansion around $y = d_e - 1$, we have

$$
\begin{aligned}
0 &= \left\{ D(-\varepsilon^2 \partial_x d^\varepsilon \partial_x u^\varepsilon + \partial_y u^\varepsilon) - \varepsilon \partial_t d^\varepsilon (\rho - u^\varepsilon) \right\} |_{(x,d^\varepsilon-1,t)} \\
&= \left\{ D(-\varepsilon^2 \partial_x d^\varepsilon \partial_x u^\varepsilon + \partial_y u^\varepsilon) - \varepsilon \partial_t d^\varepsilon (\rho - u^\varepsilon) \right\} |_{(x,d_e-1,t)} + O(\varepsilon^2) \\
&= \left\{ D(-\varepsilon^2 \partial_x d_0 \partial_x u_0 + \partial_y u_0 + \varepsilon \partial_y u_1) - \varepsilon \partial_t d_0 (\rho - u_0) \right\} |_{(x,d_e-1,t)} + O(\varepsilon^2).
\end{aligned}
$$

Since $u_0 = u_0(x,t)$, we conclude

$$D\partial_y u_1 - \partial_t d_0(\rho - u_0)|_{y=d_e-1} = O(\varepsilon). \tag{5.3.24}$$

Integrating (5.3.23) over y from $d_e - 1$ to 0 and use the symmetry condition at $y = 0$ and boundary condition at $y = d_e - 1$ to get the compatibility condition

$$(1 - d_e)\partial_t u_0 + \partial_t d_0(\rho - u_0) + \int_{d_e-1}^{0} q_0^{(1)}\partial_x u_0 dy = O(\varepsilon). \tag{5.3.25}$$

The above equation provides the leading order solution for the convection-diffusion equation. However, as remarked earlier, to improve the upscaled model we also include the first order term. To do so, we multiply (5.3.23) by $1 - d_e$ and subtract from (5.3.25) and then integrating twice, first from 0 to y and then from $d_e - 1$ to y using the symmetry conditions at $y = 0$,

$$\partial_t d_0 \frac{(\rho - u_0)y^2}{2} + (1 - d_e)Du_1 + \left(\frac{(1 - d_e)^3 y^2}{6} - \frac{(1 - d_e)y^4}{12} \right) \frac{\partial_x P_0}{2\mu} \partial_x u_0 + C(x,t) = O(\varepsilon), \tag{5.3.26}$$

where $C(x,t)$ is a constant of integration. Disregarding $O(\varepsilon)$ terms, u_1 is given by

$$u_1 = \frac{-C}{D(1 - d_e)} + \frac{\Xi(y)}{D(1 - d_e)} + O(\varepsilon),$$

where $\Xi(y)$ is defined as

$$\Xi(y) = -\partial_t d_0(\rho - u_0)\frac{y^2}{2} - \left\{\frac{(1-d_e)^3 y^2}{6} - \frac{(1-d_e)y^4}{12}\right\}\frac{\partial_x P_0 \partial_x u_0}{2\mu}. \qquad (5.3.27)$$

Straightforwardly

$$\int_{d_e-1}^0 \Xi(y)dy = \frac{(1-d_e)^3}{180}\left\{-30\partial_t d_0(\rho - u_0) - 7\frac{(1-d_e)^3}{2\mu}\partial_x P_0 \partial_x u_0\right\}, \qquad (5.3.28)$$

and hence

$$\bar{u}_1 = \frac{1}{1-d_e}\left\{\frac{-C}{D} + \frac{(1-d_e)^2}{180D}\left\{-30\partial_t d_0(\rho - u_0) - 7(1-d_e)^3\frac{\partial_x P_0 \partial_x u_0}{2\mu}\right\}\right\} + O(\varepsilon),$$
$$(5.3.29)$$

where $\bar{u}_1$ is defined in (5.3.14). The last term in (5.3.20) becomes

$$\int_{d_e-1}^0 q_e^{(1)}u_1 dy = \int_{d_e-1}^0 (y^2 - (1-d_e)^2)\frac{\partial_x P_e}{2\mu}\left\{\frac{-C}{D(1-d_e)} + \frac{\Xi(y)}{D(1-d_e)}\right\}dy + O(\varepsilon). (5.3.30)$$

Clearly

$$\int_{d_e-1}^0 (y^2 - (1-d_e)^2)\Xi(y)dy = \frac{(1-d_e)^5}{630}\left\{42\partial_t d_0(\rho - u_0) + 11(1-d_e)^3\frac{\partial_x P_0}{2\mu}\partial_x u_0\right\}.$$
$$(5.3.31)$$

Using (5.3.28),(5.3.30) , (5.3.31), and (5.3.20) give

$$\partial_x\left\{u_e\bar{q}_e - \varepsilon\bar{u}_1\bar{q}_e + \varepsilon\int_{d_e-1}^0 q_e^{(1)}u_1 dy\right\}$$

$$= \partial_x(u_e\bar{q}_e)$$

$$\quad - \frac{\varepsilon}{1-d_e}\partial_x\left\{\frac{-\partial_x P_e}{3\mu}(1-d_e)^3\left\{\frac{-C}{D} + \frac{(1-d_e)^2}{180D}\left\{-30\partial_t d_0(\rho - u_0) - 7(1-d_e)^3\partial_x u_0\frac{\partial_x P_0}{2\mu}\right\}\right\}\right\}$$

$$\quad + \varepsilon\partial_x\left\{\frac{C}{D}\frac{\partial_x P_e}{3\mu}(1-d_e)^2 + \frac{(1-d_e)^4}{630D}\frac{\partial_x P_e}{2\mu}\left\{42\partial_t d_0(\rho - u_0) + 11(1-d_e)^3\partial_x u_0\frac{\partial_x P_0}{2\mu}\right\}\right\} + O(\varepsilon)$$

$$= \partial_x\left\{u_e\bar{q}_e + \varepsilon\frac{\partial_x P_e}{D\mu}\left\{-\frac{1}{45}(1-d_e)^4\partial_t d_0(\rho - u_0) + (-\frac{4}{945})(1-d_e)^7\frac{\partial_x P_e}{2\mu}\partial_x u_0\right\}\right\} + O(\varepsilon).$$

Hence, the averaged equation reads

$$\partial_t \int_{d_e-1}^0 (u_0 + \varepsilon u_1)dy + \partial_t(d_0 + \varepsilon d_1)\rho - \varepsilon D\partial_x \int_{d_e-1}^0 (\partial_x u_0 + \varepsilon \partial_x u_1)u_1 dy$$

$$+ \partial_x \int_{d_e-1}^0 q_0^{(1)} u_0 + \varepsilon(q_0^{(1)} u_1 + q_1^{(1)} u_0)dy = O(\varepsilon^2). \qquad (5.3.32)$$

Recalling (5.3.14), this translates into

$$\partial_t((1-d_e)u_e) + \partial_t(d_e\rho) - \varepsilon D\partial_x((1-d_e)\partial_x u_e)$$

$$+ \partial_x \left\{ u_e \bar{q}_e + \varepsilon \frac{\partial_x P_e}{D\mu} \left\{ -\frac{1}{45}\partial_t d_0(\rho - u_0)(1-d_e)^4 - \frac{4}{945}(1-d_e)^7 \partial_x u_0 \frac{\partial_x P_e}{2\mu} \right\} \right\} = O(\varepsilon^2).$$

For d_e formally by using Taylor expansion of $f(u^\varepsilon, d^\varepsilon)$ around (u_e, d_e)

$$\partial_t \rho d_e = f(u^\varepsilon, \rho d^\varepsilon)$$
$$= f(u_0 + \varepsilon \bar{u}_1, \rho(d_0 + \varepsilon d_1)) + \varepsilon(u_1|_{y=d_e-1} - \bar{u}_1)\partial_1 f(u_0 + \varepsilon \bar{u}_1, \rho(d_0 + \varepsilon d_1)) + O(\varepsilon^2)$$
$$= f(u_e, \rho d_e) + \varepsilon(u_1|_{y=d_e-1} - \bar{u}_1)\partial_1 f(u_e, \rho d_e) + O(\varepsilon^2). \qquad (5.3.33)$$

By (5.3.26) and (5.3.29) we have

$$u_1|_{y=d_e-1} - \bar{u}_1 = (1-d_e) \left\{ -\frac{1}{3D}(\rho - u_e)\partial_t d_e + \frac{1}{15D}\varepsilon \bar{q}_e \partial_x u_e \right\} + O(\varepsilon),$$

where we have used the Darcy law (5.3.15). Hence the upscaled equation for $\partial_t d_e$ becomes

$$\partial_t(\rho d_e) = f(u_e, \rho d_e) + \varepsilon(1-d_e) \left\{ -\frac{1}{3D}(\rho - u_e)\partial_t d_e + \frac{1}{15D}\bar{q}_e \partial_x u_e \right\} \partial_1 f(u_e, \rho d_e) + O(\varepsilon^2).$$
$$(5.3.34)$$

For convenience, we write at one place, the upscaled equations, equations (5.3.15),(5.3.32) and (5.3.34),

$$\bar{q}_e = -(1-d_e)^3 \frac{\partial_x P_e}{3\mu} + O(\varepsilon^2),$$
$$\partial_t((1-d_e)u_e + d_e\rho) = \partial_x \left\{ -u_e \bar{q}_e + \varepsilon(1-d_e)D(1 + \frac{2\bar{q}_e^2}{105D^2})\partial_x u_e - \varepsilon \frac{\bar{q}_e}{15D}\partial_t d_e(\rho - u_e)(1-d_e) \right\}$$
$$+ O(\varepsilon^2),$$
$$\partial_t(\rho d_e) = f(u_e, \rho d_e) + \varepsilon(1-d_e) \left\{ -\frac{1}{3D}(\rho - u_e)\partial_t d_e + \frac{1}{15D}\bar{q}_e \partial_x u_e \right\} \partial_1 f(u_e, \rho d_e)$$
$$+ O(\varepsilon^2).$$

To eliminate the pressure from the first equation, we take a small slice of the half-strip of length δx, denoted by

$$Y = \{(v, w) \mid x_1 \le v \le x_1 + \delta x, |w| \le (1-d_e)\}.$$

The continuity equation and the divergence theorem give

$$0 = \int_Y \nabla \cdot \mathbf{q}^\varepsilon = \int_{-(1-d_e)}^{1-d_e} q_e^{(1)}|_{x=x_1+\delta x} dy - \int_{-(1-d_e)}^{1-d_e} q_e^{(1)}|_{x=x_1} dy + O(\varepsilon^2),$$

where we have used the no-slip boundary condition to make the boundary terms on the lateral surface equal to 0. Dividing by δx, and then taking the limit $\delta x \to 0$, we obtain

$$\partial_x \bar{q}_e = O(\varepsilon^2).$$

Hence the upscaled system of equations after neglecting $O(\varepsilon^2)$ terms from the effective equations for $\bar{q}_e, u_e, d_e$ become

$$\partial_x \bar{q}_e = 0,$$

$$\partial_t((1-d_e)u_e + d_e\rho) = \partial_x \left\{ -u_e\bar{q}_e + \varepsilon(1-d_e)D(1 + \frac{2\bar{q}_e^2}{105D^2})\partial_x u_e - \varepsilon\frac{\bar{q}_e}{15D}\partial_t d_e(\rho - u_e)(1-d_e) \right\},$$

$$\partial_t(\rho d_e) = f(u_e, \rho d_e) + \varepsilon(1-d_e) \left\{ -\frac{1}{3D}(\rho - u_e)\partial_t d_e + \frac{1}{15D}\bar{q}_e\partial_x u_e \right\} \partial_1 f(u_e, \rho d_e).$$

Remark 5.4 To compare the upscaled model for the variable geometry with that in the fixed geometry case, we refer to [46], where the following system is derived (also see the Appendix A for an alternative approach)

$$\partial_t(u_e + v_e) = \partial_x \left\{ -u_e\bar{q}_e + \varepsilon D(1 + \frac{2\bar{q}_e^2}{105D^2})\partial_x u_e - \varepsilon\frac{1}{15}\frac{\bar{q}_e}{D}f(u_e, v_e) \right\}$$

$$(1 + \varepsilon\frac{1}{3D}\partial_1 f(u_e, v_e))\partial_t v_e = f(u_e, v_e) + \varepsilon\frac{\bar{q}_e}{15D}\partial_x u_e\partial_1 f(u_e, v_e).$$

Following the ideas in [105], where in the case $\mathbf{Pe} = \mathbf{O(1)}$ the fixed geometry case is obtained as the limit of a variable geometry model, we assume that $d_e \searrow 0(\rho \to \infty)$ whereas $\rho d_e \to v_e$. Then the upscaled equations for the variable geometry case reduce to that of the fixed geometry case.   □

5.3.2   The case Pe = $O(\varepsilon^{-\alpha})$

In Section 5.3.1, we have only considered the case $\alpha = 1$. This choice was made strictly for the ease of presentation. However, other scalings may be required for different applications. For example, bringing the experiments carried out by Taylor [132] to a dimensionless model leads to either $\alpha = 1.6$, or $\alpha = 1.9$ (see [46]). Nevertheless, the asymptotic expansion procedure in the previous section can be extended to the case

$\alpha \in (0, 2)$, but with a slightly different expansion:

$$P^\varepsilon = P_0 + \varepsilon P_1 + O(\varepsilon^2),$$
$$q^{\varepsilon(1)} = q_0^{(1)} + \varepsilon q_1^{(1)} + O(\varepsilon^2),$$
$$q^{\varepsilon(2)} = q_0^{(2)} + \varepsilon q_1^{(2)} + O(\varepsilon^2),$$
$$d^\varepsilon = d_0 + \varepsilon^{2-\alpha} d_1 + O(\varepsilon^{2(2-\alpha)}),$$
$$u^\varepsilon = u_0 + \varepsilon^{2-\alpha} u_1 + O(\varepsilon^{2(2-\alpha)}).$$

For $\alpha \geq 2$ we enter into the turbulent mixing regime, and the approach considered in this chapter fails.

Following the steps outlined in the Section 5.3.1, analogous to (5.3.19) we obtain

$$\partial_t \int_{d^\varepsilon-1}^0 (u_0 + \varepsilon^{2-\alpha} u_1) dy + \partial_t (d_0 + \varepsilon^{2-\alpha} d_1)\rho - \varepsilon^\alpha D \partial_x \int_{d^\varepsilon-1}^0 (\partial_x u_0 + \varepsilon^{2-\alpha} \partial_x u_1) dy$$
$$+ \partial_x \int_{d^\varepsilon-1}^0 q_0^{(1)} u_0 + (\varepsilon^{2-\alpha} q_0^{(1)} u_1 + \varepsilon q_1^{(1)} u_0) dy = +O(\varepsilon^{3-\alpha}).$$

$$(5.3.35)$$

and the last term in the above can be expressed similarly to (5.3.20)

$$\partial_x \int_{d_e-1}^0 \left(q_0^{(1)} + \varepsilon q_1^{(1)} \right) u_0 + \varepsilon^{2-\alpha} \left(q_0^{(1)} + \varepsilon q_1^{(1)} \right) u_1 dy = \partial_x \left\{ u_e \bar{q}_e - \varepsilon^{2-\alpha} \bar{u}_1 \bar{q}_e + \varepsilon^{2-\alpha} \int_{d_e-1}^0 q_e^{(1)} u_1 dy \right\}.$$

$$(5.3.36)$$

Defining the effective quantities as

$$d_e := d_0 + \varepsilon^{2-\alpha} d_1,$$
$$u_e := u_0 + \varepsilon^{2-\alpha} \langle u_1 \rangle,$$
$$\bar{q}_e = \int_{d_e-1}^0 q_e^{(1)}(x, y, t) dy,$$
$$P_e := P_0 + \varepsilon P_1,$$

where,

$$\mathbf{q}_e := \mathbf{q}_0 + \varepsilon \mathbf{q}_1, \quad \text{and} \quad \langle u_1 \rangle = \frac{1}{1 - d_e} \int_{d_e-1}^0 u_1(x, y, t) dy,$$

the upscaled equations are

$$\partial_x \bar{q}_e = 0,$$
$$\bar{q}_e = -\frac{(1 - d_e)^3}{3\mu} \partial_x P_e.$$

$$\partial_t((1-d_e)u_e + d_e\rho) = \partial_x \left\{ -u_e\bar{q}_e \right\}$$

$$+ \partial_x \left\{ \varepsilon^\alpha(1-d_e)D(1 + \varepsilon^{2(1-\alpha)}\frac{2\bar{q}_e^2}{105D^2})\partial_x u_e \right\}$$

$$+ \partial_x \left\{ -\varepsilon^{2-\alpha}\frac{\bar{q}_e}{15D}\partial_t d_e(\rho - u_e)(1-d_e) \right\},$$

$$\partial_t(\rho d_e) = f(u_e, \rho d_e)$$

$$+ \varepsilon^{2-\alpha}(1-d_e)\left\{ -\frac{1}{3D}(\rho - u_e)\partial_t d_e + \frac{1}{15D}\bar{q}_e\partial_x u_e \right\}\partial_1 f(u_e, \rho d_e)$$

It is again to be observed that Darcy equation is retrieved by upscaling of the flow field and for the simple geometry of the strip, we obtain an explicit characteristic dependence of the permeability on the geometry, namely $\frac{(1-d_e)^3}{3}$.

The traveling wave solution approach for the upscaled equations in the case of moderate Peclét number has been studied in [105]. For the fixed geometry situation, a detailed analysis has been carried out in [45]. The analysis for the present, variable geometry model is a subject of future consideration.

5.4   Numerical validation

For the numerical experiments, we consider the case of crystal precipitation and dissolution. For this case, the reaction rate function $f(u,v)$ is given by

$$f(u,v) = k(r_p - r_d),$$

where r_p and r_d denote respectively the precipitation and dissolution rates. Here we take $r_p = r(u) = u$, whereas for r_d we follow [45] and choose $r_d = \frac{1}{2}\tilde{H}(v)$, with $\tilde{H}(\cdot)$ denoting the Heaviside graph. Since the reaction rate in this form is multivalued, we use a regularized form $H(\cdot)$ defined as,

$$H(v) = \begin{cases} 0, & v < 0, \\ \dfrac{v}{\delta}, & 0 < v < \delta, \\ 1, & v > 0, \end{cases}$$

where, for instance, $\delta = o(\varepsilon)$.

For comparison purposes, different macroscopic equations can be considered.

5.4.1   Hyperbolic Model

The first one is obtained by asymptotic expansion as carried out in the previous section, but considering only the leading order term. This involves a hyperbolic equation for the solute,

$$\partial_x \bar{q}_e = 0, \qquad\qquad \textbf{(Hyperbolic)}$$
$$\partial_t((1 - d_e)u_e + d_e\rho) = \partial_x \left\{ -\bar{q}_e u_e \right\}, \qquad\qquad (5.4.1)$$
$$\partial_t(\rho d_e) = k(r(u_e) - H(\rho d_e)).$$

We will refer this model as "**Hyperbolic**" for the numerical computations.

It is relevant to mention here that the Hyperbolic model is named only to indicate that the diffusion term is absent. This is different from the hyperbolic model some authors have used to denote the upscaled model containing mixed second order derivative term, see e.g. [94].

5.4.2   Simple Averaging

Next, a straightforward upscaling by transverse averaging provides an effective model that does not include the dispersion term, but only the original parabolic terms. Furthermore, for the chemical reactions we obtain a straightforward model. This effective model will be named in what follows as "**Simple Averaging**".

$$\partial_x \bar{q}_e = 0, \qquad\qquad \textbf{(Simple Averaging)}$$
$$\partial_t((1 - d_e)u_e + d_e\rho) = \partial_x \left\{ -u_e\bar{q}_e + \varepsilon(1 - d_e)D\partial_x u_e \right\}, \qquad\qquad (5.4.2)$$
$$\partial_t(\rho d_e) = k(r(u_e) - H(\rho d_e)).$$

5.4.3   Upscaled Model

Finally, we use the upscaled model derived for the variable geometry case:

$$\partial_x \bar{q}_e = 0, \qquad\qquad\qquad\qquad \textbf{(Upscaled)}$$
$$\partial_t((1 - d_e)u_e + d_e\rho) = \partial_x \left\{ -u_e\bar{q}_e + \varepsilon(1 - d_e)D(1 + \frac{2\bar{q}_e^2}{105D^2})\partial_x u_e - \varepsilon\frac{\bar{q}_e}{15D}\partial_t d_e(\rho - u_e)(1 - d_e) \right\},$$
$$(5.4.3)$$
$$\partial_t(\rho d_e) = k(r(u_e) - H(\rho d_e)) + \varepsilon(1 - d_e)\left\{ -\frac{1}{3D}(\rho - u_e)\partial_t d_e + \frac{1}{15D}\bar{q}_e\partial_x u_e \right\}k.$$

Henceforth, for the numerical computations, we name it as "**Upscaled**".

5.4.4   2-D Average

To compare the upscaled equations with the average of the solution of microscopic equations, we first compute the full solution of the system of equations (5.2.9) - (5.2.14) with the given initial data. To obtain the 2-D average, we compute

$$\bar{u} = \frac{1}{2(1-d^\varepsilon)} \int_{-(1-d^\varepsilon)}^{(1-d^\varepsilon)} u^\varepsilon dy. \tag{5.4.4}$$

The above computed quantity $\bar{u}$ is referred to as the 2-D average concentration. This together with the free boundary variable d^ε constitute "**2-D Average**".

5.4.5   **Numerical Computations**

For computations on the microscale model equations (5.2.9)-(5.2.14), we use the Arbitrary Lagrangian Eulerian (ALE) method. This method can be used to solve the partial differential equations on a moving domain and is a generalization of Eulerian and Lagrangian descriptions of the free boundaries. We use the ALE method as implemented in the COMSOL Multiphysics package [64], with Laplacian smoothing [42]. We refer to [42] for more details and survey of the ALE methods.

The computations are carried out for different values of D and ε. The solution of the full 2D model (microscopic model equations (5.2.9)-(5.2.14)) is approximated by a BDF time stepping combined with a finite element method (FEM). Further, the (numerical) solutions of the different upscaled models namely "**Hyperbolic** (5.4.1), **Simple Averaging** (5.4.2), **Upscaled** (5.4.3)" described above (the concentration u_e and the free boundary variable d_e) are compared at certain times with the transversal average of the concentration $\bar{u}$ (5.4.4), as well as the free boundary variable d^ε for the 2D strip.
The numerical computations for the 2D strip are assuming an initial equilibrium situation, meaning that no precipitation or dissolution is encountered. In the specific situation considered here, the equilibrium is achieved for $u = 0.5$ when $r_p = \frac{1}{2}H(v)$, meaning that the precipitation and the dissolution rates are equal. This situation is perturbed by imposing the concentration 0 at the inlet. We also assume that initially the system includes a deposition layer of thickness d_I at the lateral boundaries. The inlet flow profile is assumed parabolic, and the total water flux into the system is $2\varepsilon(1-d_I)\bar{q}_e$. Since the fluid flowing in has a low concentration of solute, dissolution will take place at the lateral boundary beginning from the inlet boundary side. Also, the strip becomes wider as the dissolution proceeds. Starting with a width $2\varepsilon(1-d_I)$, after having dis-

solved the entire precipitate the strip becomes 2ε wide.

For the numerical experiments, we take the following values: $\bar{q}_e = 1; L = 1; k = 1; \rho = 1$, whereas the initial solute concentration and layer thickness are $u(x, 0) = 0.5$ and $d(x, 0) = d_I = 0.2$.

We consider four situations. First we show that all three upscaled models agree well when ε tends to 0. Second, we fix ε, $\bar{q}_e$ and D and vary α, which basically means varying the diffusion $\varepsilon^\alpha D$. This provides information regarding the differences in results of different upscaled models with respect to variations in the value of α. Accordingly, it can be used to make informed choices for the upscaled equations for given parameters of α, ε, $\bar{q}_e$ and D. Next, we fix D, $\bar{q}_e$, α, and vary ε to study the comparisons of the upscaled models with the 2D strip. Finally, we provide the comparison with the fixed geometry and the variable geometry upscaled equations and show that the choice of the appropriate upscaled models is dictated essentially by ρ.
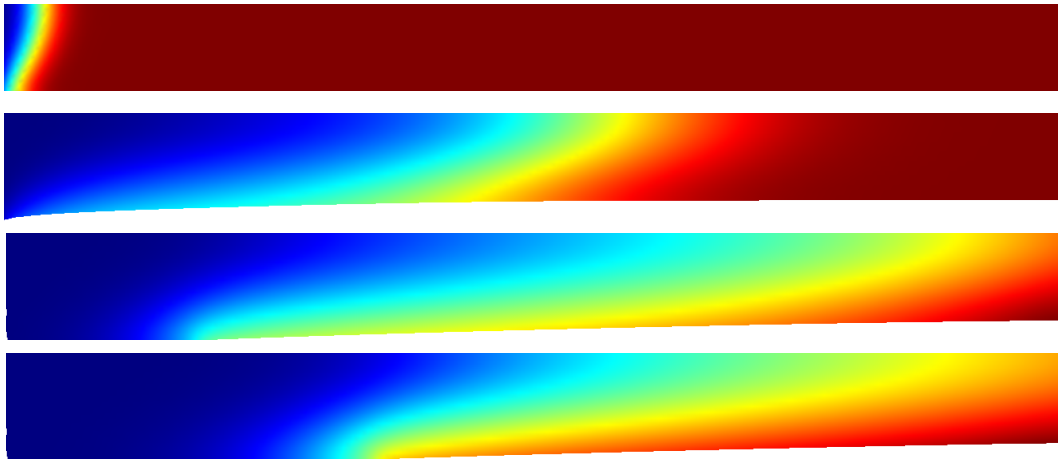
Figure 5.3: *Time snapshots showing the dissolution process taking place in the thin strip at different times, the top figure is at $t = 0.02$ and the bottom one is at $t = 1$. The parameter values are $\varepsilon = 0.1$ $D = 0.3$, $\alpha = 1.5$, $\bar{q}_e = 1$ $d(x, 0) = 0.2$. Note that the dissolution process starts at the left end and the width of the strip increases gradually as the dissolution front is moving to the right. The initial thickness of the strip is 0.08 and the final thickness after the dissolution process has finished, is 0.1.*

Figure 5.3 is the snapshot for different times for the dissolution process taking place in a thin half-strip. Close to the beginning, at $t = 0.02$, the strip has almost uniform concentration in the strip and the dissolution process starts taking place from the left end $(x = 0, y = d - \varepsilon)$, and this process continues until the entire precipitate is dissolved. At $y = 0$ symmetry conditions are used; therefore no changes in the geometry are encountered there.

Figures 5.4 and 5.5 illustrate the convergence of the different upscaled models **Simple Averaging** (5.4.2) and **Upscaled** (5.4.3) to the hyperbolic model (5.4.1) as $\varepsilon \to 0$. Letting ε decrease, it is easy to check formally that all upscaled models reduce to the hyperbolic model.

Further, the numerical results for $\alpha = 1$ and $\alpha = 1.5$ are compared in Figure 5.6 (presenting the concentration profiles) and 5.7, where the free boundary variable d is presented. As can be clearly observed, the effective model derived in Section 5.3.2 performs better than the simple averaging or the hyperbolic model.

For $\varepsilon = 0.01$, the 2D averaged concentration profile is compared to the effective concentrations in Figure 5.8. Similarly, in Figure 5.7 the corresponding free boundaries d are compared. Again, the effective model derived here outperforms the other upscaled models.

5.4.6   Fixed geometry versus variable geometry

When the changes in the geometry on the pore scale are ignored, we refer it as the fixed geometry case. The upscaling for the fixed geometry as mentioned in remark above leads to the following system of equations.

$$\partial_t(u_e + v_e) = \partial_x \left\{ -u_e \bar{q}_e + \varepsilon D(1 + \frac{2\bar{q}_e^2}{105 D^2})\partial_x u_e - \varepsilon \frac{1}{15}\frac{\bar{q}_e}{D}f(u_e, v_e) \right\} \quad \textbf{(Fixed Geometry)}$$

$$\partial_t v_e = f(u_e, v_e) + \varepsilon(-\frac{1}{3D}\partial_t v_e + \frac{1}{15D}\bar{q}_e \partial_x u_e)\partial_1 f(u_e, v_e). \quad (5.4.5)$$

To understand when it becomes important to take into account the variable geometry, we compare the solutions of **Upscaled** (5.4.3) model (for $\alpha = 1$) with the solutions of (5.4.5) for different values of ρ (density of salt in the crystal). In Figures 5.9 and Figure 5.10 the concentration, respectively the free boundary for the upscaled models in the fixed geometry, respectively variable geometry are compared. We see that as $\rho = 10$, the solutions do not differ much whereas for $\rho = 1$ case clearly indicates that the changes in the geometry can not be ignored and must be taken into account. We see that as ρ increases the difference between the two models reduce. This is consistent with the observation that in the limit $\rho \searrow \infty$, the variable geometry case reduces to the fixed geometry case. This comparison provides us useful criterion to decide if the changes in the pore geometry can be ignored.

5.5   Conclusion and outlook

In this chapter, we have derived an upscaled model for the reactive flow in a thin strip, in the case of a dominating convective transport. For simplicity, the model is presented in the case of a simple, two dimensional domain (a strip), but takes into account the changes in the microscale geometry that are due to the reactions taking place at the lateral boundaries (the pore walls). The effective model involves a dispersion term that is similar to the Taylor dispersion, whereas the transport is enhanced by reactions.

In deriving the effective equations we use formal asymptotic methods. The theoretical derivation is sustained by numerical computations, which are carried out in different cases. In all cases the results provided by the upscaled model derived here are compared with the ones obtained by other, simpler upscaled models, and with the (transversal) average of the solution to the full problem. Specifically, the following situations are considered:

- ϵ, the ratio of the width of the strip and its length, is moderate or small.

- *Pe*, the ratio of the diffusive time scale and of the convective one, is of order ε^{-1}, or larger (e.g. $\varepsilon^{-1.5}$).

- ρ, the ratio of the density of an element in the adsorbed substance, and the solute density is moderate, or high.

The following conclusions can be drawn:

- The effective model derived here provides results in excellent agreement with the averaged, solutions of the original problem.

- If ε is moderately small, the present upscaling outperforms other (simpler) models; if ε becomes very small, all models provide similar results. Therefore the present approach is recommended in intermediate regimes.

- The upscaling strategy works for $Pe = O(\varepsilon^{-\alpha})$, whenever $\alpha \in (0, 2)$. The present model clearly outperforms simpler effective models as α is increasing.

- Taking into account the changes in the pore geometry is justified especially for moderate values of ρ. In this case, any quantity of adsorbed material leads changes in the void space that cannot be neglected. As ρ increases, the differences between the effective solutions obtained in variable, respectively fixed geometries, are vanishing.

The particular pore structure considered here, a thin strip, may be seen as a representative but simplified pore geometry of a porous medium. However, applying a similar

upscaling procedure as here, but for a realistic porous media remains a challenging task. Furthermore, giving mathematically rigorous estimates of the errors involved in this upscaling process remains an open question.

(a)

(b)
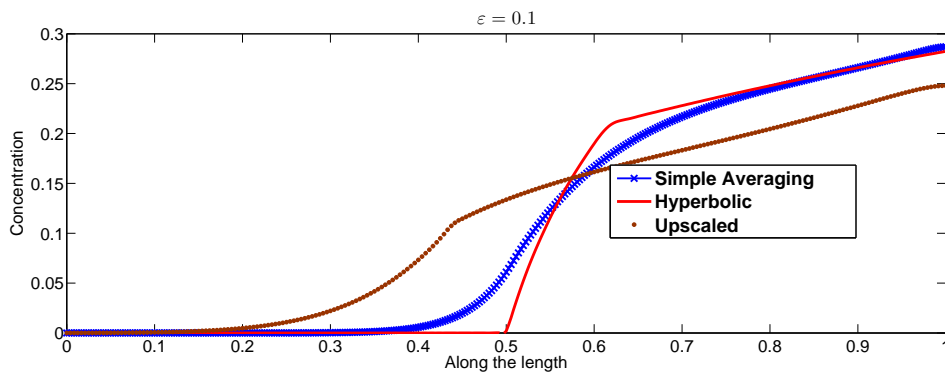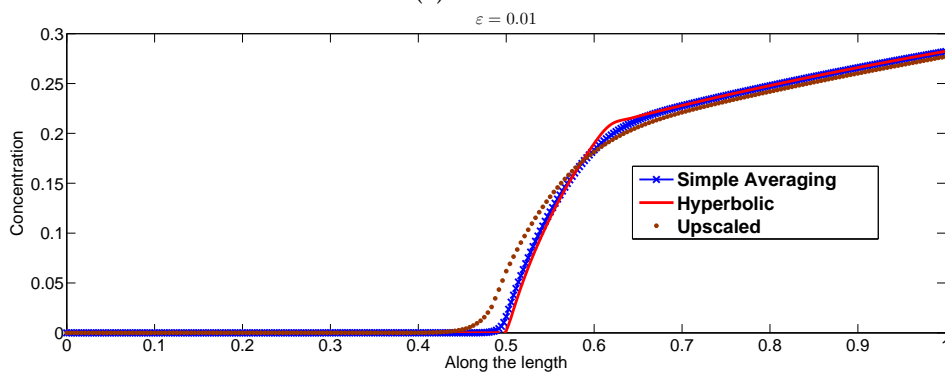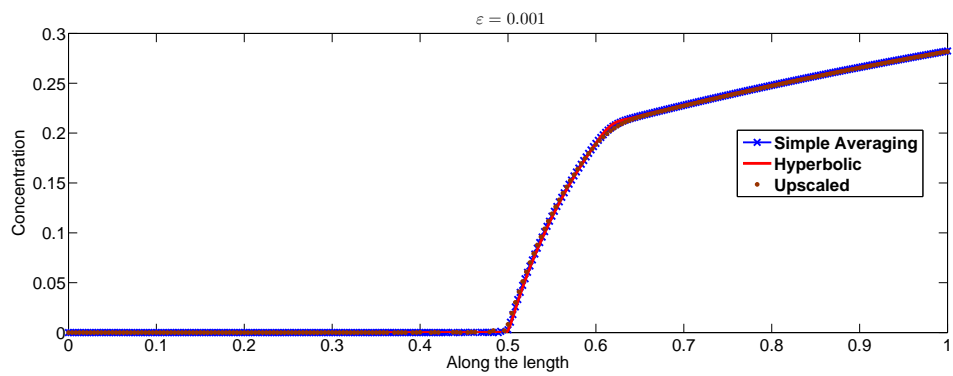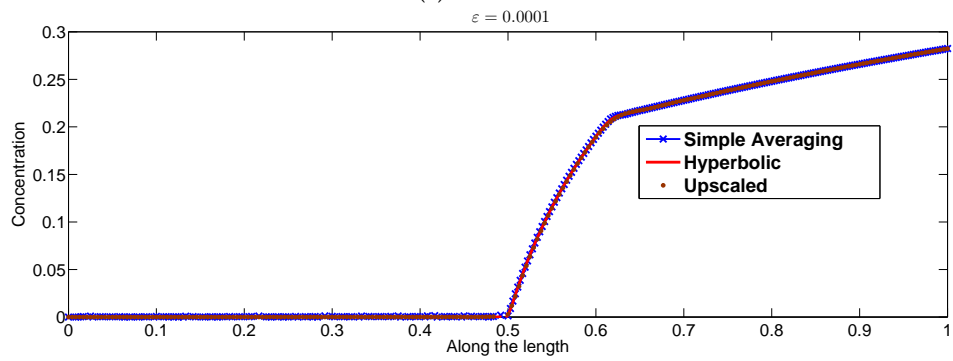
Figure 5.4: *Convergence of concentration profiles using different upscaled models for varying* $\varepsilon = 0.1, 0.01, 0.001, 0.0001$, $D = 0.5$, $\alpha = 1$, $\bar{q} = 1$. *The nomenclature refers to:* ***Simple Averaging*** *(5.4.2),* ***Upscaled*** *(5.4.3),* ***Hyperbolic*** *(5.4.1).*
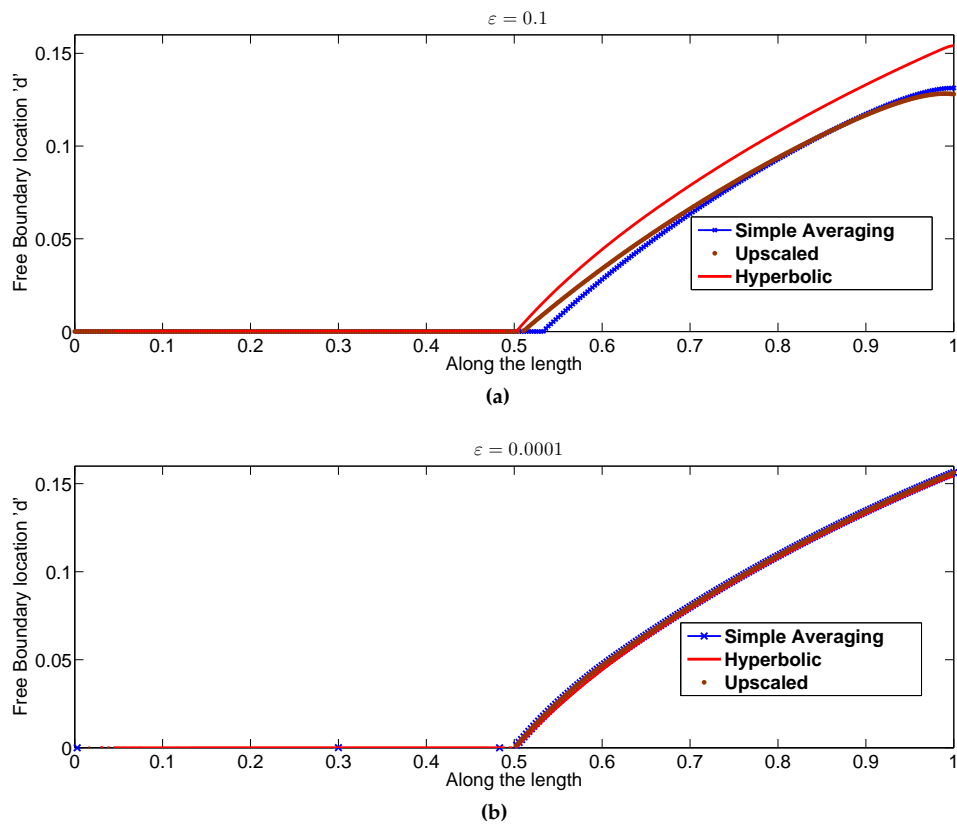
Figure 5.5: *Convergence of free boundary location d profiles using different upscaled models for varying $\varepsilon = 0.1, 0.0001$, $D = 0.5$, $\alpha = 1$, $\bar{q}_e = 1$*
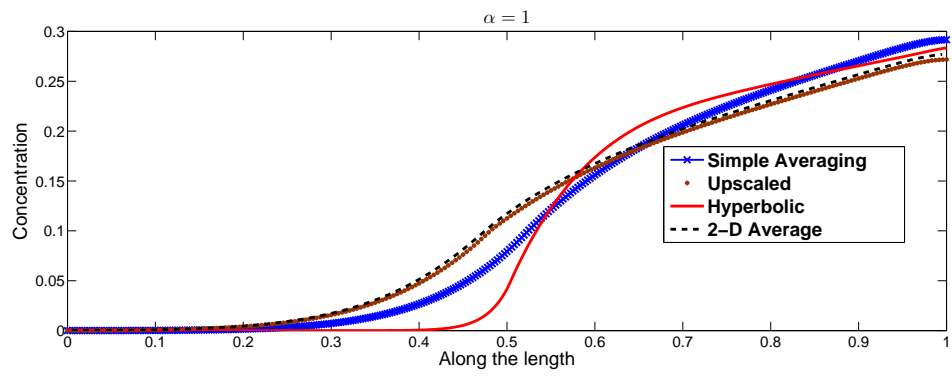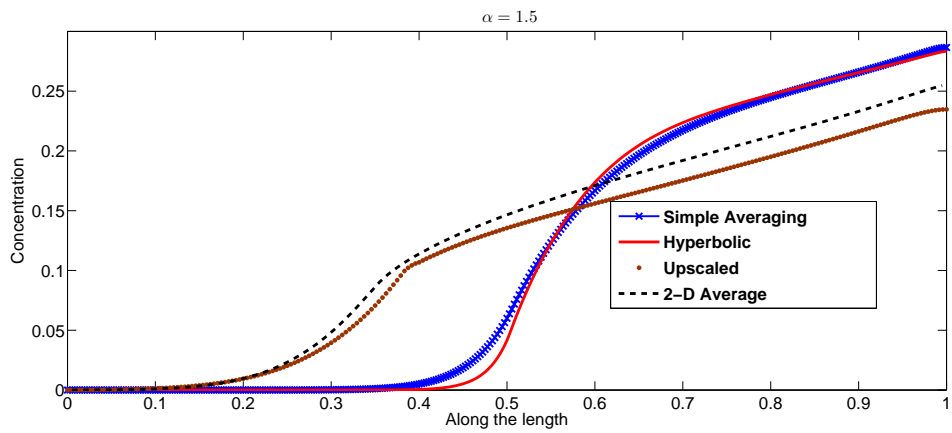
Figure 5.6: *Comparison of concentration profiles using different upscaled models for varying α, $D = 0.3$, $\varepsilon = 0.1$, $\bar{q}_e = 1$.*
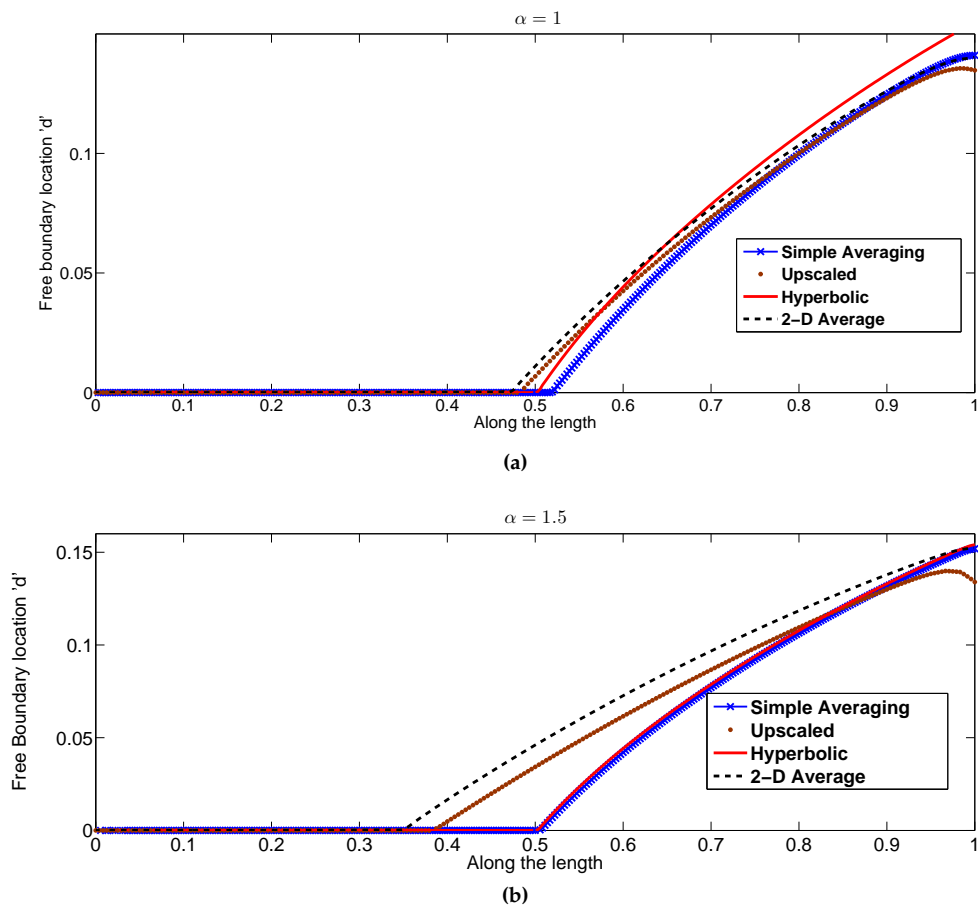
Figure 5.7: *Comparison of free boundary variable d using different upscaled models for varying* α*,* $D = 0.3$*,* $\varepsilon = 0.1$*,* $\bar{q}_e = 1$*. The nomenclature in the legend stands for: 2-D Average* (5.4.4)*, **Simple Averaging** (5.4.2), **Upscaled** (5.4.3), **Hyperbolic** (5.4.1).
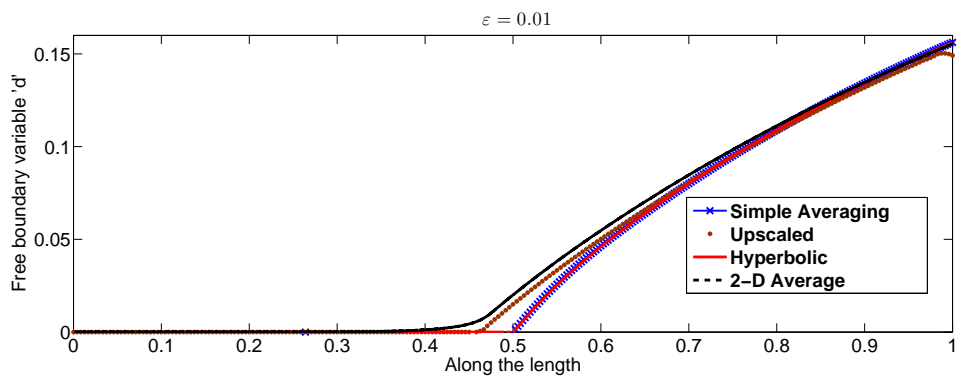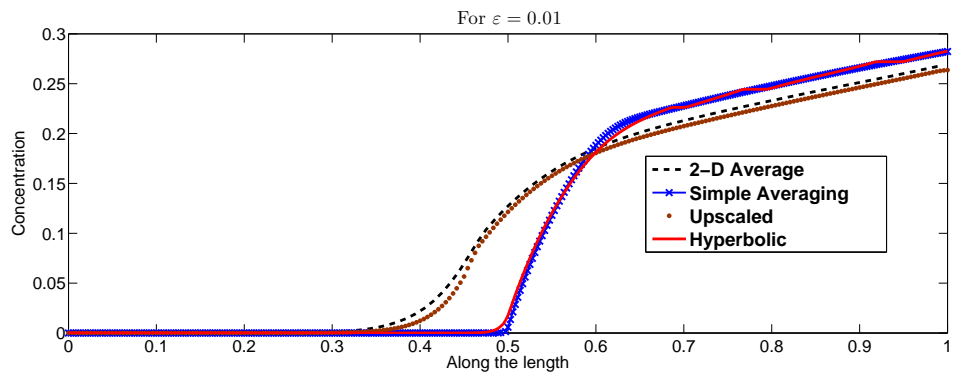
Figure 5.8: *Comparison of concentration profile and the free boundary variable d using different upscaled models for $\varepsilon = 0.01$, $D = 0.3$, $\alpha = 1.5$, $\bar{q}_e = 1$; to compare with $\varepsilon = 0.1$, see Figure 5.6(b) and Figure 5.7(b)*
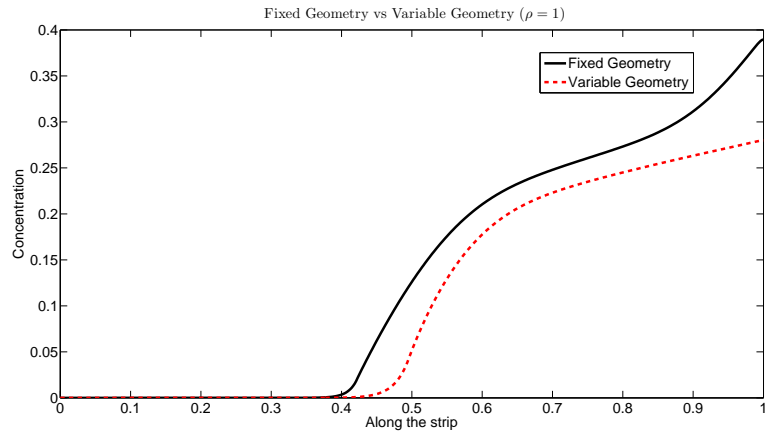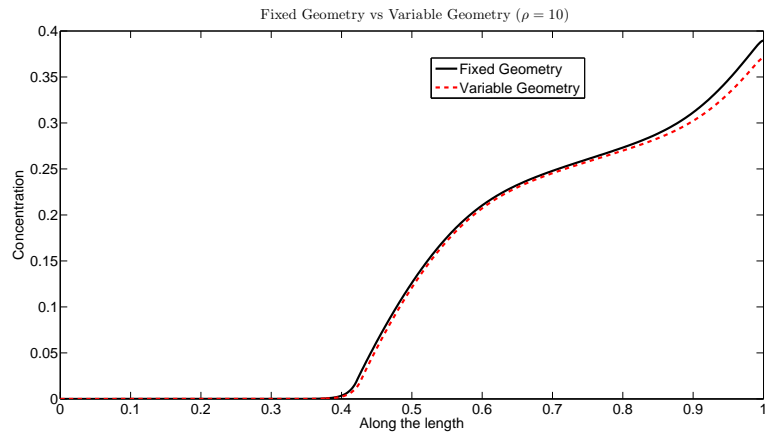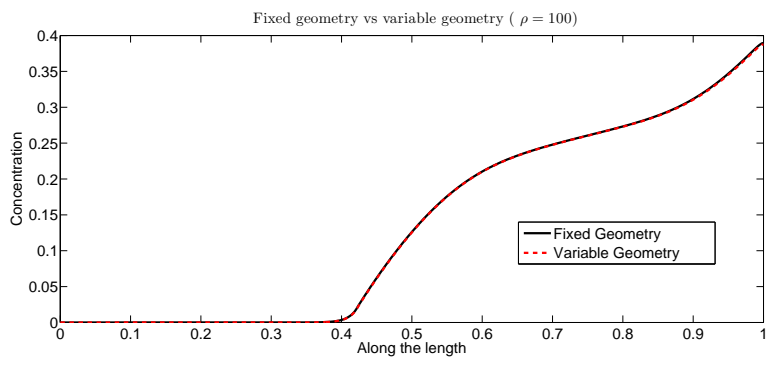
Figure 5.9: *Comparison of concentration profiles using upscaled models for variable geometry and fixed geometry, $D = 0.3$, $\alpha = 1$, $\bar{q}_e = 1$*
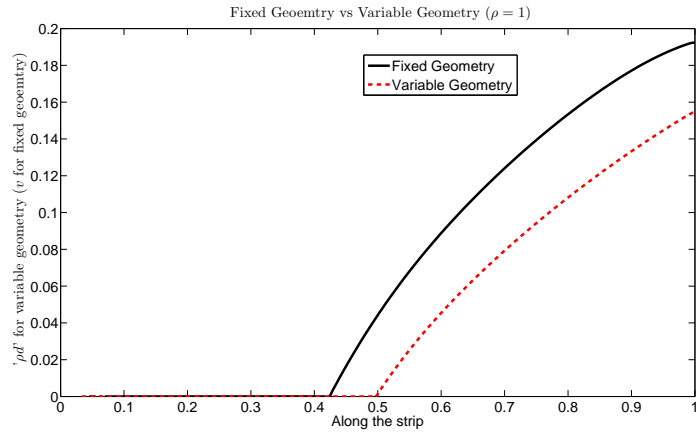
(a)
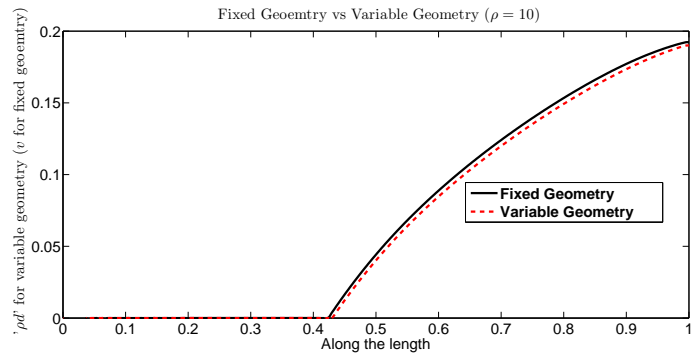
(b)
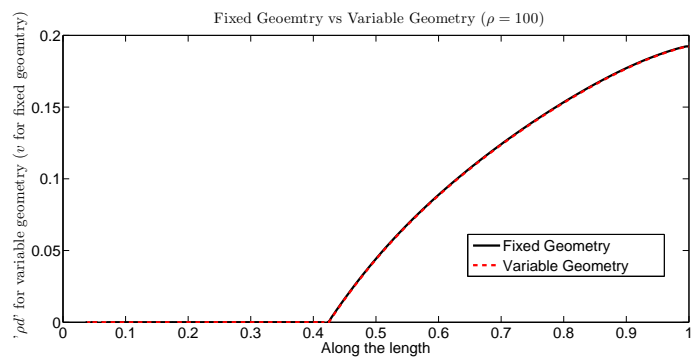
(c)

Figure 5.10: *Comparison of ρd for variable geometry and v for the fixed geometry, D =* 0.3, *α = 1,* $\bar{q}_e = 1$

Chapter 6

Homogenization of a pore-scale model

This chapter discusses the homogenization approach to derive the upscaled equations for reactive flows in a periodic medium. We define a sequence of microscopic solutions u^ε and obtain the upscaled equations as the limit of $\varepsilon \searrow 0$. We adopt the 2-scale framework to achieve this. The challenges are in dealing with the low regularity of microscopic solutions and particular non-linearities in the reaction term. This chapter closes the gap of the rigorous transition from the pore scale model given in [47] to the heuristically proposed macroscopic model in [73].

6.1 Introduction

In this chapter, we employ rigorous homogenization techniques to derive an effective model for dissolution and precipitation in a complex (porous) medium. At the micro scale, the medium consists of periodically repeating solid grains surrounded by voids (the pores). The pore space is completely filled by a fluid (e.g. water), which is flowing around the grains and by this transporting solutes, e.g. ions of species that are dissolved in the fluid. The solutes may further diffuse in the fluid, whereas at the the grain surface, they may precipitate and form a thin layer of an immobile species (salt) attached to the grain boundary. The reverse process of dissolution is also possible.

This chapter considers the micro (pore) scale model in [47], where the existence and

---

This chapter is a collaborative work with Maria Neuss-Radu and Sorin Pop.

uniqueness of a solution are proved. Using homogenization techniques, here we give
a rigorous derivation of the macro (core) scale counterpart. For the resulting upscaled
model existence and uniqueness is obtained. One important assumption is that the layer
of the species attached to the grain boundaries (the precipitate) is very thin when com-
pared to the pore thickness, so eventual changes in the the geometry at the pore-scale
can be neglected, allowing to decouple the equations modelling the flow from those
describing the chemical processes. This assumption is justified whenever the density
of the deposited layer is very large when compared to the typical density of the solute
(see [75, 104, 105]). These papers consider the alternative approach, where the precipi-
tate layer induces non-negligible changes in the pores, leading to a model involving free
boundaries at the micro scale.

The precipitation process, which is encountered at the boundary of the grains is mod-
eled by a rate function that is monotone and Lipschitz continuous with respect to the
solute concentrations, this being consistent with the mass action kinetics. For the disso-
lution, at sites on the grain boundary where precipitate is present, it will be dissolved at
a constant rate. A special situation is encountered when no precipitate is present at one
site, when certainly no dissolution is possible. However, precipitation (thus an effec-
tive gain in the immobile species) is only possible when the corresponding rate exceeds
a certain threshold value (the solubility product), when the fluid is "oversaturated".
In the "undersaturated" regime, encountered when the precipitation rate is below the
solubility product, no effective gain in the precipitate is possible. This can be seen as
an instantaneous dissolution of any precipitate formed in the undersaturated regime,
so the effective result of these processes encountered at the smallest time scale is null.
In other words, the precipitation rate is in balance with the dissolution rate. The two
regimes, oversaturation and undersaturation, are separated by the solubility product,
which is an equilibrium value. In this case neither precipitation, nor dissolution is en-
countered. Note that the undersaturated regime is encountered for any value of the
precipitation rate that is below the solubility product. This means that at sites where no
precipitate is present, the dissolution rate should take a value between 0 (no dissolution)
and the equilibrium one (the solubility product). To model this situation, we define the
dissolution rate as a member of a multi-valued graph (a scaled Heaviside graph).

The macro (core) scale model for the present problem has been proposed in [73] and
further discussed in [43–45]. Its pore scale counterpart has been analyzed in [47], where
the core scale model has been derived rigorously by a transversal averaging procedure.
In a similar context, but for the case when free boundaries are encountered at the pore
scale due to dissolution and precipitation, upscaled models are derived formally in [105]
for moderate *Peclét* numbers and in [75] for the dominated transport regime, leading
to a Taylor dispersion type model (see also [107] for a similar work related to biofilm
growth).

Here we use the 2-scale convergence concept developed in [2, 103] and extended fur-
ther in [101] to include model components defined on lower dimensional manifolds

(the grain boundaries) to derive an upscaled equation that has the same structure as the model proposed in [73]. Besides, we provide the information regarding dependence of the diffusion coefficients of macroscopic equations based on coefficients of the microscopic equations.

We mention [60, 61] for pioneering works on rigorous homogenization of reactive flow models, including the derivation of upscaled models from well-posed microscopic (pore-scale) models. Since then, many publications have considered similar problems, like [36, 89, 101]. There has been extensive work dealing with homogenization of reactive flows in porous media and we mention some of them e.g. [5, 6, 10]. The 2-scale convergence approach has been extended to include the mechanics of the porous media and finds application in several fields including the biological, mechanical etc. A recent work dealing with combining the reactive flow with the mechanics of cells is [69]. Of particular relevance to the present work is the work of [89] where non-linear reaction terms on the surface are treated using the techniques of periodic unfolding.

The major challenge in the present work is in dealing with the dissolution rates, which is a member of a the multi-valued graph. For a proper interpretation of this rate, we first consider a regularized version. Following [47], this allows to identify the dissolution rate in a unique way, as the limit of the regularized solution. However, the resulting is a dissolution rate that is non-Lipschitz and may even become discontinuous. This brings two difficulties in obtaining the rigorous results. First, for passing to the limit in the sequence of micro (pore) scale solutions one usually extends these solutions, which are defined in a perforated domain (the void space of the porous medium), to the entire domain, including the perforations (the solid grains). Further, usually shows that the extension preserves the uniform energy estimates for the original solution. The estimates for the spatial derivatives are obtained directly, from the construction of the extension. The time derivative instead needs more attention. Commonly the estimates in this case are obtained by deriving the convection-diffusion-reaction equation with respect to time. Due to the particular dissolution rate, such an approach is not allowed in the present situation. Here we show that the extension satisfies uniform estimates in the space where the solution is sought, and not a better one. In the present context, this seems to be the optimal result. Second, one has to find a proper convergence concept that is associated with the two-scale convergence for the equations on the boundary. In this chapter we follow the ideas in [102] and [89], where the concept of strong two-scale convergence is introduced, based on unfolding/localization operators [24, 35]. In particular, for the immobile species (the precipitate) we use translation estimates for obtaining compactness results and implicitly the strong convergence. These results allow us to identify the limit of the (pore scale) dissolution rate.
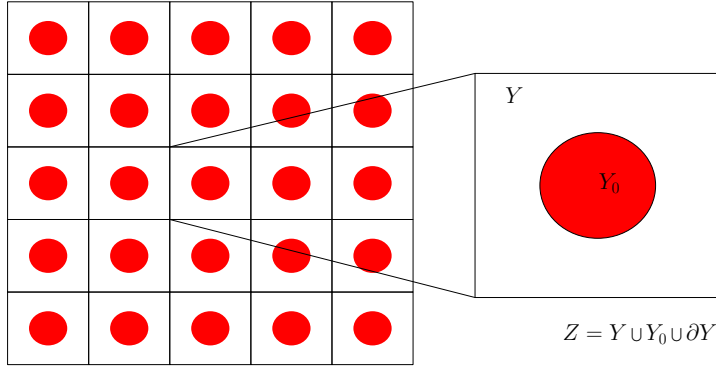
Figure 6.1: *Left: the porous medium Ω consisting of ε-scaled perforated cells distributed periodically; the total void space is Ω^ε. Right: a reference cell containing the pore Y and the solid grain Y_0 separated by the interface Γ_G. Note that the geometry remains fixed in time for a given ε.*

6.2   The mathematical model

We start with specifying the domain where the physical processes are taking place, and then introduce the model briefly. More details can be found in [47].

6.2.1   Basic geometry

The porous medium is a bounded and connected domain $\Omega \subset \mathbb{R}^d$, which includes periodically distributed grains . Its boundary $\partial\Omega$ is assumed Lipschitz. We use the following notations

- Γ_D - subset of $\partial\Omega$ where homogenous Dirichlet conditions are imposed.

- Γ_N - subset of $\partial\Omega$ where homogenous Neumann conditions are imposed.

- $\Gamma_D \bigcup \Gamma_N = \partial\Omega$ with $\Gamma_D \cap \Gamma_N = \emptyset$.

- $Z := [0,1]^d$ - the standard cell (unit cube).

- Y_0 - an open subset of Z with $\bar{Y}_0 \subset \mathbb{Z}$ representing the solid grain.

- $Y := Z \setminus \bar{Y}_0$ - the pore space.

- $\Gamma_G := \partial Y_0$ - the (piecewise smooth) boundary of Y_0 (the grain boundary).

We further assume that the $\Gamma \cap \partial Z = \emptyset$, so the closure of grain is completely included in Z.

Let $k = (k_1, \ldots, k_d)$ be a multi-index of integers and $\{\mathbf{e}_1, \ldots, \mathbf{e}_d\}$ be the canonical basis for $\mathbb{R}^d$. The translation with k of a subset Π of Z is defined by

$$\Pi^k = \Pi + \sum_{i=1}^{d} k_i \mathbf{e}_i.$$

Further, we let $1 >> \varepsilon > 0$ be a small number obtained as the ratio of the typical size of a pore (the reference micro scale length), and the typical size of the medium (the macro-scale length). Then the ε scaling of a subset Π of Z is defined by

$$\Pi^{\varepsilon} = \{\varepsilon y \mid y \in \Pi\}.$$

We assume that for a given set of multi-indices I^{ε} we have

$$\bar{\Omega} = \bigcup\{\varepsilon Z^k : k \in I^{\varepsilon}\},$$

where the translation is preceding the scaling. Then the flow domain (the total pore space) Ω^{ε} and the total grain boundary Γ_G^{ε} are defined as

$$\Omega^{\varepsilon} = \bigcup\{\varepsilon Y^k : k \in I^{\varepsilon}\}, \quad \text{and} \quad \Gamma_G^{\varepsilon} = \bigcup\{\varepsilon \Gamma_G^k : k \in I^{\varepsilon}\}.$$

The model under consideration is an evolution one. With $T > 0$ denoting a maximal time, for any $t \in (0, T]$ we define

$$Q^t = (0, t] \times Q,$$

where Q is one of the sets Ω, Ω^{ε}, Γ_G, or Γ_G^{ε}.

6.2.2 The micro scale model

The micro-scale mathematical model contains two components: the flow, and the chemistry. For the flow we consider the Stokes model

$$\begin{cases} \varepsilon^2 \triangle \mathbf{q}^{\varepsilon} &= \nabla P^{\varepsilon}, \\ \nabla \cdot \mathbf{q}^{\varepsilon} &= 0, \end{cases} \tag{6.2.1}$$

for all $x \in \Omega^{\varepsilon}$. In the above, $\mathbf{q}^{\varepsilon}$ stands for the fluid velocity, P^{ε} denotes the pressure inside the fluid. With a proper scaling, when bringing the model to a dimensionless form the dynamic viscosity becomes ε^2 (see e.g. [60], p. 45). We complement Stokes

equations by assigning no-slip boundary conditions at the grain boundary and suitable inflow and outflow boundary conditions at the outer boundary $\partial\Omega$,

$$\mathbf{q}^\varepsilon = 0, \quad \text{on } \Gamma_G^\varepsilon, \qquad \text{and} \qquad \mathbf{q}^\varepsilon = \mathbf{q}_D, \quad \text{on } \Gamma_D \cup \Gamma_N, \qquad (6.2.2)$$

where $\mathbf{q}_D$ is such that $\boldsymbol{\nu} \cdot \mathbf{q}_D = 0$ on Γ_N and $\int_{\Gamma_D} \boldsymbol{\nu} \cdot \mathbf{q}_D = 0$.

As mentioned above, we assume that the chemical processes neither change the pore scale geometry, nor the fluid properties. Therefore the flow component does not depend on the other components of the model, and can be completely decoupled. This means one can solve first the Stokes system (6.2.1) with the given boundary conditions (6.2.2) to obtain the fluid velocity $\mathbf{q}^\varepsilon$, and required a priori estimates. We further assume that $\mathbf{q}^\varepsilon$ is essentially bounded uniformly w.r.t. ε, i.e.

$$\|\mathbf{q}^\varepsilon\|_{\infty,\Omega} \leq M_q < \infty \qquad (6.2.3)$$

for some constant $M_q > 0$. For the Stokes model with homogeneous Dirichlet boundary conditions, the essential boundedness of $\mathbf{q}^\varepsilon$ holds if, for example, the domain is polygonal (see [71,82]). Here we assume that this estimate is uniform in ε.

For the chemistry two components are encountered. First, two solute (mobile) species are transported by the fluid. In the fluid, these species are diffusing, but no reactions are taking place there. The corresponding model is therefore a convection-diffusion equation in the void space, and for the time interval $(0, T)$. The chemical processes are encountered instead at the grain surface; these involve the mobile species, and the reaction result is an (immobile) species on the grain boundary. The resulting is an ordinary differential equation defined on the grain boundary, and again for $t \in (0, T)$. Finally, the partial differential equation and the ordinary one are coupled through the boundary conditions, which leads to the following system:

$$\begin{cases} \partial_t u^\varepsilon + \nabla \cdot (\mathbf{q}^\varepsilon u^\varepsilon - D\nabla u^\varepsilon) &=& 0, & \text{in } \Omega^{\varepsilon T}, \\ -D\boldsymbol{\nu} \cdot \nabla u^\varepsilon &=& \varepsilon n \partial_t v^\varepsilon, & \text{on } \Gamma_G^{\varepsilon T}, \\ \partial_t v^\varepsilon &=& k(r(u^\varepsilon) - w^\varepsilon), & \text{on } \Gamma_G^{\varepsilon T}, \\ w^\varepsilon &\in& H(v^\varepsilon), & \text{on } \Gamma_G^{\varepsilon T}. \end{cases} \qquad (6.2.4)$$

Here u^ε denotes the concentration of solutes (ions) in the fluid; v^ε denotes precipitate concentration (crystal concentration) at the solid grains and w^ε describes the dissolution rate. Note that u^ε is defined in the pore space Ω^ε and v^ε is defined on the boundaries of solid grains, Γ_G^ε. The unknowns are $u^\varepsilon, v^\varepsilon, w^\varepsilon$, and $\mathbf{q}^\varepsilon$. The physical constant D is a (given) diffusion coefficient, assumed constant. Further, k is a dimensionless reaction rate constant, which we assume constant and of moderate order w.r.t. ε. In physical sense, this means that the precipitation sites are homogeneous. The extension to the non-homogeneous case does not pose any major difficulties. Finally, n is a constant

denoting the valence of the solute. Note that only one immobile species is taken into account. This is justified if the two species are having the same diffusion coefficient (see [47,73] for details).

Clearly, $(6.2.4)_2$ relates the change in the precipitate to the normal flux of the ions at the boundaries, assuming the no-slip boundary condition for $\mathbf{q}^\varepsilon$. Also observe the appearance of ε in the boundary flux. As will be seen below, this allows to control the growth of the precipitate when passing to the limit in the homogenization step. We refer to [60] for a justification of this choice based on the geometry of the pores, and to [47] for an equivalent interpretation.

We proceed now by explaining the rates $r(u^\varepsilon)$ and w^ε in the last two equations of (6.2.4). Here $r : \mathbb{R} \to [0, \infty)$ denotes the precipitation rate and w^ε denotes the dissolution rate. Furthermore, $H(\cdot)$ denotes the Heaviside graph,

$$
H(u) = \begin{cases} 0, & \text{if } u < 0, \\ [0,1], & \text{if } u = 0, \\ 1, & \text{if } u > 0. \end{cases}
$$

For the precipitation rate we assume the following

The function r satisfies

$$
r : \mathbb{R} \to [0, \infty) \quad \text{is locally Lipschitz in} \quad \mathbb{R}. \tag{A.1}
$$

There exists a unique $u_* \geq 0$, such that

$$
r(u^\varepsilon) = \begin{cases} 0 & \text{for} \quad u^\varepsilon \leq u_*, \\ \text{strictly increasing for} \quad u^\varepsilon \geq u_* \quad \text{with} \quad r(\infty) = \infty. \end{cases} \tag{A.2}
$$

An example where these assumptions are fulfilled is given in [73], where a model based on mass-action kinetics is considered. Note that a value $u^* > 0$ exists such that

$$
r(u^*) = 1.
$$

With the proper scaling, this value is an equilibrium concentration: if $u^\varepsilon = u^*$, neither precipitation, nor dissolution is encountered (the solubility product). Finally, for the dissolution rate one has

$$
w^\varepsilon \in H(v^\varepsilon).
$$

Observe the fact that at sites where precipitate is absent (thus $v^\varepsilon = 0$), a value has to be specified for the dissolution rate. As explained in [47,73,109], in this case the rate w^ε depends also on the solute concentration. Specifically, for u^* introduced above, for $u^\varepsilon > u^*$ we take $w^\varepsilon = 1$. This is interpreted as an *oversaturated* regime, meaning that the

overall precipitation/dissolution rate is strictly positive and a net gain in the precipitate results. Whenever $u^\varepsilon \leq u^*$, thus $r(u^\varepsilon) \leq 1$, the solute concentration is insufficient for an effective gain in precipitate (the *undersaturated* regime). In this case dissolution should be avoided, implying that $\partial_t v^\varepsilon = 0$. To achieve this, we take $w^\varepsilon = r(u^\varepsilon)$ (a value between 0 and 1, by scaling) and the overall rate becomes 0. This can be summarized as

$$w^\varepsilon = \begin{cases} 0, & \text{if } v^\varepsilon < 0, \\ \min\{r(u^\varepsilon), 1\}, & \text{if } v^\varepsilon = 0, \\ 1, & \text{if } v^\varepsilon > 0. \end{cases} \tag{6.2.5}$$

Note that in the above relation, w^ε is a discontinuous function of v^ε. In what follows, we will work with the above formulation of w^ε. The system (6.2.4) is complemented by the following initial and boundary conditions,

$$\begin{cases} u^\varepsilon(0, \cdot) & = & u_I & \text{in} & \Omega^\varepsilon, \\ v^\varepsilon(0, \cdot) & = & v_I & \text{on} & \Gamma_G^\varepsilon, \\ u^\varepsilon & = & 0, & \text{on} & \Gamma_D^T. \end{cases} \tag{6.2.6}$$

6.2.3 The macro scale model

The equations (6.2.1) and (6.2.4) together with the initial and boundary conditions are giving the model at the pore scale. For completeness we provide the corresponding model at the macro-scale, which will be derived below by rigorous homogenization. Recalling that the flow is not affected by the chemistry, this component of the model can be homogenized separately. The result is a pair $(\mathbf{q}, P)$ approximating the micro scale $(\mathbf{q}^\varepsilon, P^\varepsilon)$. As shown in [1, 62, 92, 130], $\mathbf{q}$ and P satisfy the Darcy law

$$\nabla \cdot \mathbf{q} = 0, \quad \mathbf{q} = -K\nabla P, \tag{6.2.7}$$

for $x \in \Omega$, where K is the permeability tensor given by

$$k_{ij} = \frac{1}{|Y|} \int_Y \chi_i^j(y) dy,$$

for all $i, j = 1, \dots, d$. Here by χ_i^j we mean the i-th component of $\chi^j = (\chi_1^j, \cdots, \chi_d^j)$, obtained from the cell problems

$$(P_j^D) \begin{cases} -\Delta_y \chi^j(y) & = & \nabla_y \Pi^j(y) + \mathbf{e}_j, & \text{in } Y \\ \nabla_y \cdot \chi^j(y) & = & 0, & \text{in } Y \\ \chi^j(y) & = & 0, & \text{on } \Gamma_G \\ \chi^j, \Pi^j & \text{are} & Z - \text{periodic}. \end{cases}$$

Concerning the chemistry, the homogenized model reads

$$
\begin{cases}
\partial_t \left(u + n \frac{|\Gamma_G|}{|Y|} v \right) &= \nabla \cdot (S \nabla u - \mathbf{q}u), \\
\partial_t v &= k(r(u) - w), \\
w &\in H(v),
\end{cases}
\tag{6.2.8}
$$

for $x \in \Omega$ and $t \in (0, T]$, where the matrix S is defined as

$$
(S)_{i,j} = D \left[\delta_{ij} + \frac{1}{|Y|} \int_Y \partial_{y_j} w_i dy \right],
$$

and w_i solves the cell problem

$$
(P_j^C) \begin{cases}
-\Delta w_i &= 0 & \text{in } Y, \\
\mathbf{v} \cdot \nabla w_i &= \mathbf{v} \cdot \mathbf{e}_i & \text{on } \Gamma_G \\
w_i & \text{is } Z & \text{periodic.}
\end{cases}
$$

Here u and v are the upscaled concentrations for the solute, respectively the precipitate, and w is the upscaled dissolution rate, while by $\mathbf{v}$ we mean the unit normal to Γ_G pointing into the grain Y_0. The equations are complemented by the boundary and initial conditions retained from (6.2.6)

$$
\begin{cases}
u(0, \cdot) &= u_I & \text{in } \Omega^T, \\
v(0, \cdot, \cdot) &= v_I & \text{on } \Omega^T \times \Gamma_G, \\
u &= 0, & \text{on } \Gamma_D^T.
\end{cases}
\tag{6.2.9}
$$

6.3   The weak formulation

When defining the a weak solution we use common notations in the functional analysis: with Q being either Ω, Ω^ε, Γ_D, Γ_G or Γ_G^ε, we denote by $L^p(Q)$ ($p \geq 1$) the p–integrable functions on Q (in the sense of Lebesgue). The space $H_{0,\Gamma_D}^1(Q)$ restricts the space $H^1(Q)$ of functions having all first order partial derivatives in L^2 to those elements vanishing on Γ_D (in the sense of traces). $(\cdot, \cdot)_Q$ stands for the scalar product in $L^2(Q)$, or the duality pairing between $H_{0,\Gamma_D}^1(Q)$ and $H^{-1}(Q)$ – the dual of $H_{0,\Gamma_D}^1(Q)$. The corresponding norm is denoted by $\| \cdot \|_Q$, or simply $\| \cdot \|$ (where self understood). By $L^\infty(Q)$ we mean functions that are essentially bounded on Q, and the essential supremum is denoted by $\|u\|_{\infty,Q}$. Further, for a Banach space V we denote by $L^2(0, T; V)$ the corresponding Bochner space equipped with the standard inner product (where applicable) and norm. Besides, by χ_I we mean the characteristic function of the set I. Since the reaction rate constant k is immaterial in the derivation, in what follows, we simply take $k = 1$.

Before stating the definition of a weak solution, we introduce the function spaces

$$\mathcal{U}^\varepsilon := \{u \in L^2(0,T; H^1_{0,\Gamma_D}(\Omega^\varepsilon)) \quad : \quad \partial_t u \in L^2(0,T; H^{-1}(\Omega^\varepsilon))\},$$
$$\mathcal{V}^\varepsilon := H^1(0,T; L^2(\Gamma^\varepsilon_G)),$$
$$\mathcal{W}^\varepsilon := \{w \in L^\infty(\Gamma^{\varepsilon T}_G) \quad : \quad 0 \le w \le 1\}.$$

Then a weak solution is introduced in

Definition 6.3.1 *A triple* $(u^\varepsilon, v^\varepsilon, w^\varepsilon) \in \mathcal{U}^\varepsilon \times \mathcal{V}^\varepsilon \times \mathcal{W}^\varepsilon$ *is called a weak solution of* (6.2.4)-(6.2.6) *if* $u^\varepsilon(0,\cdot) = u_I, v^\varepsilon(0,\cdot) = v_I$ *and*

$$
\begin{aligned}
(\partial_t u^\varepsilon, \phi)_{\Omega^{\varepsilon T}} + D(\nabla u^\varepsilon, \nabla \phi)_{\Omega^{\varepsilon T}} - (q u^\varepsilon, \nabla \phi)_{\Omega^{\varepsilon T}} &= -\varepsilon n(\partial_t v^\varepsilon, \phi)_{\Gamma^{\varepsilon T}_G}, \\
(\partial_t v^\varepsilon, \theta)_{\Gamma^T_G} &= (r(u^\varepsilon) - w^\varepsilon, \theta)_{\Gamma^{\varepsilon T}_G}, \\
w^\varepsilon &\in H(v^\varepsilon) \quad \text{a.e. in} \quad \Gamma^{\varepsilon T}_G,
\end{aligned}
\tag{6.3.1}
$$

for all $(\phi, \theta) \in L^2(0,T; H^1_{0,\Gamma_D}(\Omega^\varepsilon)) \times L^2(\Gamma^{\varepsilon T}_G)$.

For the functions appearing as boundary and initial conditions we assume the following

$u_I \in H^1_{0,\Gamma_D}(\Omega), v_I \in H^1(\Omega) \cap L^\infty(\Omega)$, and $0 \le u_I, v_I \le M_0$ almost everywhere, (A.3)

for an ε-independent constant $M_0 > 0$. For simplicity we considered homogeneous conditions on Γ_D, but the extension to non-homogeneous ones can be carried out without major difficulties. Note that the initial and boundary conditions are compatible, and that the initial conditions are defined for the entire domain Ω.

The existence of weak solutions of (6.2.4)-(6.2.6) has been studied in [47]. There, a weak solution was obtained by regularization arguments, where the Heaviside graph modelling the dissolution process is approximated by a continuous function. For the solution $(u^\varepsilon, v^\varepsilon, w^\varepsilon)$ constructed in this way, the dissolution rate w^ε satisfies (6.2.5). Furthermore, its uniqueness is obtained from the following contraction result with respect to the initial values, see [109]:

Theorem 6.3.1 *Assume* (A.1) *and* (A.2) *and let* $(u^{(i)^\varepsilon}, v^{(i)^\varepsilon}, w^{(i)^\varepsilon}) \in \mathcal{U}^\varepsilon, \mathcal{V}^\varepsilon, \mathcal{W}^\varepsilon, i = 1,2$ *be two solutions in the sense of Definition 6.3.1, obtained for the initial values* $u_I^{(i)}, v_I^{(i)} (i = 1,2)$ *respectively. Then for any* $t \in (0,T]$ *it holds*

$$
\int_{\Omega^\varepsilon} |u^{(1)\varepsilon}(t,x) - u^{(2)\varepsilon}(t,x)| dx + \varepsilon n \int_{\Gamma^\varepsilon_G} |v^{(1)\varepsilon}(t,s) - v^{(2)\varepsilon}(t,s)| ds
$$
$$
\le |u_I^{(1)}(x) - u_I^{(2)}(x)| dx + \varepsilon n \int_{\Gamma^\varepsilon_G} |v_I^{(1)}(s) - v_I^{(2)}(s)| ds \tag{6.3.2}
$$

6.3.1 Uniform estimates for the microscopic solutions

For the rigorous derivation of the effective model we extend the micro scale solute concentration u^ε, defined in the pore space Ω^ε, to the entire domain Ω. This requires a-priori estimates that are uniform w.r.t. ε. Such estimates are obtained in [47], without considering particularly the homogenization problem. As mentioned there, the estimates are ε-uniform in the case of a periodically perforated medium, this being the case considered here. From [47, 109] one has:

Theorem 6.3.2 *Assume* (A.1) *and* (A.2), *there exists a unique weak solution of* (6.2.4). *In addition, this solution satisfies*

$$0 \le u^\varepsilon, v^\varepsilon \le M, \qquad 0 \le w^\varepsilon \le 1, \tag{6.3.3}$$

$$\|u^\varepsilon\|_{L^\infty(0,T;L^2(\Omega^\varepsilon))}^2 + \|\nabla u^\varepsilon\|_{L^2(\Omega^{\varepsilon T})}^2 + \|\partial_t u^\varepsilon\|_{L^2(0,T;H^{-1}(\Omega^\varepsilon))}^2$$
$$+ \varepsilon \|v^\varepsilon\|_{L^\infty(0,T;L^2(\Gamma_G^\varepsilon))}^2 + \varepsilon \|\partial_t v^\varepsilon\|_{L^2(\Gamma_G^{\varepsilon T})}^2 \le C, \tag{6.3.4}$$

where the constants $C > 0$ and $M > 0$ are independent of ε.

The estimates above allow extending u^ε inside the solid grain, but are insufficient for the extension of $\partial_t u^\varepsilon$. In [61, 101], additional estimates are obtained by differentiating the model with respect to time. Because of the possible jump in the reaction rate, this approach does not work here.

Here we follow the explicit extension procedure in [61, 101], and show that the estimates available here are sufficient for obtaining a well-defined extension that satisfies uniform estimates. To do so we proceed by analyzing $\partial_t u^\varepsilon$.

Estimates on $\partial_t u^\varepsilon$

The estimates on $\partial_t u^\varepsilon$ are obtained through time translations. In this sense, given a function $g : [0, T] \mapsto X$ (X being a Banach space), we extend it by its initial value on the interval $[-h, 0)$ and define

$$\triangle_h g(t) := \frac{g(t) - g(t - h)}{h},$$

for all $t \ge 0$, where $g(s) = g(0)$ whenever $s < 0$. Below we show that $\triangle_h u^\varepsilon$ is bounded uniformly with respect to h in $L^1(\Omega^\varepsilon)$ norm. Note that this does not imply $\partial_t u^\varepsilon \in L^1((-h, T) \times \Omega^\varepsilon)$, since L^1 is not reflexive. However, as we will show below, this uniform estimate is still sufficient to construct an extension of u^ε to Ω having sufficient regularity in time. We start with the following lemma.

Lemma 6.1 *Let $t \in [0, T]$, $h > 0$, and $(u^\varepsilon, v^\varepsilon, w^\varepsilon)$ be a weak solution of (6.2.4). Then the following estimate is uniform in h,*

$$\int_{\Omega^\varepsilon} |\triangle_h u^\varepsilon(t, x)| dx + \varepsilon \int_{\Gamma_G^\varepsilon} |\triangle_h v^\varepsilon(t, x)| \leq \int_{\Omega^\varepsilon} |\triangle_h u^\varepsilon(h, x)| dx + \varepsilon \int_{\Gamma_G^\varepsilon} |\triangle_h v^\varepsilon(h, x)| dx.$$

Assuming compatibility on the initial data, we obtain for any $t \geq 0$

$$\int_{\Omega^\varepsilon} |\triangle_h u^\varepsilon(t, x)| dx + \varepsilon \int_{\Gamma_G^\varepsilon} |\triangle_h v^\varepsilon(t, x)| \leq C.$$

Proof. We follow the L^1 contraction proof of Theorem 6.3.1 in [109] and define $\mathcal{T}_\delta, \mathcal{S}_\delta : \mathbb{R} \rightarrow \mathbb{R}$

$$\mathcal{T}_\delta(x) := \begin{cases} -x - \frac{\delta}{2}, & \text{if } x < -\delta, \\ \frac{x^2}{2\delta}, & \text{if } x \in [-\delta, \delta], \\ x - \frac{\delta}{2} & \text{if } x > \delta, \end{cases} \qquad \text{and} \qquad \mathcal{S}_\delta(x) = \begin{cases} -1, & \text{if } x < -\delta, \\ \frac{x}{\delta}, & \text{if } x \in [-\delta, \delta], \\ 1, & \text{if } x > \delta. \end{cases}$$

Here $\delta > 0$ is a parameter than can be taken arbitrarily small. Clearly, $\mathcal{S}_\delta = \mathcal{T}_\delta'$. Note that $\mathcal{T}_\delta$ is a regularized approximation of the absolute value, whereas $\mathcal{S}_\delta$ is the regularized sign function.

Taking $h > 0$ and $t \in (h, T]$ arbitrary, with $(\phi, \theta) \in H^1_{0,\Gamma_D}(\Omega^\varepsilon) \times L^2(\Gamma_G^\varepsilon)$ and χ_I being the characteristic function of the time interval I, we test in (6.3.1) first with $\chi_{(h,t)}(\phi, \theta)$, and then with $\chi_{(0,t-h)}(\phi, \theta)$ (both lying in $L^2(0, T; H^1_{0,\Gamma_D}(\Omega^\varepsilon)) \times L^2(\Gamma_G^{\varepsilon T}))$. Subtracting the resulting gives

$$\int_h^t (\partial_\tau \triangle_h u^\varepsilon, \phi)_{\Omega^\varepsilon} d\tau + D \int_h^t (\nabla \triangle_h u^\varepsilon, \nabla \phi)_{\Omega^\varepsilon} d\tau$$

$$- \int_h^t (\mathbf{q} \triangle_h u^\varepsilon, \nabla \phi)_{\Omega^\varepsilon} d\tau + \varepsilon n \int_h^t (\partial_t \triangle_h v^\varepsilon, \phi)_{\Gamma_G^\varepsilon}, d\tau = 0,$$

$$\varepsilon \int_h^t (\partial_\tau \triangle_h v^\varepsilon, \theta)_{\Gamma_G^\varepsilon} d\tau - \varepsilon k \int_h^t (\triangle_h r(u^\varepsilon) - \triangle_h w^\varepsilon, \theta)_{\Gamma_G^\varepsilon} d\tau = 0,$$

$$w^\varepsilon \in H(v^\varepsilon) \qquad \text{a.e. in } \Gamma_G^\varepsilon.$$

With $\phi := \mathcal{S}_\delta(\triangle_h u^\varepsilon)$ and $\theta := \varepsilon \mathcal{S}_\delta(\triangle_h v^\varepsilon)$, (6.3.6) becomes

$$\int_h^t (\triangle_h \partial_t u^\varepsilon, \mathcal{S}_\delta(\triangle_h u^\varepsilon))_{\Omega^\varepsilon} + \varepsilon(\triangle_h \partial_t v^\varepsilon, \mathcal{S}_\delta(\triangle_h v^\varepsilon))_{\Gamma_G^\varepsilon} dt$$

$$+ D \int_h^t (\nabla \triangle_h u^\varepsilon, \nabla \mathcal{S}_\delta(\triangle_h u^\varepsilon))_{\Omega^\varepsilon} dt - \int_h^t (\mathbf{q}\triangle_h u^\varepsilon, \nabla \mathcal{S}_\delta(\triangle_h u^\varepsilon))_{\Omega^\varepsilon} dt \qquad (6.3.5)$$

$$+ \varepsilon k \int_h^t (\triangle_h r(u^\varepsilon) - \triangle_h H_\delta(v^\varepsilon), \mathcal{S}_\delta(\triangle_h u^\varepsilon) - \mathcal{S}_\delta(\triangle_h v^\varepsilon))_{\Gamma_G^\varepsilon} dt = 0.$$

Denoting the terms above by $\mathcal{I}_\delta^i, i = 1, \ldots, 5$, we proceed by analyzing them separately. $\mathcal{I}_\delta^1$ gives

$$\mathcal{I}_\delta^1 = \int_h^t \int_{\Omega^\varepsilon} \partial_\tau \mathcal{T}_\delta(\triangle_h u^\varepsilon(\tau, x)) dx d\tau = \int_{\Omega^\varepsilon} \mathcal{T}_\delta(\triangle_h u^\varepsilon(t, x)) dx - \int_{\Omega^\varepsilon} \mathcal{T}_\delta((\triangle_h u^I(x))) dx. \quad (6.3.6)$$

Recall that $0 \leq \mathcal{T}_\delta(s)| \leq |s| + \delta/2$ and $u^\varepsilon(t) \in L^2(\Omega^\varepsilon)$, using the dominated convergence theorem,

$$\lim_{\delta \searrow 0} \mathcal{I}_\delta^1 = \int_{\Omega^\varepsilon} |\triangle_h u(t, x)| dx. \qquad (6.3.7)$$

In a similar manner,

$$\lim_{\delta \searrow 0} \mathcal{I}_\delta^2 = \varepsilon \int_{\Gamma_G^\varepsilon} |\triangle_h v(t, x)|. \qquad (6.3.8)$$

Next, since $\mathcal{S}_\delta' \geq 0$ a.e. on $\mathbb{R}$, one gets

$$\mathcal{I}_\delta^3 = \frac{D}{2} \int_h^t \int_{\Omega^\varepsilon} S_\delta'(\triangle_h u^\varepsilon) |\nabla \triangle_h u^\varepsilon|^2 dx dt \geq 0. \qquad (6.3.9)$$

Furthermore, for $\mathcal{I}_\delta^4$, since $\mathbf{q}$ has zero divergence, using the no-slip boundary conditions together with the vanishing trace of u^ε on Γ_D one obtains

$$\mathcal{I}_\delta^4 = \int_h^t \int_{\Omega^\varepsilon} \nabla \cdot (\mathbf{q}\mathcal{T}_\delta(\triangle_h u)) = \int_0^t \int_{\partial\Omega^\varepsilon} \boldsymbol{\nu} \cdot (\mathbf{q}\mathcal{T}_\delta(\triangle_h u)) = 0. \qquad (6.3.10)$$

With $f(u^\varepsilon(t,x), v^\varepsilon(t,x)) = r(u^\varepsilon(t,x)) - H(v^\varepsilon(t,x))$, $\mathcal{I}^5_\delta$ becomes

$$\mathcal{I}^5_\delta = \varepsilon \int_h^t \int_{\Gamma^\varepsilon_G} \left(f(u^\varepsilon(t,x), v(t,x)) - f(u^\varepsilon(t-h,x), v(t-h,x))\right) \left(\mathcal{S}_\delta(\triangle_h u^\varepsilon) - \mathcal{S}_\delta(\triangle_h v^\varepsilon)\right) dx dt.$$

(6.3.11)

Due to the a priori estimates on u^ε and v^ε and since $\mathcal{S}_\delta$ is bounded, the integration argument in $\mathcal{I}^5_\delta$ is uniformly dominated in $L^1(\Gamma^{\varepsilon T}_G)$. Therefore, for obtaining uniform estimates for $|\triangle_h u(t,x)|$, it is sufficient to prove that

$$\lim_{\delta \searrow 0} \left(f(u^\varepsilon(t,x), v^\varepsilon(t,x)) - f(u^\varepsilon(t-h,x), v^\varepsilon(t-h,x))\right) \left(\mathcal{S}_\delta(\triangle_h u^\varepsilon) - \mathcal{S}_\delta(\triangle_h v^\varepsilon)\right) \geq 0$$

a.e. on $\Gamma^{\varepsilon,T}_G$. This depends on the sign of the difference quotients $\triangle_h u^\varepsilon$ and $\triangle_h v^\varepsilon$. Without loss of generality we only consider the case when $\triangle_h u^\varepsilon \geq 0$, the proof for $\triangle_h u^\varepsilon < 0$ being similar.

Given a pair $(t,x) \in \Gamma^{\varepsilon,T}_G$, we note that if $\triangle_h u^\varepsilon > 0$ and $\triangle_h v^\varepsilon > 0$ one has

$$\lim_{\delta \searrow 0}(\mathcal{S}_\delta(\triangle_h u^\varepsilon) - \mathcal{S}_\delta(\triangle_h v^\varepsilon)) \to 0.$$

The situation is similar if $\triangle_h u^\varepsilon \geq 0$ and $\triangle_h v^\varepsilon \leq 0$. Then we use the monotonicity of f with respect to u^ε and v^ε (see also Lemma 1 in [109]) to obtain

$$f(u^\varepsilon(t,x), v^\varepsilon(t,x)) - f(u^\varepsilon(t-h,x), v^\varepsilon(t-h,x)) \geq 0.$$

Since $\mathcal{S}_\delta(\triangle_h u^\varepsilon) \geq 0 \geq \mathcal{S}_\delta(\triangle_h v^\varepsilon)$, we have

$$\lim_{\delta \searrow 0} \left(f(u^\varepsilon(t,x), v^\varepsilon(t,x)) - f(u^\varepsilon(t-h,x), v^\varepsilon(t-h,x))\right) \left(\mathcal{S}_\delta(\triangle_h u^\varepsilon) - \mathcal{S}_\delta(\triangle_h v^\varepsilon)\right) \geq 0.$$

Using the above into (6.3.5) gives

$$\int_{\Omega^\varepsilon} |\triangle_h u^\varepsilon(t,x)| dx + \varepsilon \int_{\Gamma^\varepsilon_G} |\triangle_h v^\varepsilon(t,x)| \leq \int_{\Omega^\varepsilon} |\triangle_h u^\varepsilon(h,x)| dx + \varepsilon \int_{\Gamma^\varepsilon_G} |\triangle_h v^\varepsilon(h,x)| dx$$

uniformly in h. If the initial and boundary conditions are assumed compatible (e.g. initial data $u_I \in W^{1,\alpha}, \alpha > 1$), (6.3.1) also holds for negative time arguments, and the estimate can be extended for $t \in [0,h]$.

$$\int_{\Omega^\varepsilon} |\triangle_h u^\varepsilon| dx + \varepsilon \int_{\Gamma^\varepsilon_G} |\triangle_h v^\varepsilon| \leq C,$$

(6.3.12)

which proves the lemma.   □

6.3.2 Extension results

As it has been defined in Section 6.2.1, Z and Y_0 denote the unit cell and the grain part respectively and Y represents the pore space. Let U denote the neighbourhood of ∂Y_0. First we list the results and then proceed for the proof. In the following we make use of function $m : (0, T) \mapsto \mathbb{R}$

$$m(t) := \frac{1}{|Y|} \int\limits_Y u(y) dy.$$

Lemma 6.2 *m is well-defined for a.e. t. Furthermore, $\partial_t m$ exists and $\partial_t m \in L^\infty(0, T)$.*

Lemma 6.3 *Let $u \in L^2(0, T; H^1(Y))$, $\partial_t u \in L^2(0, T; H^{-1}(Y))$ and u satisfies (6.3.12) for domain Y. Then there exists an extension $\tilde{u} \in L^2(0, T; H^1(Z))$ of $u \in L^2(0, T; H^1(Y))$ such that*

$$\|\tilde{u}\|_{L^2(0,T;H^1(Z))} \leq c \|u\|_{L^2(0,T;H^1(Y))}$$

and

$$\|\partial_t \tilde{u}\|_{L^2(0,T;H^{-1}(Z))} \leq \|\partial_t u\|_{L^2(0,T;H^{-1}(Y))}.$$

Lemma 6.4 *Let $u^\varepsilon \in L^2(0, T; H^1(\Omega^\varepsilon))$, $\partial_t u^\varepsilon \in L^2(0, T; H^1(\Omega^\varepsilon))$ and u^ε satisfies (6.3.12). Then there exists an extension $\tilde{u} \in L^2(0, T; H^1(\Omega))$ of $u^\varepsilon \in L^2(0, T; H^{-1}(\Omega^\varepsilon))$ such that*

$$\|\tilde{u}\|_{L^2(0,T;H^1(\Omega))} \leq \|u^\varepsilon\|_{L^2(0,T;H^1(\Omega^\varepsilon))}$$

and

$$\|\partial_t \tilde{u}^\varepsilon\|_{L^2(0,T;H^{-1}(\Omega))} \leq \|\partial_t u^\varepsilon\|_{L^2(0,T;H^{-1}(\Omega^\varepsilon))}.$$

Now we proceed for the proof. We construct the usual H^1 extension $\tilde{u}$ of u and use the improved regularity of $\partial_t u$ to make sure that the extension $\partial_t \tilde{u} \in L^2(0, T; H^{-1}(Z))$. For smooth enough ∂Y_0, we construct diffeomorphism

$$\Phi : \partial Y_0 \times (-\delta, \delta) \mapsto U$$

$$(y, \lambda) \mapsto x.$$

We construct an extension of u by reflection:

$$u^*(x, t) = u^*(\phi(y, \lambda)) = \begin{cases} u(\phi(y, \lambda)) & \lambda \geq 0 \\ u(\phi(y, -\lambda)) & \lambda < 0 \end{cases}$$

and extend u^* further into Z in any smooth manner. Define smooth function $\psi : Z \mapsto [0,1]$ with compact support in Y_0 and $\psi \equiv 1$ in $Y_0 \setminus U$. With m as defined above in 6.2, we define the extension $\tilde{u}$ as follows

$$\tilde{u} := (1-\psi)(u^* - m) + m.$$

Proof. (Lemma 6.2) To prove Lemma 6.2 recall that for a.e. t, $m(t)$ is well-defined and $m \in L^\infty(0,T)$ since $u \in L^\infty(0,T;L^2(Y))$. For a.e. t

$$\left| \frac{m(t+h) - m(t)}{h} \right| = \frac{1}{|Y|} \left| \int_Y \frac{u(t+h) - u(t)}{h} \right|$$

$$\leq \frac{1}{|Y|} \int_Y \left| \frac{u(t+h) - u(t)}{h} \right| \leq C$$

using Lemma 6.1.with C independent of h and dependent on the initial data. Taking limit $h \searrow 0$ and using Riesz-Frechet-Kolmogorov compactness criterion, we conclude that the sequence $\triangle_h m$ converges to $\partial_t m \in L^\infty(0,T)$.
$\square$

Proof. (Lemma 6.3) We need to make sure that $\tilde{u} \in L^2(0,T;H^1(Z))$. For a.e. $t \in (0,T)$, we have

$$\|\tilde{u}\|^2_{L^2(Y_0)} = \int_{Y_0} |(1-\psi)(u^* - m) + m|^2 dy$$

$$= \int_{Y_0 \cap U} |(1-\psi)u^* + \psi m|^2 dy + \int_{Y_0 \setminus U} m^2 dy$$

$$\leq C\|u\|^2_{L^2(Y)}$$

since $\displaystyle\int_{Y_0 \cap U} \left(\frac{1}{|Y|} \int_Y u \right)^2 \leq \int_{Y_0 \cap U} \frac{1}{|Y|} \left(\int_Y u^2 \right) \leq \frac{|Y_0|}{|Y|} \|u\|^2_{L^2(Y)}.$

For the derivative we compute

$$
\begin{aligned}
\|\nabla \tilde{u}\|_{L^2(Y_0)} &= \int_{Y_0} |\nabla((1-\psi)(u^* - m))|^2 dy \\
&\leq C \left(\int_{Y_0 \cap U} |u^* - m|^2 |\nabla(1-\psi)|^2 dy + \int_{Y_0 \cap U} |1-\psi|^2 |\nabla u^*|^2 dy \right) \\
&\leq C \left(\int_{Y_0 \cap U} |u^* - m|^2 dy + \int_{Y_0 \cap U} |\nabla u^*|^2 dy \right) \\
&\leq C \int_{Y_0 \cap U} \|\nabla u^*\|^2 dy \\
&\leq C \|\nabla u\|_{L^2(Y)}^2
\end{aligned}
$$

where we have used the Poincare inequality for $\int_{Y_0 \cap U} |u^* - m|^2$. With $\partial_t m$ obtained from

Lemma 6.2, we define the extension $\partial_t \tilde{u}$

$$
\partial_t \tilde{u} := (1-\psi)(\partial_t u^* - \partial_t m) + \partial_t m,
$$

As $\partial_t u^* \in L^2(0, T; H^{-1}(Z))$ and $\partial_t m \in L^\infty(0, T)$, the definition above is well defined and $\partial_t \tilde{u} \in L^2(0, T; H^{-1}(Z))$. Also for a.e. t,

$$
\|\partial_t \tilde{u}\|_{H^{-1}(Z)} = \sup_{\xi \in H^1(Z), \|\xi\|=1} |\langle \partial_t \tilde{u}, \xi \rangle| = \partial_t m + \sup_{\xi \in H^1(Z), \|\xi\|=1} |\langle (1-\psi)\partial_t u^*, \xi \rangle|.
$$

Hence,

$$
\|\partial_t \tilde{u}\|_{H^{-1}(Z)} \leq C \|\partial_t u\|_{H^{-1}(Y)},
$$

which implies Lemma 6.3. $\qquad\square$

Proof. (Lemma 6.4) To prove the first part of Lemma 6.4 we use a simple scaling argument,

$$
\begin{aligned}
\|\tilde{u}^\varepsilon\|_{H^1(\Omega)} &= \sum_{\varepsilon Z^k \subset \Omega} \int_{\varepsilon Z^k} \left\{ |\tilde{u}^\varepsilon(x)|^2 + |\nabla \tilde{u}^\varepsilon(x)|^2 dx \right\} \\
&= \sum_{\varepsilon Z^k \subset \Omega} \int_{Z^k} \left\{ |\tilde{u}^\varepsilon(\varepsilon y)|^2 + \varepsilon^{-2} |\nabla_y \tilde{u}^\varepsilon(\varepsilon y)|^2 \right\} dy \\
&\leq C \sum_{\varepsilon Z^k \subset \Omega} \int_{Y^k} \left\{ |u^\varepsilon(\varepsilon y)|^2 + \varepsilon^{-2} |\nabla_y u^\varepsilon(\varepsilon y)|^2 \right\} dy \\
&= C \sum_{\varepsilon Z^k \subset \Omega} \int_{\varepsilon Y^k} \left\{ |u^\varepsilon(x)|^2 + |\nabla_y u^\varepsilon(x)|^2 \right\} dx \\
&= C \|u^\varepsilon\|_{H^1(\Omega^\varepsilon)}.
\end{aligned}
$$

By a simple scaling argument similar to that used above completes the proof for Lemma 6.4. □

6.4   Two-scale convergence

First we note down the definitions of two-scale convergence and a lemma that would found to be useful later. Following definitions are standard (e.g. [2, 101]).

Definition 6.4.1 *A sequence $u^\varepsilon \in L^2(\Omega^\varepsilon)$ is said to converge two-scale to a limit $u \in L^2(\Omega \times Z)$ iff*

$$\lim_{\varepsilon \searrow 0} \int_{\Omega^\varepsilon} u^\varepsilon(x)\phi(x, \frac{x}{\varepsilon})dx = \int_\Omega \int_Z u(x,y)\phi(x,y)dxdy$$

for all $\phi \in \mathcal{D}(\Omega; C^\infty_{per}(Z))$.

Definition 6.4.2 *A sequence $v^\varepsilon \in L^2(\Gamma^\varepsilon_G)$ is said to converge two-scale to a limit $v \in L^2(\Omega \times \Gamma_G))$ iff*

$$\lim_{\varepsilon \searrow 0} \varepsilon \int_{\Gamma^\varepsilon_G} v^\varepsilon(x)\phi(x, \frac{x}{\varepsilon})dx = \int_\Omega \int_{\Gamma_G} v(x,y)\phi(x,y)dxdy$$

for all $\phi \in \mathcal{D}(\Omega; C^\infty_{per}(\Gamma_G))$.

We state the Oscillation Lemma for the lower dimensional manifold (see [101] Lemma 1.3.2)

Lemma 6.5 *For any function $f \in C^0(\bar{\Omega}; C^0_{per}(\Gamma))$ holds*

$$\lim_{\varepsilon \searrow 0} \varepsilon \int_{\Gamma^\varepsilon_G} f\left(x, \frac{x}{\varepsilon}\right) dx = \int_\Omega \int_{\Gamma_G} f(x,y)dxdy.$$

Next, we consider the estimates (6.3.4). Using the extension theorem and denoting $\tilde{u}^\varepsilon$ by u^ε for the ease of presentation; compactness arguments provide us the following:

Lemma 6.6 *There exists a limit u such that up to a subsequence*

(i). *$u^\varepsilon \rightharpoonup u$ weakly in $L^2(0, T; H^1(\Omega))$,*

(ii). *$\partial_t u^\varepsilon \rightharpoonup \partial_t u$ weakly in $L^2(0, T; H^{-1}(\Omega))$,*

(iii). $u^\varepsilon \to u$ *in* $C^0(0, T; H^{-s}(\Omega)) \cap L^2(0, T; H^s(\Omega)), s \in (0, 1).$

Since u^ε converges weakly to u in $L^2(0, T; H^1(\Omega))$, and with $\partial_t u^\varepsilon \in L^2(0, T; H^{-1}(\Omega))$ implies the strong convergence in $L^2(0, T; L^2(\Omega))$; the compactness arguments ([2,101]) imply the two-scale convergence to the same u and there exists functions $u \in L^2(0, T; H^1(\Omega))$, $u_1 \in L^2(0, T; L^2(\Omega; H^1_{\text{per}}(Z)))$ such that up to a subsequence

Lemma 6.7 *It holds that*

(i). u^ε *two-scale converges to u.*

(ii). ∇u^ε *two-scale converges to* $\nabla_x u + \nabla_y u_1$.

Furthermore, for $v^\varepsilon, w^\varepsilon$ and $\partial_t v^\varepsilon$:

Lemma 6.8 *Up to a subsequence*

(i). v^ε *two-scale converges to v.*

(ii). $\partial_t v^\varepsilon$ *two-scale converges to $\partial_t v$.*

(iii). w^ε *two-scale converges to w.*

6.4.1 The macroscopic equation

Up to now we have obtained the existence of a limit triple (u, v, w) for the sequence $(u^\varepsilon, v^\varepsilon, w^\varepsilon)$. Here we proceed by identifying this limit as the solution of the upscaled system of equations (6.2.8), with the initial and boundary conditions (6.2.9). To be precise, with matrix S defined as

$$(S)_{i,j} = |Y|\delta_{ij} + \int_Y \partial_{y_j} w_i;$$

and w_i solving the cell problem

$$-\triangle w_i = 0 \text{ in } Y, \quad \nabla \cdot w_i = \mathbf{e}_i \cdot \boldsymbol{\nu} \text{ on } \partial Y,$$

we have the following definition for the weak solution of the upscaled equations (6.2.8)-(6.2.9).

Definition 6.4.3 *The triple (u, v, w) with $u \in L^2(0, T; H^1(\Omega))$; $\partial_t u \in L^2(0, T; H^{-1}(\Omega))$, $v \in L^\infty(0, T; L^2(\Omega \times \Gamma_G)), w \in L^\infty(0, T; L^2(\Omega \times \Gamma_G))$ is called a weak solution of (6.2.8) and*

(6.2.9) *if* $(u(0), v(0)) = (u_I, v_I)$ *and if*

$$(\partial_t u, \phi)_{\Omega^T} + D(S\nabla u, \nabla \phi)_{\Omega^T} = -(qu, \nabla \phi)_{\Omega^T} - (\partial_t v, \phi)_{\Omega^T \times \Gamma_G}$$
$$(\partial_t v, \theta)_{L^2(\Omega^T \times \Gamma_G)} = (r(u) - w, \theta)_{L^2(\Omega^T \times \Gamma_G)} \quad (6.4.1)$$
$$w \in H(v)$$

for all $(\phi, \theta) \in (L^2(0, T, H^1_{0,\Gamma_D}(\Omega)), L^2(0, T; L^2(\Omega \times \Gamma_G)))$.

The main result is as follows:

Theorem 6.4.1 *As* $\varepsilon \searrow 0$, *the sequence of solutions* $(u^\varepsilon, v^\varepsilon, w^\varepsilon)$ *of the microscopic problem* (6.3.1) *converges to the weak solution* (u, v, w) *in the sense of Definition 6.4.3.*

In view of two-scale convergence results, the derivation of limit problem for $(6.3.1)_1$ is straightforward. We defer the derivation of the limit problem and the cell problem to the end of this section. We begin by considering $(6.3.1)_2$ which contains the nonlinearities. Passing to the limit as $\varepsilon \searrow 0$ for the left hand side is straightforward ; we deal with the right hand side which contains the non-linear terms. Specifically, we consider the term

$$\varepsilon \int_0^T \int_{\Gamma_G^\varepsilon} (r(u^\varepsilon) - w^\varepsilon) \left(\phi_0(t, x) + \varepsilon \phi_1(t, x, \frac{x}{\varepsilon}) \right) dx dt.$$

Note that

$$u^\varepsilon \to u \text{ in } C^0(0, T; H^{-s}(\Omega)) \cap L^2(0, T; H^s(\Omega)), s \in (0, 1).$$

By a slight modification in the proof of Lemma 3 of [61] there exists a constant $C > 0$, independent of ε, such that

$$\varepsilon \|u^\varepsilon - u\|^2_{\Gamma_G^\varepsilon} \le C(\|u^\varepsilon - u\|^2_\Omega + \varepsilon^2 \|\nabla u^\varepsilon - \nabla u\|^2_\Omega),$$

and hence we obtain (see [89], Lemma 4.2)

$$\varepsilon \|u^\varepsilon - u\|^2_{\Gamma_G^{\varepsilon T}} \le C\|u^\varepsilon - u\|^2_{L^2(0,T;H^s(\Omega^\varepsilon))} \le C\|u^\varepsilon - u\|^2_{L^2(0,T;H^s(\Omega))}.$$

This gives using the Lipschitz continuity of r

$$\varepsilon \|r(u^\varepsilon) - r(u)\|^2_{L^2(0,T;L^2(\Gamma_G^\varepsilon))} \le C\varepsilon \|u^\varepsilon - u\|^2_{\Gamma_G^{\varepsilon T}}$$
$$\le C\|u^\varepsilon - u\|^2_{L^2(0,T;H^s(\Omega^\varepsilon))} \le C\|u^\varepsilon - u\|^2_{L^2(0,T;H^s(\Omega))} \searrow 0 \quad (6.4.2)$$

because of the interpolation inequality. To correspond to the definition of two-scale convergence we estimate

$$\left| \int\limits_{\Gamma_G^\varepsilon} \varepsilon r(u^\varepsilon)\phi(x,\frac{x}{\varepsilon}) - \int\limits_{\Omega}\int\limits_{\Gamma_G} r(u)\phi(x,y) \right| \leq$$

$$\int\limits_{\Gamma_G^\varepsilon} \left| \varepsilon(r(u^\varepsilon) - r(u))\phi(x,\frac{x}{\varepsilon}) \right| + \left| \int\limits_{\Gamma_G^\varepsilon} \varepsilon r(u)\phi(x,\frac{x}{\varepsilon}) - \int\limits_{\Omega}\int\limits_{\Gamma_G} r(u)\phi(x,y) \right|$$

and using (6.4.2) first term on the right vanishes and the second term tends to 0 because of the Oscillation Lemma 6.5 thereby implying $r(u^\varepsilon)$ converges 2-scale to $r(u)$.

Even though w^ε converges two-scale to w, however this does not provide explicit form for the function w. To obtain this identification first we need to consider the convergence of v^ε to v in more details. We follow the ideas in [24, 35] and use the unfolding operator to establish the strong two-scale convergence for v^ε.

Definition 6.4.4 *For a given $\varepsilon > 0$, we define an unfolding operator T^ε mapping measurable functions on $(0,T) \times \Gamma_G^\varepsilon$ to measurable functions on $(0,T) \times \Omega \times \Gamma_G$ by*

$$T^\varepsilon f(t,x,y) = f(t,\varepsilon[\frac{x}{\varepsilon}] + \varepsilon y), \quad y \in \Gamma_G, \quad (t,x) \in (0,T) \times \Omega.$$

We extend T^ε from Γ_G to $\bigcup_k(\Gamma_G + k)$ periodically.

Basically, the two-scale convergence on Γ_G^ε becomes weak convergence of unfolded functions on $\Gamma_G \times \Omega$ and the strong two-scale convergence is equivalent to the strong convergence of unfolded functions on $\Gamma_G \times \Omega$. We establish first the strong convergence of the unfolded sequence $T^\varepsilon v^\varepsilon$. This is stated in the following lemmas. Following [89], denote $L^2_{\text{per}}(\Gamma_G)$ the space of functions f such that $f \in L^2(\Gamma_G)$ and then is periodically extended to $\bigcup_k(\Gamma_G + k)$.

Lemma 6.9 *If $T^\varepsilon v^\varepsilon \to v^*$ weakly in $L^2(0,T;L^2(\Omega);L^2_{\text{per}}(\Gamma_G))$ and v^ε converges two-scale to v then $v^* = v$ a.e. on $(0,T) \times \Omega \times \Gamma_G$.*

Proof. See Lemma 4.6, [89] (see also [24]). □

Lemma 6.10 *$T^\varepsilon v^\varepsilon$ converges strongly in $L^2(0,T;L^2(\Omega);L^2_{\text{per}}(\Gamma_G))$.*

Proof. We will be using the translation estimates and Riesz-Frechet-Kolmogorov theorem (e.g. see (IV.26 in [25] and its converse)) to prove the strong convergence. Notice that by virtue of $\partial_t v^\varepsilon$ uniformly bounded in $L^2(\Gamma_G^{\varepsilon T})$, the translations in time are already controlled. What we need is to control the translations in space. In doing so, let us

recall (6.2.5), and conclude that w^ε is monotonically increasing with respect to v^ε. This also implies that $T^\varepsilon w^\varepsilon$ is monotone with respect to $T^\varepsilon v^\varepsilon$. With the change in variable $x \mapsto \varepsilon[\frac{x}{\varepsilon}] + \varepsilon y, y \in \Gamma_G$ the equation $(6.3.1)_2$ reads

$$\partial_t T^\varepsilon v^\varepsilon = T^\varepsilon r(u^\varepsilon) - T^\varepsilon w^\varepsilon$$

in the sense of distributions.

Our approach is close to that used in [102]. Note that, with respect to x, $T^\varepsilon v^\varepsilon$ are step functions and to obtain equicontinuity with respect to translations in L^2, one needs to compare solutions from different cells and we need to control these translations with respect to x. The strong convergence of $r(u^\varepsilon)$ to $r(u)$ in $L^2(0, T; \Gamma_G)$ and the monotonicity of $T^\varepsilon w^\varepsilon$ are essentially used to achieve this. The control of translation with respect to y is similar. Here, we show the calculations for $x-$translation. Let Ω_h be an arbitrary compact subset of Ω and let $h \in (0, dist(\Omega_h, \partial\Omega))$. We compute

$$\frac{d}{dt}\|T^\varepsilon v^\varepsilon(t, x+h, y) - T^\varepsilon v^\varepsilon(t, x, y)\|^2_{L^2(\Gamma_G \times \Omega_h)} =$$
$$\int_{\Gamma_G \times \Omega_h} \{T^\varepsilon v^\varepsilon(t, x+h, y) - T^\varepsilon v^\varepsilon(t, x, y)\} \ldots$$
$$\{T^\varepsilon r(u^\varepsilon(t, x+h, y)) - T^\varepsilon w^\varepsilon(t, x+h, y) - T^\varepsilon r(u^\varepsilon(t, x, y)) + T^\varepsilon w^\varepsilon(t, x, y)\} \, dxdy.$$
$$(6.4.3)$$

The monotonicity of $T^\varepsilon w^\varepsilon$ with respect to $T^\varepsilon v^\varepsilon$ has the property,

$$\{T^\varepsilon v^\varepsilon(t, x+h, y) - T^\varepsilon v^\varepsilon(t, x, y)\}\{T^\varepsilon w^\varepsilon(t, x+h, y) - T^\varepsilon w^\varepsilon(t, x, y)\} \geq 0. \qquad (6.4.4)$$

Using (6.4.4) in (6.4.3), the right hand side is estimated as

$$\frac{d}{dt}\|T^\varepsilon v^\varepsilon(t, x+h, y) - T^\varepsilon v^\varepsilon(t, x, y)\|^2_{L^2(\Gamma_G \times \Omega_h)}$$
$$\leq \int_{\Gamma_G \times \Omega_h} \{T^\varepsilon v^\varepsilon(t, x+h, y) - T^\varepsilon v^\varepsilon(t, x, y)\}\{T^\varepsilon r(u^\varepsilon(t, x+h, y)) - T^\varepsilon r(u^\varepsilon(t, x, y))\} \, dxdy$$
$$\leq \frac{1}{2}\|T^\varepsilon v^\varepsilon(t, x+h, y) - T^\varepsilon v^\varepsilon(t, x, y)\|^2_{L^2(\Gamma_G \times \Omega_h)}$$
$$+\frac{1}{2}\|T^\varepsilon r(u^\varepsilon(t, x+h, y)) - T^\varepsilon r(u^\varepsilon(t, x, y))\|^2_{L^2(\Gamma_G \times \Omega_h)}.$$

Now integrate in time and notice that as $h \searrow 0$, due to strong convergence of $T^\varepsilon r(u^\varepsilon)$ the second term goes to 0 uniformly with respect to h (IV.26 in [25]). Using Gronwall's lemma we conclude that

$$\|T^\varepsilon v^\varepsilon(t, x+h, y) - T^\varepsilon v^\varepsilon(t, x, y)\|^2_{L^2(\Gamma_G^T \times \Omega_h)} \to 0 \text{ as } h \searrow 0$$

uniformly and hence establishing the strong convergence of $T^\varepsilon v^\varepsilon$ in $L^2(0, T; L^2(\Omega); L^2_{\text{per}}(\Gamma_G))$ (IV.26 in [25] and its converse). □

Remark 6.11 Note that w^ε may have discontinuities with respect to t, x which makes dealing with $T^\varepsilon w^\varepsilon$ a delicate task. In the present situation, we are rescued by the fact that $T^\varepsilon w^\varepsilon$ is monotone with respect to $T^\varepsilon v^\varepsilon$ and hence, the property (6.4.4) has a good sign which we use in (6.4.3). An alternative approach would be to formulate the boundary conditions as a variational inequality and then use the monotonicity arguments e.g. in [62]. □

Next, we prove that $w \in H(v)$. Recall that from above discussions, we have the following information:

$$
\begin{aligned}
T^\varepsilon v^\varepsilon &\to v \quad \text{strongly in} \quad L^2(0, T; L^2(\Omega); L^2_{\text{per}}(\Gamma_G)), \\
T^\varepsilon w^\varepsilon &\to w \quad \text{weakly in} \quad L^2(0, T; L^2(\Omega); L^2_{\text{per}}(\Gamma_G)), \\
T^\varepsilon w^\varepsilon &\in H(T^\varepsilon v^\varepsilon).
\end{aligned}
$$

Since $T^\varepsilon v^\varepsilon \to v$ strongly in $L^2(0, T; L^2(\Omega); L^2_{\text{per}}(\Gamma_G))$ we have $T^\varepsilon v^\varepsilon \to v$ a.e. We have only two situations, either $v(t, x, y) > 0$ or $v(t, x, y) = 0$. In the first case and with $\mu := v(t, x, y)/2 > 0$, the pointwise convergence implies the existence of a $\varepsilon_\mu > 0$ such that $T^\varepsilon v^\varepsilon > \mu$ for all $\varepsilon \le \varepsilon_\mu$. Then for any $\varepsilon \le \varepsilon_\mu$ we have $T^\varepsilon w^\varepsilon = 1$ implying $w = 1$. For the case when $v = 0$, we consider the following situations:

(a) $u > u^*$

From the pointwise convergence of $T^\varepsilon u^\varepsilon$, there exists an ε^* such that for $\varepsilon \le \varepsilon^*$, we have $u^\varepsilon > u^*$. This gives, using monotonicity of r, $r(T^\varepsilon u^\varepsilon) > 1$ and recall the definition (6.2.5) to obtain $T^\varepsilon w^\varepsilon = 1$. This implies that $T^\varepsilon w^\varepsilon \to 1$ pointwise a.e.

(b) $u \in [0, u^*)$

Again the pointwise convergence of $T^\varepsilon u^\varepsilon$ implies that for small enough ε, $u^\varepsilon \in (0, u^*)$. In this case, $r(T^\varepsilon u^\varepsilon) < 1$ leading to $T^\varepsilon w^\varepsilon = r(T^\varepsilon u^\varepsilon)$ using (6.2.5). With strong convergence of r, we get $T^\varepsilon w^\varepsilon$ converges to $r(u)$ pointwise a.e..

(c) $u = u^*$

Using similar arguments as above, $r(u) = 1$ and for sufficiently small ε, $r(T^\varepsilon u^\varepsilon) \to 1$ pointwise a.e.. Hence, $T^\varepsilon w^\varepsilon = \min(r(T^\varepsilon u^\varepsilon), 1) \to 1$ pointwise a.e..

Collecting the above cases, $T^\varepsilon w^\varepsilon$ converges pointwise a.e. to $\widetilde{w}$ where

$$
\widetilde{w} = \begin{cases} 1, & v > 0, \\ \min(r(u), 1), & v = 0, \\ 0, & v < 0. \end{cases} \tag{6.4.5}
$$

Next, both $T^\varepsilon w^\varepsilon$ and $\widetilde{w}$ are essentially bounded which implies that along a sequence $\varepsilon \searrow 0$, $T^\varepsilon w^\varepsilon \to \widetilde{w}$ strongly in $L^2(\Omega^T, L^2_{\text{per}}(\Gamma_G))$ but weakly* to w. By the uniqueness of

limit, one has $w = \widetilde{w}$ a.e. implying that w has the structure of (6.2.5). This completes the identification of w. The above discussions are summarized in the following:

Lemma 6.12 *The two-scale limit functions v, w satisfy*

$$(\partial_t v, \theta)_{\Omega^T \times \Gamma_G} = \int\limits_{\Omega^T \times \Gamma_G} (r(u) - w)\,\theta \qquad \text{for all} \qquad \theta \in C^\infty(\Omega^T, C^\infty_{\text{per}}(\Gamma_G)),$$

$$w \in H(v).$$

With the above Lemma providing us the limit equations for $(6.3.1)_{2,3}$, we proceed to complete the proof of Theorem 6.4.1.

Proof.   Proof of Theorem 6.4.1

Now we pass to the limit in $(6.3.1)_1$ to obtain the limiting equation and the cell problem. We rewrite the weak formulation $(6.3.1)_1$ to obtain

$$(\partial_t u^\varepsilon, \chi^\varepsilon \phi)_{\Omega^T} + D(\nabla u^\varepsilon, \chi^\varepsilon \nabla \phi)_{\Omega^T} - (\mathbf{q}^\varepsilon \chi^\varepsilon u^\varepsilon, \nabla \phi)_{\Omega^T} = -\varepsilon n(\partial_t v^\varepsilon, \phi)_{\Gamma_G^{\varepsilon T}}, \qquad (6.4.6)$$

for all $\phi \in L^2(0, T; H^1_{0, \Gamma_D}(\Omega))$, where χ^ε is the characteristic function for Ω^ε.
Choose for the test function $\phi = \phi_0(t, x) + \varepsilon \phi_1(t, x, \frac{x}{\varepsilon})$ with $\phi_0 \in C^\infty_0(0, T; C^\infty_0(\Omega))$ and $\phi_1 \in C^\infty_0(0, T; C^\infty_{\text{per}}(\Omega))$.

$$\int\limits_{\Omega^T} \partial_t u^\varepsilon \chi(\frac{x}{\varepsilon})\left(\phi_0(t, x) + \varepsilon \phi_1(t, x, \frac{x}{\varepsilon})\right) +$$

$$D \int\limits_{\Omega^T} \nabla_x u^\varepsilon(t, x) \cdot \chi(\frac{x}{\varepsilon})\left(\nabla_x \phi_0(t, x) + \varepsilon \nabla_x \phi_1(t, x, \frac{x}{\varepsilon})\right) + \nabla_y \phi_1(t, x, \frac{x}{\varepsilon}) +$$

$$\varepsilon n \int\limits_0^T \int\limits_{\Gamma_G^\varepsilon} \left(\partial_t v^\varepsilon, \phi_0(t, x) + \phi_1(t, x, \frac{x}{\varepsilon})\right) = 0$$

With $\varepsilon \searrow 0$ and using Theorem 6.6, Lemma 6.7, Lemma 6.12, we obtain

$$|Y| \int\limits_{\Omega^T} \partial_t u \phi_0 + D \int\limits_0^T \int\limits_{\Omega \times Y} \left(\nabla_x u(t, x) + \nabla_y u_1(t, x, y)\right)\left(\partial_x \phi_0(t, x) + \nabla_y \phi_1(t, x, y)\right) +$$

$$\int\limits_0^T \int\limits_\Omega \mathbf{q} u \nabla \phi + \int\limits_0^T \int\limits_{\Omega \times \Gamma_G} (r(u) - H(v))\,\phi_0 = 0.$$

Here, to pass to the limit in term containing $\mathbf{q}^\varepsilon$, we have used the strong convergence of $\mathbf{q}^\varepsilon$ to $\mathbf{q}$ as proved in [62].

Next, setting $\phi_0 \equiv 0$ we obtain

$$\int\limits_0^T \int\limits_{\Omega \times Y} \left(\nabla_x u(t,x) + \nabla_y u_1 \right) \cdot \nabla_y \phi_1(t,x,y) = 0, \text{ for all } \phi_1 \in C_0^\infty(0,T;C_{\text{per}}^\infty(\Omega)),$$

which is a weak form for the cell problem. Further,

$$D \int\limits_0^T \int\limits_{\Omega \times Y} \left(\nabla_x u(t,x) + \nabla_y u_1 \right) \nabla_x \phi_0 = D \int\limits_0^T \int\limits_{\Omega} S \nabla_x \phi_0 \nabla_x u,$$

where

$$(S)_{i,j} = |Y|\delta_{ij} + \int\limits_Y \partial_{y_j} w_i; \qquad -\triangle w_i = 0 \text{ in } Y, \quad \nabla \cdot w_i = \mathbf{e}_i \cdot \boldsymbol{\nu} \text{ on } \partial Y.$$

Collecting the above results in combination with Lemma 6.12, we conclude that (u,v,w) is a weak solution as introduced in Definition 6.4.3. This completes the proof of Theorem 6.4.1. □

6.4.2 Uniqueness of the macroscopic model

Theorem 6.4.2 *Uniqueness:* (6.2.8)-(6.2.9) *has unique solution.*

Proof. We follow the ideas from [45] and [47]. Here we only provide the sketch of the proof. Assume (u_1,v_1,w_1) and (u_2,v_2,w_2) both solve the weak formulation (6.4.1). We proceed as usual by defining:

$$U := u_1 - u_2, \quad V := v_1 - v_2, \quad W := w_1 - w_2.$$

We have the resulting equations as:

$$(\partial_t U, \phi) + (D\nabla U, \nabla \phi) + (\nabla \cdot (\mathbf{q}U), \phi) = \frac{|\Gamma_G|}{|Y|}(r(u_1) - r(u_2) - w_1 + w_2, \phi), \quad (6.4.7)$$

$$(\partial_t V, \theta) = (r(u_1) - r(u_2) - W, \theta), \quad (6.4.8)$$

$$W \in H(v_1) - H(v_2), \quad (6.4.9)$$

for all $(\phi, \theta) \in (L^2(0,T,H_{0,\Gamma_D}^1(\Omega)), L^2(0,T;L^2(\Omega))$.

Using (6.4.8) and choose $\theta = V$, using Young's inequality, Lipschitz continuity of r and

monotonicity of W we obtain

$$\|V(t)\|^2 \leq L_r^2 \int\limits_0^t \|U(\tau)\|^2 d\tau + \int\limits_0^t \|V(\tau)\|^2 d\tau,$$

and using Gronwall's lemma we obtain

$$\|V(t)\|^2 \leq \exp(t) L^2 \int\limits_0^t \|U(\tau)\|^2 d\tau,$$

$$\int\limits_0^t \|V(\tau)\|^2 d\tau \leq (\exp(t) - 1) L^2 \int\limits_0^t \|U(\tau)\|^2 d\tau.$$

Use for the test function $\phi = \int\limits_t^s U(\tau, x) d\tau$ in (6.4.7) and doing straightforward computations, we obtain [47]

$$\int\limits_0^s \|U(t)\|^2 dt + S \int\limits_\Omega \left| \int\limits_0^t \|\nabla U(\tau)\| d\tau \right|^2 dx \leq C M_q^2 \int\limits_0^s \int\limits_\Omega \left| \int\limits_0^t \|\nabla U(\tau)\| d\tau \right|^2 dx dt$$

and using Gronwall's lemma gives,

$$\int\limits_\Omega \int\limits_0^t \|\nabla U(\tau)\|^2 d\tau dx = 0$$

and consequently,

$$\int\limits_0^s \|U(t)\|^2 dt = 0,$$

for small enough s. Combining this with the estimates for $\|V(t)\|$ establishes uniqueness. $\qquad\square$

Remark 6.13

Alternatively, one can use L-1 contraction to show the uniqueness. One can follow the proof as given in [109]; in the given situation, the proof follows the same line. $\qquad\square$

Chapter 7

Numerical analysis of an upscaled model: conformal formulation

In this chapter we discuss the numerical analysis of an upscaled (core scale) model describing the transport, precipitation and dissolution of solutes in a porous medium. The particularity lies in the modeling of the reaction term, especially the dissolution term, which has a multivalued character. We consider the weak formulation for the upscaled equation and provide rigorous stability and convergence results for both the semi-discrete (time discretization) and the fully discrete scheme. In doing so, compactness arguments are employed.

7.1 Introduction

In this chapter we consider a model for the reactive flow in a porous medium, where the ions/solutes are being transported through the combined process of convection and diffusion. Such models are encountered in many real-life applications, like the spreading of chemical and the resulting ground water contamination (see [128] and references therein), biological applications such as tissue and bone formation, pharmaceutical applications [91], or the operation of solid state batteries. Of particular interest are the reactive processes, where precipitation and dissolution fronts develop as a result of re-

---

This chapter is a collaborative work with Sorin Pop and Florin Radu and it has been submitted to Numerische Mathematik.

actions (see [97,115,118] and references therein). In a related context, [23] discusses the presence of stiff dissolution fronts involving the applications in the nuclear waste disposal.

Here we concentrate on a macroscale (upscaled) model, meaning that the model is defined at the Darcy scale. Therefore no distinction is made between the solid grains and the pore space, and the equations are defined everywhere in the domain of interest. The interesting aspect of the flow is the description of reactions taking place which have a particular structure. These reactions model the precipitation and dissolution processes taking place due to the interactions of ions (cations and anions). The reactions lead to the formation of crystal which are immobile species. Since, the model is considered at macroscale, both the crystals and the ions are defined everywhere. We take the model which was first proposed in [73] and then followed in a series of papers [43–45]. In [47], the corresponding pore scale model was presented. Further, the upscaled model is derived rigorously in a simplified situation of a 2D strip. For a similar situation, but now involving free boundaries at the pore scale, formal upscaling has been discussed in [75] and [104].

Our main goal here is to provide the convergence of a conforming FEM discretization for an upscaled model for dissolution and precipitation in porous media, involving a multi-valued dissolution rate. Before discussing the details, we briefly review some of the numerical work that is related to the present context. Conformal FEM schemes for reactive porous media flow models are discussed in [14,15], where non-Lipschitz, but Hölder continuous rates are considered. Similarly, for Hölder continuous rates (including equilibrium and non-equilibrium cases) mixed FEM methods are analyzed rigorously in [120,123], whereas [121] provides error estimates for the coupled system describing unsaturated flow and reactive transport. In all these cases, the continuity of the reaction rates allows obtaining error estimates. Further, for continuously differentiable rates, the convergence of (adaptive) finite volume discretizations is studied in [72,111]; see also [28] for the convergence of a finite volume discretization of a copper-leaching model. In a similar framework, discontinuous Galerkin methods are discussed in [127] and upwind mixed FEM are considered in [38,39]; combined finite volume-mixed hybrid finite elements are employed in [52,59].

The primary motivation for the work here is to develop and analyse the appropriate numerical schemes to compute the solutions of macroscale equations. In the treatment here, we assume the flow to be given. Our primary focus is therefore to deal with the convection-diffusion-reaction equation where the non-linearities are in the reaction term. To avoid dealing with the inclusions as the dissolution rate is multi-valued, we use approximation schemes and consider both the semi-discrete and the fully discrete numerical schemes along these approximations (regularization). The resulting discrete equations are non-linear and the solutions depend on the regularization parameter. We prove their convergence to the time-continuous macroscale equations via a limiting procedure using compactness arguments. Whereas in the case of semi-discrete case,

we use translation estimates to improve the convergence needed to deal with the non-linearities, in the fully-discrete case, we use the properties of Lagrange interpolation operator (see [34]) to achieve the required convergence. Of particular relevance to the work presented here is [41] where a semi-discrete numerical scheme for pore scale model is considered and the convergence is proved. Here, we consider both semi-discrete and fully discrete cases and for the latter we use finite element method to treat the spatial discretization. As a by-product of the convergence proof, we also obtain an alternative proof for existence of solutions for the macroscale equations. The present work should be considered as a first step towards an eventual plan to consider both the flow and the reactions coupled together (for example, Richards' equation coupled with precipitation-dissolution reaction models).

The chapter is structured as follows. We begin with a brief description of the model in Section 7.2 where we also define the weak formulation of the model. We proceed to define the time-discrete formulation in Section 7.3 where the numerical scheme is analyzed and the convergence is proved. Next, in Section 7.4, we consider the fully discrete formulation and treat the convergence issue. The numerical experiments are shown in Section 7.5 followed by the conclusions and discussions in Section 7.6.

7.2 The model

We present here a brief description of the precipitation-dissolution model under consideration here. We refer to [43, 44, 73] for the details of the model. It is relevant to mention that despite the simplification of the model under consideration, we retain the essence and thereby the interesting mathematical character of the model. Let $\Omega \subset \mathbb{R}^2$ be the domain occupied by the porous medium, and assume Ω be open, connected, bounded and polygonal with Lipschitz boundary Γ. Further, let $T > 0$ be a fixed but arbitrarily chosen time, and define

$$\Omega^T = (0, T] \times \Omega, \quad \text{and} \quad \Gamma^T = (0, T] \times \Gamma.$$

While the reactions take place between the cations and anions, for the model considered here, we study only one mobile species (cation, though the choice is immaterial). This makes sense if the boundary and initial data are compatible (see [43], or [44]). Then, denoting by v the concentration of the (immobile) precipitate, and by u the cation concentration, the model reduces to

$$\begin{cases} \partial_t(u + v) + \nabla \cdot (\mathbf{q}u - \nabla u) &= 0, & \text{in } \Omega^T, \\ u &= 0, & \text{on } \Gamma^T, \\ u &= u_I, & \text{in } \Omega, \text{ for } t = 0, \end{cases} \quad (7.2.1)$$

for the ion transport, and

$$\begin{cases} \partial_t v & = & (r(u) - w), & \text{on } \Omega^T, \\ w & \in & H(v), & \text{on } \Omega^T, \\ v & = & v_I, & \text{on } \Omega, \text{ for } t = 0, \end{cases} \tag{7.2.2}$$

for the precipitate. The rate of change in the precipitate concentration is the net process of precipitation and dissolution. Here **q** stands for the Darcy fluid velocity. We assume that **q** is a known, divergence free velocity

$$\nabla \cdot \mathbf{q} = 0 \quad \text{in} \quad \Omega.$$

For the ease of presentation we restrict to homogeneous Dirichlet boundary conditions. The initial data u_I and v_I are assumed non–negative and essentially bounded. Moreover, for simplicity we assume that both $u_I, v_I \in H_0^1(\Omega)$, the space of H^1 functions defined on Ω and having a vanishing trace on Γ.

All quantities and variables in the above are assumed dimensionless. The diffusion is assumed 1, the extension to a positive definite diffusion tensor being straightforward. Further, we assume that the Damköhler number is scaled to 1, as well as an eventual factor in the time derivative of v in $(7.2.2)_1$, appearing in the transition (homogenization) from the pore scale to the core scale. For the precipitation rate r we assume

(A1) $r(\cdot) : \mathbb{R} \to [0, \infty)$ is locally Lipschitz continuous in $\mathbb{R}$.

(A2) There exists a unique $u_* \geq 0$, such that

$$r(u) = \begin{cases} 0 & \text{for} \quad u \leq u_*, \\ \text{strictly increasing for} \quad u \geq u_* & \text{with} \quad r(\infty) = \infty. \end{cases} \tag{7.2.3}$$

The dissolution rate has a particular structure. It is assumed constant (1, by scaling) at some $(t, x) \in \Omega^T$ where the precipitate is present, i.e. if $v(t, x) > 0$. In the absence of the precipitate, the overall rate (precipitate minus dissolution) is either zero if the solute present there is insufficient to produce a net precipitation gain, or positive in case the solute exceeds certain threshold value. In the presence of the precipitate, the dissolution strength is constant as it is a surface process. Further, the absence of net precipitation gain under insufficient amount of solutes being present, is related to the time-scale of observation. The derivation of the precipitation-dissolution is based on chemical kinetics and the ideas of solubility product for the crystals. For further discussions and derivation of this model, we refer to [45, 73]. For the dissolution process, the rate law

can be summarized as

$$w \in H(v), \quad \text{where} \quad H(v) = \begin{cases} 0, & \text{if} \quad v < 0, \\ [0,1], & \text{if} \quad v = 0, \\ 1, & \text{if} \quad v > 0. \end{cases} \qquad (7.2.4)$$

Remark 7.1 Since the precipitation rate r is monotonically increasing, under the setting above, a unique u^* exists for which $r(u^*) = 1$. Then u^* can be interpreted as an equilibrium value: within an open set $A \subset \Omega^T$ where $u = u^*$, no precipitation or dissolution occurs, and the precipitation rate is balanced by the dissolution rate regardless of the presence or absence of crystals. Then, as follows from [47, 73, 109],

$$w = 1 \quad \text{a.e. in} \quad A.$$

$\square$

Remark 7.2 The upscaled model under discussion, proposed originally in [73] (see also [43–45]), and can be obtained by homogenization techniques, starting from the pore scale counterpart in [47]. $\square$

We emphasize on the particularity of the present model, which is in the description of the dissolution and precipitation processes, involving a multi–valued dissolution rate. Clearly, classical solutions do not exist, except for some particular cases. Therefore we resort to defining appropriate weak solutions. We treat here the conformal weak formulation which one formally obtains by multiplying the equations, e.g. (7.2.1), (7.2.2) by smooth test functions and using partial integration, if necessary. We give a formal definition in Section 7.2.2.

7.2.1 Notations and assumptions

We adopt the following standard notations from the functional analysis. By $(\cdot, \cdot)$ we mean $L^2(\Omega)$ inner product or the duality pairing between H_0^1 and H^{-1}; the $L^2(\Omega^T)$ inner product is denoted by $(\cdot, \cdot)_{\Omega^T}$. Further, $\| \cdot \|$ stands for the norms induced by L^2 inner product, $L^2(0, T; X)$ denotes the usual Bochner spaces for a given Banach space X. For other norms, we explicitly state it. Furthermore, C denotes the generic constant and the value of which might change from line to line and is independent of unknown variables or the discretization parameters. Let L_r denote the Lipschitz constant of r and $\|\mathbf{q}\|_{L^\infty(\Omega)} \leq M_q$ where M_q is known.

We assume $\Omega \subset \mathbb{R}^2$ to be an open bounded and polygonal subset and define the follow-

ing sets

$$
\begin{aligned}
\mathcal{U} &:= \{u \in L^2((0,T); H_0^1(\Omega)) : \partial_t u \in L^2((0,T); H^{-1}(\Omega))\}, \\
\mathcal{V} &:= \{v \in H^1((0,T); L^2(\Omega))\}, \\
\mathcal{W} &:= \{w \in L^\infty(\Omega^T) : 0 \le w \le 1\}.
\end{aligned}
$$

Since, Ω is polygonal, it has a regular decomposition into triangles and the errors due to nonpolygonal domains are avoided. Let $\mathcal{T}_h$ be a regular decomposition of $\Omega \subset \mathbb{R}^2$ into closed triangles; h stands for the mesh-size. For the fully discrete situation, we will use the discrete subspace $\mathcal{U}_h \subset H_0^1(\Omega)$ defined as

$$
\mathcal{U}_h := \{\theta \in C(\bar\Omega) \mid \theta \in \mathcal{P}_1(T), \quad T \in \mathcal{T}_h, \text{ and } \theta = 0 \text{ on } \partial\Omega\},
$$

where $\mathcal{P}_1(T)$ is the space of first order polynomials in two variables, defined on a triangle T. In other words, $\mathcal{U}_h$ denotes the space of piecewise linear functions. Recall that $\mathcal{U}_h \subset H_0^1(\Omega)$ (see [33], p. 64). We also define the following projection:

$$
P_h : L^2(\Omega) \mapsto \mathcal{U}_h, (P_h\theta - \theta, \psi_h) = 0, \tag{7.2.5}
$$

for all $\psi_h \in \mathcal{U}_h$. Note that P_h satisfies ([33], p. 138)

$$
\|P_h\theta - \theta\| \le Ch\|\nabla\theta\|, \tag{7.2.6}
$$

for all $\theta \in H_0^1(\Omega)$, for some $C > 0$ not depending on θ.

Moreover, let $\mathbf{q}_h$ be the discrete approximation of $\mathbf{q}$ and we assume $\nabla \cdot \mathbf{q}_h = 0$ with

$$
\|\mathbf{q} - \mathbf{q}_h\| \searrow 0
$$

uniformly as $h \searrow 0$. Further, we assume that $\mathbf{q}_h$ also obeys the maximum principle so that $\|\mathbf{q}_h\|_{L^\infty(\Omega)} \le M_q$.

7.2.2 Weak formulation

We start with defining the conformal weak formulation for (7.2.1)-(7.2.2).

Definition 7.2.1 *A triple* $(u,v,w) \in \mathcal{U} \times \mathcal{V} \times \mathcal{W}$ *is a weak solution of* (7.2.1) *and* (7.2.2) *if* $(u_{|t=0}, v_{|t=0}) = (u_I, v_I)$, *and for all* $(\phi, \theta) \in (L^2(0,T,H_0^1(\Omega)), L^2(0,T;L^2(\Omega))$

$$
\begin{aligned}
(\partial_t u + \partial_t v, \phi)_{\Omega^T} + (\nabla u, \nabla\phi)_{\Omega^T} + (qu, \nabla\phi)_{\Omega^T} &= 0, \\
(\partial_t v, \theta)_{\Omega^T} - (r(u) - w, \theta)_{\Omega^T} &= 0, \\
w &\in H(v), \text{ a.e. in } \Omega^T.
\end{aligned} \tag{7.2.7}
$$

The existence of a solution will be proved in Theorems 7.3.1 and 7.4.1 below. Alternatively, one can obtain the existence as an outcome of the rigorous homogenization procedure, starting from the model at the pore scale. The uniqueness follows by standard contraction arguments. In what follows we propose numerical schemes for the above weak formulation and perform their analysis, namely proving the convergence of these discretized equations to the macroscale equations (7.2.7). First, we start with time-discrete formulation which we refer to as semi-discrete scheme. Consideration of this case provides a good understanding of the mathematical issues encountered in the convergence proofs and prepares for considering the fully-discrete case where we discretize in both space and time. The proofs in the latter case follow the same line of arguments as in the semi-discrete case and in some cases, the results can be directly borrowed. However, there are important differences and we comment on these as we proceed for the proofs.

As it has been remarked before, the study of numerical schemes and the convergence of these schemes to the macroscale equations provide us with an alternative proof for existence of solutions. We begin with the time-discrete formulation.

7.3   Semi-discrete scheme

Before defining the time-discretization, let us note the presence of a multi-valued rate in $(7.2.7)_3$, which impedes obtaining a priori estimates. Therefore we consider a regularized approximation of the original model (and pass later to the limit). We make sure that the estimates are independent of the regularization parameter, which is essential for passing to the limit. With $\delta > 0$, define the regularized Heaviside function

$$H_\delta(v) = \begin{cases} 0, & \text{if } v < 0, \\ \frac{v}{\delta}, & \text{if } 0 \le v \le \delta, \\ 1, & \text{if } v > \delta. \end{cases} \qquad (7.3.1)$$

We start with defining the time-discrete scheme which we refer to $\mathbf{P}_\delta^n$ with subscript stressing the dependence of solution on the regularization parameter δ. We then proceed to prove the convergence of the sequence of solutions of $\mathbf{P}_\delta^n$, passing to a subsequence, if necessary. Our steps for the proof of convergence follow the usual procedure. First, we obtain the a priori estimates which are independent of the discretization parameters and then define a time-continuous approximation for the solution. The estimates for these approximations then pave the way for using convergence results. In the wake of non-linearities involved, we need to improve the convergence, which we obtain by translation estimates in the semi-discrete situation.

Next, with $N \in \mathbb{N}, \tau = \frac{T}{N}$ and $t_n = n\tau, n = 1, \ldots, N$, we consider a uniform time stepping that is implicit in u and explicit in v. Starting with $u_\delta^0 = u_I, v_\delta^0 = v_I$, with

$n \in \{1, \dots, N\}$, the approximation (u_δ^n, v_δ^n) of $(u(t_n), v(t_n))$ solves

Problem P_δ^n : Given $(u_\delta^{n-1}, v_\delta^{n-1}) \in \left(H_0^1(\Omega) \times L^2(\Omega) \right)$, find $(u_\delta^n, v_\delta^n) \in \left(H_0^1(\Omega) \times \in L^2(\Omega) \right)$ such that

$$\left(\frac{u_\delta^n - u_\delta^{n-1}}{\tau}, \phi \right) + (\nabla u_\delta^n, \nabla \phi) - (\mathbf{q} u_\delta^n, \nabla \phi) + \left(\frac{v_\delta^n - v_\delta^{n-1}}{\tau}, \phi \right) = 0$$
$$\left(\frac{v_\delta^n - v_\delta^{n-1}}{\tau}, \theta \right) = \left(r(u_\delta^n) - H_\delta(v_\delta^{n-1}), \theta \right) \tag{7.3.2}$$

for all $\phi \in H_0^1(\Omega), \theta \in L^2(\Omega)$. For completeness, we define

$$w_\delta^n := H_\delta(v_\delta^n).$$

For stability reasons, we choose $\delta = O(\tau^{\frac{1}{2}})$ (see [41] for detailed arguments).

This is a system of elliptic equations for u_δ^n, v_δ^n given $u_\delta^{n-1} \in H_0^1(\Omega), v_\delta^{n-1} \in L^2(\Omega)$. Note that the first equation is decoupled from the second equation since it can be written in the form

$$\left(\frac{u_\delta^n - u_\delta^{n-1}}{\tau}, \phi \right) + (\nabla u_\delta^n, \nabla \phi) - (\mathbf{q} u_\delta^n, \nabla \phi) + \left(r(u_\delta^n) - H_\delta(v_\delta^{n-1}), \phi \right) = 0.$$

With reaction term r being Lipschitz and monotonic; standard monotonicity arguments can be used to show the existence and uniqueness of u_δ^n given u_δ^{n-1} [83]. After u_δ^n is computed, for the second equation, computing v_δ^n is straightforward as it is an explicit discretization in time. We summarize the above result:

Lemma 7.3 *Problem P_δ^n has a unique solution pair (u_δ^n, v_δ^n).*

For the continuous formulation, (7.2.7), u, v are positive and essentially bounded. We proceed to establish that this property is also respected by the time-discrete formulation. With $M_u := \max\{\|u_I\|_{L^\infty}, u^*\}, M_v := \|v_I\|_{L^\infty}$, we note that $r(M_u) \geq 1$. Let us first prove the positivity of the solution pair (u_δ^n, v_δ^n).

Lemma 7.4 *If $u_\delta^{n-1}, v_\delta^{n-1} \geq 0$ then $u_\delta^n, v_\delta^n \geq 0$.*

Proof. We start with the estimate for v_δ^n. In $(7.3.2)_2$, for $\theta = [v_\delta^{n-1}]_-$, with $[\cdot]_-$ denoting the non-positive part, we get

$$\|[v_\delta^n]_-\|^2 = (v_\delta^{n-1}, [v_\delta^n]_-) + \tau(r(u_\delta^n) - H_\delta(v_\delta^{n-1}), [v_\delta^n]_-).$$

By assumption $v_\delta^{n-1} \geq 0$, $\delta = O(\tau^{\frac{1}{2}})$ and $r(u_\delta^n) \geq 0$, we are left to consider

$$v_\delta^{n-1} - \tau H_\delta(v_\delta^{n-1}) \geq v_\delta^{n-1}(1 - \tau/\delta) \geq 0.$$

Hence $\|[v_\delta^n]_-\|^2 \leq 0$ implying $v_\delta^n \geq 0$.

Next we prove that u_δ^n is nonnegative. For $\phi = [u_\delta^n]_-$ in $(7.3.2)_2$

$$\|[u_\delta^n]_-\|^2 + \tau\|\nabla[u_\delta^n]_-\|^2 - \tau(\mathbf{q}u_\delta^n, \nabla[u_\delta^n]_-) + (v_\delta^n - v_\delta^{n-1}, [u_\delta^n]_-) \leq (u_\delta^{n-1}, [u_\delta^n]_-).$$

The first two terms are nonnegative, whereas the third term vanishes:

$$(\mathbf{q}u_\delta^n, \nabla[u_\delta^n]_-) = \frac{1}{2}(\mathbf{q}, \nabla[u_\delta^n]_-^2) = \frac{1}{2}(\nu \cdot \mathbf{q}, [u_\delta^n]_-^2)_\Gamma - \frac{1}{2}(\nabla \cdot \mathbf{q}, [u_\delta^n]_-^2) = 0$$

by the boundary conditions for u_δ^n on Γ and $\nabla \cdot \mathbf{q} = 0$ in Ω. Further using $(7.3.2)_2$ we have

$$(v_\delta^n - v_\delta^{n-1}, [u_\delta^n]_-) = \tau(r(u_\delta^n) - H_\delta(v_\delta^{n-1}), [u_\delta^n]_-) = -\tau(H_\delta(v_\delta^{n-1}), [u_\delta^n]_-) \geq 0$$

where we have used the positivity of $r(u_\delta^{n-1})$ and non-negativity of H_δ. Now by assumption $u_\delta^{n-1} \geq 0$, we obtain $u_\delta^n \geq 0$. $\qquad\square$

The next lemma provides the pointwise bound for the concentration u_δ^n for any n. The following lemma and a simple induction argument give this bound.

Lemma 7.5 *If $u_\delta^{n-1} \leq M_u$ then $u_\delta^n \leq M_u$.*

Proof. Test $(7.3.2)_1$ with $\phi = [u_\delta^n - M_u]_+$ (the non-negative part of $u_\delta^n - M_u$) to obtain

$$\|[u_\delta^n - M_u]_+\|^2 + \tau\|\nabla[u_\delta^n - M_u]_+\|^2 - \tau(\mathbf{q}u_\delta^n, \nabla[u_\delta^n - M_u]_+)$$
$$+ (v_\delta^n - v_\delta^{n-1}, [u_\delta^n - M_u]_+) \leq (u_\delta^{n-1} - M_u, [u_\delta^n - M_u]_+). \tag{7.3.3}$$

Again the third term vanishes using the arguments in the previous proof. Also

$$(u_\delta^{n-1} - M_u, [u_\delta^n - M_u]_+) \leq 0 \text{ as } u_\delta^{n-1} - M_u \leq 0.$$

Furthermore,

$$(v_\delta^n - v_\delta^{n-1}, [u_\delta^n - M_u]_+) = (r(u_\delta^n) - H_\delta(v_\delta^{n-1}), [u_\delta^n - M_u]_+) \geq 0 \text{ since } r(u_\delta^n) - H_\delta(v_\delta^{n-1}) \geq 0$$

for $u_\delta^n \leq M_u$. $\qquad\square$

For the concentration of the crystal v_δ^n, the situation is a bit different but expected as is evident from its ODE nature. Indeed, we have the following lemma:

Lemma 7.6 *Let $C = \frac{L_r M_u}{M_v}$ and assume that $v_\delta^{n-1} \leq M_v e^{C(n-1)\tau}$, then $v_\delta^n \leq M_v e^{Cn\tau}$.*

Proof. We use $\theta := [v_\delta^n - M_v e^{Cn\tau}]_+$ in $(7.3.2)_2$ to obtain

$$
\begin{aligned}
\|[v_\delta^n - M_v e^{Cn\tau}]_+\|^2 &= \left(v_\delta^{n-1} - M_v e^{C(n-1)\tau}, [v_\delta^n - M_v e^{Cn\tau}]_+ \right) \\
&\quad + M_v \left(e^{C(n-1)\tau} - e^{Cn\tau}, [v_\delta^n - M_v e^{Cn\tau}]_+ \right) \\
&\quad \tau \left(r(u_\delta^n) - H_\delta(v_\delta^{n-1}), [v_\delta^n - M_v e^{Cn\tau}]_+ \right).
\end{aligned}
\tag{7.3.4}
$$

Since, $r(u_\delta^n)$ is Lipschitz and $H_\delta(\cdot)$ is positive, we obtain

$$
\tau \left(r(u_\delta^n) - H_\delta(v_\delta^{n-1}), [v_\delta^n - M_v e^{Cn\tau}]_+ \right) \leq \tau (CM_v, [v_\delta^n - M_v e^{Cn\tau}]_+),
$$

and

$$
M_v \left(e^{C(n-1)\tau} - e^{Cn\tau}, [v_\delta^n - M_v e^{Cn\tau}]_+ \right) \leq M_v \left(1 - e^{C\tau}, [v_\delta^n - M_v e^{Cn\tau}]_+ \right).
$$

Here, we have used $e^{C(n-1)\tau} \geq 1$. Next,

$$
\begin{aligned}
\tau \left(CM_v, [v_\delta^n - M_v e^{Cn\tau}]_+ \right) &+ M_v \left(1 - e^{C\tau}, [v_\delta^n - M_v e^{Cn\tau}]_+ \right) \\
&\leq M_v \left(C\tau + 1 - e^{C\tau}, [v_\delta^n - M_v e^{Cn\tau}]_+ \right) \leq 0
\end{aligned}
$$

since $1 + x - e^x \leq 0$ for $x \geq 0$.

By assumption on v_δ^{n-1}, $\left(v_\delta^{n-1} - M_v e^{C(n-1)\tau}, [v_\delta^n - M_v e^{Cn\tau}]_+ \right) \leq 0$ and using above in (7.3.4), we conclude

$$
\|[v_\delta^n - M_v e^{Cn\tau}]_+\|^2 \leq 0
$$

leading to the assertion.   □

As $n\tau \leq T$, we conclude that the estimates shown above are independent of δ and τ.

7.3.1   The a priori estimates

With the pointwise bounds for the Problem $\mathbf{P}_\delta^n$ already established, we proceed to obtain energy estimates. These estimates will be used later for compactness arguments. These are similar to estimates for parabolic equations but here restricted to discrete time steps. We have the following lemma:

Lemma 7.7 *The following estimates hold*

$$\|v_\delta^n\| \leq \|v_I\| + Cr(M_u),\tag{7.3.5}$$

$$\|v_\delta^n - v_\delta^{n-1}\| \leq C\tau,\tag{7.3.6}$$

$$\tau \sum_{n=1}^{N} \|\nabla u_\delta^n\|^2 \leq C,\tag{7.3.7}$$

$$\sum_{n=1}^{N} \|u_\delta^n - u_\delta^{n-1}\|^2 \leq C\tau,\tag{7.3.8}$$

$$\sum_{n=1}^{N} \|\nabla(u_\delta^n - u_\delta^{n-1})\|^2 \leq C,\tag{7.3.9}$$

where C is independent of τ and δ.

Proof. To prove (7.3.5) we choose the test function $\phi = v_\delta^n$ in (7.3.2)$_1$ to obtain

$$(v_\delta^n - v_\delta^{n-1}, v_\delta^n) = \tau(r(u_\delta^n) - H_\delta(v_\delta^{n-1}), v_\delta^n),$$

which leads to using Cauchy-Schwarz inequality and $H_\delta, v_\delta^n \geq 0$

$$\|v_\delta^n\|^2 \leq \|v_\delta^n\|(\|v_\delta^{n-1}\| + C\tau r(M_u)).$$

The above equation can be re-written as

$$\|v_\delta^n\| - \|v_\delta^{n-1}\| \leq C\tau r(M_u)$$

which we sum over n to arrive at the assertion (7.3.5).
To prove (7.3.6), we consider (7.3.2)$_2$ and use $\theta = v_\delta^n - v_\delta^{n-1}$ to obtain

$$\|v_\delta^n - v_\delta^{n-1}\|^2 = \tau(r(u_\delta^n) - H_\delta(v_\delta^n), v_\delta^n - v_\delta^{n-1})$$
$$\leq \tau^2 \frac{1}{2}(r(M_u))^2 + \frac{1}{2}\tau^2 + \frac{1}{2}\|v_\delta^n - v_\delta^{n-1}\|^2,$$

leading to (7.3.6).
For (7.3.7), choosing $\phi = u_\delta^n$ in (7.3.2)$_1$ gives

$$(u_\delta^n - u_\delta^{n-1}, u_\delta^n) + \tau\|\nabla u_\delta^n\|^2 + \tau(\mathbf{q}u_\delta^n, \nabla u_\delta^n) + (v_\delta^n - v_\delta^{n-1}, u_\delta^n) = 0.$$

We rewrite the left hand side to get

$$\frac{1}{2}\left(\|u_\delta^n\|^2 - \|u_\delta^{n-1}\|^2 + \|u_\delta^n - u_\delta^{n-1}\|^2\right) + \tau\|\nabla u_\delta^n\|^2 \leq \|v_\delta^n - v_\delta^{n-1}\|\|u_\delta^n\| \leq C\tau.$$

Summing over n we obtain

$$\frac{1}{2}\|u_\delta^N\|^2 + \frac{1}{2}\sum_{n=1}^{N}\|u_\delta^n - u_\delta^{n-1}\|^2 + \tau\sum_{n=1}^{N}\|\nabla u_\delta^n\|^2 \leq \frac{1}{2}\|u_I\|^2 + C \leq C.$$

leading to (7.3.7).

We proceed further to prove (7.3.8) and (7.3.9). We choose for the test function $\phi = u_\delta^n - u_\delta^{n-1}$ in (7.3.2)$_1$ to obtain

$$\|u_\delta^n - u_\delta^{n-1}\|^2 + \tau(\nabla u_\delta^n, \nabla(u_\delta^n - u_\delta^{n-1})) + \tau(\mathbf{q}u_\delta^n, \nabla(u_\delta^n - u_\delta^{n-1})) + (v_\delta^n - v_\delta^{n-1}, u_\delta^n - u_\delta^{n-1}) = 0.$$

Treating the terms on the left hand side separately

$$\tau(\nabla u_\delta^n, \nabla(u_\delta^n - u_\delta^{n-1})) = \tau\frac{1}{2}\left(\|\nabla u_\delta^n\|^2 - \|\nabla u_\delta^{n-1}\|^2 + \|\nabla(u_\delta^n - u_\delta^{n-1})\|^2\right),$$

$$\tau\left|(\nabla\cdot(\mathbf{q}u_\delta^n), (u_\delta^n - u_\delta^{n-1}))\right| \leq \frac{\tau^2 M_q^2\|\nabla u_\delta^n\|^2}{2} + \frac{1}{2}\|u_\delta^n - u_\delta^{n-1}\|^2,$$

$$\left|(v_\delta^n - v_\delta^{n-1}, u_\delta^n - u_\delta^{n-1})\right| \leq \left(\|v_\delta^n - v_\delta^{n-1}\|^2 + \frac{1}{4}\|u_\delta^n - u_\delta^{n-1}\|^2\right) \leq \tau^2 CM_u^2 + \frac{1}{4}\|u_\delta^n - u_\delta^{n-1}\|^2,$$

where for the last line we have used (7.3.6). Using above, we obtain by summing over $n = 1,\ldots,N$

$$\frac{1}{4}\sum_{n=1}^{N}\|u_\delta^n - u_\delta^{n-1}\|^2 + \tau\|\nabla u_\delta^N\|^2 + \sum_{n=1}^{N}\tau\|\nabla(u_\delta^n - u_\delta^{n-1})\|^2 \leq C\tau + CM_q^2\tau + \tau\|\nabla u_I\|^2 \leq C\tau.$$

$\square$

7.3.2 Convergence

We consider the sequence of time discrete $(u_\delta^n, v_\delta^n, w_\delta^n)$ solving problem $\mathbf{P}_\delta^n$, and construct a time continuous approximation by taking linear interpolation. We define,

$$U^\tau(t) := u_\delta^n\frac{(t - t_{n-1})}{\tau} + u_\delta^{n-1}\frac{(t_n - t)}{\tau},$$
$$V^\tau(t) := v_\delta^n\frac{(t - t_{n-1})}{\tau} + v_\delta^{n-1}\frac{(t_n - t)}{\tau},$$
$$W^\tau(t) := H_\delta(V^\tau(t)).$$

We will use compactness arguments for time-continuous triples (U^τ, V^τ, W^τ) to identify the limit points and the system that these limit points satisfy. Note that this triple depends on δ however, for notational convenience we have suppressed the subscript. Using the estimates obtained in (7.3.5)-(7.3.9), we obtain similar estimates for (U^τ, V^τ, W^τ).

Lemma 7.8 *We have the following estimates:*

$$0 \leq U^\tau \leq M_u, 0 \leq V^\tau \leq M_v e^{CT}, 0 \leq W^\tau \leq 1 \tag{7.3.10}$$

$$\|U^\tau\|^2 + \|V^\tau\|^2 \leq C, \tag{7.3.11}$$

$$\|\partial_t U^\tau\|^2 + \|\nabla U^\tau\|^2 + \|\partial_t V^\tau\|^2 \leq C, \tag{7.3.12}$$

where C is a constant independent of τ, δ.

Proof. Clearly, (7.3.10), (7.3.11) follow from L^∞ estimates for u_δ^n, v_δ^n. We proceed with the gradient estimates. We rewrite the interpolation scheme,

$$U^\tau = u_\delta^{n-1} + \frac{t - t_{n-1}}{\tau}(u_\delta^n - u_\delta^{n-1})$$

from which we obtain

$$\nabla U^\tau = \nabla u_\delta^{n-1} + \frac{t - t_{n-1}}{\tau}(\nabla u_\delta^n - \nabla u_\delta^{n-1}).$$

Computing the $L^2(\Omega)$ norm and using the elementary inequality,

$$\|\nabla U^\tau\|^2 \leq 2\|\nabla u_\delta^{n-1}\|^2 + 2\frac{(t - t_{n-1})^2}{\tau^2}\|\nabla(u_\delta^n - u_\delta^{n-1})\|^2,$$

and integrating over t and since $u_\delta^{n-1}, u_\delta^n$ are constant in (t_{n-1}, t_n) we obtain

$$
\begin{aligned}
\int_0^T \|\nabla U^\tau\|^2 dt &\leq \sum_{n=1}^N 2 \int_{t_{n-1}}^{t_n} \|\nabla u_\delta^{n-1}\|^2 dt + 2\sum_{n=1}^N \int_{t_{n-1}}^{t_n} \frac{(t-t_{n-1})^2}{\tau^2}\|\nabla(u_\delta^n - u_\delta^{n-1})\|^2 dt, \\
&\leq \sum_{n=1}^N 2\tau\|\nabla u_\delta^{n-1}\|^2 + \sum_{n=1}^N \frac{2\tau}{3}\|\nabla(u_\delta^n - u_\delta^{n-1})\|^2,
\end{aligned}
$$

and stability estimates (7.3.7), (7.3.9) imply

$$\|\nabla U^\tau\|_{L^2(\Omega^T)}^2 \leq C.$$

To estimate $\|\partial_t V^\tau\|_{L^2(\Omega^T)}$ we note that whenever $t \in (t_{n-1}, t_n]$

$$\partial_t V^\tau = \frac{v_\delta^n - v_\delta^{n-1}}{\tau}$$

implying

$$\int_0^T \|\partial_t V^\tau\|^2 dt = \sum_{n=1}^N \int_{t_{n-1}}^{t_n} \|\frac{v_\delta^n - v_\delta^{n-1}}{\tau}\|^2 dt \leq \sum_{n=1}^N \tau\|\frac{v_\delta^n - v_\delta^{n-1}}{\tau}\|^2 \leq CN\tau \leq CT \leq C,$$

where we have used the estimate (7.3.6). To prove the estimate (7.3.12) is similar as above. Again, for $\|\partial_t U^\tau\|_{L^2(0,T;L^2(\Omega))}^2$ term, we note that whenever $t \in (t_{n-1}, t_n]$

$$\partial_t U^\tau = \frac{u_\delta^n - u_\delta^{n-1}}{\tau}$$

of which square of L^2 norm upon integrating over t yields

$$\int_0^T \|\partial_t U^\tau\|^2 dt = \sum_{n=1}^N \int_{t_{n-1}}^{t_n} \|\frac{u_\delta^n - u_\delta^{n-1}}{\tau}\|^2 dt \leq \sum_{n=1}^N \tau \|\frac{u_\delta^n - u_\delta^{n-1}}{\tau}\|^2 \leq CN\tau \leq CT \leq C,$$

where we have used the estimate (7.3.8). This proves the lemma. $\square$

The next lemma provides the convergence results based on the estimates obtained above.

Lemma 7.9 *The estimates obtained are uniform in τ and δ and furthermore we have $(U^\tau, V^\tau, W^\tau) \in \mathcal{U} \times \mathcal{V} \times L^\infty(\Omega)$. Clearly, $\tau \searrow 0$ with $\delta = O(\tau^{\frac{1}{2}})$ implies that both $\delta, \frac{\tau}{\delta} \searrow 0$. The compactness arguments from the bounds established in Lemma 7.8 lead to the following convergence results*

(i). $U^\tau \rightharpoonup u$ *weakly in* $L^2((0, T); H_0^1(\Omega))$,

(ii). $\partial_t U^\tau \rightharpoonup \partial_t u$ *weakly in* $L^2((0, T); H^{-1}(\Omega))$,

(iii). $V^\tau \rightharpoonup v$ *weakly in* $L^2((0, T); L^2(\Omega))$,

(iv). $\partial_t V^\tau \rightharpoonup \partial_t v$ *weakly in* $L^2((0, T); L^2(\Omega))$,

(v). $W^\tau \rightharpoonup w$ *weakly-star in* $L^\infty(\Omega)$.

The compactness results above only provides the existence of these limit points and it remains to be shown that these points satisfy the weak formulation in the sense of Definition 7.2.1. In what follows, we proceed to prove the same.

Notice that the weak convergence for U^τ in $L^2((0, T); H_0^1(\Omega))$ together with $\partial_t U^\tau \rightharpoonup \partial_t u$ weakly in $L^2((0, T); H^{-1}(\Omega))$ imply

$$U^\tau \to u \quad \text{strongly in} \quad L^2((0, T); L^2(\Omega)) \tag{7.3.13}$$

The lemma above provides only a weak convergence for V^τ and in the wake of nonlinearities, to facilitate getting the limit equations, we improve the convergence for V^τ and show that under H^1 regularity of the initial datum, we obtain strong convergence. This is achieved by the translation estimates.

Fixing a $t \in (t_{n-1}, t_n](0 < n \leq N)$ we define $\triangle_\xi$ as the translation operator

$$\triangle_\xi f(y, t) = f(y, t) - f(y + \xi, t).$$

We have the following lemma that provides the required translation estimate.

Lemma 7.10 *If $v_I \in H^1(\Omega)$ then the following estimate holds*

$$\left\|\triangle_\xi v_\delta^N\right\|^2 + \sum_{n=1}^N \left\|\triangle_\xi (v_\delta^n - v_\delta^{n-1})\right\|^2 \leq C \left\|\triangle_\xi v_I\right\|^2 + C\tau \sum_{n=1}^N \left\|\triangle_\xi u_\delta^n\right\|^2 \tag{7.3.14}$$

Proof. For $\theta = \triangle_\xi v_\delta^n$ in $(7.3.2)_2$, we get

$$\left(\triangle_\xi v_\delta^n - \triangle_\xi v_\delta^{n-1}, \triangle_\xi v_\delta^n\right) = \tau\left(\triangle_\xi r(u_\delta^n), \triangle_\xi v_\delta^n\right) - \tau\left(\triangle_\xi H_\delta(v_\delta^{n-1}), \triangle_\xi v_\delta^n\right).$$

We rewrite the last term in the above identity,

$$\left(\triangle_\xi H_\delta(v_\delta^{n-1}), \triangle_\xi v_\delta^n\right) = \left(\triangle_\xi H_\delta(v_\delta^{n-1}), \triangle_\xi v_\delta^{n-1}\right) + \left(\triangle_\xi H_\delta(v_\delta^{n-1}), \triangle_\xi(v_\delta^n - v_\delta^{n-1})\right).$$

The monotonicity of H_δ implies that the first term on the right hand side is positive, that is,

$$\left(\triangle_\xi H_\delta(v_\delta^{n-1}), \triangle_\xi v_\delta^{n-1}\right) \geq 0.$$

For the left hand side, we use the identity

$$\left(\triangle_\xi v_\delta^n - \triangle_\xi v_\delta^{n-1}, \triangle_\xi v_\delta^n\right) = \frac{1}{2}\left(\|\triangle_\xi v_\delta^n\|^2 - \left\|\triangle_\xi v_\delta^{n-1}\right\|^2 + \left\|\triangle_\xi(v_\delta^n - v_\delta^{n-1})\right\|^2\right).$$

Using the above identity and Cauchy-Schwarz for the first term on the right hand side, we have

$$\frac{1}{2}\left(\|\triangle_\xi v_\delta^n\|^2 - \left\|\triangle_\xi v_\delta^{n-1}\right\|^2 + \left\|\triangle_\xi(v_\delta^n - v_\delta^{n-1})\right\|^2\right) \leq \tau L_r \|\triangle_\xi u_\delta^n\| \|\triangle_\xi v_\delta^n\|$$
$$+ \tau\left(\triangle_\xi H_\delta(v_\delta^{n-1}), \triangle_\xi(v_\delta^n - v_\delta^{n-1})\right)$$
$$\leq L_r \tfrac{\tau}{2}\|\triangle_\xi u_\delta^n\|^2 + \tfrac{\tau}{2}\|\triangle_\xi v_\delta^n\|^2 + \tau^2\left\|\triangle_\xi H_\delta(v_\delta^{n-1})\right\|^2 + \tfrac{1}{4}\left\|\triangle_\xi(v_\delta^n - v_\delta^{n-1})\right\|^2$$

which gives further

$$\frac{1}{2}\left(\|\triangle_\xi v_\delta^n\|^2 - \left\|\triangle_\xi v_\delta^{n-1}\right\|^2 + \left\|\triangle_\xi(v_\delta^n - v_\delta^{n-1})\right\|^2\right) \leq \tfrac{1}{2}L_r\tau\|\triangle_\xi u_\delta^n\|^2 + \tfrac{1}{2}\tau\|\triangle_\xi v_\delta^n\|^2$$
$$+ \tfrac{\tau^2}{\delta^2}\|\triangle_\xi v_\delta^{n-1}\|^2 + \tfrac{1}{4}\|\triangle_\xi(v_\delta^n - v_\delta^{n-1})\|^2. \tag{7.3.15}$$

Summing over $n = 1, \ldots, N$

$$\left\|\triangle_\xi v_\delta^N\right\|^2 + \tfrac{1}{2}\sum_{n=1}^N\left\|\triangle_\xi(v_\delta^n - v_\delta^{n-1})\right\|^2 \leq \|\triangle_\xi v_I\|^2 + L_r\tau\sum_{n=1}^N\|\triangle_\xi u_\delta^n\|^2$$
$$+ \tau\sum_{n=1}^N\|\triangle_\xi v_\delta^n\|^2 + \sum_{n=1}^N\tfrac{2\tau^2}{\delta^2}\|\triangle_\xi v_\delta^{n-1}\|^2. \tag{7.3.16}$$

Choose for $\delta = O(\sqrt{\tau})$ and using Gronwall's lemma we obtain (since we can re-do the steps for any chosen $k \leq N$, $k \in \mathbb{Z}_+$)

$$\sup_{k=1,\ldots,N}\left\|\triangle_\xi v_\delta^k\right\|^2 \leq C\tau\sum_{n=1}^N\|\triangle_\xi u_\delta^n\|^2 + \|\triangle_\xi v_I\|^2. \tag{7.3.17}$$

$\square$

Using the translation estimate in above Lemma 7.10, we now show the strong conver-

gence of V^τ.

Lemma 7.11 *It holds that*

$$V^\tau \to v \quad strongly\ in \quad L^2(0, T; L^2(\Omega)). \tag{7.3.18}$$

Proof.   We use the translation in space and time to prove this strong convergence. First, let Ω' denote an arbitrary compact subset of Ω and $\xi \in (0, dist(\Gamma, \Omega'))$. It is well known that the strong convergence is tantamount to proving that (Prop. 9.3, p.267, [25])

$$\mathcal{I} := \int_{\Omega'^T} |V^\tau(t + h_t, x + \xi) - V^\tau(t, x)|^2 dxdt \searrow 0 \quad as \quad |(h_t, \xi)'| \searrow 0.$$

Since $\partial_t V^\tau$ is bounded uniformly in $L^2(0, T; L^2(\Omega))$, the estimates for the translation with respect to time is easily obtained. We now consider the translation with respect to space. We have using the definition of V^τ,

$$\triangle_\xi V^\tau = \frac{t_n - t}{\tau} \triangle_\xi v_\delta^{n-1} + \frac{t - t_{n-1}}{\tau} \triangle_\xi v_\delta^n.$$

We define the piecewise constant interpolation $\bar{U}^n$ for u_δ^n so that

$$\bar{U}^n = u_\delta^n, \quad t \in [t_{n-1}, t_n). \tag{7.3.19}$$

Squaring and integrating the left hand side over $\Omega' \times (0, T)$, we obtain

$$\int_0^T \int_{\Omega'} |\triangle_\xi V^\tau|^2 \le \sum_{n=1}^N \|\triangle_\xi v_\delta^n\|^2$$

and using (7.3.17) and replacing u_δ^n by $\bar{U}^n$, the right hand side is estimated as

$$\int_{\Omega'} |\triangle_\xi V^\tau(t, x) dx|^2 \le CT\tau \sum_{n=1}^N \|\triangle_\xi \bar{U}^n\|^2 + CT \|\triangle_\xi v_I\|^2.$$

We exploit a general result (for example, see [85]) which connects the convergence of piecewise linear interpolations with that of the piecewise constant interpolations. This ensures that the strong convergence of affine interpolation U^τ in $L^2(0, T; L^2(\Omega))$ implies strong convergence for piece-wise constant interpolation $\bar{U}^n$. Having this strong convergence for $\bar{U}^n$ implies that the space translation is controlled, namely

$$\tau \sum_{n=1}^N \|\triangle_\xi \bar{U}^n\|^2 \searrow 0 \quad as \quad |\xi| \searrow 0.$$

Since the initial conditions are in $H^1(\Omega)$, $\|\triangle_\xi v_I\|^2 \searrow 0$ as $|\xi| \searrow 0$. With this, $\mathcal{I} \searrow 0$ as $|\xi| \searrow 0$ which leads to the strong convergence of V^τ. $\qquad\square$

With the strong convergence established for V^τ, our preparation is complete to show that the limits points (u, v, w) obtained in Lemma 7.9 satisfy the weak formulation (7.2.7). This is considered in the following theorem.

Theorem 7.3.1 *The limit triple (u, v, w) satisfy the weak formulation stated in Definition 7.2.1.*

Proof. By the weak convergence, the estimates in Lemma 7.8 carry over for the limit triple (u, v, w). Moreover,

$$\int_0^T (\partial_t U^\tau, \phi) dt + \int_0^T (\nabla U^\tau, \nabla \phi) dt + \int_0^T (\mathbf{q} \cdot \nabla U^\tau, \phi) dt + \int_0^T (\partial_t V^\tau, \phi) dt$$
$$= \sum_{n=1}^N \int_{t_{n-1}}^{t_n} ((\nabla U^\tau - \nabla u_\delta^n), \nabla \phi) dt + \sum_{n=1}^N \int_{t_{n-1}}^{t_n} (\mathbf{q} \cdot (\nabla U^\tau - \nabla u_\delta^n), \phi) dt,$$

for all $\phi \in L^2(0, T; H_0^1)$. By Lemma 7.9, the left hand side converges to the desired limit. We are thus required to show that the right hand side vanishes. Denote the integrals of the right hand side by $\mathcal{I}_1$ and $\mathcal{I}_2$ and we obtain

$$|\mathcal{I}_1| \leq \left(\sum_{n=1}^N \tau C \|\nabla u_\delta^n - \nabla u_\delta^{n-1}\|^2 \right)^{\frac{1}{2}} \left(\int_0^T \|\nabla \phi\|^2 dt \right)^{\frac{1}{2}} \to 0$$

since $\sum_{n=1}^N \tau \|\nabla u_\delta^n - \nabla u_\delta^{n-1}\|^2 \searrow 0$ because of estimate (7.3.9). Similarly,

$$|\mathcal{I}_2| \leq \left(\sum_{n=1}^N \tau M_q \|\nabla(u_\delta^n - u_\delta^{n-1})\|^2 \right)^{\frac{1}{2}} \left(\int_0^T \|\phi\|^2 dt \right)^{\frac{1}{2}}$$

and due to (7.3.9), $|\mathcal{I}_2|$ vanishes as well.
For the limiting equation for V^τ, we have using $(7.3.2)_2$

$$\int_0^T (\partial_t V^\tau, \theta) dt = \int_0^T (r(U^\tau) - W^\tau) dt + \sum_{n=1}^N \int_{t_{n-1}}^{t_n} (r(u_\delta^n) - r(U^\tau), \theta) dt$$
$$+ \sum_{n=1}^N \int_{t_{n-1}}^{t_n} (W^\tau - H_\delta(v_\delta^{n-1}), \theta) dt.$$

We would retrieve the desired limiting equations once we prove that the last two integrals on the right hand side vanish. Let us denote the last two integrals by $\mathcal{I}_3$ and $\mathcal{I}_4$ respectively. We have

$$|\mathcal{I}_3| \leq \left(\sum_{n=1}^N \tau L_r^2 \|u_\delta^n - u_\delta^{n-1}\|^2 \right)^{\frac{1}{2}} \left(\int_0^T \|\theta\|^2 dt \right)^{\frac{1}{2}}$$

and using (7.3.8), we obtain $\mathcal{I}_3 \searrow 0$.
For $\mathcal{I}_4$, use the definition of W^τ and Lipschitz continuity of H_δ in order to obtain

$$|\mathcal{I}_4| \leq \sum_{n=1}^N \int_{t_{n-1}}^{t_n} \frac{1}{\delta} \|v_\delta^n - v_\delta^{n-1}\| \|\theta\| dt \leq \sum_{n=1}^N C \tau \frac{\tau}{\delta} \|\theta\| dt$$

by using (7.3.5) and further using Cauchy Schwarz and $\tau/\delta \searrow 0$ (by the construction of δ) we obtain $\mathcal{I}_4 \searrow 0$.

Next, we need to prove $w = H(v)$. Since we have V^τ strongly converging, we also obtain $V^\tau \to v$ pointwise a.e.. Further,

$$(W^\tau, \theta) = (w, \theta)$$

and by definition, $W^\tau = H_\delta(V^\tau)$; and

$$(H_\delta(V^\tau), \theta) = (w, \theta).$$

By construction, as $\tau \searrow 0$, $\delta \searrow 0$. Now, for any given $(t, x) \in \Omega$, either $v > 0$ or $v = 0$. For the case when $v > 0$, we have $W^\tau = 1$ and hence $w = 1$. For the case when $v = 0$, since $\partial_t v \in L^2(\Omega)$, $\partial_t v = 0$ leading to $w = r(u)$ with $0 \leq w \leq 1$ and hence we can establish the required result. □

7.4   Fully discrete system

We consider the fully discrete system (discretized in both space and time) and show the convergence of the numerical method. In particular, we consider the finite element discretization in space and for the time we retain the discretization as in the semi-discrete case. The steps for the proof of convergence are similar to the semi-discrete situation and where ever the proof is based on the time-discrete case treated above, we suppress the details of the proof. Further, to simplify notation, henceforth, we suppress the subscript δ.

To obtain the fully discrete formulation for the weak solution of (7.2.1)–(7.2.2), we take Euler's implicit discretization for the diffusion and reaction terms. Next, with $N \in \mathbb{N}, \tau = \frac{T}{N}$ and $t_n = n\tau, n = 1, \ldots, N$, we consider a uniform time stepping that is implicit in u and explicit in v. For the space discretization, we have Ω discretized in the $2-$ dimensional simplices (triangles) $\mathcal{T}_h$ with mesh-size h. We have assumed Ω to be polygonal as has been stated in Section 7.2.1. Further, we give definitions, in Section 7.2.1, of function spaces that will be used here. Starting with $u_h^0 = u_I, v_h^0 = v_I$, with $n \in \{1, \ldots, N\}$, the approximation (u_h^n, v_h^n) of $(u(t_n), v(t_n))$ at $\mathcal{T}_h$ solves

Problem $\mathbf{P}_h^n$: Given $(u_h^{n-1}, v_h^{n-1}, w_h^{n-1}) \in \mathcal{U}_h \times \mathcal{U}_h \times L^\infty(\Omega)$, find $(u_h^n, v_h^n, w_h^n) \in \mathcal{U}_h \times \mathcal{U}_h \times L^\infty(\Omega)$ such that

$$(u_h^n - u_h^{n-1}, \phi_h) + \tau(\nabla u_h^n, \nabla \phi_h) - (\mathbf{q}_h u_h^n, \nabla \phi_h) + (v_h^n - v_h^{n-1}, \phi_h) = 0,$$
$$(v_h^n - v_h^{n-1}, \theta_h) = \tau(r(u_h^n), \theta_h) - \tau(H_\delta(v_h^{n-1}), \theta_h) \qquad (7.4.1)$$

for all $\phi_h, \theta_h \in \mathcal{U}_h$.
To complete the solution we define

$$w_h^n := H_\delta(v_h^{n-1}).$$

Note that the solutions for $\mathbf{P}_h^n$ are defined in a finite dimensional vector space. In what follows we analyse the fully discrete case.

7.4.1 Existence and uniqueness

The discretization above in (7.4.1) provides a sequence of elliptic equations for u_h^n, v_h^n given $u_h^{n-1}, v_h^{n-1} \in \mathcal{U}_h$. For stability reasons, we choose $\delta = O(\tau^{\frac{1}{2}})$.
The first task here is to obtain the existence and uniqueness for problem $\mathbf{P}_h^n$. Since $\mathbf{P}_h^n$ is defined on a finite dimensional space, the proof for existence and uniqueness is not difficult, as for example it follows from [133]. However, we present here a fixed point argument based on linearization techniques (see [116]). It also provides a numerical method in addition to providing the existence and uniqueness. We use this method to perform numerical computations, hence we find it relevant to present this argument.
We assume that u_h^{n-1} and v_h^{n-1} are given with their corresponding $H_0^1(\Omega)$ and $L^2(\Omega)$ norms uniformly bounded. To construct the iteration scheme, we decouple the ion-transport equation and rewrite $(7.4.1)_1$ using $(7.4.1)_2$

$$(u_h^n - u_h^{n-1}, \phi_h) + \tau(\nabla u_h^n, \nabla \phi_h) - \tau(\mathbf{q}_h u_h^n, \nabla \phi_h) + \tau(r(u_h^n) - H_\delta(v_h^{n-1}), \phi_h) = 0 \quad (7.4.2)$$

for all $\phi_h \in \mathcal{U}_h$.
We make some preparation for applying the fixed point iteration. We define the norm

$$|||u|||^2 := \|u\|^2 + \frac{2\tau}{2 + \tau L_r} \|\nabla u\|^2$$

so that we can obtain the contraction. Recall that L_r is the Lipschitz constant of the precipitation term $r(\cdot)$. Further, we define the closed set

$$\mathcal{K} := \{u \in \mathcal{U}_h, \quad |||u||| \leq C\}.$$

Assuming $u_h^{n-1} \in \mathcal{K}$, we define the mapping $\mathcal{T}$

$$u_{i-1} \mapsto u_i = \mathcal{T} u_{i-1}$$

where u_i solves

$$(u_i, \phi_h) + \tau(\nabla u_i, \nabla \phi_h) - \tau(\mathbf{q}_h u_i, \nabla \phi_h) + \tau L_r(u_i, \phi_h) = \tau L_r(u_{i-1}, \phi_h) - \tau(r(u_{i-1}), \phi_h)$$
$$+ (u_h^{n-1}, \phi_h) + \tau(H_\delta(v_h^{n-1}), \phi_h)$$
$$(7.4.3)$$

for all $\phi_h \in \mathcal{U}_h$. A good initial value for the iteration is $u_0 = u_h^{n-1}$. We have suppressed the superscript n in the iteration for the sake of presentation. In the iterative scheme considered here, we note that the fixed point satisfies (7.4.2) as the terms involving L_r gets canceled in the case of convergence. The problem of proving existence and uniqueness of solution of problem $\mathbf{P}_h^n$ is, thus, tantamount to proving that of the fixed point of (7.4.3). Such constructions are common and we refer to [41] and the references therein for another application.

Next, we define

$$e_i := u_i - u_{i-1}.$$

We have the following result for the mapping $\mathcal{T}$.

Lemma 7.12 *It holds that $\mathcal{T}$ maps $u_{i-1} \in \mathcal{K}$ to $u_i = \mathcal{T}u_{i-1} \in \mathcal{K}$ and is a contraction with respect to the $||| \cdot |||$ norm.*

Proof. Note that standard Lax-Milgram arguments provide that $\mathcal{T}$ maps $\mathcal{K}$ into H^1. Next, we show that it is a contraction and hence maps $\mathcal{K}$ to itself. Using (7.4.3) and subtract the equation for u_{i-1} to obtain

$$(e_i, \phi_h) + \tau(\nabla e_i, \nabla \phi_h) - \tau(\mathbf{q}_h e_i, \nabla \phi_h) + \tau L_r(e_i, \phi_h) = \tau L_r(e_{i-1}, \phi_h)$$
$$- \tau(r(u_{i-1}) - r(u_{i-2}), \phi_h). \quad (7.4.4)$$

Choosing for $\phi_h = e_i$, we obtain

$$(1 + \tau L_r)\|e_i\|^2 + \tau\|\nabla e_i\|^2 - \tau(\mathbf{q}_h e_i, \nabla e_i) = \tau(L_r e_{i-1} - r(u_{i-1}) + r(u_{i-2}), e_i) \quad (7.4.5)$$

and since r is Lipschitz continuous, we use mean value theorem to obtain

$$(1 + \tau L_r)\|e_i\|^2 + \tau\|\nabla e_i\|^2 - \tau(\mathbf{q}_h e_i, \nabla \phi) = \tau(L_r e_{i-1} - r'(\xi)e_{i-1}, e_i) \quad (7.4.6)$$

for some $\xi \in (u_{i-1}, u_{i-2})$. Further, note that the contribution due to convection term vanishes, using the divergence free $\mathbf{q}_h$ we have

$$(\mathbf{q}_h e_i, \nabla e_i) = \frac{1}{2}\int_\Omega \nabla \cdot (\mathbf{q}_h e_i^2)dx = \frac{1}{2}\int_{\partial\Omega} \nu \cdot \mathbf{q}_h e_i^2 ds = 0$$

because of boundary condition for e_i.

Next, with $0 \le L_r - r'(\xi) \le L_r$, the right hand side of (7.4.6) can be estimated as

$$(1 + \tau L_r)\|e_i\|^2 + \tau\|\nabla e_i\|^2 \le \tau L_r\|e_{i-1}\|\|e_i\| \le \frac{1}{2}\tau L_r\left(\|e_i\|^2 + \|e_{i-1}\|^2\right)$$

which gives,

$$(1 + \frac{1}{2}\tau L_r)\|e_i\|^2 + \tau\|\nabla e_i\|^2 \le \frac{1}{2}\tau L_r\|e_{i-1}\|^2$$

or rewriting

$$\|e_i\|^2 + \frac{\tau}{1 + \frac{1}{2}\tau L_r} \|\nabla e_i\|^2 \leq \frac{1}{2} \frac{\tau L_r}{1 + \frac{1}{2}\tau L_r} \|e_{i-1}\|^2 \leq \gamma |||e_{i-1}|||^2$$

with $\gamma = \frac{\tau L_r}{2 + \tau L_r}$ and using $\tau L_r > 0$ we obtain $\gamma < 1$. Hence, the map $\mathcal{T}$

$$u_{i-1} \mapsto u_i = \mathcal{T}u_{i-1}$$

is a contraction and therefore has a unique fixed point by Banach fixed point theorem.
$\square$

Using the above lemma, we immediately obtain that u_i converges to the fixed point of (7.4.2) as $i \nearrow \infty$. Clearly, the limit is u_h^n; after obtaining it, computing v_h^n is straightforward as it is an explicit discretization in time. In other words,

Lemma 7.13 *Problem $\mathbf{P}_h^n$ has a unique solution triple (u_h^n, v_h^n, w_h^n).*

Remark 7.14 The numerical scheme presented here has a linear convergence rate with respect to H^1 norm as opposed to say Newton's iteration which is quadratic. This is compensated by the fact that the convergence is guaranteed for any choice of parameters. The error converges to 0 as the iteration index approaches ∞. In practice, however, only 3-4 iterations are needed. Also, in L^2 norm, one expects a faster convergence since, as τ decreases the factor γ tends to 0 and the norm defined for the mapping $\mathcal{T}$ is independent of τ for L^2 part of the norm.

We have not investigated the stability in time of this iteration process. For computing the solution, at each time step, by performing this iterative scheme, we accumulate the error. It can be shown that the error accumulated in time vanishes as τ tends to 0. Since our focus is to show the existence and uniqueness of the solution for the discrete problem $\mathbf{P}_h^n$ we do not investigate this aspect. For a discussion on this issue, we refer to [41], Lemma 3.6.
$\square$

7.4.2 A priori estimates

We start with the a priori estimates for Problem $\mathbf{P}_h^n$. These are similar to estimates for parabolic equations but here restricted to discrete time steps. We have the following lemma:

Lemma 7.15 *The following estimates hold*

$$\sup_{k=1,\dots,N} \|u_h^k\|^2 \le C, \tag{7.4.7}$$

$$\tau \sum_{n=1}^N \|\nabla u_h^n\|^2 \le C, \tag{7.4.8}$$

$$\|v_h^n - v_h^{n-1}\| \le C\tau, \tag{7.4.9}$$

$$\sup_{k=1,\dots,N} \|v_h^k\| \le C, \tag{7.4.10}$$

$$\sum_{n=1}^N \|u_h^n - u_h^{n-1}\|^2 \le C\tau, \tag{7.4.11}$$

$$\sum_{n=1}^N \|\nabla(u_h^n - u_h^{n-1})\|^2 \le C, \tag{7.4.12}$$

where C is independent of τ and δ.

Proof.   These a priori estimates are similar to the estimates as derived in the proof of Lemma 7.7. However, the technique used for obtaining the maximum principle in the continuous case, does not apply here due to inadmissibility of the test function. We therefore, derive the estimates in the following manner: Consider $(7.4.1)_1$ and choose $\phi_h = u_h^n$ to obtain

$$(u_h^n - u_h^{n-1}, u_h^n) + \tau(\nabla u_h^n, \nabla u_h^n) - \tau(\mathbf{q}_h u_h^n, \nabla u_h^n) + (v_h^n - v_h^{n-1}, u_h^n) = 0, \tag{7.4.13}$$

and use $(7.4.1)_2$ to replace the last term on the left hand side,

$$(u_h^n - u_h^{n-1}, u_h^n) + \tau(\nabla u_h^n, \nabla u_h^n) + \tau(r(u_h^n), u_h^n) = \tau(\mathbf{q}_h u_h^n, \nabla u_h^n) - \tau(H_\delta(v_h^{n-1}), u_h^n). \tag{7.4.14}$$

Using the identity for the left hand side

$$(u_h^n - u_h^{n-1}, u_h^n) = \frac{1}{2}\left(\|u_h^n\|^2 - \|u_h^{n-1}\|^2 + \|u_h^n - u_h^{n-1}\|^2\right)$$

and for the right hand side, use Cauchy-Schwarz to obtain

$$\frac{1}{2}\left(\|u_h^n\|^2 - \|u_h^{n-1}\|^2 + \|u_h^n - u_h^{n-1}\|^2\right) + \frac{1}{2}\tau\|\nabla u_h^n\|^2 + \tau L_r\|u_h^n\|^2$$
$$\le \frac{1}{2}\tau M_q\|u_h^n\|^2 + C\tau + \frac{1}{2}\tau\|u_h^n\|^2, \tag{7.4.15}$$

and sum over $n = 1, \ldots, N$ to get

$$\frac{1}{2} \|u_h^N\|^2 + \frac{1}{2} \sum_{n=1}^{N} \|u_h^n - u_h^{n-1}\|^2 + \frac{1}{2}\tau \sum_{n=1}^{N} \|\nabla u_h^n\|^2 + L_r\tau \sum_{n=1}^{N} \|u_h^n\|^2 \leq C\tau \sum_{n=1}^{N} \|u_h^n\|^2 + C.$$

(7.4.16)

Using Gronwall's lemma provides

$$\sup_{k=1,\ldots,N} \|u_h^k\|^2 \leq C$$

which is (7.4.7). Use this in above to obtain

$$\tau \sum_{n=1}^{N} \|\nabla u_h^n\|^2 \leq C$$

which is (7.4.8). We proceed further to prove (7.4.9) and (7.4.10). Choose for $\theta = v_h^n - v_h^{n-1}$ in $(7.4.1)_2$ and applying Cauchy-Schwarz inequality for the right hand side,

$$\left\| v_h^n - v_h^{n-1} \right\|^2 \leq \tau \|r(u_h^n)\| \left\| v_h^n - v_h^{n-1} \right\| + \tau \left\| H_\delta(v_h^{n-1}) \right\| \left\| v_h^n - v_h^{n-1} \right\|$$

which implies using bound (7.4.7) for u_h^n,

$$\left\| v_h^n - v_h^{n-1} \right\| \leq C\tau$$

which is (7.4.9).

Next to prove (7.4.10), choose $\theta = v_h^n$ in $(7.4.1)_2$ to obtain

$$(v_h^n - v_h^{n-1}, v_h^n) = \tau(r(u_h^n), v_h^n) - \tau(H_\delta(v_h^{n-1}), v_h^n).$$

(7.4.17)

The left hand side can be rewritten as

$$(v_h^n - v_h^{n-1}, v_h^n) = \frac{1}{2} \left(\|v_h^n\|^2 - \|v_h^{n-1}\|^2 + \|v_h^n - v_h^{n-1}\|^2 \right).$$

We rewrite the last term on the right hand side

$$\left(H_\delta(v_h^{n-1}), v_h^n \right) = \left(H_\delta(v_h^{n-1}), v_h^{n-1} \right) - \left(H_\delta(v_h^{n-1}), v_h^{n-1} - v_h^n \right).$$

Substituting these in (7.4.10),

$$\|v_h^n\|^2 - \left\| v_h^{n-1} \right\|^2 + \left\| v_h^n - v_h^{n-1} \right\|^2 = 2\tau \left(r(u_h^n), v_h^n \right) - 2 \left(H_\delta(v_h^{n-1}), v_h^{n-1} \right) + 2 \left(H_\delta(v_h^{n-1}), v_h^{n-1} - v_h^n \right).$$

Since $H(\cdot)$ is monotone, $(H_\delta(v_h^{n-1}), v_h^{n-1}) \geq 0$ and further use Cauchy-Schwarz inequality to get

$$\|v_h^n\|^2 - \left\|v_h^{n-1}\right\|^2 + \left\|v_h^n - v_h^{n-1}\right\|^2 \leq 2\tau C \|u_h^n\| \|v_h^n\| + 2\tau \left(H_\delta(v_h^{n-1}), v_h^n - v_h^{n-1}\right).$$

Now use Young's inequality for the terms on the right hand side to obtain

$$\|v_h^n\|^2 - \left\|v_h^{n-1}\right\|^2 + \frac{1}{2} \left\|v_h^n - v_h^{n-1}\right\|^2 \leq C\tau \|v_h^n\|^2 + C\tau \|u_h^n\|^2 + 2\tau^2 \|H_\delta\|^2.$$

Summing over $n = 1, \dots, N$ gives

$$
\begin{aligned}
\left\|v_h^N\right\|^2 + \tfrac{1}{2} \sum_{n=1}^N \left\|v_h^n - v_h^{n-1}\right\|^2 &\leq \|v_I\|^2 + C\tau \sum_{n=1}^N \|v_h^n\|^2 + C\tau \sum_{n=1}^N \|u_h^n\|^2 + \sum_{n=1}^N 2\tau^2 \|H_\delta\|^2 \\
&\leq \tau \sum_{n=1}^N \|v_\delta^n\|^2 + C + C\tau
\end{aligned}
$$

where we have used bounds on u_h^n and on initial data. Now use Gronwall's lemma to conclude (7.4.10).

The estimates (7.4.11) and (7.4.12) follow from the steps in the proof of (7.3.8) and (7.3.9). We omit the details. □

7.4.3   Convergence

As in the semi-discrete case, we consider the sequence of time discrete (u_h^n, v_h^n, w_h^n) solving problem $\mathbf{P}_h^n$, and construct a time continuous approximation by taking linear interpolation. We define,

$$
\begin{aligned}
U_h^\tau(t) &:= u_h^n \frac{(t - t_{n-1})}{\tau} + u_h^{n-1} \frac{(t_n - t)}{\tau}, \\
V_h^\tau(t) &:= v_h^n \frac{(t - t_{n-1})}{\tau} + v_h^{n-1} \frac{(t_n - t)}{\tau}, \\
W_h^\tau(t) &:= H_\delta(V_h^\tau(t)).
\end{aligned}
$$

We will use compactness arguments for time-continuous triples $(U_h^\tau, V_h^\tau, W_h^\tau)$ to identify the limit points and the system that these limit points satisfy. Using the estimates obtained in (7.4.9)-(7.4.12), we obtain similar estimates for $(U_h^\tau, V_h^\tau, W_h^\tau)$.

Lemma 7.16 *We have the following estimates:*

$$\|U_h^\tau\|^2 + \|V_h^\tau\|^2 \leq C, \tag{7.4.18}$$

$$\|\partial_t U_h^\tau\|^2 + \|\nabla U_h^\tau\|^2 + \|\partial_t V_h^\tau\|^2 \leq C, \tag{7.4.19}$$

$$0 \leq W_h^\tau \leq 1 \tag{7.4.20}$$

where the norms are taken with respect to $L^2(0, T; L^2(\Omega))$ and C is a constant independent of τ, δ.

Proof. Estimate (7.4.18) follows from the L^2 estimate for u_h^k and v_h^k. For instance,

$$\|U_h^\tau\|_{L^2(0,T;L^2(\Omega))}^2 \leq 2\tau \sum_{n=1}^{N} \|u_h^n\|^2 + 2\tau \sum_{n=1}^{N} \|u_h^{n-1}\|^2 \leq CN\tau \leq C$$

using (7.4.7). Similarly the estimate for V_h^τ follows from (7.4.10). The other estimates follow the steps in semi-discrete case. We omit the details. $\square$

The estimates above provide us with the convergence results. We state this in the next lemma.

Lemma 7.17 *The estimates obtained are uniform in discretization parameters (τ, h) and regularization parameter δ and furthermore we have $(U_h^\tau, V_h^\tau, W_h^\tau) \in \mathcal{U} \times \mathcal{V} \times L^\infty(\Omega)$. Clearly, $\tau \searrow 0$ with $\delta = O(\sqrt{\tau})$, implies that both $\delta, \frac{\tau}{\delta} \searrow 0$. The compactness arguments from the Lemma 7.16 lead to the following convergence results. As $(h, \tau) \searrow 0$, it holds that*

(i). $U_h^\tau \rightharpoonup u$ *weakly in* $L^2((0, T); H_0^1(\Omega))$,

(ii). $\partial_t U_h^\tau \rightharpoonup \partial_t u$ *weakly in* $L^2((0, T); L^2(\Omega))$,

(iii). $V_h^\tau \rightharpoonup v$ *weakly in* $L^2((0, T); L^2(\Omega))$,

(iv). $\partial_t V_h^\tau \rightharpoonup \partial_t v$ *weakly in* $L^2((0, T); L^2(\Omega))$,

(v). $W_h^\tau \rightharpoonup w$ *weakly-star in* $L^\infty(\Omega)$.

Once again, it remains to be proved that the limit points are the desired functions that satisfy the weak formulation in the sense of Definition 7.2.1. In this respect, to identify the limit object for the dissolution term, we need the strong convergence of V_h^τ. Here, the translation estimates can not be applied straightforwardly as the test functions after translation may leave the space $\mathcal{U}_h$. This is due to the fact that the translations are not remaining within the same triangle. To prove the strong convergence, we use the ideas from [34]. In this context, we use the higher regularity of v_I to improve the convergence. We start with the following proposition that we are going to use later.

Proposition 7.4.1 *Let Π be the interpolation operator that maps $H^1(\Omega) \cap C(\bar{\Omega})$ to the space $\mathcal{U}_h$. Let $g : \mathbb{R} \mapsto \mathbb{R}$ be a Lipschitz function with Lipschitz constant L_g, and let $f : \Omega \mapsto \mathbb{R}$ defined by $f = g(u)$. Then for any $u \in \mathcal{U}_h$ it holds that*

$$\|\nabla \Pi f\| \leq L_g \|\nabla u\|. \tag{7.4.21}$$

Proof. We follow the computations of [34] (Page 469) and only provide a brief sketch and cite the results directly (also see [49]). Following the notations of [34], let $A_i^T = (x_i, y_i)$ denote the vertices of the triangle T with $i = 1, 2,$ or 3. Note that f is an H^1 function. Since Πf is piecewise linear,

$$\Pi f = \sum_{i=1}^{3} (a_i^T x + b_i^T y + c_i^T) \Pi f(A_i^T),$$

with

$$a_i^T = \frac{1}{2|T|}(y_j - y_k),$$

$$b_i^T = \frac{1}{2|T|}(x_k - x_j),$$

$$c_i^T = \frac{1}{2|T|}(x_j y_k - x_k y_j)$$

with cyclic permutation of the indices i, j, k and $|T|$ representing the area of the triangle. The equation (2.5), page 469 of [34] reads for the given context here,

$$\|\nabla \Pi f\|^2 = \sum_{T \in \mathcal{T}_h} \frac{1}{4|T|} \{(A_k^T A_i^T, A_k^T A_j^T)|f(A_i^T) - f(A_j^T)|^2\} \tag{7.4.22}$$

where $A_k^T A_i^T$ is a vector connecting vertex i to k of triangle T. This provides using the Lipschitz continuity of g,

$$\|\nabla \Pi f\|^2 \leq L_g^2 \sum_{T \in \mathcal{T}_h} \frac{1}{4|T|} \{(A_k^T A_i^T, A_k^T A_j^T)|u(A_i^T) - u(A_j^T)|^2\}$$

$$= L_g^2 \|\nabla u\|^2 \tag{7.4.23}$$

establishing the proposition. □

Remark 7.18 It is important to note that the constant of the bound is indeed L_g, the Lipschitz constant. We need this fact below in the proof of the next Lemma. □

Lemma 7.19 *If $v_I \in H^1(\Omega)$, it holds that as $(\tau, h) \searrow 0$*

$$V_h^\tau \to v \quad \text{strongly in} \quad L^2(0, T; L^2(\Omega)). \tag{7.4.24}$$

Proof. From $(7.4.1)_2$ we have

$$(v_h^n - v_h^{n-1}, \theta_h) = \tau(r(u_h^n) - H_\delta(v_h^{n-1}), \theta_h)$$

for all $\theta_h \in \mathcal{U}_h$ which provides

$$v_h^n = \tau \Pi r(u_h^n) - \Pi(v_h^{n-1} - \tau H_\delta(v_h^{n-1}))$$

as v_h^n and v_h^{n-1} are in $\mathcal{P}_1$. Next, note that $(v_h^{n-1} - \tau H_\delta(v_h^{n-1}))$ is a Lipschitz function of v_h^{n-1} with Lipschitz constant $1 - \frac{\tau}{\delta}$. Hence, using the above Proposition 7.4.1, we have

$$\|\nabla \Pi(v_h^{n-1} - \tau H_\delta(v_h^{n-1}))\| \le (1 - \frac{\tau}{\delta})\|\nabla v_h^{n-1}\| \le \|\nabla v_h^{n-1}\|$$

as we choose $\delta = O(\sqrt{\tau})$. This gives,

$$\|\nabla v_h^n\| - \|\nabla v_h^{n-1}\| \le \tau L_r \|\nabla u_h^n\|$$

by first considering pointwise gradients and then taking the $L^2(\Omega)$ norm. Summing over $n = 1, \ldots, k$ we obtain

$$\|\nabla v_h^k\| \le \|\nabla v_I\| + \sum_{n=1}^k \tau L_r \|\nabla u_h^n\|$$

which implies that (since, this holds for any $k \in \mathbb{Z}_+$, $k \le N$)

$$\sup_k \|\nabla v_h^k\| \le C. \tag{7.4.25}$$

Using the definition of V_h^τ, we have

$$\nabla V_h^\tau = \nabla u_h^n + \frac{t - t_{n-1}}{\tau} \nabla u_h^{n-1}$$

and taking L^2 norm on both sides,

$$\|\nabla V_h^\tau\|^2 \le 2\|\nabla v_h^n\|^2 + 2\|\nabla v_h^{n-1}\|^2.$$

Integrate in time and use preceding bound (7.4.25) to conclude

$$\int_0^T \int_\Omega |\nabla V_h^\tau|^2 dx dt \le C.$$

The estimate above provides a weak convergence of V_h^τ in $L^2(0, T; H^1(\Omega))$ and combining with $\partial_t V_h^\tau \in L^2(0, T; L^2(\Omega))$ provides strong convergence of V_h^τ in $L^2(0, T; L^2(\Omega))$.
$\square$

7.4.4 Limit equations

In what follows, we show that these limits satisfy the weak formulation (7.2.7). This is considered in the following theorem.

Theorem 7.4.1 *The limit triple (u, v, w) satisfy the weak formulation (7.2.7).*

Proof. By the weak convergence, the estimates in Lemma 7.16 carry over for the limit triple (u, v, w). By 7.4.1, for (U_h^τ, V_h^τ) we have

$$
\int_0^T (\partial_t U_h^\tau, \phi) dt + \int_0^T (\nabla U_h^\tau, \nabla \phi) dt + \int_0^T (\mathbf{q}_h \cdot \nabla U_h^\tau, \phi) dt + \int_0^T (\partial_t V_h^\tau, \phi) dt
$$
$$
= \sum_{n=1}^N \int_{t_{n-1}}^{t_n} (\partial_t V_h^\tau, \phi - \phi_h) + \sum_{n=1}^N \int_{t_{n-1}}^{t_n} (\partial_t U_h^\tau, \phi - \phi_h) dt + \sum_{n=1}^N \int_{t_{n-1}}^{t_n} (\nabla U_h^\tau, \nabla (\phi - \phi_h)) dt
$$
$$
+ \sum_{n=1}^N \int_{t_{n-1}}^{t_n} ((\nabla U_h^\tau - \nabla u_h^n), \nabla \phi_h) dt - \sum_{n=1}^N \int_{t_{n-1}}^{t_n} (\mathbf{q}_h U_h^\tau, (\nabla \phi - \nabla \phi_h)) dt
$$
$$
- \sum_{n=1}^N \int_{t_{n-1}}^{t_n} (\mathbf{q}_h (U_h^\tau - u_h^n), \nabla \phi_h) dt,
$$
(7.4.26)

for all $\phi \in L^2(0, T; H_0^1(\Omega))$, where $\phi_h = P_h \phi$ is the projection of ϕ defined in (7.2.5). We proceed by showing that the terms on the right are vanishing as the discretization parameters h and τ are approaching 0. To this aim we first taken test functions that are H^2 in space, i.e. $\phi \in L^2(0, T; H_0^2(\Omega))$. As will be seen below, this extra regularity allows us to control terms involving $\nabla(\phi - \phi_h)$. By this we prove that (u, v) satisfy $(7.2.7)_1$, but only for test functions having a better regularity in space. Once this is established, density arguments ensure that the equality is satisfied also for test functions in $L^2(0, T; H_0^1(\Omega))$.

By Lemma 7.17, all terms on the left hand side converge to the desired limits. This is obvious except for the third term where a simple argument takes us through:

$$
\int_0^T (\mathbf{q}_h \cdot \nabla U_h^\tau, \phi) dt = \int_0^T (\mathbf{q} \cdot \nabla U_h^\tau, \phi) dt + \int_0^T ((\mathbf{q}_h - \mathbf{q}) \cdot \nabla U_h^\tau, \phi) dt. \tag{7.4.27}
$$

The first term on the right hand side of (7.4.27) passes to the desired limit. We show that the second term vanishes in the limit. Note that $\mathbf{q}_h - \mathbf{q} \in L^\infty(\Omega)$ and hence, $(\mathbf{q}_h - \mathbf{q})\nabla U_h^\tau$ has a weak limit. Now choose $\phi \in L^2(0, T; C_c^\infty(\Omega))$ so that $\phi \in L^\infty(\Omega)$ and use the strong convergence of $\mathbf{q}_h$ in L^2 (uniform with respect to h) to conclude that the weak limit is indeed 0.

We are thus required to show that the right hand side of (7.4.26) vanishes in the limit. We treat each term on the right hand side separately. Denote the successive terms in r.h.s. by $\mathcal{I}_i$ with $i = 1, \ldots, 6$. We have

$$
|\mathcal{I}_1| \le \left(\int_0^T \|\partial_t V_h^n\|^2 dt \right)^{\frac{1}{2}} \left(\sum_{n=1}^N \int_{t_{n-1}}^{t_n} \|\phi - \phi_h\|^2 dt \right)^{\frac{1}{2}} \le Ch \|\nabla \phi\|_{L^2(0,T;L^2(\Omega))} \searrow 0
$$

as $h \searrow 0$.

For $\mathcal{I}_2$ we have the similar argument as in the case of $\mathcal{I}_1$. Next,

$$|\mathcal{I}_3| \leq \left(\int_0^T \|\nabla U_h^\tau\|^2 dt \right)^{\frac{1}{2}} \left(\sum_{n=1}^N \int_{t_{n-1}}^{t_n} \|\nabla(\phi - \phi_h)\|^2 dt \right)^{\frac{1}{2}} \leq Ch\|\phi\|_{L^2(0,T;H_0^2(\Omega))}$$

and hence, $\mathcal{I}_3 \searrow 0$ as $h \searrow 0$. Here we use the fact that $\phi \in L^2(0,T;H_0^2(\Omega))$, and hence,

$$\|\nabla(\phi - \phi_h)\| \leq Ch\|\phi\|_{H_0^2(\Omega)}.$$

For $\mathcal{I}_4$, we obtain

$$|\mathcal{I}_4| \leq \left(\sum_{n=1}^N \tau\|\nabla u_h^n - \nabla u_h^{n-1}\|^2 \right)^{\frac{1}{2}} \left(\sum_{n=1}^N \tau\|\nabla \phi_h\|^2 \right)^{\frac{1}{2}} \to 0$$

since $\sum_{n=1}^N \tau\|\nabla u_h^n - \nabla u_h^{n-1}\|^2 \searrow 0$ because of estimate (7.4.12).

To continue,

$$|\mathcal{I}_5| \leq \left(\int_0^T \|\mathbf{q}_h U_h^\tau\|^2 dt \right)^{\frac{1}{2}} \left(\sum_{n=1}^N \int_{t_{n-1}}^{t_n} \|\nabla(\phi - \phi_h)\|^2 dt \right)^{\frac{1}{2}} \leq Ch\|\phi\|_{L^2(0,T;H_0^2(\Omega))}$$

leading to $\mathcal{I}_5$ vanishing in the limit. For $\mathcal{I}_6$ we have

$$|\mathcal{I}_6| \leq M_q \left(\sum_{n=1}^N \tau\|u_h^n - u_h^{n-1}\|^2 dt \right)^{\frac{1}{2}} \left(\sum_{n=1}^N \tau\|\nabla \phi_h\|^2 dt \right)^{\frac{1}{2}} \searrow 0$$

because of (7.4.11).

Concerning the second equation in (7.2.7), by (7.4.1)$_2$ we have

$$\int_0^T (\partial_t V^\tau, \theta) dt - \int_0^T (r(U^\tau) - W_h^\tau, \theta) dt = \sum_{n=1}^N \int_{t_{n-1}}^{t_n} (\partial_t V_h^\tau, \theta - \theta_h) dt$$
$$+ \sum_{n=1}^N \int_{t_{n-1}}^{t_n} (r(u_h^n) - r(U^\tau), \theta_h) dt + \sum_{n=1}^N \int_{t_{n-1}}^{t_n} (r(U_h^\tau), \theta_h - \theta) dt$$
$$+ \sum_{n=1}^N \int_{t_{n-1}}^{t_n} (W_h^\tau - H_\delta(v_h^{n-1}), \theta_h) dt$$
$$+ \sum_{n=1}^N \int_{t_{n-1}}^{t_n} (W_h^\tau, \theta - \theta_h) dt.$$

for all $\theta \in L^2(0,T;H_0^1(\Omega))$, and with $\theta_h = P_h\theta$. Recall that (see [33])

$$\|\theta - \theta_h\| \leq Ch\|\nabla\theta\|. \tag{7.4.28}$$

We would retrieve the desired limiting equations once we prove that the integrals on the right hand side vanish. Let us denote the successive integrals by $\mathcal{I}_i$, $i = 1, \ldots, 5$

respectively. For $\mathcal{I}_1$ we get

$$|\mathcal{I}_1| \leq \left(\int_0^T \|\partial_t V_h^\tau\|^2 dt\right)^{\frac{1}{2}} \left(\sum_{n=1}^N \int_{t_{n-1}}^{t_n} \|(\theta - \theta_h)\|^2 dt\right)^{\frac{1}{2}} \leq Ch\|\theta\|_{L^2(0,T;H_0^1(\Omega))}$$

which vanishes in the limit as $h \searrow 0$. Next, we consider

$$|\mathcal{I}_2| \leq \left(\sum_{n=1}^N \tau L_r^2 \|u_h^n - u_h^{n-1}\|^2\right)^{\frac{1}{2}} \left(\sum_{n=1}^N \tau \|\theta_h\|^2\right)^{\frac{1}{2}}$$

and using the estimate (7.4.11), we obtain $\mathcal{I}_2 \searrow 0$.
For $\mathcal{I}_3$,

$$|\mathcal{I}_3| \leq L_r \left(\int_0^T \|U_h^\tau\|^2 dt\right)^{\frac{1}{2}} \left(\sum_{n=1}^N \int_{t_{n-1}}^{t_n} \|(\theta - \theta_h)\|^2 dt\right)^{\frac{1}{2}} \leq Ch\|\theta\|_{L^2(0,T;H_0^1(\Omega))} \searrow 0$$

as $h \searrow 0$.
Further, for $\mathcal{I}_4$, we use the definition of W^τ and Lipschitz continuity of H_δ to obtain

$$|\mathcal{I}_4| \leq \sum_{n=1}^N \tau \frac{1}{\delta} \|v_h^n - v_h^{n-1}\| \|\theta_h\| \leq \sum_{n=1}^N \tau C \frac{\tau}{\delta} \|\theta_h\|$$

by using (7.4.8) and further using $\tau/\delta \searrow 0$ by the construction of δ we obtain $\mathcal{I}_4 \searrow 0$.
Finally, we treat $\mathcal{I}_5$

$$|\mathcal{I}_5| \leq C \left(\sum_{n=1}^N \int_{t_{n-1}}^{t_n} \|\theta - \theta_h\|^2 dt\right)^{\frac{1}{2}} \leq Ch\|\nabla\theta\|_{L^2(0,T;L^2(\Omega))} \searrow 0 \quad \text{as} \quad h \searrow 0$$

because of (7.4.28).
Next, we need to prove $w = H(v)$. Since we have V_h^τ strongly converging, we also obtain $V_h^\tau \to v$ pointwise a.e.. Further,

$$(W_h^\tau, \theta) = (w, \theta)$$

and by definition, $W_h^\tau = H_\delta(V_h^\tau)$; and further,

$$(H_\delta(V_h^\tau), \theta) = (w, \theta).$$

As $\tau \searrow 0$, by construction $\delta \searrow 0$. Now, for any given $(t, x) \in \Omega$, either $v > 0$ or $v = 0$. For the case when $v > 0$, we have $W_h^\tau = 1$ and hence $w = 1$. For the case when $v = 0$, since $\partial_t v \in L^2(\Omega)$, $\partial_t v = 0$ leading to $w = r(u)$ with $0 \leq w \leq 1$.
Note that the limit triple (u, v, w) indeed satisfies (7.2.7), but for test functions having a better regularity in space: $\phi \in L^2(0, T; H_0^2(\Omega))$ and $\theta \in L^2(0, T; H_0^1(\Omega))$. In view of

the regularity of u and v, density arguments can be employed to show that the limit equations also hold for $\phi \in L^2(0, T; H_0^1(\Omega))$ and $\theta \in L^2(0, T; L^2(\Omega))$, which completes the proof. $\qquad\qquad\qquad\qquad\qquad\qquad\qquad\qquad\qquad\qquad\qquad\qquad\qquad\qquad\square$

7.5   Numerical experiments

For the numerical experiments, we study different situations. For simplicity and vali-dation exercise, let us consider a 1D situation where we study the concentration profile and the dissolution fronts,

$$\Omega = (0, L)$$

with $L = 1$ and we choose the following parameters

$$D = 1e - 2, \quad r(u) = ku, \quad k = 1, \quad q = 1;$$

and the boundary conditions are

$$u = 1, \quad \text{at} \quad x = 0, \quad \text{and} \quad \frac{\partial u}{\partial x} = 0, \quad \text{at} \quad x = 1.$$

For initial condition, we make the following choices

$$u_I = 1, \quad v_I = 0.2, \quad x \in [0, 1].$$

Note that for this initial and boundary conditions, initially, $H(v_I) = 1$ as $v_I > 0$ and

$$r(u_I) - H(v_I) = u_I - H(v_I) = 0.$$

Hence, in the beginning, it is an equilibrium situation where the dissolution and pre-cipitation processes balance each other. However, this equilibrium is disturbed at $x = 0$ because of boundary condition ($u = 0$). This leads to the initiation of dissolution and this process moves forward as t increases. Note also that the dissolution process takes some time before v becomes 0 at $x = 0$. We call this time as t_s. The computation of t_s follows from a simple calculation. For $x = 0$,

$$\int_{v_I}^{0} \partial_t v \, dt = \int_{0}^{t_s} u - H(v) \, dt = -t_s$$

which gives,

$$t_s = v_I = 0.2.$$

Computations are performed for $t \in (0, 1)$ and the discretization in space is obtained on a regular grid of size $h = 1e - 3$. Further, we choose standard first order upwinding for the transport term. For the time discretization, we choose $\tau = 1e - 3$ and we use
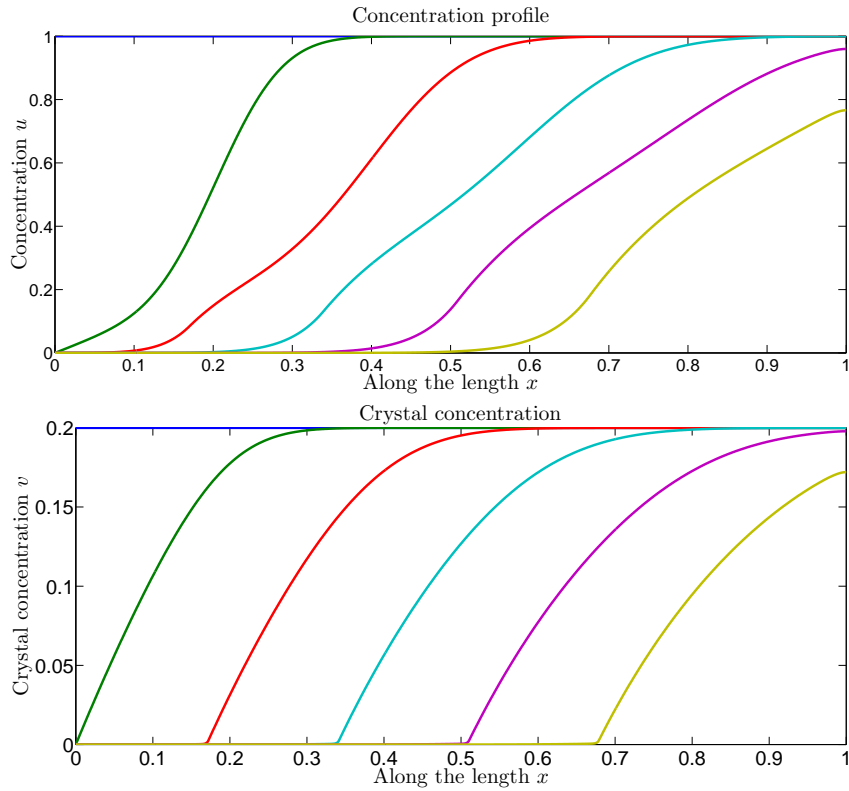
Figure 7.5.1: *The profiles for the concentration u and the crystal precipitate v for different times, t = 0, 0.2, 0.4, 0.6, 0.8, 1. Note that initially u = 1 and v = 0.2 and as t increases, the dissolution front moves forward. For the concentration profile, the effect of reactions is clearly visible.*

regularized Heaviside function (7.3.1) for the dissolution rate for the 1D problem. For the regularization parameter δ, we choose $\delta = 0.1(\tau^{0.5})$.
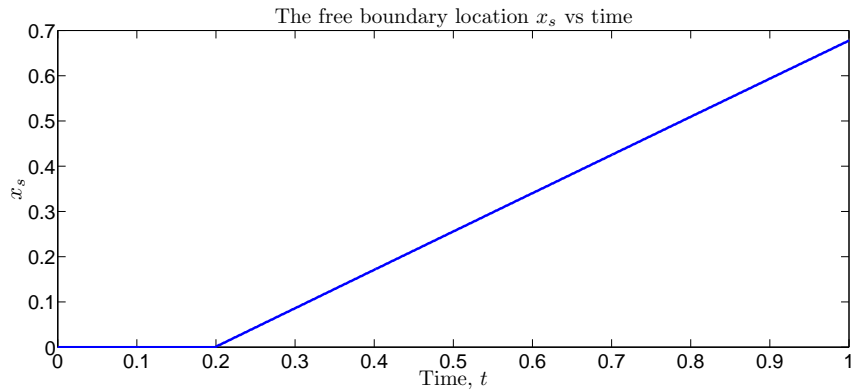
Figure 7.5.2: *The free boundary location, x_s. Note the starting time $t_s = 0.2$ for the beginning of the dissolution front. Also, the slope of the free boundary is equal to Q_v.*
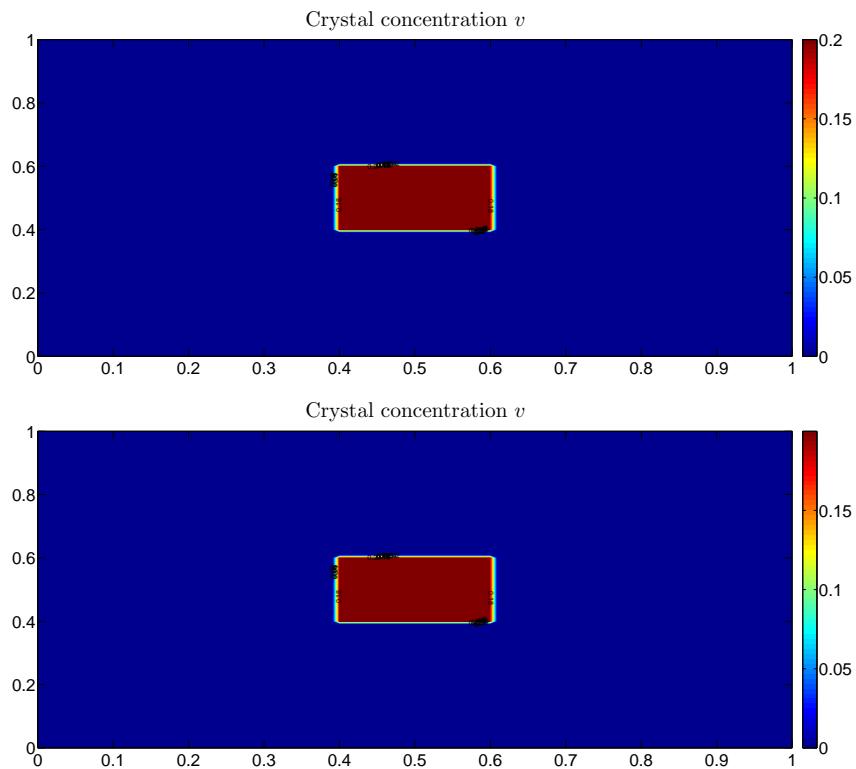
Figure 7.5.3: *The profiles for the crystal precipitate v for different times, $t = 0$ and $t = 0.5$. Note that initially $v = 0.2$ and as t increases, no changes take place in the profile of v. This is an equilibrium situation where the dissolution rates and the precipitation rates annul each other.*
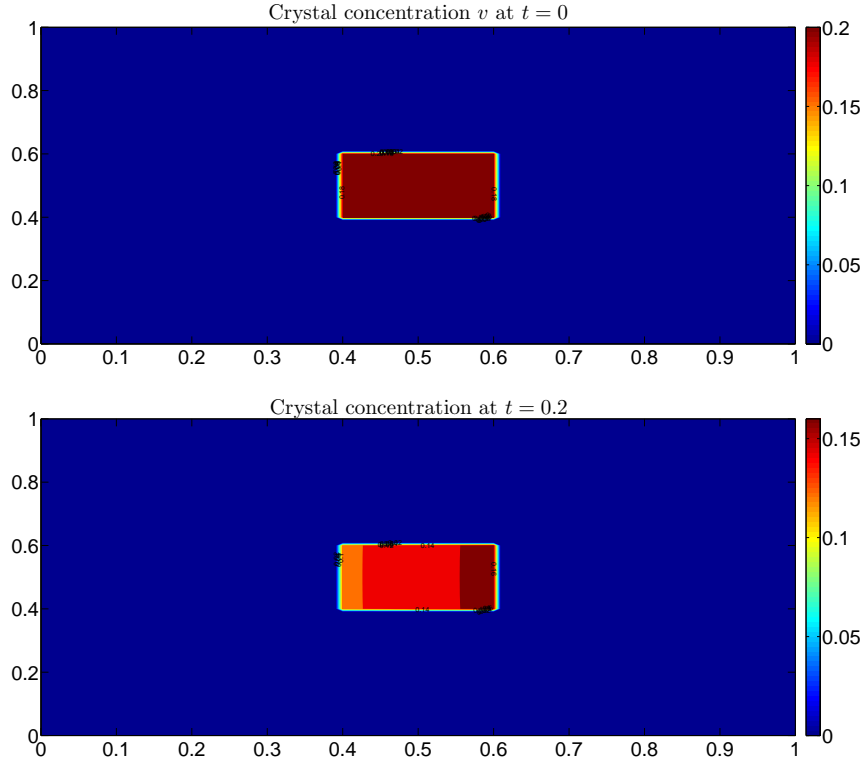
Figure 7.5.4: *The profiles for the crystal precipitate v for different times, $t = 0$ and $t = 0.2$. Note that initially $v = 0.2$ in Ω_v and as t increases, dissolution process starts taking place because of the boundary condition imposed at $x = 0$ ($u = 0$). The net dissolution process then starts taking place and further, we observe that the left hand side experiences more erosion than the right hand side due to the boundary condition effect at $x = 0$.*

The concentration profiles $u(x, t)$ and the dissolution fronts $v(x, t)$ corresponding to different times have been shown in Figure 7.5.1. As expected, the dissolution fronts propagate forward almost in a parallel manner and also there is a correspondence with the concentration profile. The 1D case has been studied in literature [47]. There are two quantities that may be of interest here. One is the speed of the dissolution front Q_v given by (see Proposition 1.2 of [45])

$$Q_v = q\frac{u^*}{u^* + v_I} \approx 0.833.$$

Secondly, the starting time for dissolution process $t_s = 0.2$ as computed above. These two information are contained in considering the free boundary location x_s which is defined as

$$x_s(t) := \{ \sup_{x \in (0,L)} x, \quad \text{s.t.} \quad v(x, t) = 0\}.$$

In Figure 7.5.2, we plot $x_s(t)$ and we notice the time t_s, the time when the dissolution starts at $x = 0$ and the slope of the plot which provides us information about the speed of the free boundary. Numerically, we obtain for the $t_s = 0.199$ and for the $Q_v = 0.8464$. We see that the matching is excellent. This provides us a validation exercise of the numerical scheme considered here.

For the second situation, we consider a 2D problem. For Ω we choose

$$\Omega = (0, 1) \times (0, 1).$$

We choose the following parameters

$$D = 1, \quad r(u) = ku, \quad k = 1, \quad \mathbf{q} = 0.01y(1 - y)\mathbf{e}_1;$$

that is, we use a linear reaction rate and for the convection, we have used parabolic profile. With the iterative scheme (7.4.3) in Section 7.4.1, the nonlinear reaction rates are also straightforward to compute, however, we stick to linear rates for simplicity of exposition. We choose small convection so that the changes in the concentrations are slow enough for the time scale of our observation ($T = 1$). For choosing the initial conditions, let us define,

$$\Omega_v \subset \Omega; \quad \Omega_v := \{(x, y); 0.4 \leq x \leq 0.6, \quad 0.4 \leq y \leq 0.6\},$$

that is, there is a small square Ω_v contained in the square domain Ω. Further, we choose, at $t = 0$, $u_I = 1$ and for v

$$v_I = 1, \quad (x, y) \in \Omega_v; \quad v_I = 0 \quad (x, y) \in \Omega \setminus \Omega_v.$$

At $x = 0$ we choose $u = 1$ and note that for this choice, $r(u) = 1$ at $t = 0$ and for Ω_v, $H(v) = 1$ as $v > 0$. Further, for $\Omega \setminus \Omega_v$, we put $v = 0$ which means that

$$H(v) = \min(r(u), 1) = 1.$$

Hence, $\partial_t v = u - H(v) = 0$ implying that this is an equilibrium situation. For the computations, we choose a uniform space discretization with $h = 1e - 2$ and for time stepping $\tau = 1e - 3$. For the convection term, we use standard upwinding. For diffusion, convection and reaction, we use implicit in time. We plot the precipitate concentration v in Figure 7.5.3 for two different times $t = 0$ and $t = 0.5$. As it is clearly seen, v does not change with time.

Next, we consider the case when we perturb the equilibrium by prescribing the boundary condition $u = 0$ at $x = 0$. This leads to the beginning of the dissolution process taking place and the concentration of v decreases in Ω_v. We have included the concentration profile and the crystal concentration at different times. Notice that the dissolu-
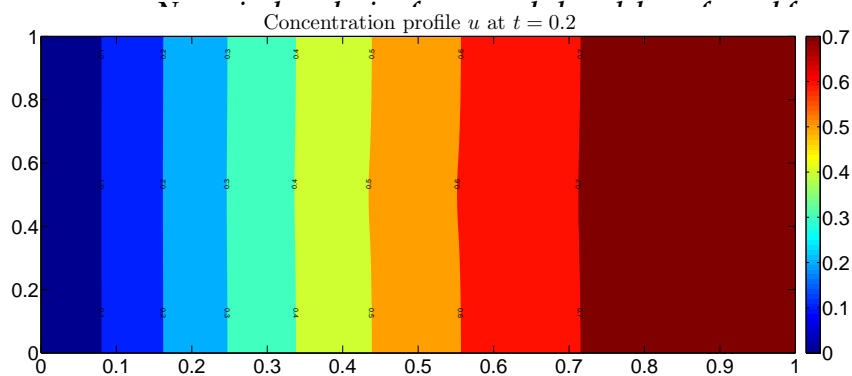
Figure 7.5.5: *The profiles for the concentration u at t = 0.2. Note that initially u = 1 and as t increases, u starts decreasing because of the homogeneous Dirichlet boundary condition at x = 0. Clearly, u = v = 0 is the equilibrium situation and we see that the effect of reduction is more prominent on the left side compared to the right side.*

7.6   Conclusions and discussions

We have considered both semi-discrete and fully discrete schemes for the macroscale equations. For the fully discrete case, we consider the linear finite elements on the triangular meshes. These schemes have been analyzed for their convergence and the proof relies on a priori estimates and the compactness arguments. To deal with the multivalued dissolution rate, we consider these numerical schemes along a regularizing sequence. For the a priori estimates, we make sure that the estimates remain independent of the discretization as well as the regularization parameters. The proofs for the semi-discrete and the fully discrete cases follow similar strategy, however, there are some important differences. Whereas the semi-discrete case retains the maximum principle, we have to rely on different estimates in the fully discrete case. Also, the translation estimates to obtain the strong convergence are easily applicable for the semi-discrete situation, the same is not true for the fully discrete case. For the choice of basis functions taken here, that is, piecewise linear elements on a triangle, the usual method of obtaining pointwise estimates does not work in fully discrete case thereby not necessarily having the maximum principle. Next, instead of using the discrete analogue of translation estimates, the properties of Lagrangian interpolation operator on a triangle are used to obtain the strong convergence needed to deal with the nonlinearities.

The numerical experiments have been carried out which present several interesting aspects of the model. In 1D model, we have shown the dissolution fronts propagating forward. Further, we have plotted the free boundary location and shown its evolution. We find an excellent agreement with the theoretical predictions. For the 2D model, we have shown that the model indeed maintains the equilibrium in the absence of crystal

($v = 0$) when the precipitation concentration is not sufficient. Further, for the case when the crystals are present and dissolution process starts taking place due to the boundary effect, we clearly see the evolution of dissolution processes taking place.

Chapter 8

Numerical analysis of an upscaled model: mixed schemes

This chapter deals with the numerical analysis of an upscaled model describing the reactive flow in a porous medium. The solutes are transported by advection and diffusion and undergo precipitation and dissolution. The reaction term and, in particular, the dissolution term has a particular, multi-valued character, which leads to stiff dissolution fronts. We consider the Euler implicit method for the temporal discretization and the mixed finite element for the discretization in space. More precisely, we use the lowest order Raviart-Thomas elements. As an intermediate step we consider also a semi-discrete mixed variational formulation (continuous in space). We analyse the numerical schemes and prove the convergence to the continuous formulation. Apart from the proof for the convergence, this also yields an existence proof for the solution of the model in mixed variational formulation. Numerical experiments are performed to study the convergence behavior.

8.1 Introduction

In this chapter, we consider an upscaled model defined on a Darcy scale. This implies that the solid grains and the pore space are not distinguished and the equations are defined everywhere. Consequently, the crystals formed as a result of reactions among ions and the ions themselves are defined everywhere in the domain. Such models fall in the

general category of reactive porous media flow models. For Darcy-scale models related directly to precipitation and dissolution processes we refer to [23, 97, 115, 118] (see also the references therein). Here we adopt the ideas proposed first in [73], and extended in a series of papers [43–45]. These papers are referring to Darcy scale models; the porescale counterpart is considered in [47], where distinction is made for the domains delineating the pore space and the solid grains. The transition from the porescale model to the up-scaled model is obtained, for instance, via homogenization arguments. For a simplified situation of a 2D strip, the rigorous arguments are provided in [47]; see also [4, 94] for the upscaling procedure in transport dominated flow regimes. For a similar situation, but tracking the geometry changes due to the reactions leading to the free boundary problems, the formal arguments are presented in [75] and [105].

We are motivated by analyzing appropriate numerical methods for solving the reactive flows for an upscaled model. Considering the mixed variational formulation is an at-tractive proposition as it preserves the mass locally. Our main goal here is to provide the convergence of a mixed finite element discretization for such a model for disso-lution and precipitation in porous media, involving a multi-valued dissolution rate. Before discussing the details and specifics, we briefly review some of the relevant nu-merical work. For continuously differentiable rates the convergence of (adaptive) fi-nite volume discretizations is studied in [72, 111]; see also [28] for the convergence of a finite volume discretization of a copper-leaching model. In a similar framework, dis-continuous Galerkin methods are discussed in [127] and upwind mixed FEM are con-sidered in [38, 39]; combined finite volume-mixed hybrid finite elements are employed in [52, 59]. Non-Lipschitz, but Hölder continuous rates are considered using conformal FEM schemes in [14, 15]. Similarly, for Hölder continuous rates (including equilibrium and non-equilibrium cases) mixed FEM methods are analyzed rigorously in [120, 123], whereas [121] provides error estimates for the coupled system describing unsaturated flow and reactive transport. In all these cases, the continuity of the reaction rates al-lows obtaining error estimates. A characteristic mixed-finite element method for the advection dominated transport has been treated in [8] and characteristic FEM scheme for contaminant transport giving rise to possibly non-Lipschitz reaction rates are treated in [40] where the convergence and the error estimates have been provided. A parabolic problem coupled with linear ODEs at the boundary have been treated in [7] using char-acteristic MFEM method. Conformal schemes both for the semi-discrete and fully dis-crete (FEM) cases for the upscaled model under consideration have been treated in [80].

The main difficulty here is due to the particular description of the dissolution rate in-volving differential inclusions. To deal with this, we consider a regularization of this term and the corresponding sequence of regularized equations. The regularization pa-rameter δ is dependent on the time discretization parameter τ in such a way that as $\tau \searrow 0$, it is ensured that $\delta \searrow 0$. Thus, obtaining the limit of discretized scheme au-tomatically yields, by virtue of the regularization parameter also vanishing, the origi-nal equation. In proving the convergence results, the compactness arguments are em-

ployed. These arguments rely on a priori estimates providing weak convergence. However, strong convergence is needed to deal with the non-linear terms in the reaction rates. Translation estimates are used to achieve this.

We consider both the semi-discrete and the fully discrete cases with the proof for the latter case following closely the ideas of semi-discrete case. However, there are important differences particularly in the way the translation estimates are obtained. Whereas in the semi-discrete case, we use the dual problem for obtaining the translation estimates; in the fully discrete case, we use the properties of discrete H_0^1 norm following the finite volume framework [51]. The convergence analysis of appropriate numerical schemes for the problem considered here is a stepping stone for coupled flow and reactive transport problem (for example, Richards' equation coupled with precipitation-dissolution reaction models).

The chapter is structured as follows. We begin with a brief description of the model in Section 8.2 followed by Section 8.3 which deals with the notations used in this work. We proceed to define the mixed variational formulation in Section 8.4 where we prove the uniqueness of the solution with the existence coming from the convergence proof. Next, in sections 8.5 and 8.6 the time-discrete, respectively fully discrete numerical schemes are considered and the proofs for the convergence are provided. The numerical experiments are shown in Section 8.7 followed by the conclusions and discussions in Section 8.8.

8.2 The mathematical model

We consider a Darcy scale model that describes the reactive transport of the ions/solutes in a porous medium. The solutes are subjected to convective transport and in addition they undergo diffusion and reactions in the bulk. Below we provide a brief description and the assumptions of the model; we refer to [43], or [44] for more details.

Let $\Omega \subset \mathbb{R}^2$ be the domain occupied by the porous medium, and assume Ω be open, connected, bounded and with Lipschitz boundary Γ. Further, let $T > 0$ be a fixed but arbitrarily chosen time, and define

$$\Omega^T = (0, T] \times \Omega, \quad \text{and} \quad \Gamma^T = (0, T] \times \Gamma.$$

At the outset, we assume that the fluid velocity $\mathbf{q}$ is known, divergence free and essentially bounded

$$\nabla \cdot \mathbf{q} = 0 \quad \text{in} \quad \Omega.$$

Usually, two or more different types of ions react to produce precipitate (an immobile species). A simplified model will be considered here where we include only one mobile

species. This makes sense if the boundary and initial data are compatible (see [43], or [44]). Then, denoting by v the concentration of the (immobile) precipitate, and by u the cation concentration, the model reduces to

$$\begin{cases} \partial_t(u+v) + \nabla \cdot (\mathbf{q}u - \nabla u) &= 0, & \text{in } \Omega^T, \\ u &= 0, & \text{on } \Gamma^T, \\ u &= u_I, & \text{in } \Omega, \text{ for } t = 0, \end{cases} \tag{8.2.1}$$

for the ion transport, and

$$\begin{cases} \partial_t v &= (r(u) - w), & \text{on } \Omega^T, \\ w &\in H(v), & \text{on } \Omega^T, \\ v &= v_I, & \text{on } \Omega, \text{ for } t = 0, \end{cases} \tag{8.2.2}$$

for the precipitate. For the ease of presentation we restrict to homogeneous Dirichlet boundary conditions. The assumptions for the initial conditions will be given below. In the system considered above, we assume all the quantities and variables as dimensionless. To simplify the exposition, the diffusion is assumed 1, the extension to a positive definite diffusion tensor being straightforward. Further, we assume that the Damköhler number is scaled to 1, as well as an eventual factor in the time derivative of v in $(8.2.2)_1$, appearing in the transition form the pore scale to the core scale.

The assumptions on the precipitation rate r are

(A.r1) $r(\cdot) : \mathbb{R} \to [0, \infty)$ is Lipschitz in $\mathbb{R}$ with the constant L_r.

(A.r2) There exists a unique $u_* \geq 0$, such that

$$r(u) = \begin{cases} 0 & \text{for } \quad u \leq u_*, \\ \text{strictly increasing for} & u \geq u_* \quad \text{with} \quad r(\infty) = \infty. \end{cases} \tag{8.2.3}$$

The interesting part is the structure of the dissolution rate. We interpret it as a process encountered strictly at the surface of the precipitate layer, so the rate is assumed constant (1, by scaling) at some $(t, x) \in \Omega^T$ where the precipitate is present, i.e. if $v(t, x) > 0$. In the absence of the precipitate, the overall rate (precipitate minus dissolution) is either zero, if the solute present there is insufficient to produce a net precipitation gain, or positive. This can be summarized as

$$w \in H(v), \quad \text{where} \quad H(v) = \begin{cases} 0, & \text{if } \quad v < 0, \\ [0, 1], & \text{if } \quad v = 0, \\ 1, & \text{if } \quad v > 0. \end{cases} \tag{8.2.4}$$

In the setting above, a unique u^* exists for which $r(u^*) = 1$. If $u = u^*$ for all t and x, then the system is in equilibrium: no precipitation or dissolution occurs, since the precipitation rate is balanced by the dissolution rate regardless of the presence of absence of crystals (see [80], Section 5 for some illustrations). Then, as follows from [47, 73, 109], for a.e. $(t, x) \in \Omega^T$ where $v = 0$, the dissolution rate satisfies

$$w = \begin{cases} r(u) & \text{if} \quad u < u^*, \\ 1 & \text{if} \quad u \geq u^*. \end{cases} \tag{8.2.5}$$

Since, we will work with the model in the mixed formulation, we define the flux as

$$\mathbf{Q} = -\nabla u + \mathbf{q}u. \tag{8.2.6}$$

Except for some particular situations, one cannot expect the existence of classical solutions to (8.2.1)-(8.2.2). To rectify this, we resort to defining appropriate weak solutions which implies satisfying the equations in some average sense. Formally, these solutions are obtained by multiplying by smooth functions and using partial integration wherever required thereby reducing the regularity of solutions otherwise needed in the strong form. In this work, we write the equations in a mixed variational form which means that we separate the equation for the flux $\mathbf{Q}$ and retain the local mass conservation property (see [120–122] for similar problems).

8.3   Notations

We adopt the following notations from the functional analysis. In particular, by $H_0^1(\Omega)$ we mean the space of functions in $H^1(\Omega)$ and having a vanishing trace on Γ and H^{-1} is its dual. By $(\cdot, \cdot)$ we mean L^2 inner product or the duality pairing between H_0^1 and H^{-1}. Further, $\| \cdot \|$ stands for the norms induced by L^2 inner product. For other norms, we explicitly state it. The functions in $H(div; \Omega)$ are vector valued having a L^2 divergence. Furthermore, C denotes a generic constant and the value of which might change from line to line and is independent of unknown variables or the discretization parameters.

Having introduced these notations we can state the assumptions on the initial conditions:

(A.I1) The initial data u_I and v_I are non–negative and essentially bounded.

(A.I2) $u_I, v_I \in H_0^1(\Omega)$.

We have taken the initial conditions in H_0^1 to avoid technicalities. Alternatively, one can approximate the initial conditions by taking the convolutions with smooth functions.

The H_0^1 regularity for v_I is used for obtaining strong convergence results, for which L^2 regularity is not sufficient.

We furthermore assume that Ω is polygonal. Therefore it admits regular decompositions into simplices and the errors due to nonpolygonal domains are avoided. The spatial discretization will be defined on such a regular decomposition $\mathcal{T}_h$ into 2D simplices (triangles); h stands for the mesh-size. We provide the exposition for 2D but extending the results to 3D is similar.

We define the following sets

$$
\begin{aligned}
\mathcal{V} &:= \{v \mid v \in H^1((0,T); L^2(\Omega))\}, \\
\mathcal{S} &:= \{\mathbf{Q} \mid \mathbf{Q} \in L^2((0,T); H(div; \Omega))\}, \\
\mathcal{W} &:= \{w \in L^\infty(\Omega^T) \mid 0 \le w \le 1\}.
\end{aligned}
$$

In addition, for the fully discrete situation, we use the following discrete subspaces $\mathcal{V}_h \subset L^2(\Omega)$ and $\mathcal{S}_h \subset H(div; \Omega)$ defined as follows

$$
\begin{aligned}
\mathcal{V}_h &:= \{u \in L^2(\Omega) \mid u \text{ is constant on each element } T \in \mathcal{T}_h\} \\
\mathcal{S}_h &:= \{\mathbf{Q} \in H(\text{div}; \Omega) \mid \mathbf{Q}_{|_T} = \mathbf{a} + b\mathbf{x} \text{ for all } T \in \mathcal{T}_h\}.
\end{aligned}
$$

In other words, $\mathcal{V}_h$ denotes the space of piecewise constant functions, while $\mathcal{S}_h$ is the RT_0 space. Clearly from the above definitions, $\nabla \cdot \mathbf{Q} \in \mathcal{V}_h$ for any $\mathbf{Q} \in \mathcal{S}_h$.

We also define the following usual projections:

$$
P_h : L^2(\Omega) \mapsto \mathcal{V}_h, \langle P_h v - v, v_h \rangle = 0
$$

for all $v_h \in \mathcal{V}_h$. Similarly, the projection Π_h is defined on $(H^1(\Omega))^d$ such that

$$
\Pi_h : (H^1(\Omega))^d \mapsto \mathcal{S}_h, \langle \nabla \cdot (\Pi_h \mathbf{Q} - \mathbf{Q}), v_h \rangle = 0
$$

for all $v_h \in \mathcal{V}_h$. Following [119], p.237 (also see [26]), this operator can be extended to $H(div; \Omega)$ and also for the above operators there holds

$$
\|v - P_h v\| \le Ch\|v\|_{H^1(\Omega)} \tag{8.3.1}
$$

and further,

$$
\begin{aligned}
\|\mathbf{Q} - \Pi_h \mathbf{Q}\| &\le Ch\|\mathbf{Q}\|_{H^1(\Omega)} \\
\|\nabla \cdot \mathbf{Q} - \nabla \cdot (\Pi_h \mathbf{Q})\| &\le Ch\|\mathbf{Q}\|_{H^2(\Omega)}.
\end{aligned}
\tag{8.3.2}
$$

For the spatial discretization we will work with the approximation $\mathbf{q}_h$ of the Darcy ve-

locity $\mathbf{q}$, defined on the given mesh $\mathcal{T}_h$. For this approximation we assume that there exists a $M_q > 0$ s.t. $\|\mathbf{q}_h\|_{L^\infty} \leq M_q$ (uniformly in h; the same estimate being valid for $\mathbf{q}$), and as $h \searrow 0$

$$\|\mathbf{q}_h - \mathbf{q}\|_{L^2(\Omega)^2} \searrow 0. \tag{8.3.3}$$

Having stated the assumptions, we proceed by introducing the mixed variational formulation and analyzing the convergence of its discretization.

8.4 Continuous mixed variational formulation

A weak solution of (8.2.1)–(8.2.2) written in mixed form is defined as follows.

Definition 8.4.1 *A quadruple* $(u, \mathbf{Q}, v, w) \in (\mathcal{V} \times \mathcal{S} \times \mathcal{V} \times \mathcal{W}$ *with* $u_{|t=0} = u_I, v_{|t=0} = v_I$ *is a mixed weak solution of* (8.2.1)–(8.2.2) *if* $w \in H(v)$ *a.e. and for all* $t \in (0, T)$ *and* $(\phi, \theta, \boldsymbol{\psi}) \in H^1(\Omega) \times L^2(\Omega) \times H(div; \Omega)$ *we have*

$$\begin{aligned}
(\partial_t u, \phi) + (\nabla \cdot \mathbf{Q}, \phi) + (\partial_t v, \phi) &= 0, \\
(\partial_t v, \theta) - (r(u) - w, \theta) &= 0, \\
(\mathbf{Q}, \boldsymbol{\psi}) - (u, \nabla \cdot \boldsymbol{\psi}) - (qu, \boldsymbol{\psi}) &= 0.
\end{aligned} \tag{8.4.1}$$

The proof for the existence of solution for (8.4.1) is obtained by the convergence of the numerical schemes considered below. Therefore, we give the proof for the uniqueness of a solution. The following lemma shows the uniqueness without further details on w. As mentioned in (8.2.5) the inclusion $w \in H(v)$ can be made more precise.

Lemma 8.1 *The mixed weak formulation* (8.4.1) *has at most one solution.*

Proof. Assume there exist two solution quadruples $(u_1, \mathbf{Q}_1, v_1, w_1)$ and $(u_2, \mathbf{Q}_2, v_2, w2)$, and define

$$u := u_1 - u_2, \quad \mathbf{Q} := \mathbf{Q}_1 - \mathbf{Q}_2, \quad v := v_1 - v_2, \quad w := w_1 - w_2.$$

Clearly, at $t = 0$ we have $u(0, x) = 0$ and $v(0, x) = 0$ for all x.
Subtracting $(8.4.1)_2$ for u_2, v_2 and w_2 from the equation for u_1, v_1 and w_1 and taking (for $t \leq T$ arbitrary) $\theta = \chi_{(0,t)} v$, using monotonicity of H and the Lipschitz continuity of $r(\cdot)$ leads to

$$\begin{aligned}
\|v(t, \cdot)\|^2 &= \int_0^t \int_\Omega (r(u_1) - r(u_2)) v(s, x) dx ds - \int_0^t \int_\Omega (H(v_1) - H(v_2)) v(s, x) dx ds \\
&\leq \frac{1}{2} \int_0^t L_r^2 \|u(s, \cdot)\|^2 ds + \frac{1}{2} \int_0^t \|v(s, \cdot)\|^2 ds.
\end{aligned}$$

Then Gronwall's lemma gives

$$\|v(t,\cdot)\|^2 \le Ce^t \int_0^t \|u(s,\cdot)\|^2 ds \le C \int_0^t \|u(s,\cdot)\|^2 ds. \tag{8.4.2}$$

Next, we choose for $\phi = \chi_{(0,t)} u(t,x)$ in the difference between the two equalities $(8.4.1)_1$ to get

$$\|u(t,\cdot)\|^2 + \left(\int_0^t \nabla \cdot \mathbf{Q}(s,\cdot) ds, u(t,\cdot) \right) + (v(t,\cdot), u(t,\cdot)) = 0. \tag{8.4.3}$$

Similarly, choosing $\psi = \int_0^t \mathbf{Q}(s) ds$ in $(8.4.1)_3$ (written for a.e. t) yields

$$\int_\Omega \left(\mathbf{Q}(t,x) \int_0^t \mathbf{Q}(s,x) ds \right) dx - \int_\Omega u(t,x) \left(\int_0^t \nabla \cdot \mathbf{Q}(s,x) ds \right) dx$$
$$- \int_\Omega \mathbf{q} u(t,x) \left(\int_0^t \mathbf{Q}(s,x) ds \right) dx = 0. \tag{8.4.4}$$

Combining (8.4.3) and (8.4.4) we have

$$\|u(t,\cdot)\|^2 + \int_\Omega v(t,x) u(t,x) dx + \int_\Omega \mathbf{Q}(t,x) \int_0^t \mathbf{Q}(s,x) ds dx = \int_\Omega \mathbf{q} u(t,x) \int_0^t \mathbf{Q} ds dx$$
$$\le \frac{1}{4} \|u(t,\cdot)\|^2 + M_q^2 \left\| \int_0^t \mathbf{Q}(s,\cdot) ds \right\|^2,$$

which implies,

$$\|u(t,\cdot)\|^2 + (\mathbf{Q}(t,\cdot), \int_0^t \mathbf{Q}(s,\cdot) ds) \le \frac{1}{2} \|u(t,\cdot)\|^2 + M_q^2 \left\| \int_0^t \mathbf{Q} ds \right\|^2 + \|v(t,\cdot)\|^2.$$

Using (8.4.2) we obtain

$$\frac{1}{2} \|u(t,\cdot)\|^2 + (\mathbf{Q}(t,\cdot), \int_0^t \mathbf{Q}(s,\cdot) ds) \le C \int_0^t \|u(s,\cdot)\|^2 ds + M_q^2 \left\| \int_0^t \mathbf{Q}(s,\cdot) ds \right\|^2. \tag{8.4.5}$$

Defining,

$$E(t) := \frac{1}{2} \int_0^t \|u(s,\cdot)\|^2 ds + \frac{1}{2} \left\| \int_0^t \mathbf{Q}(s) ds \right\|^2$$

we have $E \ge 0$ and $E(0) = 0$ because of initial conditions. Then (8.4.5) rewrites

$$\frac{dE}{dt} \le CE.$$

This immediately gives $E(t) = 0$ for all t implying

$$\int_0^t \|u(s, \cdot)\|^2 ds = 0, \text{ and } \int_0^t \mathbf{Q}(s) ds = 0$$

for all t. Hence $u = 0, \mathbf{Q} = 0$ and using this in (8.4.2) we conclude $v = 0$. $\qquad \square$

8.5 Semi-discrete mixed variational formulation

As announced, to avoid dealing with inclusion in the description of dissolution rate, the numerical scheme relies on the regularization of the Heaviside graph. With this aim, with $\delta > 0$ we define

$$H_\delta(z) := \begin{cases} 1, & z > \delta, \\ \frac{z}{\delta}, & 0 \le z \le \delta, \\ 0, & z < 0. \end{cases} \tag{8.5.1}$$

Next, with $N \in \mathbb{N}, \tau = \frac{T}{N}$ and $t_n = n\tau, n = 1, \ldots, N$, we consider a first order time discretization with uniform time stepping, which is implicit in u and explicit in v. At each time step t_n we use $(u_\delta^{n-1}, v_\delta^{n-1}) \in \left(L^2(\Omega), L^2(\Omega) \right)$ determined at t_{n-1} to find the next approximation $(u_\delta^n, \mathbf{Q}_\delta^n, v_\delta^n, w^n)$. The procedure is initiated with $u^0 = u_I, v^0 = v_I$. Specifically, we look for $(u_\delta^n, v_\delta^n, \mathbf{Q}_\delta^n) \in H^1(\Omega), L^2(\Omega), H(div; \Omega)$ satisfying the time discrete

Problem $\mathbf{P}_\delta^{mvf,n}$: Given $(u_\delta^{n-1}, v_\delta^{n-1}) \in \left(L^2(\Omega), L^2(\Omega) \right)$, find $(u_\delta^n, \mathbf{Q}_\delta^n, v_\delta^n, w_\delta^n)$
$\in \left(L^2(\Omega), H(div; \Omega), \ L^2(\Omega), L^\infty(\Omega) \right)$ such that

$$\begin{aligned}
(u_\delta^n - u_\delta^{n-1}, \phi) + \tau(\nabla \cdot \mathbf{Q}_\delta^n, \phi) + (v_\delta^n - v_\delta^{n-1}, \phi) &= 0, \\
(v_\delta^n - v_\delta^{n-1}, \theta) - \tau(r(u_\delta^n), \theta) - \tau(H_\delta(v_\delta^{n-1}), \theta) &= 0, \\
(\mathbf{Q}_\delta^n, \boldsymbol{\psi}) - (u_\delta^n, \nabla \cdot \boldsymbol{\psi}) - (\mathbf{q}u_\delta^n, \boldsymbol{\psi}) &= 0
\end{aligned} \tag{8.5.2}$$

for all $(\phi, \theta, \boldsymbol{\psi}) \in \left(H^1(\Omega), L^2(\Omega), H(div; \Omega) \right)$. For completeness we define

$$w_\delta^n = H_\delta(v_\delta^n).$$

This is a system of elliptic equations for $u_\delta^n, \mathbf{Q}_\delta^n, v_\delta^n$ given $u_\delta^{n-1} \in H_{0,\Gamma_D}^1(\Omega), v_\delta^{n-1} \in L^2(\Omega)$. For stability reasons, we choose $\delta = O(\tau^{\frac{1}{2}})$ (see [41, 80] for detailed arguments) which implies that $\frac{\tau}{\delta}$ goes to 0 as $\tau \searrow 0$. This in turn allows us to consider the solutions along the sequence of regularized Heaviside function with the regularization parameter δ automatically vanishing in the limit of $\tau \searrow 0$.

The existence of a solution for Problem $\mathbf{P}_\delta^{mvf,n}$ will result from the convergence of the fully discrete scheme, which is proved in the Appendix B by keeping τ and δ fixed, and passing to the limit $h \searrow 0$. Note that it suffices to compute u_δ^n, as v_δ^n can be obtained straightforwardly. For now, we prove the uniqueness of the solution.

Lemma 8.2 *Problem $\mathbf{P}_\delta^{mvf,n}$ has at most one solution triple $(u_\delta^n, \mathbf{Q}_\delta^n, v_\delta^n)$.*

Proof. Since $w_\delta^n = H_\delta(v_\delta^n)$, it has no influence on the existence or uniqueness of the solution. Therefore, we consider only the triples $(u_\delta^n, \mathbf{Q}_\delta^n, v_\delta^n)$. Assume that for the same $(u_\delta^{n-1}, v_\delta^{n-1})$ there are two solution triples $(u_{\delta,i}^n, \mathbf{Q}_{\delta,i}^n, v_{\delta,i}^n)$, $i = 1, 2$ providing a solution to Problem $\mathbf{P}_\delta^{mvf,n}$. Define

$$u_\delta^n := u_{\delta,1}^n - u_{\delta,2}^n, \quad \mathbf{Q}_\delta^n := \mathbf{Q}_{\delta,1}^n - \mathbf{Q}_{\delta,2}^n, \quad v_\delta^n := v_{\delta,1}^n - v_{\delta,2}^n.$$

We follow the usual approach and consider the equations for the difference above. Taking $\theta = v_\delta^n$ in $(8.5.2)_2$ gives

$$\|v_\delta^n\|^2 = \tau(r(u_{\delta,1}^n) - r(u_{\delta,2}^n), v_\delta^n) \le \tau L_r \|u_\delta\| \|v\|$$

as the H_δ terms cancel because of explicit discretization. This gives,

$$\|v_\delta^n\| \le C\tau \|u_\delta^n\|. \tag{8.5.3}$$

Further, with $\phi = u_\delta^n, \theta = u_\delta^n, \psi = \tau \mathbf{Q}_\delta^n$, from (8.5.2) we obtain

$$\|u_\delta^n\|^2 + \tau\|\mathbf{Q}_\delta^n\|^2 + \tau(r(u_{\delta,1}^n) - r(u_{\delta,2}^n), u_\delta^n) = \tau(\mathbf{q}u_\delta^n, \mathbf{Q}_\delta^n).$$

Since r is monotone, the Cauchy inequality and boundedness of $\mathbf{q}$ give

$$\|u_\delta^n\|^2 + \frac{1}{2}\tau\|\mathbf{Q}_\delta^n\|^2 \le \tau\frac{1}{2}M_q^2\|u_\delta^n\|^2.$$

For $\tau < \frac{2}{M_q^2}$, we obtain

$$\|u_\delta^n\| = 0 \text{ and thereby } \|\mathbf{Q}_\delta^n\| = 0.$$

Together with (8.5.3) we conclude $u_\delta^n = v_\delta^n = 0$ and $\mathbf{Q}_\delta^n = \mathbf{0}$. $\qquad\square$

8.5.1   The a priori estimates

We start with the following stability estimates.

Lemma 8.3 *It holds that*

$$\sup_{k=1,\ldots,N} \left\| u_\delta^k \right\| \le C, \tag{8.5.4}$$

$$\left\| v_\delta^n - v_\delta^{n-1} \right\| \le C\tau, \tag{8.5.5}$$

$$\sup_{k=1,\ldots,N} \left\| v_\delta^k \right\| \le C, \tag{8.5.6}$$

$$\sup_{k=1,\ldots,N} \left\| Q_\delta^k \right\| \le C, \tag{8.5.7}$$

$$\sum_{n=1}^{N} \left\| u_\delta^n - u_\delta^{n-1} \right\|^2 \le C\tau, \tag{8.5.8}$$

$$\sum_{n=1}^{N} \left\| Q_\delta^n - Q_\delta^{n-1} \right\|^2 \le C, \tag{8.5.9}$$

$$\sum_{n=1}^{N} \tau \left\| \nabla \cdot Q_\delta^n \right\|^2 \le C, \tag{8.5.10}$$

$$\sum_{n=1}^{N} \tau \left\| \nabla \cdot (Q_\delta^n - Q_\delta^{n-1}) \right\|^2 \le C. \tag{8.5.11}$$

Proof. We start by showing (8.5.4). To this aim we chose

$$\phi = u_\delta^n, \quad \psi = \tau Q_\delta^n, \quad \theta = u_\delta^n$$

as test functions in (8.5.2), and add the resulting to obtain

$$(u_\delta^n - u_\delta^{n-1}, u_\delta^n) + \tau \|Q_\delta^n\|^2 - \tau(qu_\delta^n, Q_\delta^n) + \tau(r(u_\delta^n), u_\delta^n) = \tau(H_\delta(v_\delta^{n-1}), u_\delta^n). \tag{8.5.12}$$

Using the equality

$$(u_\delta^n - u_\delta^{n-1}, u_\delta^n) = \frac{1}{2} \left(\|u_\delta^n\|^2 - \|u_\delta^{n-1}\|^2 + \|u^n - u_\delta^{n-1}\|^2 \right)$$

since $\mathbf{q}$ and H_δ are bounded and $r(u_\delta^n)u_\delta^n \ge 0$, by Young's inequality we get

$$\|u_\delta^n\|^2 - \left\| u_\delta^{n-1} \right\|^2 + \left\| u_\delta^n - u_\delta^{n-1} \right\|^2 + 2\tau \|Q_\delta^n\|^2 + 2\tau(r(u_\delta^n), u_\delta^n)$$
$$= 2\tau(qu_\delta^n, Q_\delta^n) + 2\tau(H_\delta(v_\delta^{n-1}), u_\delta^n) \le \tau \|Q_\delta^n\|^2 + C\tau \|u_\delta^n\|^2 + C\tau + C\tau \|u_\delta^n\|^2.$$

Summing over $n = 1, \ldots, k$ (where $k \in \{, 1, \ldots, N\}$ is arbitrary) gives

$$\left\| u_\delta^k \right\|^2 + \sum_{n=1}^{k} \left\| u_\delta^n - u_\delta^{n-1} \right\|^2 + \tau \sum_{n=1}^{k} \|Q_\delta^n\|^2 \le \|u_I\|^2 + C + C\tau \sum_{n=1}^{k} \|u_\delta^n\|^2, \tag{8.5.13}$$

and (8.5.4) follows from the discrete Gronwall lemma.

For (8.5.5) we choose for $\theta = v_\delta^n - v_\delta^{n-1}$ in $(8.5.2)_2$ and apply the Cauchy Schwarz inequality for the right hand side,

$$\left\| v_\delta^n - v_\delta^{n-1} \right\|^2 \leq \tau \left\| r(u_\delta^n) \right\| \left\| v_\delta^n - v_\delta^{n-1} \right\| + \tau \left\| H_\delta(v_\delta^{n-1}) \right\| \left\| v_\delta^n - v_\delta^{n-1} \right\|.$$

Using (8.5.4), the boundedness of H_δ and the Lipschitz continuity of r this implies

$$\left\| v_\delta^n - v_\delta^{n-1} \right\| \leq C\tau.$$

To prove (8.5.6), choose $\theta = v_\delta^n$ in $(8.5.2)_2$ to obtain

$$(v_\delta^n - v_\delta^{n-1}, v_\delta^n) = \tau(r(u_\delta^n), v_\delta^n) - \tau(H_\delta(v_\delta^{n-1}), v_\delta^n).$$

The left hand side can be rewritten as

$$(v_\delta^n - v_\delta^{n-1}, v_\delta^n) = \frac{1}{2} \left(\|v_\delta^n\|^2 - \|v_\delta^{n-1}\|^2 + \|v_\delta^n - v_\delta^{n-1}\|^2 \right).$$

We write the last term on the right hand side as

$$\left(H_\delta(v_\delta^{n-1}), v_\delta^n \right) = \left(H_\delta(v_\delta^{n-1}), v_\delta^{n-1} \right) - \left(H_\delta(v_\delta^{n-1}), v_\delta^{n-1} - v_\delta^n \right).$$

and substitute it in above to obtain

$$\|v_\delta^n\|^2 - \left\| v_\delta^{n-1} \right\|^2 + \left\| v_\delta^n - v_\delta^{n-1} \right\|^2 = 2\tau \left(r(u_\delta^n), v_\delta^n \right) - \left(H_\delta(v_\delta^{n-1}), v_\delta^{n-1} \right) + \left(H_\delta(v_\delta^{n-1}), v_\delta^{n-1} - v_\delta^n \right).$$

Since $H(\cdot)$ is monotone, $(H_\delta(v_\delta^{n-1}), v_\delta^{n-1}) \geq 0$, now the Cauchy Schwarz inequality gives

$$\|v_\delta^n\|^2 - \left\| v_\delta^{n-1} \right\|^2 + \left\| v_\delta^n - v_\delta^{n-1} \right\|^2 \leq 2\tau C \|u_\delta^n\| \|v_\delta^n\| + 2\tau \left(H_\delta(v_\delta^{n-1}), v_\delta^n - v_\delta^{n-1} \right).$$

By Young's inequality this leads to

$$\|v_\delta^n\|^2 - \left\| v_\delta^{n-1} \right\|^2 + \frac{1}{2} \left\| v_\delta^n - v_\delta^{n-1} \right\|^2 \leq \tau \|v_\delta^n\|^2 + C\tau \|u_\delta^n\|^2 + 2\tau^2 \|H_\delta\|^2.$$

Summing over $n = 1, \ldots, k$ (with $k \in \{1, \ldots, N\}$ arbitrary) this gives

$$\begin{aligned}
\left\| v_\delta^k \right\|^2 + \sum_{n=1}^k \left\| v_\delta^n - v_\delta^{n-1} \right\|^2 &\leq \|v_I\|^2 + \tau \sum_{n=1}^k \|v_\delta^n\|^2 + C\tau \sum_{n=1}^k \|u_\delta^n\|^2 + \sum_{n=1}^k 4\tau^2 \|H_\delta\|^2 \\
&\leq \tau \sum_{n=1}^k \|v_\delta^n\|^2 + C + C\tau
\end{aligned}$$

where we have used the estimates proved before and the bounds on initial data. Now (8.5.6) follows from the Discrete Gronwall Lemma.

We proceed with the estimate (8.5.7). To this aim, we need to specify the initial flux: $\mathbf{Q}_\delta^0 = -\nabla u_I + \mathbf{q} u_I \in (L^2(\Omega))^d$. With $\phi = u_\delta^n - u_\delta^{n-1}$, $(8.5.2)_1$ gives

$$\left\| u_\delta^n - u_\delta^{n-1} \right\|^2 + \tau \left(\nabla \cdot \mathbf{Q}_\delta^n, u_\delta^n - u_\delta^{n-1} \right) + \left(v_\delta^n - v_\delta^{n-1}, u_\delta^n - u_\delta^{n-1} \right) = 0. \qquad (8.5.14)$$

Now take $\psi = \tau \mathbf{Q}_\delta^n$ to get

$$\tau \left(\mathbf{Q}_\delta^n, \mathbf{Q}_\delta^n \right) - \tau \left(u_\delta^n, \nabla \cdot \mathbf{Q}_\delta^n \right) - \tau \left(\mathbf{q} u_\delta^n, \mathbf{Q}_\delta^n \right) = 0, \qquad (8.5.15)$$

and next choose $\psi = \tau \mathbf{Q}_\delta^n$ for the equation corresponding to $(n-1)$-th time step

$$\tau \left(\mathbf{Q}_\delta^{n-1}, \mathbf{Q}_\delta^n \right) - \tau \left(u_\delta^{n-1}, \nabla \cdot \mathbf{Q}_\delta^n \right) - \tau \left(\mathbf{q} u_\delta^{n-1}, \mathbf{Q}_\delta^n \right) = 0. \qquad (8.5.16)$$

Subtract (8.5.16) from (8.5.15) to obtain

$$\tau \left(\mathbf{Q}_\delta^n - \mathbf{Q}_\delta^{n-1}, \mathbf{Q}_\delta^n \right) - \tau \left(u_\delta^n - u_\delta^{n-1}, \nabla \cdot \mathbf{Q}_\delta^n \right) - \tau \left(\mathbf{q}(u_\delta^n - u_\delta^{n-1}), \mathbf{Q}_\delta^n \right) = 0.$$

Further, use (8.5.14) in above to obtain

$$\left\| u_\delta^n - u_\delta^{n-1} \right\|^2 + \tau \left(\mathbf{Q}_\delta^n - \mathbf{Q}_\delta^{n-1}, \mathbf{Q}_\delta^n \right) = \tau \left(\mathbf{q}(u_\delta^n - u_\delta^{n-1}), \mathbf{Q}_\delta^n \right) - (v_\delta^n - v_\delta^{n-1}, u_\delta^n - u_\delta^{n-1}). \qquad (8.5.17)$$

As before, we can rewrite $\left(\mathbf{Q}_\delta^n - \mathbf{Q}_\delta^{n-1}, \mathbf{Q}_\delta^n \right)$ as

$$\left(\mathbf{Q}_\delta^n - \mathbf{Q}_\delta^{n-1}, \mathbf{Q}_\delta^n \right) = \frac{1}{2} \left(\|\mathbf{Q}_\delta^n\|^2 - \|\mathbf{Q}_\delta^{n-1}\|^2 + \|\mathbf{Q}_\delta^n - \mathbf{Q}_\delta^{n-1}\|^2 \right).$$

Substituting the above in (8.5.17) we obtain

$$2 \left\| u_\delta^n - u_\delta^{n-1} \right\|^2 + \tau \|\mathbf{Q}_\delta^n\|^2 - \tau \left\| \mathbf{Q}_\delta^{n-1} \right\|^2 + \tau \left\| \mathbf{Q}_\delta^n - \mathbf{Q}_\delta^{n-1} \right\|^2$$
$$= 2\tau(\mathbf{q}(u_\delta^n - u_\delta^{n-1}), \mathbf{Q}_\delta^n) - 2(v_\delta^n - v_\delta^{n-1}, u_\delta^n - u_\delta^{n-1})$$

The right hand side can be estimated using Young's inequality in a straightforward manner

$$2 \left\| u_\delta^n - u_\delta^{n-1} \right\|^2 + \tau \|\mathbf{Q}_\delta^n\|^2 - \tau \left\| \mathbf{Q}_\delta^{n-1} \right\|^2 + \tau \left\| \mathbf{Q}_\delta^n - \mathbf{Q}_\delta^{n-1} \right\|^2$$
$$\leq \left\| u_\delta^n - u_\delta^{n-1} \right\|^2 + M_q^2 \tau^2 \|\mathbf{Q}_\delta^n\|^2 + 2 \left\| v_\delta^n - v_\delta^{n-1} \right\|^2.$$

Summing over $n = 1, \ldots, k$ ($k \in \{1, \ldots, N\}$ arbitrary) we obtain

$$\sum_{n=1}^{k} \left\| u_\delta^n - u_\delta^{n-1} \right\|^2 + \tau \left\| \mathbf{Q}_\delta^k \right\|^2 + \tau \sum_{n=1}^{k} \left\| \mathbf{Q}_\delta^n - \mathbf{Q}_\delta^{n-1} \right\|^2 \leq C\tau + C\tau^2 \sum_{n=1}^{k} \|\mathbf{Q}_\delta^n\|^2 + \tau \|\mathbf{Q}_I\|^2.$$
$$(8.5.18)$$

The estimate (8.5.7) follows now by the Discrete Gronwall lemma. Moreover, from (8.5.18) we also get (8.5.8) and (8.5.9).

Finally, to prove (8.5.10) we take $\phi = \nabla \cdot \mathbf{Q}_\delta^n$ in (8.5.2)$_1$ and use Young's inequality for the right hand side to obtain

$$\tau^2 \left\| \nabla \cdot \mathbf{Q}_\delta^n \right\|^2 \leq \left\| u_\delta^n - u_\delta^{n-1} \right\|^2 + \left\| v_\delta^n - v_\delta^{n-1} \right\|^2 + \frac{1}{2}\tau^2 \left\| \nabla \cdot \mathbf{Q}_\delta^n \right\|^2 ,$$

Summing over $n = 1 \dots, N$ and using (8.5.5) and (8.5.8) gives (8.5.10).

Finally, to prove the estimate (8.5.11), we simply use the Triangle inequality in (8.5.10).
$\square$

8.5.2   Enhanced compactness

As will be seen below, the above estimates are not sufficient to retrieve the desired limiting equations. To complete the proof of convergence, stronger compactness properties are needed. These are obtained by translation estimates. To this aim, we define the translation in space
$$\triangle_\xi f(\cdot) := f(\cdot) - f(\cdot + \xi), \quad \xi \in \mathbb{R}^2.$$
Further, with $\xi \in \mathbb{R}^2$ we consider $\Omega_\xi \subset \Omega$ such that

$$\Omega_\xi := \{ x \in \Omega \mid \operatorname{dist}(x, \Gamma) > |\xi| \}.$$

In this way, the translations $\triangle_\xi f(x)$ with $x \in \Omega$ are well-defined.
For reasons of brevity, the norms and the inner products for the translations should be understood with respect to Ω_ξ unless explicitly stated otherwise. First, we consider the translation for u_δ^n.

Lemma 8.4 *It holds that*
$$\sum_{n=1}^{N} \tau \left\| \triangle_\xi u_\delta^n \right\|^2 \leq C|\xi|.$$

Proof.   For (8.5.2)$_3$ we have after translation in space

$$(\triangle_\xi \mathbf{Q}_\delta^n, \boldsymbol{\psi}) - (\triangle_\xi u_\delta^n, \nabla \cdot \boldsymbol{\psi}) - (\triangle_\xi (\mathbf{q} u_\delta^n), \boldsymbol{\psi}) = 0.$$

We construct an appropriate test function to obtain the estimate above. Take η^n such that
$$\begin{cases} -\triangle \eta^n = \triangle_\xi u_\delta^n & \text{in} \quad \Omega, \\ \eta^n = 0 & \text{on} \quad \partial\Omega, \end{cases}$$

and choose $\boldsymbol{\psi} = \nabla \eta^n$ (note that $\boldsymbol{\psi} \in H(div; \Omega)$) to obtain

$$(\triangle_\xi \mathbf{Q}^n_\delta, \nabla \eta^n) + (\triangle_\xi u^n_\delta, \triangle_\xi u^n_\delta) - (\triangle_\xi(\mathbf{q}u^n_\delta), \nabla \eta^n) = 0. \tag{8.5.19}$$

Note that η^n satisfies $\|\triangle \eta^n\| = \|\triangle_\xi u^n_\delta\|$, and therefore

$$\|\eta^n\|_{H^2(\Omega)} \le C(\Omega) \|\triangle_\xi u^n_\delta\|.$$

This implies that translations of $\nabla \eta^n$ are controlled,

$$\|\nabla(\triangle_\xi \eta^n)\|_{L^2(\Omega)} \le C|\xi| \|\nabla \cdot (\nabla \eta^n)\| \le C(\Omega)|\xi| \|\triangle_\xi u^n_\delta\|. \tag{8.5.20}$$

Recalling (8.5.4), this gives

$$\|\nabla(\triangle_\xi \eta^n\|_{L^2(\Omega)} \le C(\Omega)|\xi| \|\triangle_\xi u^n_\delta\| \le C|\xi|. \tag{8.5.21}$$

Thus we have the following estimate

$$\begin{aligned} \tau \sum_{n=1}^N \|\triangle_\xi u^n_\delta\|^2 &= \tau \sum_{n=1}^N (\mathbf{q}u^n_\delta, \nabla(\triangle_\xi \eta^n)) + \tau \sum_{n=1}^N (\mathbf{Q}^n_\delta, \nabla(\triangle_\xi \eta^n)) \\ &\le \tau \sum_{n=1}^N \|\mathbf{Q}^n_\delta\| \|\nabla(\triangle_\xi \eta^n)\| + \tau \sum_{n=1}^N \|\mathbf{q}\|_{L^\infty(\Omega)} \|u^n_\delta\| \|\nabla(\triangle_\xi \eta^n)\| \end{aligned} \tag{8.5.22}$$

The conclusion follows by (8.5.4), (8.5.7), the Young inequality and (8.5.21). $\qquad\square$

The translation estimates for v^n_δ are bounded by those for u^n_δ. This is the essence of the next lemma.

Lemma 8.5 *The following estimates hold true*

$$\sup_{k=1,\dots N} \left\|\triangle_\xi v^k_\delta\right\|^2 + \sum_{n=1}^N \left\|\triangle_\xi(v^n_\delta - v^{n-1}_\delta)\right\|^2 \le C \left\|\triangle_\xi v^I\right\|^2 + C\tau \sum_{n=1}^N \|\triangle_\xi u^n_\delta\|^2, \tag{8.5.23}$$

$$\sum_{n=1}^N \|\triangle_\xi v^n_\delta\|^2 \le C|\xi|. \tag{8.5.24}$$

Proof. With $\theta = \triangle_\xi v^n_\delta$ in $(8.5.2)_2$, we get

$$\left(\triangle_\xi v^n_\delta - \triangle_\xi v^{n-1}_\delta, \triangle_\xi v^n_\delta\right) = \tau \left(\triangle_\xi r(u^n_\delta), \triangle_\xi v^n_\delta\right) - \tau \left(\triangle_\xi H_\delta(v^{n-1}_\delta), \triangle_\xi v^n_\delta\right)$$

The last term in the above rewrites as

$$\left(\triangle_\xi H_\delta(v^{n-1}_\delta), \triangle_\xi v^n_\delta\right) = \left(\triangle_\xi H_\delta(v^{n-1}_\delta), \triangle_\xi v^{n-1}_\delta\right) + \left(\triangle_\xi H_\delta(v^{n-1}_\delta), \triangle_\xi(v^n_\delta - v^{n-1}_\delta)\right).$$

The monotonicity of H_δ implies that the first term on the right hand side is positive

$$\left(\triangle_\xi H_\delta(v^{n-1}_\delta), \triangle_\xi v^n_\delta\right) \ge 0.$$

For the left hand side, we use the identity

$$\left(\triangle_\xi v_\delta^{n-1}, \triangle_\xi v_\delta^n\right) = \frac{1}{2}\left(\|\triangle_\xi v_\delta^n\|^2 - \left\|\triangle_\xi v_\delta^{n-1}\right\|^2 + \left\|\triangle_\xi(v_\delta^n - v_\delta^{n-1})\right\|^2\right),$$

which, together with the Cauchy-Schwarz inequality for the first term on the right hand side gives

$$\begin{aligned}
\tfrac{1}{2}&\left(\|\triangle_\xi v_\delta^n\|^2 - \left\|\triangle_\xi v_\delta^{n-1}\right\|^2 + \left\|\triangle_\xi(v_\delta^n - v_\delta^{n-1})\right\|^2\right) \\
&\leq \tau L_r \|\triangle_\xi u_\delta^n\| \|\triangle_\xi v_\delta^n\| + \tau\left(\triangle_\xi H_\delta(v_\delta^{n-1}), \triangle_\xi(v_\delta^n - v_\delta^{n-1})\right) \\
&\leq L_r \tfrac{\tau}{2}\|\triangle_\xi u_\delta^n\|^2 + \tfrac{\tau}{2}\|\triangle_\xi v_\delta^n\|^2 + \tau^2\left\|\triangle_\xi H_\delta(v_\delta^{n-1})\right\|^2 + \tfrac{1}{4}\left\|\triangle_\xi(v_\delta^n - v_\delta^{n-1})\right\|^2 \\
&\leq \tfrac{1}{2}L_r\tau\|\triangle_\xi u_\delta^n\|^2 + \tfrac{1}{2}\tau\|\triangle_\xi v_\delta^n\|^2 + \tfrac{\tau^2}{\delta^2}\|\triangle_\xi v_\delta^{n-1}\|^2 + \tfrac{1}{4}\|\triangle_\xi(v_\delta^n - v_\delta^{n-1})\|^2.
\end{aligned}$$

Summing over $n = 1, \ldots, k$ ($k \in \{1, \ldots, N\}$) yields

$$\begin{aligned}
\left\|\triangle_\xi v_\delta^k\right\|^2 &+ \frac{1}{2}\sum_{n=1}^{k}\left\|\triangle_\xi(v_\delta^n - v_\delta^{n-1})\right\|^2 \\
&\leq \left\|\triangle_\xi v^I\right\|^2 + L_r\tau\sum_{n=1}^{k}\|\triangle_\xi u_\delta^n\|^2 + \tau\sum_{n=1}^{k}\|\triangle_\xi v_\delta^n\|^2 + \sum_{n=1}^{k}\frac{2\tau^2}{\delta^2}\|\triangle_\xi v_\delta^{n-1}\|^2.
\end{aligned}$$

$$(8.5.25)$$

Using Lemma 8.4 and Gronwall's lemma we obtain

$$\sup_{k=1,\ldots,N}\left\|\triangle_\xi v_\delta^k\right\|^2 \leq C\tau\sum_{n=1}^{N}\|\triangle_\xi u_\delta^n\|^2 + \|\triangle_\xi v_I\|^2. \tag{8.5.26}$$

The estimate (8.5.23) follows from the above and from (8.5.25), whereas (8.5.24) is a direct consequence of Lemma 8.4 and the assumptions on v_I. $\qquad\square$

From the above we also get

Lemma 8.6 *The following estimate holds:*

$$\sum_{n=1}^{N}\left\|\triangle_\xi(v_\delta^n - v_\delta^{n-1})\right\|^2 \leq C\tau. \tag{8.5.27}$$

Proof. Testing in $(8.5.2)_2$ with $\theta = v_\delta^n - v_\delta^{n-1}$ gives

$$\begin{aligned}
\left\|\triangle_\xi(v_\delta^n - v_\delta^{n-1})\right\|^2 &= \tau(\triangle_\xi r(u_\delta^n) - H_\delta(v_\delta^{n-1}), \triangle_\xi(v_\delta^n - v_\delta^{n-1})) \\
&\leq \tau^2\|\triangle_\xi r(u_\delta^n)\|^2 + \tfrac{1}{2}\|\triangle_\xi(v_\delta^n - v_\delta^{n-1})\|^2 + \tau^2\|H_\delta(v_\delta^{n-1})\|^2.
\end{aligned}$$

$$(8.5.28)$$

Using the Lipschitz property of r and the estimates above we obtain

$$\left\|\triangle_\xi(v_\delta^n - v_\delta^{n-1})\right\|^2 \le \tau^2 C,$$

and the conclusion follows by summing over $n = 1, \dots, N$. □

8.5.3 Convergence

For proving the convergence of the time discretization scheme, we consider the sequence of time discrete quadruples $\{(u_\delta^n, \mathbf{Q}_\delta^n, v_\delta^n, w_\delta^n), n = 0, \dots, N\}$ solving Problem $\mathbf{P}_\delta^{mvf,n}$, and construct a time continuous approximation by linear interpolation. In this sense, for $t \in [t_{n-1}, t_n]$ $(n = 1, \dots, N)$ we define

$$
\begin{aligned}
U^\tau(t) &:= u_\delta^n \frac{(t - t_{n-1})}{\tau} + u_\delta^{n-1} \frac{(t_n - t)}{\tau}, \\
V^\tau(t) &:= v_\delta^n \frac{(t - t_{n-1})}{\tau} + v_\delta^{n-1} \frac{(t_n - t)}{\tau}, \\
\mathbf{Q}^\tau(t) &:= \mathbf{Q}_\delta^n \frac{(t - t_{n-1})}{\tau} + \mathbf{Q}_\delta^{n-1} \frac{(t_n - t)}{\tau}, \\
W^\tau(t) &:= H_\delta(V^\tau(t)).
\end{aligned}
\tag{8.5.29}
$$

The estimates in Lemma 8.3 can be translated directly to $(U^\tau, \mathbf{Q}^\tau, V^\tau, W^\tau)$:

Lemma 8.7 *A constant $C > 0$ exists s.t. for any τ and $\delta = O(\sqrt{\tau})$ the following $L^2(0, T; L^2(\Omega))$ estimates hold*

$$\|U^\tau\|^2 + \|V^\tau\|^2 + \|\mathbf{Q}^\tau\|^2 \le C, \tag{8.5.30}$$

$$\|\partial_t U^\tau\| + \|\partial_t V^\tau\|^2 + \|\nabla \cdot \mathbf{Q}^\tau\|^2 \le C. \tag{8.5.31}$$

Proof. (8.5.30) follows easily from (8.5.4). For instance,

$$\|U^\tau\|^2 \le 2\|u_\delta^n\|^2 + 2\|u_\delta^{n-1}\|^2 \le C$$

and similarly other estimates follow. To estimate $\|\partial_t V^\tau\|^2_{L^2(0,T;L^2(\Omega))}$ we note that, whenever $t \in (t_{n-1}, t_n]$,

$$\partial_t V^\tau = \frac{v_\delta^n - v_\delta^{n-1}}{\tau}$$

implying

$$\int_0^T \|\partial_t V^\tau\|^2 dt = \sum_{n=1}^N \int_{t_{n-1}}^{t_n} \|\frac{v_\delta^n - v_\delta^{n-1}}{\tau}\|^2_{L^2(\Omega)} dt \le \sum_{n=1}^N \tau \|\frac{v_\delta^n - v_\delta^{n-1}}{\tau}\|^2_{L^2(\Omega)} \le C\tau N \le C,$$

where we have used the estimate (8.5.4).

The proof for $\partial_t U^\tau$ is the same as above and uses the estimate (8.5.8). The only remaining part in (8.5.31) is to show that $\nabla \cdot \mathbf{Q}^\tau \in L^2(0, T; L^2(\Omega))$. To see this note that

$$\nabla \cdot \mathbf{Q}^\tau = \nabla \cdot \mathbf{Q}_\delta^{n-1} + \frac{t - t_{n-1}}{\tau} \nabla \cdot (\mathbf{Q}_\delta^n - \mathbf{Q}_\delta^{n-1}).$$

Squaring both sides and using the elementary inequality

$$\|\nabla \cdot \mathbf{Q}^\tau\|_{L^2(\Omega)}^2 \leq 2\|\nabla \cdot \mathbf{Q}_\delta^{n-1}\|^2 + 2\frac{(t - t_{n-1})^2}{\tau^2}\|\nabla \cdot (\mathbf{Q}_\delta^n - \mathbf{Q}_\delta^{n-1})\|^2,$$

integrating over t from 0 to T, since $\nabla \cdot \mathbf{Q}_\delta^{n-1}$ and $\nabla \cdot \mathbf{Q}_\delta^n$ are constant in (t_{n-1}, t_n) gives

$$\int_0^T \|\nabla \cdot \mathbf{Q}^\tau\|^2 dt \leq 2\tau \sum_{n=1}^N \|\nabla \cdot \mathbf{Q}_\delta^{n-1}\|^2 + 2\sum_{n=1}^N \int_{t_{n-1}}^{t_n} \frac{(t-t_{n-1})^2}{\tau^2}\|\nabla \cdot (\mathbf{Q}_\delta^n - \mathbf{Q}_\delta^{n-1})\|^2 dt$$
$$\leq 2\tau \sum_{n=1}^N \|\nabla \cdot \mathbf{Q}_\delta^{n-1}\|^2 + 2\sum_{n=1}^N \frac{2\tau}{3}\|\nabla \cdot (\mathbf{Q}_\delta^n - \mathbf{Q}_\delta^{n-1})\|^2.$$

Now use (8.5.10)–(8.5.11) to obtain

$$\int_0^T \|\nabla \cdot \mathbf{Q}^\tau\|^2 \leq C.$$

$\square$

Note that the estimates above are uniform in τ, if $\delta = O(\sqrt{\tau})$ and we have $(U^\tau, \mathbf{Q}^\tau, V^\tau, W^\tau) \in \mathcal{V} \times \mathcal{S} \times \mathcal{V} \times L^\infty(\Omega^T)$. Moreover, we have

Lemma 8.8 *A quadruple* $(u, \mathbf{Q}, v, w) \in \mathcal{V} \times \mathcal{S} \times \mathcal{V} \times L^\infty(\Omega^T)$ *exists s.t. along a sequence* $\tau \searrow 0$ *(and with* $\delta = O(\tau^{\frac{1}{2}})$*) we have*

(i). $U^\tau \rightharpoonup u$ *weakly in* $L^2((0, T); L^2(\Omega))$,

(ii). $\partial_t U^\tau \rightharpoonup \partial_t u$ *weakly in* $L^2((0, T); L^2(\Omega))$,

(iii). $\mathbf{Q}^\tau \rightharpoonup \mathbf{Q}$ *weakly in* $L^2((0, T); L^2(\Omega)^d)$,

(iv). $\nabla \cdot \mathbf{Q}^\tau \rightharpoonup \nabla \cdot \mathbf{Q}$ *weakly in* $L^2((0, T); L^2(\Omega))$,

(v). $V^\tau \rightharpoonup v$ *weakly in* $L^2((0, T); L^2(\Omega))$,

(vi). $\partial_t V^\tau \rightharpoonup \partial_t v$ *weakly in* $L^2((0, T); L^2(\Omega))$,

(vii). $W^\tau \rightharpoonup w$ *weakly-star in* $L^\infty(\Omega)$.

In the above only weak convergence of U^τ in $L^2(0, T; L^2(\Omega))$ is obtained, which is not sufficient for passing to the limit for non-linear term $r(U^\tau)$. To obtain strong convergence, we use translation estimates as derived in Lemma 8.4.

Lemma 8.9 *It holds that*

$$U^\tau \to u \text{ strongly in } L^2((0,T); L^2(\Omega)).$$

Proof. In view of $\partial_t U^\tau \in L^2(0,T; L^2(\Omega))$, the translation in time is already controlled. What we need is to control the translation in space. Due to [25] (Prop. 9.3, p.267), we need to prove that

$$\mathcal{I}_\xi := \int_0^T \int_\Omega |\triangle_\xi U^\tau|^2 \to 0 \text{ as } |\xi| \searrow 0.$$

The definition of U^τ immediately implies that

$$|\mathcal{I}_\xi| \le \sum_{n=1}^N \tau \left(2\|\triangle_\xi u_\delta^n\|^2 + 2\|\triangle_\xi u_\delta^{n-1}\|^2 \right).$$

Using Lemma 8.4 we find that

$$|\mathcal{I}_\xi| \le C|\xi|$$

where C is independent of τ and δ, implying the strong convergence. $\qquad\square$

To identify w with $H(v)$ we further need the strong convergence of V^τ. This ia a consequence of lemmas 8.5 and 8.9.

Lemma 8.10 *For V^τ, it holds that*

$$V^\tau \to v \text{ strongly in } L^2((0,T); L^2(\Omega)).$$

Proof. Once again, we use the translation estimate and note that the regularity of $\partial_t V^\tau$ ensures the control of the translation in time. What remains is to prove the following estimate

$$\mathcal{I}_\xi := \int_0^T \int_{\Omega_\xi} |\triangle_\xi V^\tau|^2 \to 0 \text{ as } |\xi| \searrow 0.$$

Using the definition of V^τ we have

$$\mathcal{I}_\xi \le \sum_{n=1}^N \tau \left(2\|\triangle_\xi v_\delta^n\|^2 + 2\|\triangle_\xi v_\delta^{n-1}\|^2 \right).$$

Thanks to Lemma 8.5 we have

$$\mathcal{I}_\xi \le C|\xi|$$

where C is independent of τ and δ, thus establishing the strong convergence. $\qquad\square$

8.5.4 The limit equations

Once the strong convergence is obtained, the following theorem provides the existence of the weak solution in the mixed variational formulation.

Theorem 8.5.1 *The limit quadruple $(u, \mathbf{Q}, v, w)$ is a solution in the sense of Definition 8.4.1.*

Proof.   By the weak convergence, the estimates in Lemma 8.7 carry over for the limit quadruple $(u, \mathbf{Q}, v, w)$. Moreover, the time continuous approximation in (8.5.29) satisfies

$$(\partial_t U^\tau, \phi) + (\nabla \cdot \mathbf{Q}^\tau, \phi) + (\partial_t V^\tau, \phi) = (\nabla \cdot (\mathbf{Q}^\tau - \mathbf{Q}_\delta^n), \phi), \tag{8.5.32}$$

$$(\partial_t V^\tau, \theta) - (r(U^\tau) - W^\tau, \theta) = \left(H_\delta(V^\tau) - H_\delta(v_\delta^{n-1}, \theta \right) + (r(u_\delta^n) - r(U^\tau), \theta) \tag{8.5.33}$$

$$(\mathbf{Q}^\tau, \boldsymbol{\psi}) - (U^\tau, \nabla \cdot \boldsymbol{\psi}) - (\mathbf{q}U^\tau, \boldsymbol{\psi}) = (\mathbf{Q}^\tau - \mathbf{Q}_\delta^n, \boldsymbol{\psi}) - (U^\tau - u_\delta^n, \nabla \cdot \boldsymbol{\psi}) - (\mathbf{q}(U^\tau - u_\delta^n), \boldsymbol{\psi}) \tag{8.5.34}$$

for all $(\phi, \theta, \boldsymbol{\psi}) \in L^2(0, T; H_0^1(\Omega)), \mathcal{V}, \mathcal{S}$. Note that, in fact, (8.5.32) also holds for $\phi \in \mathcal{V}$. Here we choose a better space to identify the limit, where we prove that the term on the right is vanishing along a sequence $\tau \searrow 0$. By density arguments, the limit will hold for $\phi \in \mathcal{V}$.

Consider first (8.5.32) and note that by Lemma 8.8, the left hand side converges to the desired limit. It only remains to show that the right hand side, denoted by $\mathcal{I}_1$, vanishes as $\tau \searrow 0$. Integrating by parts, which is allowed due to the choice of $\phi \in L^2(0, T; H_0^1(\Omega))$, one has

$$|\mathcal{I}_1| \leq \left(\sum_{n=1}^N \tau C \|\mathbf{Q}_\delta^n - \mathbf{Q}_\delta^{n-1}\|^2 \right)^{\frac{1}{2}} \left(\int_0^T \|\nabla \phi\|^2 \right)^{\frac{1}{2}}.$$

Due to the estimate (8.5.9), $\sum_{n=1}^N \tau \|\mathbf{Q}_\delta^n - \mathbf{Q}_\delta^{n-1}\|^2 \to 0$.

Next, we consider (8.5.33). First we prove that the last two integrals on the right hand side vanish, denoted by $\mathcal{I}_2$ and $\mathcal{I}_3$ vanish. For $\mathcal{I}_2$ we use the Lipschitz continuity of H_δ and the definition of V^τ to obtain

$$|\mathcal{I}_2| \leq \left(\sum_{n=1}^N \frac{\tau}{\delta^2} \|v_\delta^n - v_\delta^{n-1}\|^2 \right)^{\frac{1}{2}} \left(\int_0^T \|\theta\|^2 \right)^{\frac{1}{2}}.$$

Using (8.5.5) we have

$$|\mathcal{I}_2| \leq C \frac{\tau}{\delta} \left(\int_0^T \|\theta\|^2 \right)^{\frac{1}{2}}.$$

By the choice of δ, $\frac{\tau}{\delta} \searrow 0$ as $\tau \searrow 0$, implying that $\mathcal{I}_2$ vanishes in the limit.

For $\mathcal{I}_3$ we use the Lipschitz continuity of r and (8.5.8) to get

$$|\mathcal{I}_3| \leq \left(\sum_{n=1}^{N} \tau L_r \|u_\delta^n - u_\delta^{n-1}\|^2 \right)^{\frac{1}{2}} \left(\int_0^T \|\psi\|^2 \right)^{\frac{1}{2}} \to 0.$$

For the first term on the left in (8.5.32), the limit is straightforward. For the limit of the second term, with strong convergence of U^τ and weak-* convergence of W^τ we get

$$\lim_{\tau \searrow 0} \left(r(U^\tau) - W^\tau, \theta \right) = \left(r(u) - w, \theta \right),$$

leading to the limiting equation

$$(\partial_t v, \theta) = (r(u) - w, \theta) \ \text{ for all } \theta \in \mathcal{V}. \tag{8.5.35}$$

Now we consider (8.5.34) and denote the corresponding integrals on the right hand side respectively by $\mathcal{I}_4, \mathcal{I}_5$, and $\mathcal{I}_6$. By the definition of $\mathbf{Q}^\tau$ and (8.5.9), as $\tau \searrow 0$ we obtain

$$|\mathcal{I}_4| \leq \left(\sum_{n=1}^{N} \tau \|\mathbf{Q}_\delta^n - \mathbf{Q}_\delta^{n-1}\|^2 \right)^{\frac{1}{2}} \left(\int_0^T \|\psi\|^2 \right)^{\frac{1}{2}} \to 0.$$

Similarly, for $\mathcal{I}_5$ and $\mathcal{I}_5$, using (8.5.8)

$$|\mathcal{I}_4| \leq \left(\sum_{n=1}^{N} \tau \|u_\delta^n - u_\delta^{n-1}\|^2 \right)^{\frac{1}{2}} \left(\int_0^T \|\psi\|^2 \right)^{\frac{1}{2}} \to 0, \ \text{ and}$$

$$|\mathcal{I}_5| \leq \left(\sum_{n=1}^{N} \tau M_q^2 \|u_\delta^n - u_\delta^{n-1}\|^2 \right)^{\frac{1}{2}} \left(\int_0^T \|\psi\|^2 \right)^{\frac{1}{2}} \to 0.$$

With this the limit equation takes the form

$$(\mathbf{Q}, \psi) - (u, \nabla \cdot \psi) - (\mathbf{q}u, \psi) = 0. \tag{8.5.36}$$

To conclude the proof what remains is to show that $w = H(v)$. Since we have V^τ strongly converging, we also obtain $V^\tau \to v$ pointwise a.e. and further, as $\tau \searrow 0$, by construction $\delta \searrow 0$. For the set $R_+ := \{(t, x) : v(t, x) > 0\}$, let us assume $\mu := v(t, x, z)/2 > 0$. Then the pointwise convergence implies the existence of a $\varepsilon_\mu > 0$ such that $V^\tau > \mu$ for all $\varepsilon \leq \varepsilon_\mu$. Then for any $\varepsilon \leq \varepsilon_\mu$ we have $W^\tau = 1$ implying $w = 1$. A similar conclusion also holds for R_- where $R_- := \{(t, x) : v(t, x) < 0\}$.
For the case when $v = 0$; consider the set $R_0 := \{(t, x, z) : v(t, x, z) = 0\}$. Now in the interior of the set R_0, $\partial_t v = 0$. Next, from the weak convergence of $\partial_t V^\tau, W^\tau, r(U^\tau)$, we

have the following limit equation

$$(\partial_t v, \theta) = (r(u) - w, \theta).$$

Hence, for the interior of the set R_0, we obtain $w = r(u)$. Furthermore, the bounds $0 \leq W^\tau \leq 1$ with weak- convergence of W_h^τ to w imply the same bounds on w and hence $w = r(u)$ with $0 \leq r(u) \leq 1$. □

8.6   The mixed finite element formulation

Following the semi-discrete scheme, we now consider the fully discrete system (discretized in both space and time) and show the convergence of the numerical method. In particular, we consider the mixed finite element discretization in space and for the time we retain the discretization as in the semi-discrete case. The steps for the proof of convergence are similar to the semi-discrete situation and where ever the proof is similar to time-discrete case treated above, we suppress the details. Further, to simplify notation, henceforth, we suppress the subscript δ.

The fully discrete formulation for the weak solution of (8.2.1)–(8.2.2) builds on the time discretization in (8.5.2), and consider a uniform time stepping that is implicit in u and explicit in v. For the space discretization, we have Ω decomposed in $2-$ dimensional simplices (triangles) denoted by $\mathcal{T}_h$ and having the mesh-size h. We assume Ω to be polygonal as has been stated in Section 8.3. The function spaces used here are already introduced in Section 8.3.

Starting with $u_h^0 = u_I, v_h^0 = v_I$, with $n \in \{1, \ldots, N\}$, the approximation $(u_h^n, v_h^n, \mathbf{Q}_h^n, w_h^n)$ of $(u(t_n), v(t_n), \mathbf{Q}(t_n), w(t_n))$ at $t = t_n$ solves :

Problem $\mathbf{P}_h^n$: Given $(u_h^{n-1}, v_h^{n-1}) \in (\mathcal{V}_h, \mathcal{V}_h)$ find $(u_h^n, v_h^n, \mathbf{Q}_h^n, w_h^n) \in (\mathcal{V}_h, \mathcal{V}_h, \mathcal{S}_h, L^\infty(\Omega))$ satisfying

$$
\begin{aligned}
(u_h^n - u_h^{n-1}, \phi) + \tau(\nabla \cdot \mathbf{Q}_h^n, \phi) + (v_h^n - v_h^{n-1}, \phi) &= 0, \\
(v_h^n - v_h^n, \theta) - \tau(r(u_h^n), \theta) - \tau(H_\delta(v_h^{n-1}), \theta) &= 0, \qquad (8.6.1) \\
(\mathbf{Q}_h^n, \boldsymbol{\psi}) - (u_h^n, \nabla \cdot \boldsymbol{\psi}) - (\mathbf{q}_h u_h^n, \boldsymbol{\psi}) &= 0,
\end{aligned}
$$

for all $(\phi, \theta, \boldsymbol{\psi}) \in \mathcal{V}_h \times \mathcal{V}_h \times \mathcal{S}_h$. For completion, we define

$$w_h^n = H_\delta(v_h^n).$$

For stability reasons, as before, we choose $\delta = O(\tau^{\frac{1}{2}})$ (see [41, 80] for detailed arguments).

The fully discrete scheme (8.6.1) seeks solution on a finite dimensional vector space for

any given discretization parameters. From $(8.6.1)_1$ and $(8.6.1)_2$, we eliminate v_h^n, which is computed after having obtained $(u_h^n, \mathbf{Q}_h^n)$ satisfying for all $(\phi, \boldsymbol{\psi}) \in (\mathcal{V}_h, \mathcal{S}_h)$

$$
\begin{aligned}
(u_h^n - u_h^{n-1}, \phi) + \tau(\nabla \cdot \mathbf{Q}_h^n, \phi) + \tau(r(u_h^n) - H_\delta(v_h^{n-1}), \phi) &= 0, \\
(\mathbf{Q}_h^n, \boldsymbol{\psi}) - (u_h^n, \nabla \cdot \boldsymbol{\psi}) - (\mathbf{q}_h u_h^n, \boldsymbol{\psi}) &= 0.
\end{aligned}
\tag{8.6.2}
$$

In the above formulation, the nonlinearities only involve u_h^n; the H_δ is known, from the previous time step and is in L^∞.

The existence follows from [121], Theorem 4.3, which treats a more general case. Its proof is based on [133] (Lemma 1.4, p.140). Following the ideas in Section 8.5, one can prove that (8.6.2) has a unique solution pair $(u_h^n, \mathbf{Q}_h^n)$. This also determines v_h^n and w_h^n uniquely. We summarize the above result

Lemma 8.11 *Problem P_h^n has a unique solution pair $(u_h^n, \mathbf{Q}_h^n, v_h^n, w_h^n)$.*

8.6.1 The a priori estimates

We proceed with the energy estimates which are analogous to the semi-discrete case. We simply state the results as their proof follows as in the semi-discrete case.

Lemma 8.12 *The following estimates hold*

$$
\sup_{k=1,\dots,N} \left\| u_h^k \right\| \le C,
\tag{8.6.3}
$$

$$
\left\| v_h^n - v_h^{n-1} \right\| \le C\tau,
\tag{8.6.4}
$$

$$
\sup_{k=1,\dots,N} \left\| v_h^k \right\| \le C,
\tag{8.6.5}
$$

$$
\sup_{k=1,\dots,N} \left\| \mathbf{Q}_h^k \right\| \le C,
\tag{8.6.6}
$$

$$
\sum_{n=1}^{N} \left\| u_h^n - u_h^{n-1} \right\|^2 \le C\tau,
\tag{8.6.7}
$$

$$
\sum_{n=1}^{N} \left\| \mathbf{Q}_h^n - \mathbf{Q}_h^{n-1} \right\|^2 \le C,
\tag{8.6.8}
$$

$$
\sum_{n=1}^{N} \tau \left\| \nabla \cdot \mathbf{Q}_h^n \right\|^2 \le C,
\tag{8.6.9}
$$

$$
\sum_{n=1}^{N} \tau \left\| \nabla \cdot (\mathbf{Q}_h^n - \mathbf{Q}_h^{n-1}) \right\|^2 \le C.
\tag{8.6.10}
$$

We continue with the steps analogous to the semi-discrete situation. As in (8.5.29) we consider the time-continuous approximation by the piecewise linear interpolations of the time discrete solutions. With $t \in [t_{n-1}, t_n]$, define

$$Z_h^\tau(t) := \frac{(t - t_{n-1})}{\tau} z_h^n + \frac{(t_n - t)}{\tau} z_h^{n-1}, \qquad (8.6.11)$$

$$(8.6.12)$$

where z_h^n, z_h^{n-1} are the time-discrete solutions from which we construct the corresponding time-continuous approximation Z_h^τ. The symbol z may be replaced here by either $u, v,$ or $\mathbf{Q}$, and the same holds for Z. As before, the estimates in Lemma 8.12 carry over for the time-continuous approximation (the proof is omitted) and we obtain

Lemma 8.13 *The time-continuous approximations satisfy the following estimates*

$$\|\partial_t U_h^\tau\|^2 + \|\nabla \cdot \mathbf{Q}_h^\tau\|^2 + \|U_h^\tau\|^2 + \|V_h^\tau\|^2 + \|\mathbf{Q}_h^\tau\|^2 \leq C, \qquad (8.6.13)$$

$$0 \leq W_h^\tau \leq 1. \qquad (8.6.14)$$

Here the norms are taken with respect to $L^2(0, T; L^2(\Omega))$. The estimates are uniform in τ and δ and furthermore we have $(U_h^\tau, \mathbf{Q}_h^\tau, V_h^\tau, W_h^\tau) \in \mathcal{V} \times \mathcal{S} \times \mathcal{V} \times L^\infty(\Omega)$. Clearly, if $\tau \searrow 0$ with $\delta = O(\tau^{\frac{1}{2}})$ implies that both $\delta, \frac{\tau}{\delta} \searrow 0$. The compactness arguments from the Lemma 8.13 lead to the following convergence result:

Lemma 8.14 *Along a sequence $\tau \searrow 0$, it holds that*

  (i). $U_h^\tau \rightharpoonup u$ weakly in $L^2((0, T); L^2(\Omega))$,

  (ii). $\partial_t U_h^\tau \rightharpoonup \partial_t u$ weakly in $L^2((0, T); H^{-1}(\Omega))$,

  (iii). $\mathbf{Q}_h^\tau \rightharpoonup \mathbf{Q}$ weakly in $L^2((0, T); L^2(\Omega)^d)$,

  (iv). $\nabla \cdot \mathbf{Q}_h^\tau \rightharpoonup \chi$ weakly in $L^2((0, T); L^2(\Omega))$,

  (v). $V_h^\tau \rightharpoonup v$ weakly in $L^2((0, T); L^2(\Omega))$,

  (vi). $\partial_t V_h^\tau \rightharpoonup \partial_t v$ weakly in $L^2((0, T); L^2(\Omega))$,

  (vii). $W_h^\tau \rightharpoonup w$ weakly-star in $L^\infty(\Omega)$.

As in the semi-discrete case, identification of the above limit χ with $\nabla \cdot \mathbf{Q}$ is obtained via smooth test functions. Note that the above lemma only provides weak convergence for U_h^τ, V_h^τ; in the wake of nonlinearities, the strong convergence is needed. However, the techniques from the semi-discrete case can not be applied directly. This is because the translation of a function that is piecewise constant on the given mesh need not be piecewise constant on that mesh. We therefore adopt the finite volume framework in [51] in order to overcome this difficulty.

8.6.2 Strong convergence

In what follows, we establish the required strong convergence of U_h^τ followed by that of V_h^τ. We provide the notations used below in the framework of finite volumes. Let $\mathcal{E}$ denote the set of edges of the simplices $\mathcal{T}_h$. Also, we have that $\mathcal{E} = \mathcal{E}_{int} \cup \mathcal{E}_{ext}$ with $\mathcal{E}_{ext} = \mathcal{E} \cap \partial\Omega$ and $\mathcal{E}_{int} = \mathcal{E} \setminus \mathcal{E}_{ext}$. We adopt the following notation:

$$
\begin{aligned}
|T| &- \text{ the area of } T \in \mathcal{T}_h, \\
\mathbf{x}_i &- \text{ the centre of the circumcircle of } T, \\
l_{ij} &- \text{ the edge between } T_i \text{ and } T_j, \\
d_{ij} &- \text{ the distance from } \mathbf{x}_i \text{ to } l_{ij}, \\
\sigma_{ij} &- \frac{|l_{ij}|}{d_{ij}},
\end{aligned}
\tag{8.6.15}
$$

In analogy with the spatially continuous case, we define the following discrete inner product for any $u_h^n, v_h^n \in \mathcal{V}_h$

$$
(u_h^n, v_h^n)_h := \sum_{T_i \in \mathcal{T}_h} |T_i| u_{h,i}^n v_{h,i}^n, \quad (u_h^n, v_h^n)_{1,h} := \sum_{l_{ij} \in \mathcal{E}} |\sigma_{ij}| (u_{h,i}^n - u_{h,j}^n)(v_{h,i}^n - v_{h,j}^n). \tag{8.6.16}
$$

The discrete inner product gives rise to discrete H_0^1 norm, which is

$$
\|u_h^n\|_{1,h} = \sum_{l_{ij} \in \mathcal{E}} |\sigma_{ij}| (u_{h,i}^n - u_{h,j}^n)^2. \tag{8.6.17}
$$

In [51], the following discrete Poincare inequality is proved

$$
\|u_h^n\| \le C \|u_h^n\|_{1,h}, \tag{8.6.18}
$$

with C independent of h or u_h^n. Based on Lemma 4 in [51], below we show that the translations are controlled by the discrete $\|\cdot\|_{1,h}$ norm.

Lemma 8.15 *Let Ω be an open bounded set of $\mathbb{R}^2$ and let $\mathcal{T}_h$ be an admissible mesh. For a given u defined in Ω and extended to $\bar{u}$ by 0 outside Ω we have*

$$
\|\triangle_\xi \bar{u}\|_{L^2(\mathbb{R}^2)}^2 \le \|u\|_{1,h}^2 |\xi|(|\xi| + C\mathrm{size}(\mathcal{T}_h)), \text{ for all } \xi \in \mathbb{R}^2. \tag{8.6.19}
$$

This shows that for a sequence $\{u_h^n\}$ having the discrete H_0^1 norm uniformly bounded, the L^2- norm of the translations $\triangle_\xi u_h^n$ vanishes uniformly with respect to h as $\eta \searrow 0$. This is an essential step in proving the strong L^2- convergence for h_h^n. Here we only need to show that u_h^n has bounded discrete H_0^1 norm

Lemma 8.16 *For the sequence u_h^n, the following inequality holds uniformly with respect to h,*

$$
\|u_h^n\|_{1,h} \le C(\|Q_h^n\| + \|u_h^n\|). \tag{8.6.20}
$$

Proof. The approach is inspired from the semi-discrete situation and is adapted to the present context by defining appropriate test function. Define

$$|T_i| f_h^n(T_i) := \sum_{e_{ij}} \frac{|l_{ij}|}{d_{ij}} (u_{h,i}^n - u_{h,j}^n) \qquad (8.6.21)$$

and note that by the definition of $\| \cdot \|_{1,h}^2$,

$$(f_h^n, u_h^n) = \sum_i T_i f_h^n(T_i) u_h^n(T_i) = \sum_{e_{ij}} \frac{l_{ij}}{d_{ij}} |u_{h,i}^n - u_{h,j}^n|^2 = \|u_h^n\|_{1,h}^2. \qquad (8.6.22)$$

Further, by using Cauchy-Schwarz we obtain

$$\|f_h^n\|_{L^2(\Omega)}^2 = \sum_i |T_i| |f_h^n(T_i)|^2 \le \sum_{e_{ij}} \frac{|l_{ij}|}{d_{ij}} (u_i^n - u_j^n)^2 \frac{1}{|T_i|} \sum_{e_{ij}} \frac{|l_{ij}|}{d_{ij}}$$

which implies that

$$\|f_h^n\| \le \|u_h^n\|_{1,h}. \qquad (8.6.23)$$

Note that $f_h^n \in L^2(\Omega)$ and hence, there exists $\boldsymbol{\psi}_h \in \mathcal{S}_h$ which satisfies

$$\nabla \cdot \boldsymbol{\psi}_h = f_h^n \quad \text{in} \quad \Omega, \qquad (8.6.24)$$
$$\boldsymbol{\psi}_h = 0 \quad \text{on} \quad \partial\Omega. \qquad (8.6.25)$$

By (8.6.23), it also holds that

$$\|\boldsymbol{\psi}_h\|_{L^2(\Omega)} \le C \|f_h^n\|_{L^2(\Omega)} \le C \|u_h^n\|_{1,h}. \qquad (8.6.26)$$

Now choose for the test function $\boldsymbol{\psi} = \boldsymbol{\psi}_h$ in $(8.6.1)_3$

$$(\mathbf{Q}_h^n, \boldsymbol{\psi}_h) - (u_h^n, \nabla \cdot \boldsymbol{\psi}_h) - (\mathbf{q}_h u_h^n, \boldsymbol{\psi}_h) = 0.$$

Note that by (8.6.22)
$$(u_h^n, \nabla \cdot \boldsymbol{\psi}_h) = (u_h^n, f_h^n) = \|u_h^n\|_{1,h}^2.$$

This implies that

$$\begin{aligned}
\|u_h^n\|_{1,h}^2 &= (u_h^n, \nabla \cdot \boldsymbol{\psi}_h) = (\mathbf{Q}_h^n, \boldsymbol{\psi}_h) - (\mathbf{q}_h u_h^n, \boldsymbol{\psi}_h) \\
&\le \|\mathbf{Q}_h^n\| \|\boldsymbol{\psi}_h\| + M_q \|u_h^n\| \|\boldsymbol{\psi}_h\| \le C \|\mathbf{Q}_h^n\| \|u_h^n\|_{1,h} + CM_q \|u_h^n\| \|u_h^n\|_{1,h}
\end{aligned}$$

and the conclusion follows. $\qquad \square$

In view of the above lemma, obtaining the relative compactness in L^2 is straightforward.

Lemma 8.17 *Along a sequence (τ, h) converging to $(0,0)$ (and with $\delta = O(\sqrt{\tau})$), U_h^τ converges strongly in $L^2(0, T; L^2(\Omega))$.*

Proof. Since, $\partial_t U_h^\tau$ is in L^2, the translation with respect to time is already controlled. What remains is to consider the translation with respect to space. Take (8.6.20) and sum over $n = 1, \dots, N$ to obtain

$$\tau \sum_{n=1}^{N} \|u_h^n\|_{1,h}^2 \leq C\tau \sum_{n=1}^{N} (\|Q_h^n\|^2 + \|u_h^n\|^2) \leq C \qquad (8.6.27)$$

and using (8.6.3) and (8.6.6) gives

$$\tau \sum_{n=1}^{N} \|u_h^n\|_{1,h}^2 \leq C.$$

Now use Lemma 8.15 to control the translations by the $\|\cdot\|_{1,h}$ norm (after extending u_h^n by 0 outside Ω; for simplicity retain the same notation)

$$\tau \sum_{n=1}^{N} \|u_h^n(\cdot + \xi) - u_h^n\|_{L^2(\mathbb{R}^2)}^2 \leq C|\xi|(|\xi| + \mathrm{size}(\mathcal{T}_h)),$$

which, in turn, provides similar estimate for U_h^τ

$$\tau \sum_{n=1}^{N} \|U_h^\tau(\cdot + \xi) - U_h^\tau\|_{L^2(\mathbb{R}^2)}^2 \leq C|\xi|(|\xi| + \mathrm{size}(\mathcal{T}_h)).$$

The Kolomogorov compactness theorem proves the assertion. $\qquad \square$

The strong convergence of U_h^τ gives the strong convergence of V_h^τ.

Lemma 8.18 *Along a sequence (τ, h) converging to $(0,0)$, V_h^τ converges strongly to v in $L^2(0, T; L^2(\Omega))$.*

Proof. As before, the translations with respect to time are already controlled by virtue of $\partial_t V_h^\tau \in L^2$. We now consider the case for the translation with respect to space. Since both u_h^n, v_h^n are piecewise constants in each simplex T, we have for every $x \in T$

$$v_h^n(x) = v_h^{n-1}(x) + \tau \left(r(u_h^n(x)) - \tau H_\delta(v_h^{n-1}(x)) \right)$$

$$v_h^n(x + \xi) = v_h^{n-1}(x + \xi) + \tau \left(r(u_h^n(x + \xi)) - \tau H_\delta(v_h^{n-1}(x + \xi)) \right)$$

so that for any $x \in \Omega_\xi$ we have

$$\triangle_\xi(v_h^n - v_h^{n-1}) = \tau \triangle_\xi r(u_h^n) - \tau \triangle_\xi H_\delta(v_h^{n-1})$$

Multiplying by $\triangle_\xi v_h^{n-1}$ and rewriting the left hand side, we have

$$\frac{1}{2}\left\{|\triangle_\xi v_h^n|^2 - |\triangle_\xi v_h^{n-1}|^2 + |\triangle_\xi(v_h^n - v_h^{n-1})|^2\right\} \tag{8.6.28}$$

$$\leq \tau L_r |\triangle_\xi u_h^n||\triangle_\xi v_h^n| - \tau\left(\triangle_\xi H_\delta(v_h^n - 1)\right)\triangle_\xi v_h^n.$$

The term involving the $\triangle_\xi H_\delta$ can be rewritten as

$$\left(\triangle_\xi H_\delta(v_h^{n-1})\right)\triangle_\xi v_h^n = \left(\triangle_\xi H_\delta(v_h^{n-1})\right)\triangle_\xi v_h^{n-1} + \left(\triangle_\xi H_\delta(v_h^{n-1})\right)\left(\triangle_\xi(v_h^n - v_h^{n-1})\right)$$

and due to monotonicity of H_δ, we have

$$\left(\triangle_\xi H_\delta(v_h^{n-1})\right)\triangle_\xi v_h^{n-1} \geq 0.$$

Using above in (8.6.28) gives

$$\frac{1}{2}\left\{|\triangle_\xi v_h^n|^2 - |\triangle_\xi v_h^{n-1}|^2 + |\triangle_\xi(v_h^n - v_h^{n-1})|^2\right\}$$

$$\leq \tau L_r^2 |\triangle_\xi u_h^n|^2 + \frac{1}{4}|\triangle_\xi v_h^n|^2 + \frac{1}{4}|\triangle_\xi(v_h^n - v_h^{n-1})|^2 + \frac{\tau^2}{\delta^2}|\triangle_\xi v_h^{n-1}|^2.$$

Integrating over Ω_ξ and summing over $n = 1, \cdots, k$ for any $k \in \{1, \dots, N\}$ gives

$$\frac{1}{2}\|\triangle_\xi v_h^k\|^2 + \frac{1}{4}\sum_{n=1}^{k}\|\triangle_\xi(v_h^n - v_h^{n-1})\|^2$$

$$\leq \|\triangle_\xi v_{I,h}\|^2 + \tau\sum_{n=1}^{k} L_r^2\|\triangle_\xi u_h^n\|^2 + \frac{1}{4}\tau\sum_{n=1}^{k}\|\triangle_\xi v_h^n\|^2 + \sum_{n=1}^{k}\frac{\tau^2}{\delta^2}\|\triangle_\xi v_h^{n-1}\|^2,$$

where the norms are taken with respect to Ω_ξ. Choosing $\delta = O(\tau^{\frac{1}{2}})$ leads to

$$\frac{1}{2}\|\triangle_\xi v_h^k\|^2 + \frac{1}{4}\sum_{n=1}^{k}\|\triangle_\xi(v_h^n - v_h^{n-1})\|^2 \leq \|\triangle_\xi v_{I,h}\|^2 + \tau\sum_{n=1}^{k} L_r^2\|\triangle_\xi u_h^n\|^2 + C\tau\sum_{n=1}^{k}\|\triangle_\xi v_h^n\|^2.$$

Applying the Gronwall lemma provides

$$\sup_{k=1,\dots,N}\|\triangle_\xi v_h^k\|^2 \leq C\|\triangle_\xi v_{I,h}\|^2 + C\tau\sum_{n=1}^{N}\|\triangle_\xi u_h^n\|^2.$$

The strong convergence of U_h^τ in $L^2(0, T; L^2(\Omega))$ implies that the last term vanishes in the limit of $\xi \searrow 0$ (see the proof of Lemma 8.17).

To estimate the translations for the initial condition we consider $v_{I,h}$ as the finite volume approximation of v_I defined (formally) by

$$-\Delta v_{I,h} = -\Delta v_I, \qquad \text{in } \Omega,$$

with homogenous Dirichlet boundary conditions. This implies

$$\|v\|_{1,h} \leq C\|\nabla v_I\| \leq C.$$

Since the translations are approaching 0 if $\|v_{I,h}\|_{1,h} \leq C$ (uniformly in h), $\|\triangle_\xi v_{I,h}\| \to 0$ as $\xi \searrow 0$. From the above we conclude that $\|\triangle_\xi v_h^k\|^2 \to 0$ as $|\xi|$ goes to 0.

Finally, note that the definition of V_h^τ implies the rough estimate

$$\int_0^T \|\triangle_\xi V_h^\tau\|^2 dt \leq 2\tau \sum_{n=1}^N \|\triangle_\xi v_h^n\|^2 + 2\tau \sum_{n=1}^N \|\triangle_\xi v_h^{n-1}\|^2,$$

and the right hand side vanishes uniformly in h as $\xi \searrow 0$, hence V_h^τ converges strongly. $\square$

8.6.3 The limit equations

Up to now we obtained the convergence of the fully discrete triples $(U_h^\tau, V_h^\tau, \mathbf{Q}_h^\tau)$ along a sequence (τ, h) approaching $(0,0)$ with $\delta = O(\sqrt{\tau})$. Clearly, the (L^∞ weakly*) convergence extends to the sequence $W_h^\tau = H_\delta(V_h^\tau)$. In what follows, we identify the limit discussed in the preceding section as the weak formulation (8.4.1).

Theorem 8.6.1 *The limit quadruple* $(u, \mathbf{Q}, v, w)$ *is a weak solution in the sense of Definition 8.4.1.*

Proof. By the weak convergence, the estimates in Lemma 8.13 carry over for the limit triple $(u, \mathbf{Q}, v)$. By $(8.6.1)_1$ we have

$$
\begin{aligned}
\int_0^T (\partial_t U_h^\tau, \phi) dt &+ \int_0^T (\nabla \cdot \mathbf{Q}_h^\tau, \phi) dt + \int_0^T (\partial_t V_h^\tau, \phi) dt \\
&= \sum_{n=1}^N \int_{t_{n-1}}^{t_n} (\partial_t U_h^\tau, \phi - \phi_h) dt + \sum_{n=1}^N \int_{t_{n-1}}^{t_n} (\nabla \cdot \mathbf{Q}_h^\tau - \nabla \cdot \mathbf{Q}_h^n, \phi) dt \\
&+ \sum_{n=1}^N \int_{t_{n-1}}^{t_n} (\nabla \cdot \mathbf{Q}_h^\tau, \phi - \phi_h) dt + \sum_{n=1}^N \int_{t_{n-1}}^{t_n} (\nabla \cdot \mathbf{Q}_h^\tau - \nabla \cdot \mathbf{Q}_h^n, \phi_h - \phi) dt \\
&+ \sum_{n=1}^N \int_{t_{n-1}}^{t_n} (\partial_t V_h^\tau, \phi - \phi_h) dt.
\end{aligned}
\tag{8.6.29}
$$

for all $\phi \in L^2(0, T; H_0^1(\Omega))$, and where ϕ_h is the projection $\phi_h = P\phi$ introduced in Section 8.3. Note that we assume again an H^1 regularity in space for the test function ϕ. We use this to control the terms involving $\|\phi - \phi_h\|$ by using the property (8.3.1). A usual density argument lets the result hold for all $\phi \in \mathcal{V}$.

The left hand side gives the desired limit terms; it only remains to show that the right

hand side vanishes in the limit. Denote the successive integrals on the right by $\mathcal{I}_i, i = 1, \ldots, 5$. We deal with each term separately.

For $\mathcal{I}_1$ we use (8.6.13) to obtain that as $h \searrow 0$

$$|\mathcal{I}_1| \leq \|\partial_t U_h^\tau\|_{L^2(0,T;L^2(\Omega))} \left(\sum_{n=1}^{N} \tau \|\phi - \phi_h\|_{L^2(\Omega)}^2 \right)^{\frac{1}{2}} \leq Ch\|\nabla\phi\|_{L^2(0,T;L^2(\Omega))} \searrow 0.$$

Similarly, by (8.6.8), for $\mathcal{I}_2$ one gets

$$|\mathcal{I}_2| \leq \left(\sum_{n=1}^{N} \tau \|\mathbf{Q}_h^n - \mathbf{Q}_h^{n-1}\|^2 \right)^{\frac{1}{2}} \left(\sum_{n=1}^{N} \tau \|\nabla\phi\|_{L^2(\Omega)}^2 \right)^{\frac{1}{2}} \leq C\tau.$$

Clearly $\mathcal{I}_2$ vanishes in the limit of $\tau \searrow 0$. Next, for $\mathcal{I}_3$, we have

$$|\mathcal{I}_3| \leq \|\nabla \cdot \mathbf{Q}_h^\tau\|_{L^2(0,T;L^2(\Omega))} \left(\sum_{n=1}^{N} \tau \|\phi - \phi_h\|^2 \right)^{\frac{1}{2}} \leq Ch\|\nabla\phi\|_{L^2(0,T;L^2(\Omega))}$$

using (8.6.13). Hence, $\mathcal{I}_3$ goes to 0 as $h \searrow 0$. Proceeding in the similar way, for $\mathcal{I}_4$

$$|\mathcal{I}_4| \leq \left(\sum_{n=1}^{N} \tau \|\nabla \cdot \mathbf{Q}_h^n - \nabla \cdot \mathbf{Q}_h^{n-1}\|^2 \right)^{\frac{1}{2}} \left(\sum_{n=1}^{N} \tau \|\phi - \phi_h\|_{L^2(\Omega)}^2 \right)^{\frac{1}{2}} \leq Ch\|\nabla\phi\|_{L^2(0,T;L^2(\Omega))}$$

by using (8.6.10) implying that $\mathcal{I}_4$ vanishes in the limit.

In the same manner, for $\mathcal{I}_5$ we use the bounds for $\partial_t V_h^\tau$ and obtain

$$|\mathcal{I}_4| \leq \|\partial_t V_h^\tau\|_{L^2(0,T;L^2(\Omega))} \left(\sum_{n=1}^{N} \tau \|\phi - \phi_h\|_{L^2(\Omega)}^2 \right)^{\frac{1}{2}} \leq Ch\|\nabla\phi\|_{L^2(0,T;L^2(\Omega))}.$$

Next we consider $(8.6.1)_2$, which we rewrite as

$$\int_0^T (\partial_t V_h^\tau, \theta) dt - \int_0^T (r(U_h^\tau) - W_h^\tau, \theta) \, dt$$

$$= \int_0^T (\partial_t V_h^\tau, \theta - \theta_h) \, dt + \sum_{n=1}^{N} \int_{t_{n-1}}^{t_n} \left(H_\delta(V_h^\tau) - H_\delta(v_h^{n-1}), \theta \right) dt$$

$$+ \sum_{n=1}^{N} \int_{t_{n-1}}^{t_n} \left(H_\delta(v_h^{n-1}), \theta - \theta_h \right) dt + \sum_{n=1}^{N} \int_{t_{n-1}}^{t_n} \left(r(u_h^n) - r(U_h^\tau), \theta \right) dt$$

$$+ \sum_{n=1}^{N} \int_{t_{n-1}}^{t_n} \left(r(u_h^n), \theta_h - \theta \right) dt.$$

for $\theta \in L^2(0, T; H_0^1(\Omega))$ and θ_h is the P_h projection of θ. A better regularity of θ is again chosen for identifying the limits and controlling the errors due to the projections. We would retrieve the desired limiting equations once we prove that the integrals on the right hand side vanish. Let us denote the successive integrals by $\mathcal{I}_i, \ i = 1, \ldots, 5$

respectively. For $\mathcal{I}_1$ we get by using (8.6.13) and recalling the projection estimate (8.3.1)

$$|\mathcal{I}_1| \leq \left(\int_0^T \|\partial_t V_h^\tau\|^2 dt \right)^{\frac{1}{2}} \left(\sum_{n=1}^N \int_{t_{n-1}}^{t_n} \|(\theta - \theta_h)\|^2 dt \right)^{\frac{1}{2}} \leq Ch\|\theta\|_{L^2(0,T;H_0^1(\Omega))}$$

which vanishes in the limit as $h \searrow 0$. For $\mathcal{I}_2$, we use the definition of W^τ and Lipschitz continuity of H_δ to obtain

$$|\mathcal{I}_2| \leq \sum_{n=1}^N \tau \frac{1}{\delta} \|v_h^n - v_h^{n-1}\| \|\theta_h\| \leq \sum_{n=1}^N \tau C \frac{\tau}{\delta} \|\theta_h\|$$

by using (8.6.4) and further using $\tau/\delta \searrow 0$ by the construction of δ we obtain $\mathcal{I}_2 \searrow 0$. Next, we consider $\mathcal{I}_3$

$$|\mathcal{I}_3| \leq C \left(\sum_{n=1}^N \int_{t_{n-1}}^{t_n} \|\theta - \theta_h\|^2 dt \right)^{\frac{1}{2}} \leq Ch\|\nabla\theta\|_{L^2(0,T;L^2(\Omega))} \searrow 0 \quad \text{as} \quad h \searrow 0$$

because of (8.3.1). To continue,

$$|\mathcal{I}_4| \leq \left(\sum_{n=1}^N \tau L_r^2 \|u_h^n - u_h^{n-1}\|^2 \right)^{\frac{1}{2}} \left(\sum_{n=1}^N \tau \|\theta_h\|^2 \right)^{\frac{1}{2}}$$

and using the estimate (8.6.7), we obtain $\mathcal{I}_4 \searrow 0$.
For $\mathcal{I}_5$, as $h \searrow 0$,

$$|\mathcal{I}_5| \leq L_r \left(\sum_{n=1}^N \tau \|u_h^n\|^2 dt \right)^{\frac{1}{2}} \left(\sum_{n=1}^N \int_{t_{n-1}}^{t_n} \|(\theta - \theta_h)\|^2 dt \right)^{\frac{1}{2}} \leq Ch\|\theta\|_{L^2(0,T;H_0^1(\Omega))} \searrow 0.$$

Let us consider the next equation, that is, $(8.6.1)_3$. We have by realigning the terms,

$$\begin{aligned}
\int_0^T (\mathbf{Q}_h^\tau, \boldsymbol{\psi}) dt &- \int_0^T (U_h^\tau, \nabla \cdot \boldsymbol{\psi}) dt - \int_0^T (\mathbf{q}_h U_h^\tau, \boldsymbol{\psi}) dt \\
&= \sum_{n=1}^N \int_{t_{n-1}}^{t_n} (\mathbf{Q}_h^\tau - \mathbf{Q}_h^n, \boldsymbol{\psi}) dt + \sum_{n=1}^N \int_{t_{n-1}}^{t_n} (\mathbf{Q}_h^n, \boldsymbol{\psi} - \boldsymbol{\psi}_h) dt \\
&\quad + \sum_{n=1}^N \int_{t_{n-1}}^{t_n} (u_h^n - U_h^\tau, \nabla \cdot \boldsymbol{\psi}) dt + \sum_{n=1}^N \int_{t_{n-1}}^{t_n} (U_h^n, \nabla \cdot (\boldsymbol{\psi}_h - \boldsymbol{\psi})) dt \\
&\quad + \sum_{n=1}^N \int_{t_{n-1}}^{t_n} (\mathbf{q}_h(u_h^n - U_h^\tau), \boldsymbol{\psi}) dt + \sum_{n=1}^N \int_{t_{n-1}}^{t_n} (\mathbf{q}_h u_h^n, \boldsymbol{\psi}_h - \boldsymbol{\psi}) dt
\end{aligned} \tag{8.6.30}$$

for all $\boldsymbol{\psi} \in L^2(0,T;H^2(\Omega))$ and where $\boldsymbol{\psi}_h$ is chosen as the Π_h projection of $\boldsymbol{\psi}$. As before the left hand side converges to the desired limits. This is obvious except for the third term where we use the L^∞ and strong convergence of $\mathbf{q}_h$. Indeed,

$$\int_0^T (\mathbf{q}_h U_h^\tau, \boldsymbol{\psi})dt = \int_0^T (\mathbf{q} U_h^\tau, \boldsymbol{\psi})dt + \int_0^T ((\mathbf{q}_h - \mathbf{q})U_h^\tau, \boldsymbol{\psi})dt \qquad (8.6.31)$$

and the first term on the right hand side passes to the desired limit. We show that the second term vanishes in the limit. Note that $\mathbf{q}_h - \mathbf{q} \in (L^\infty(\Omega))^2$ and hence, $(\mathbf{q}_h - \mathbf{q})U_h^\tau$ has a weak limit. Now choose $\boldsymbol{\psi} \in L^2(0,T;(C_c^\infty(\Omega))^d), d = 2$ so that $\boldsymbol{\psi} \in (L^\infty(\Omega))^2$. Now

$$\|(\mathbf{q}_h - \mathbf{q})U_h^\tau\|_{(L^1(\Omega))^2} \leq \|\mathbf{q}_h - \mathbf{q}\|_{(L^2(\Omega))^2}\|U_h^\tau\|_{(L^2(\Omega))^2}$$

and use the strong convergence of $\mathbf{q}_h$ in L^2 (uniform with respect to h) to conclude that the weak limit is indeed 0.

Now we show that the right hand side of (8.6.30) indeed vanishes in the limit. Let us denote the integrals by $\mathcal{I}_i, i = 1, \ldots, 6$. The successive terms will be treated as before. We begin with $\mathcal{I}_1$

$$|\mathcal{I}_1| \leq \|\boldsymbol{\psi}\|_{L^2(0,T;H^1(\Omega))} \left(\sum_{n=1}^N \tau\|\mathbf{Q}_h^n - \mathbf{Q}_h^{n-1}\|^2\right)^{\frac{1}{2}} \leq C\tau$$

using bounds given in (8.6.8). Thus, $\mathcal{I}_1$ goes to 0 in the limit. For $\mathcal{I}_2$, recalling the bound (8.6.6) and the projection estimate (8.3.2)

$$|\mathcal{I}_2| \leq \left(\sum_{n=1}^N \tau\|\mathbf{Q}_h^n\|^2\right)^{\frac{1}{2}} \left(\sum_{n=1}^N \tau\|\boldsymbol{\psi} - \boldsymbol{\psi}_h\|_{L^2(\Omega)}\right)^{\frac{1}{2}} \leq Ch\|\boldsymbol{\psi}\|_{L^2(0,T;H(div,\Omega))} \searrow 0$$

as $h \searrow 0$.
Let us deal with the next term using (8.6.7),

$$|\mathcal{I}_3| \leq \left(\sum_{n=1}^N \|u_h^n - u_h^{n-1}\|^2\right)^{\frac{1}{2}} \left(\int_0^T \|\nabla \cdot \boldsymbol{\psi}\|^2 dt\right)^{\frac{1}{2}} \leq C\tau$$

which vanishes in the limit $\tau \searrow 0$. For $\mathcal{I}_4$, we have

$$|\mathcal{I}_4| \leq \left(\sum_{n=1}^N \tau\|u_h^n\|^2\right)^{\frac{1}{2}} \left(\sum_{n=1}^N \tau\|\nabla \cdot (\boldsymbol{\psi} - \boldsymbol{\psi}_h)\|^2\right)^{\frac{1}{2}}$$

and further by using (8.6.7) and (8.3.2),

$$|\mathcal{I}_4| \leq Ch\|\boldsymbol{\psi}\|_{L^2(0,T;H^1(\Omega))}$$

which tends to 0 as $h \searrow 0$. To proceed,

$$|\mathcal{I}_5| \leq M_q \left(\sum_{n=1}^{N} \tau \|u_h^n - u_h^{n-1}\|^2 \right)^{\frac{1}{2}} \|\psi\|_{L^2(0,T;L^2(\Omega))} \leq C\tau$$

with similar conclusion. Finally,

$$|\mathcal{I}_6| \leq M_q \left(\sum_{n=1}^{N} \tau \|u_h^n\|^2 \right)^{\frac{1}{2}} \left(\sum_{n=1}^{N} \tau \|(\psi - \psi_h)\|^2 \right)^{\frac{1}{2}}$$

with vanishing limit due to the projection estimate (8.3.2) and by (8.6.3).

The identification of w with $H(v)$ is identical to the semi-discrete case.

Note that the limit quadruple $(u, \mathbf{Q}, v, w)$ indeed satisfies (8.4.1), but for test functions having a better regularity in space: $\phi \in L^2(0, T; H_0^1(\Omega))$, $\theta \in L^2(0, T; H_0^1(\Omega))$ and $\psi \in L^2(0, T; H^2(\Omega))$. In view of the regularity of $u, v, \mathbf{Q}$, density arguments can be employed to show that the limit equations also hold for $\phi \in L^2(0, T; L^2(\Omega)), \theta \in L^2(0, T; L^2(\Omega)), \psi \in L^2(0, T; H(div, \Omega))$, which completes the proof. $\qquad\square$

8.7   Numerical computations

We consider a test problem similar to (8.2.1)–(8.2.2), but including a right hand side in the first equation (see [79] where we first announced part of these results). This is chosen in such a way that the problem has an exact solution, which is used then to test the convergence of the mixed finite element scheme. Specifically, for $T = 1$ and $\Omega = (0, 5) \times (0, 1)$, and with $r(u) = [u]_+^2$ (where $[u]_+ := \max\{0, u\}$), we consider the problem

$$\begin{cases} \partial_t(u + v) + \nabla \cdot (\mathbf{q}u - \nabla u) &=& f, & \text{in } \Omega^T, \\ \partial_t v &=& (r(u) - w), & \text{on } \Omega^T, \\ w &\in& H(v), & \text{on } \Omega^T. \end{cases}$$

Here $\mathbf{q} = (1, 0)$ is a constant velocity, whereas

$$f(t, x, y) = \frac{1}{2}e^{x-t-5}\left(1 - e^{x-t-5}\right)^{-\frac{3}{2}}\left(1 - \frac{1}{2}e^{x-t-5}\right) - \begin{cases} 0, & \text{if } x < t, \\ e^{x-t-5}, & \text{if } x \geq t, \end{cases}$$

and the boundary and initial conditions are such that

$$u(t, x, y) = \left(1 - e^{x-t-5}\right)^{\frac{1}{2}} \quad \text{and} \quad v(t, x, y) = \begin{cases} 0, & \text{if } x < t, \\ \frac{e^{x-t}-1}{e^5} & \text{if } x \geq t, \end{cases}$$

$$\text{providing} \quad w(t, x, y) = \begin{cases} 1, & \text{if } x < t, \\ 1 - e^{x-t-5} & \text{if } x \geq t, \end{cases}$$

form a solution triple.

We consider the mixed finite element discretization of the problem above, based on the time stepping in Section 8.6 and the lowest order Raviart-Thomas elements RT_0. The numerical scheme was implemented in the software package *ug* [16]. The simulations are carried out for a constant mesh diameter h and time step τ, satisfying $\tau = h$. Further, we take $\delta = \sqrt{h}$ as regularizing parameter. We start with $h = 0.2$, and refine the mesh (and correspondingly τ and δ) four times successively by halving h up to $h = 0.0125$. We compute the errors for u and v in the L^2 norms,

$$E_u^h = \|u - U^\tau\|_{L^2(\Omega^T)}, \quad \text{respectively} \quad E_v^h = \|v - V^\tau\|_{L^2(\Omega^T)}.$$

These are presented in Table 8.1. Although theoretically no error estimates could be given due to the particular character of the dissolution rate, Table 8.1 also includes an estimate of the convergence order, based on the reduction factor between two successive calculations:

$$\alpha = \log_2(E_u^h/E_u^{\frac{h}{2}}), \quad \text{and} \quad \beta = \log_2(E_v^h/E_v^{\frac{h}{2}}).$$

For this simple test case, the method converges linearly.

h	$\|u - U^\tau\|$	α	$\|v - V^\tau\|$	β
0.2	1.1700e-01		1.8409e-01	
0.1	6.414e-02	0.87	9.927e-02	0.89
0.05	3.396e-02	0.91	5.317e-02	0.90
0.025	1.726e-02	0.98	2.785e-02	0.93
0.0125	8.42e-03	1.03	1.420e-02	0.97

Table 8.1: *Convergence results for the mixed discretization, with explicit for v; $h = \tau$ and $\delta = \sqrt{\tau}$.*

A natural question is to investigate the case when we take the implicit discretization for v. This leads to a set of coupled nonlinear equation for the triple $(u_h^n, \mathbf{Q}_h^n, v_h^n)$. Newton's iteration is used to solve the resulting system (see [120, 127] where Newton method is applied to similar problems). We consider this case for the numerical experiments and the results are tabulated in Table 8.2. We see that for the test problem, we obtain a linear convergence rate.

8.8 Conclusions

We have considered the semi-discrete and fully discrete numerical methods for the up-scaled equations. These equations describe the transport and reactions of the solutes.

h	$\|u - U^\tau\|$	α	$\|v - V^\tau\|$	β
0.2	1.031e-01		1.593e-01	
0.1	5.925e-02	0.79	9.023e-02	0.82
0.05	3.247e-02	0.87	5.031e-02	0.84
0.025	1.686e-02	0.95	2.703e-02	0.90
0.0125	8.313e-03	1.02	1.3980e-02	0.95

Table 8.2: *Convergence results for the mixed discretization, with implicit for v ; $h = \tau$ and $\delta = \sqrt{\tau}$.*

The numerical methods are based on mixed variational formulation where we have a separate equation for the flux. These numerical methods retain the local mass conservation property. The reaction terms are nonlinear and the dissolution term is multi-valued described by Heaviside graph. To avoid dealing with the inclusions, we use the regularized Heaviside function with the regularization parameter δ dependent on the time step τ. This implies that in the limit of vanishing discretization parameters automatically yields $\delta \searrow 0$. For the fully discrete situation, we have used Mixed finite element method. The convergence analysis of both formulations have been proved using the compactness arguments, in particular the translation estimates. The proof for the fully discrete situation mirrors the proof for the semi-discrete situation however, there are important differences especially dealing with the translation estimates where we use discrete H_0^1 norm to obtain compactness.

The work is complemented by the numerical experiments where we study a test case where we compare the numerical solution to the exact solution. The study provides us convergence rates for the problem studied here.

Appendix A

Dispersion for fixed geometry case

For the case of thin strip, in Chapter 5, we have discussed the upscaling problem for the situation when the geometry changes are taken into account. Here we give a derivation of the upscaled equations for the case when the pore-scale geometry does not change as a result of reactions taking place. The derivation differs slightly from the one in [46] where the same situation is considered. While the cited work uses anisotropic singular perturbation technique [129] to obtain the upscaled equations, here the formal homogenization techniques have been used. As will be seen below, the results agree well. The two dimensional bounded domain representing the strip is given by:

$$\Omega_\varepsilon := \{(x, y) \in \mathbb{R} | 0 < x < 1, -\varepsilon \leq y \leq \varepsilon\}$$

The boundaries of Ω_ε are then defined by the lateral boundary Γ_ε given by:

$$\Gamma_\varepsilon := \{(x, y) | 0 \leq x \leq 1, y \in \{-\varepsilon, \varepsilon\}\},$$

the inlet boundary Γ_i,

$$\Gamma_i := \{(x, y) | x = 0, -\varepsilon \leq y \leq \varepsilon\},$$

and the outflow boundary Γ_o,

$$\Gamma_o := \{(x, y) | x = 1, -\varepsilon \leq y \leq \varepsilon\}.$$

For modeling the crystal precipitation/dissolution, we consider the following dimensionless system of equations that describe the flow of the solutes in a fixed geometry.

$$u_t^\varepsilon = \nabla \cdot (\varepsilon D \nabla u^\varepsilon - \mathbf{q}^\varepsilon u^\varepsilon), \quad \text{in} \quad \Omega_\varepsilon$$

$$\varepsilon^2 \mu \Delta \mathbf{q}^\varepsilon = \nabla p^\varepsilon, \quad \text{in} \quad \Omega_\varepsilon$$

$$\nabla \cdot \mathbf{q}^\varepsilon = 0, \quad \text{in} \quad \Omega_\varepsilon$$

$$v_t^\varepsilon = \varepsilon f(u^\varepsilon, v^\varepsilon) \quad \text{on} \quad \Gamma_\varepsilon,$$

$$-\boldsymbol{\nu}^\varepsilon \cdot \varepsilon D \nabla u^\varepsilon = v_t^\varepsilon \quad \text{on} \quad \Gamma_\varepsilon,$$

$$\mathbf{q}^\varepsilon = 0, \quad \text{on} \quad \Gamma_\varepsilon,$$

$$u^\varepsilon = u_{b_i}, \quad \text{on} \quad \Gamma_i,$$

$$\mathbf{q}^\varepsilon = \mathbf{q}_{b_i}, \quad \text{on} \quad \Gamma_i,$$

$$\boldsymbol{\nu} \cdot \nabla u^\varepsilon = 0, \quad \text{on} \quad \Gamma_o,$$

$$\mathbf{q}^\varepsilon = \mathbf{q}_{b_0}, \quad \text{on} \quad \Gamma_o,$$

$$u^\varepsilon(x, y, 0) = u_0(x, y),$$

$$v^\varepsilon(x, 0) = v_0(x).$$

Recall that the pore geometry is fixed and so, to take into account the thickness of the deposition, another variable v is needed to account for the reactant/product on the lateral boundaries. After rescaling $x := x$; $y = y/\varepsilon$, we obtain considering only equations which are relevant to the present discussion:

$$u_t^\varepsilon + \nabla \cdot (\mathbf{q}^\varepsilon u^\varepsilon) = \varepsilon D(\partial_{xx} u^\varepsilon + \varepsilon^{-2} \partial_{yy} u^\varepsilon), \quad \text{in} \quad \Omega_\varepsilon \tag{A.0.1}$$

$$\varepsilon^2 \mu (\partial_{xx} q^{(1)\varepsilon} + \varepsilon^{-2} \partial_{yy} q^{(1)\varepsilon}, \partial_{xx} q^{(2)\varepsilon}, \varepsilon^{-2} \partial_{yy} q^{(2)\varepsilon})^T = (\partial_x p^\varepsilon, \varepsilon^{-1} \partial_y p^\varepsilon)^T, \quad \text{in} \quad \Omega_\varepsilon \tag{A.0.2}$$

$$\partial_x q^{(1)\varepsilon} + \varepsilon^{-1} \partial_y q^{(2)\varepsilon} = 0, \quad \text{in} \quad \Omega_\varepsilon \tag{A.0.3}$$

$$v_t^\varepsilon = f(u^\varepsilon, v^\varepsilon) \quad \text{on} \quad \Gamma_\varepsilon, \tag{A.0.4}$$

$$-\boldsymbol{\nu}^\varepsilon \cdot \varepsilon D(\partial_x u^\varepsilon, \varepsilon^{-1} \partial_y u^\varepsilon) = \varepsilon v_t^\varepsilon \quad \text{on} \quad \Gamma_\varepsilon, \tag{A.0.5}$$

$$\mathbf{q}^\varepsilon = 0, \quad \text{on} \quad \Gamma_\varepsilon. \tag{A.0.6}$$

Since, the geometry is assumed to be fixed, we can solve the Stokes equation (A.0.2)-(A.0.3) with the no-slip boundary condition (A.0.6), if we assume a parabolic inlet flow profile (Poiseuille flow)

$$q^{(1)\varepsilon}(y) = Q(1 - y^2), \quad q^{(2)\varepsilon} = 0,$$

where $Q > 0$ is a given constant, depending upon the pressure gradient.

We assume the following asymptotic expansion for u^ε and v^ε

$$u^\varepsilon = u_0 + \varepsilon u_1 + O(\varepsilon^2),$$
$$v^\varepsilon = v_0 + \varepsilon v_1 + O(\varepsilon^2).$$

Using the expansion above in the convection-diffusion equation (A.0.1) with boundary condition(A.0.5), we obtain

$$\partial_t u_0 + \varepsilon \partial_t u_1 = \varepsilon D \partial_{xx} u_0 + \varepsilon^{-1} D \partial_{yy} u_0 + \varepsilon^2 D \partial_{xx} u_1 + D \partial_{yy} u_1$$
$$- Q(1 - y^2)\partial_x (u_0 + \varepsilon u_1) + O(\varepsilon^2), \quad \text{in} \quad \Omega_\varepsilon, \qquad (A.0.7)$$
$$D(\partial_y u_0 + \varepsilon \partial_y u_1) = \varepsilon \partial_t v_0 + \varepsilon^2 \partial_t v_1 + O(\varepsilon^3) \quad \text{on} \quad \Gamma_\varepsilon, \qquad (A.0.8)$$

- ε^{-1} term:

$$D \partial_{yy} u_0 = 0,$$
$$D \partial_y u_0 = 0, \quad \text{at} \quad y = \{-1, 1\},$$

and hence, we conclude

$$u_0(x, y, t) = u_0(x, t).$$

- ε^0 term:

$$\partial_t u_0 - D \partial_{yy} u_1 + Q(1 - y^2)\partial_x u_0 = 0, \qquad (A.0.9)$$
$$-D \partial_y u_1 = \partial_t v_0, \quad \text{at} \quad y = 1, \qquad (A.0.10)$$
$$\partial_y u_1 = 0, \quad \text{at} \quad y = 0. \qquad (A.0.11)$$

Integrating the first equation from $y = 0$ to 1, and using the boundary conditions, (A.0.10) and (A.0.11) gives

$$\partial_t u_0 + \partial_t v_0 + \frac{2}{3} Q \partial_x u_0 = 0. \qquad (A.0.12)$$

To obtain an expression for u_1, we eliminate $\partial_t u_0$ from equation (A.0.9). Subtracting (A.0.12) from (A.0.9), gives

$$-D \partial_{yy} u_1 + Q(\frac{1}{3} - y^2)\partial_x u_0 - \partial_t v_0 = 0. \qquad (A.0.13)$$

Successively integrating (A.0.13) with respect to y, we get for $u_1(x, y, t)$ as

$$u_1(x, y, t) = \frac{Q}{D}\left(\frac{y^2}{6} - \frac{y^4}{12} + C_0(x, t)\right)\partial_x u_0 + \frac{1}{D}\left(\frac{-y^2}{2} + C_1(x, t)\right)\partial_t v_0, \qquad \text{(A.0.14)}$$

where C_0, C_1 are constants of integration. As will be seen later, there is no need for specifying the expressions for C_0, C_1, since their effects get canceled in the averaging process.

- ε^1 term:

$$\partial_t u_1 - D(\partial_{xx} u_0 + \partial_{yy} u_2) + Q(1 - y^2)\partial_x u_1 = 0, \qquad \text{(A.0.15)}$$

$$-D\partial_y u_2 = \partial_t v_1. \qquad \text{(A.0.16)}$$

Integrating (A.0.15) from $y = 0$ to $y = 1$ we obtain

$$\partial_t \int_0^1 u_1 - D\partial_{xx} u_0 + k\partial_t v_1 + Q \int_0^1 (1 - y^2)\partial_x u_1 dy = 0. \qquad \text{(A.0.17)}$$

Define

$$\bar{u}_1 = \int_0^1 u_1 dy,$$

and with this definition (A.0.17) becomes

$$\partial_t \bar{u}_1 - D\partial_{xx} u_0 + \partial_t v_1 + Q\partial_x \bar{u}_1 = Q \int_0^1 y^2 \partial_x u_1 dy. \qquad \text{(A.0.18)}$$

Adding (A.0.18) and (A.0.12) gives

$$\partial_t(u_0 + \varepsilon\bar{u}_1) - \varepsilon D\partial_{xx} u_0 + \partial_t(v_0 + \varepsilon v_1) + \frac{2}{3}Q\partial_x(u_0 + \varepsilon\bar{u}_1) = \varepsilon Q\left(\int_0^1 y^2 \partial_x \bar{u}_1 dy - \frac{1}{3}\int_0^1 \partial_x \bar{u}_1 dy\right), \qquad \text{(A.0.19)}$$

Define:

$$u_e = u_0 + \varepsilon\bar{u}_1,$$
$$v_e = v_0 + \varepsilon v_1.$$

With this definition, (A.0.19) becomes

$$\partial_t(u_e + v_e) - \varepsilon D\partial_{xx} u_e + \frac{2}{3}Q\partial_x u_e = -\varepsilon^2 D\partial_{xx}\bar{u}_1 + \varepsilon Q \int_0^1 (y^2 - \frac{1}{3})\partial_x \bar{u}_1. \qquad \text{(A.0.20)}$$

To compute the $\int_0^1 (y^2 - \frac{1}{3}) \partial_x \bar{u}_1$, we can use the expression for u_1 as obtained in equation (A.0.14). Basically, we need to compute the following integrals

$$\int_0^1 (y^2 - \frac{1}{3})(\frac{y^2}{6} - \frac{y^4}{12} + C_0)dy = \frac{8}{945},$$

and

$$\int_0^1 (y^2 - \frac{1}{3})(C_1 - \frac{y^2}{2})dy = \frac{-2}{45}.$$

Here, it is to be noted that the precise expressions for C_0, C_1 are of no consequence. Substituting the value of $\int_0^1 (y^2 - \frac{1}{3})\partial_x \bar{u}_1$, using the integrals computed above, in equation (A.0.20),

$$\partial_t(u_e + v_e) - \varepsilon D \partial_{xx} u_e + \frac{2Q}{3} \partial_x u_e = -\varepsilon^2 D \partial_{xx} \bar{u}_1 + \frac{8\varepsilon}{945} \frac{Q^2}{D} \partial_{xx} u_0 - \frac{\varepsilon Q}{D} \frac{2}{45} \partial_{xt} v_0. \quad \text{(A.0.21)}$$

Hence, the upscaled equation takes the form,

$$\begin{aligned}
\partial_t(u_e + v_e) - \varepsilon D \partial_{xx} u_e + \frac{2Q}{3} \partial_x u_e &= -\varepsilon^2 D \partial_{xx} \bar{u}_1 \\
&\quad + \frac{8\varepsilon}{945} \frac{Q^2}{D} \partial_{xx} u_0 + \varepsilon^2 \frac{8}{945} \frac{Q^2}{D} \partial_{xx} \bar{u}_1 \\
&\quad - \varepsilon^2 \frac{8}{945} \frac{Q^2}{D} \partial_{xx} \bar{u}_1 - \frac{\varepsilon Q}{D} \frac{2}{45} \partial_{xt} v_0 \\
&\quad - \varepsilon^2 \frac{Q}{D} \frac{2}{45} \partial_{xt} v_1 + \varepsilon^2 \frac{Q}{D} \frac{2}{45} \partial_{xt} v_1.
\end{aligned}$$

This can be then rewritten up to an error of order $O(\varepsilon^2)$ as

$$\begin{aligned}
\partial_t(u_e + v_e) - \varepsilon D \partial_{xx} u_e + \frac{2Q}{3} \partial_x u_e &= -\varepsilon^2 D \partial_{xx} \bar{u}_1 \\
&\quad + \frac{8\varepsilon}{945} \frac{Q^2}{D} (\partial_{xx}(u_0 + \varepsilon \bar{u}_1)) \\
&\quad - \varepsilon^2 \frac{8}{945} \frac{Q^2}{D} \partial_{xx} u_1 - \varepsilon \frac{Q}{D} \frac{2}{45} (\partial_{xt}(v_0 + \varepsilon v_1)) \\
&\quad + \varepsilon^2 \frac{Q}{D} \frac{2}{45} \partial_{xt} v_1.
\end{aligned}$$

For v_e, we can have, formally, by using Taylor expansion of $f(u^\varepsilon, v^\varepsilon)$ around (u_e, v_e),

$$\begin{aligned}
\partial_t v_e = f(u^\varepsilon, v^\varepsilon) &= f(u_0 + \varepsilon \bar{u}_1, v_0 + \varepsilon v_1) + \varepsilon(u_1|_{y=1} - \bar{u}_1)\partial_1 f(u_0 + \varepsilon \bar{u}_1, v_0 + \varepsilon v_1)) + O(\varepsilon^2) \\
&= f(u_e, v_e) + \varepsilon(u_1|_{y=1} - \bar{u}_1)\partial_1 f(u_e, v_e) + O(\varepsilon^2). \quad \text{(A.0.22)}
\end{aligned}$$

And from the expression for u_1 using equation (A.0.14), we have

$$
\begin{aligned}
u_1(y = 1) - \bar{u}_1 &= \frac{Q}{D}(\frac{1}{12} + C_0 - \frac{7}{180} - C_0)\partial_x u_0 + \partial_t v_0 \frac{1}{D}(C_1 - \frac{1}{2} - C_1 + \frac{1}{6}) \\
&= \frac{Q}{D}\frac{2}{45}\partial_x u_0 - \frac{1}{3}\frac{1}{D}\partial_t v_0.
\end{aligned} \tag{A.0.23}
$$

Once again, we note that the values of C_0, C_1 are immaterial. Equations (A.0.22) and (A.0.23) give us the final expression for v_e,

$$
\partial_t v_e = f(u_e, v_e) + \varepsilon \left\{ \frac{Q}{D}\frac{2}{45}\partial_x u_0 - \frac{1}{3}\frac{1}{D}\partial_t v_0 \right\} \partial_1 f(u_e, v_e).
$$

To summarize, we obtain the set of effective equations for the fixed geometry case up to $O(\varepsilon^2)$,

$$
\partial_t(u_e + v_e) = \partial_x \left\{ -u_e\bar{q}_e + \varepsilon D(1 + \frac{2\bar{q}_e^2}{105D^2})\partial_x u_e - \varepsilon \frac{1}{15}\frac{\bar{q}_e}{D}f(u_e, v_e) \right\}
$$

$$
\partial_t v_e = f(u_e, v_e) + \varepsilon(-\frac{1}{3D}\partial_t v_e + \frac{1}{15D}\bar{q}_e\partial_x u_e)\partial_1 f(u_e, v_e).
$$

Appendix B

Existence of solution for semi discrete scheme (8.5.2)

In Chapter 8, we have already obtained the existence of fully discrete scheme (8.6.1), $\mathbf{P}_h^n$. What remains to show is the existence of the solution for semi-discrete (8.5.2), that is, Problem $\mathbf{P}_\delta^{mvf,n}$. We show this in this Appendix. The symbols refer to the Chapter 8.

In this respect we keep τ and δ fixed and let $h \searrow 0$ in the fully discrete problem (8.6.1), $\mathbf{P}_h^n$. The limit will solve Problem $\mathbf{P}_\delta^{mvf,n}$. All the steps are similar to the fully discrete case discussed before in the Section 8.6, Chapter 8, therefore, we only give the outline of the proof. Along a sequence $h \searrow 0$, Lemma 8.12 provides the following convergence results:

(i). $u_h^n \rightharpoonup u_\delta^n$ weakly in $L^2(\Omega)$,

(ii). $\mathbf{Q}_h^n \rightharpoonup \mathbf{Q}_\delta^n$ weakly in $L^2(\Omega)^d$,

(iii). $\nabla \cdot \mathbf{Q}_h^n \rightharpoonup \chi$ weakly in $L^2(\Omega)$,

(iv). $v_h^n \rightharpoonup v_\delta^n$ weakly in $L^2(\Omega)$.

As before, identification of χ with $\nabla \cdot \mathbf{Q}_\delta^n$ takes place via standard arguments. Further, Lemma 8.16 with the estimates (8.6.3) and (8.6.6) gives

$$\|u_h^n\|_{1,h} \leq C$$

and after extending u_h^n by 0, Lemma 8.15 implies

$$\|\triangle_\xi u_h^n\|_{L^2(\mathbb{R}^2)} \leq C|\xi|(|\xi| + \text{size}(\mathcal{T}_h)).$$

Since the right hand side vanishes uniformly as $|\xi| \searrow 0$, the use of Kolmogorov compactness theorem yields strong convergence of u_h^n to u_δ^n. Now one can use the projection properties and pass $h \searrow 0$ to show that the limit solves $\mathbf{P}_\delta^{mvf,n}$. Note that having v discretized explicitly in $(8.6.1)_2$, no nonlinearities in v_h^n are involved and therefore there is no need for strong convergence for v_h^n.

Bibliography

[1] G. Allaire. Homogenization of the Stokes flow in a connected porous medium. *Asymptotic Anal.*, 2(3):203–222, 1989.

[2] G. Allaire. Homogenization and two-scale convergence. *SIAM J. Math. Anal.*, 23(6):1482–1518, 1992.

[3] G. Allaire and M. Amar. Boundary layer tails in periodic homogenization. *ESAIM Control Optim. Calc. Var.*, 4:209–243 (electronic), 1999.

[4] G. Allaire, R. Brizzi, and A. Mikelić. Two-scale expansion with drift approach to the Taylor dispersion for reactive transport through porous media. *Chemical Engineering Science*, 65:2292–2300, 2010.

[5] G. Allaire, A. Mikelić, and A. Piatnitski. Homogenization approach to the dispersion theory for reactive transport through porous media. *SIAM J. Math. Anal.*, 42(1):125–144, 2010.

[6] G. Allaire, A. Mikelić, and A. Piatnitski. Homogenization of the linearized ionic transport equations in rigid periodic porous media. *J. Math. Phys.*, 51(12):123103, 18, 2010.

[7] T. Arbogast, M. Obeyesekere, and M. F. Wheeler. Numerical methods for the simulation of flow in root-soil systems. *SIAM J. Numer. Anal.*, 30(6):1677–1702, 1993.

[8] T. Arbogast and M. F. Wheeler. A characteristics-mixed finite element method for advection-dominated transport problems. *SIAM J. Numer. Anal.*, 32(2):404–424, 1995.

[9] J. M. Arrieta and S. M. Bruschi. Very rapidly varying boundaries in equations with nonlinear boundary conditions. The case of a non uniformly Lipschitz deformation. *Discrete Contin. Dyn. Syst. Ser. B*, 14(2):327–351, 2010.

[10] J. M. Arrieta and M. C. Pereira. Elliptic problems in thin domains with highly oscillating boundaries. *Bol. Soc. Esp. Mat. Apl. SēMA*, (51):17–24, 2010.

[11] J. M. Arrieta and M. C. Pereira. Homogenization in a thin domain with an oscillatory boundary. *J. Math. Pures Appl. (9)*, 96(1):29–57, 2011.

[12] J. L. Auriault and P. M. Adler. Dispersion in porous media: by multiple scale expansions. *Adv. Water Resour.*, 18(4):211–226, 1995.

[13] K. Baber, K. Mosthaf, B. Flemisch, R. Helmig, S. Müthing, and B. Wohlmuth. Numerical scheme for coupling two-phase compositional porous-media flow and one-phase compositional free flow. *IMA J. Appl. Math.*, (to appear), 2012.

[14] J. W. Barrett and P. Knabner. Finite element approximation of the transport of reactive solutes in porous media. I. Error estimates for nonequilibrium adsorption processes. *SIAM J. Numer. Anal.*, 34(1):201–227, 1997.

[15] J. W. Barrett and P. Knabner. Finite element approximation of the transport of reactive solutes in porous media. II. Error estimates for equilibrium adsorption processes. *SIAM J. Numer. Anal.*, 34(2):455–479, 1997.

[16] P. Bastian, K. Birken, K. Johannsen, S. Lang, N. Neuss, H. Rentz-Reichert, and C. Wieners. UG – a flexible software toolbox for solving partial differential equations. *Comput. and Vis. in Science*, 1:27–40, 1997.

[17] J. Bear. *Dynamics of fluids in porous media*. American Elsevier, New York, 1972.

[18] A. Bensoussan, J.-L. Lions, and G. Papanicolaou. *Asymptotic analysis for periodic structures*, volume 5 of *Studies in Mathematics and its Applications*. North-Holland Publishing Co., Amsterdam, 1978.

[19] C. W. J. Berentsen, M. L. Verlaan, and C. P. J. W. van Kruijsdijk. Upscaling and reversibility of Taylor dispersion in heterogeneous porous media. *Phys. Rev. E*, 71(4):046308, Apr 2005.

[20] J. Bogers. Well-posedness, upscaling and numerical schemes for problems involving a nonlinear transmission condition. *Masters Thesis, Technische Universiteit Eindhoven*, pages 100–101, 2011.

[21] J. Bogers, K. Kumar, P.H.L. Notten, J.F.M. Oudenhoven, and I.S. Pop. A multiscale domain decomposition approach for chemical vapor deposition. *CASA Report 12-11*, 2012.

[22] J. F. Bonder, R. Orive, and J. D. Rossi. The best Sobolev trace constant in a domain with oscillating boundary. *Nonlinear Anal.*, 67(4):1173–1180, 2007.

[23] N. Bouillard, R. Eymard, R. Herbin, and P. Montarnal. Diffusion with dissolution and precipitation in a porous medium: mathematical analysis and numerical approximation of a simplified model. *M2AN Math. Model. Numer. Anal.*, 41(6):975–1000, 2007.

[24] A. Bourgeat, S. Luckhaus, and A. Mikelić. Convergence of the homogenization process for a double-porosity model of immiscible two-phase flow. *SIAM J. Math. Anal.*, 27(6):1520–1543, 1996.

[25] H. Brezis. *Analyse fonctionnelle*. Collection Mathématiques Appliquées pour la Maîtrise. [Collection of Applied Mathematics for the Master's Degree]. Masson, Paris, 1983. Théorie et applications. [Theory and applications].

[26] F. Brezzi and M. Fortin. *Mixed and hybrid finite element methods*, volume 15 of *Springer Series in Computational Mathematics*. Springer-Verlag, New York, 1991.

[27] C. Cancès. An existence result for multidimensional immiscible two-phase flows with discontinuous capillary pressure field. *UPMC Univ Paris*, 2011.

[28] E. Cariaga, F. Concha, I. S. Pop, and M. Sepúlveda. Convergence analysis of a vertex-centered finite volume scheme for a copper heap leaching model. *Math. Methods Appl. Sci.*, 33(9):1059–1077, 2010.

[29] G. A. Chechkin, A. Friedman, and A. L. Piatnitski. The boundary-value problem in domains with very rapidly oscillating boundary. *J. Math. Anal. Appl.*, 231(1):213–234, 1999.

[30] W. Chen, H. J. H. Brouwers, and Z. H. Shui. Three-dimensional computer modeling of slag cement hydration. *Journal of Materials Science*, 42(23):9595–9610, 2007.

[31] C. Choquet and A. Mikelić. Laplace transform approach to the rigorous upscaling of the infinite adsorption rate reactive flow under dominant Peclet number through a pore. *Appl. Anal.*, 87:1373 – 1395, 2008.

[32] C. Choquet and A. Mikelić. Rigorous upscaling of the reactive flow with finite kinetics and under dominant peclet number. *Continuum Mechanics and Thermodynamics*, 21:125–140, 2009.

[33] P. G. Ciarlet. *The finite element method for elliptic problems*. North-Holland Publishing Co., Amsterdam, 1978. Studies in Mathematics and its Applications, Vol. 4.

[34] J. F. Ciavaldini. Analyse numerique d'un problème de Stefan à deux phases par une methode d'éléments finis. *SIAM J. Numer. Anal.*, 12:464–487, 1975.

[35] D. Cioranescu, A. Damlamian, and G. Griso. The periodic unfolding method in homogenization. *SIAM J. Math. Anal.*, 40(4):1585–1620, 2008.

[36] C. Conca, J. I. Díaz, and C. Timofte. Effective chemical processes in porous media. *Math. Models Methods Appl. Sci.*, 13(10):1437–1462, 2003.

[37] A. Damlamian and K. Pettersson. Homogenization of oscillating boundaries. *Discrete Contin. Dyn. Syst.*, 23(1-2):197–219, 2009.

[38] C. Dawson. Analysis of an upwind-mixed finite element method for nonlinear contaminant transport equations. *SIAM J. Numer. Anal.*, 35(5):1709–1724, 1998.

[39] C. Dawson and V. Aizinger. Upwind-mixed methods for transport equations. *Comput. Geosci.*, 3(2):93–110, 1999.

[40] C. N. Dawson, C. J. van Duijn, and M. F. Wheeler. Characteristic-Galerkin methods for contaminant transport with nonequilibrium adsorption kinetics. *SIAM J. Numer. Anal.*, 31(4):982–999, 1994.

[41] V. M. Devigne, I. S. Pop, C. J. van Duijn, and T. Clopeau. A numerical scheme for the pore-scale simulation of crystal dissolution and precipitation in porous media. *SIAM J. Numer. Anal.*, 46(2):895–919, 2008.

[42] J. Donea, A. Huerta, J.-Ph. Ponthot, and A. Rodrguez-Ferran. Arbitrary Lagrangian-Eulerian methods. *The Encyclopedia of Computational Mechanics, Wiley*, 1(14):413–437, 2004.

[43] C. J. van Duijn and P. Knabner. Solute transport through porous media with slow adsorption. In *Free boundary problems: theory and applications, Vol. I (Irsee, 1987)*, volume 185 of *Pitman Res. Notes Math. Ser.*, pages 375–388. Longman Sci. Tech., Harlow, 1990.

[44] C. J. van Duijn and P. Knabner. Solute transport in porous media with equilibrium and nonequilibrium multiple-site adsorption: travelling waves. *J. Reine Angew. Math.*, 415:1–49, 1991.

[45] C. J. van Duijn and P. Knabner. Travelling wave behaviour of crystal dissolution in porous media flow. *European J. Appl. Math.*, 8(1):49–72, 1997.

[46] C. J. van Duijn, A. Mikelic, C. Rosier, and I. S. Pop. Effective dispersion equations for reactive flows with dominant peclet and damkohler numbers. *Advances in Chemical Engineering*, 34:1–45, 2008.

[47] C. J. van Duijn and I. S. Pop. Crystal dissolution and precipitation in porous media: pore scale analysis. *J. Reine Angew. Math.*, 577:171–211, 2004.

[48] J. Eberhard. Upscaling for stationary transport in heterogeneous porous media. *Multiscale Model. Simul.*, 3(4):957–976 (electronic), 2005.

[49] C. M. Elliott. Error analysis of the enthalpy method for the Stefan problem. *IMA J. Numer. Anal.*, 7(1):61–71, 1987.

[50] L. C. Evans. *Partial differential equations*, volume 19 of *Graduate Studies in Mathematics*. American Mathematical Society, Providence, RI, 1998.

[51] R. Eymard, T. Gallouët, and R. Herbin. Convergence of finite volume schemes for semilinear convection diffusion equations. *Numer. Math.*, 82(1):91–116, 1999.

[52] R. Eymard, D. Hilhorst, and M. Vohralík. A combined finite volume–nonconforming/mixed-hybrid finite element scheme for degenerate parabolic problems. *Numer. Math.*, 105(1):73–131, 2006.

[53] T. Fatima, N. Arab, E. P. Zemskov, and A. Muntean. Homogenization of a reaction-diffusion system modeling sulfate corrosion of concrete in locally periodic perforated domains. *J. Engrg. Math.*, 69(2-3):261–276, 2011.

[54] A. Friedman and B. Hu. A non-stationary multi-scale oscillating free boundary for the Laplace and heat equations. *J. Differential Equations*, 137(1):119–165, 1997.

[55] A. Friedman, B. Hu, and Y. Liu. A boundary value problem for the Poisson equation with multi-scale oscillating boundary. *J. Differential Equations*, 137(1):54–93, 1997.

[56] M. K. Gobbert and C. A. Ringhofer. An asymptotic analysis for a model of chemical vapor deposition on a microstructured surface. *SIAM J. Appl. Math.*, 58(3):737–752 (electronic), 1998.

[57] F. Golfier, B.D. Wood, L. Orgogozo, M. Quintard, and M. Buès. Biofilms in porous media: Development of macroscopic transport equations via volume averaging with closure for local mass equilibrium. *Adv. Water Res.*, 32:463–485, 2009.

[58] F. Hesse, F. A. Radu, M. Thullner, and S. Attinger. Upscaling of the advection-diffusion-reaction equation with monod reaction. *Adv. Water Resour.*, 32(8):1336–1351, 2009.

[59] D. Hilhorst and M. Vohralík. A posteriori error estimates for combined finite volume–finite element discretizations of reactive transport equations on non-matching grids. *Comput. Methods Appl. Mech. Engrg.*, 200(5-8):597–613, 2011.

[60] U. Hornung. Introduction: homogenization and porous media. pages 1–25, 1997.

[61] U. Hornung and W. Jäger. Diffusion, convection, adsorption, and reaction of chemicals in porous media. *J. Differential Equations*, 92(2):199–225, 1991.

[62] U. Hornung, W. Jäger, and A. Mikelić. Reactive transport through an array of cells with semi-permeable membranes. *RAIRO Modél. Math. Anal. Numér.*, 28(1):59–94, 1994.

[63] O. Iliev, A. Mikelić, and P. Popov. On upscaling certain flows in deformable porous media. *Multiscale Model. Simul.*, 7(1):93–123, 2008.

[64] COMSOL Inc. `http://www.comsol.com`.

[65] W. Jäger and N. Kutev. Discontinuous solutions of the nonlinear transmission problem for quasilinear elliptic equations. *Preprint der IWR Universität Heidelberg*.

[66] W. Jäger and A. Mikelić. On the boundary conditions at the contact interface between a porous medium and a free fluid. *Ann. Scuola Norm. Sup. Pisa Cl. Sci. (4)*, 23(3):403–465, 1996.

[67] W. Jäger and A. Mikelić. On the interface boundary condition of Beavers, Joseph, and Saffman. *SIAM J. Appl. Math.*, 60(4):1111–1127 (electronic), 2000.

[68] W. Jäger and A. Mikelić. On the roughness-induced effective boundary conditions for an incompressible viscous flow. *J. Differential Equations*, 170(1):96–122, 2001.

[69] W. Jäger, A. Mikelić, and M. Neuss-Radu. Homogenization limit of a model system for interaction of flow, chemical reactions, and mechanics in cell tissues. *SIAM J. Math. Anal.*, 43(3):1390–1435, 2011.

[70] E. Javierre, F. J. Vermolen, C. Vuik, and S. van der Zwaag. A mathematical analysis of physiological and morphological aspects of wound closure. *J. Math. Biol.*, 59(5):605–630, 2009.

[71] R. B. Kellogg and J. E. Osborn. A regularity result for the Stokes problem in a convex polygon. *J. Functional Analysis*, 21(4):397–431, 1976.

[72] R. Klöfkorn, D. Kröner, and M. Ohlberger. Local adaptive methods for convection dominated problems. *Internat. J. Numer. Methods Fluids*, 40(1-2):79–91, 2002. ICFD Conference on Numerical Methods for Fluid Dynamics (Oxford, 2001).

[73] P. Knabner, C. J. van Duijn, and S. Hengst. An analysis of crystal dissolution fronts in flows through porous media. part 1: Compatible boundary conditions. *Adv. Water Resour.*, 18:171–185, 1995.

[74] K. Kumar, M. Neuss-Radu, and I. S. Pop. Homogenization of crystal precipitation and dissolution model in a porous medium. *In Preparation*, (Chapter **6**).

[75] K. Kumar, T. L. van Noorden, and I. S. Pop. Effective dispersion equations for reactive flows involving free boundaries at the microscale. *Multiscale Model. Simul.*, 9(1):29–58, 2011 (Chapter **5**).

[76] K. Kumar, T.L. van Noorden, and I.S. Pop. Upscaling of reactive flows in domains with moving oscillating boundaries. *CASA Report 12-12*, 2012 (Chapter **4**).

[77] K. Kumar, M. Pisarenco, M. Rudnaya, and V. Savcenco. A note on analysis and numerics of algae growth. *Nonlinear Analysis Series B: Real World Applications (submitted)*.

[78] K. Kumar, M. Pisarenco, M. Rudnaya, V. Savcenco, and S. Srivastava. Shape reconstruction techniques for optical sectioning of arbitrary objects. *Mathematics-in-Industry Case Studies*, 3:19–36, 2011.

[79] K. Kumar, I. S. Pop, and F. A. Radu. A numerical analysis for the upscaled equations describing dissolution and precipitation in porous media. *Enumath Proceedings Volume*, 2011.

[80] K. Kumar, I. S. Pop, and F. A. Radu. Convergence analysis for a conformal discretization of a model for precipitation and dissolution in porous media. *CASA Report 12-08*, 2012 (Chapter **7**).

[81] K. Kumar, I. S. Pop, and F. A. Radu. Convergence analysis of mixed numerical schemes for reactive flow in a porous medium. *CASA Report 12-20*, 2012 (Chapter **8**).

[82] J. R. Kweon and R. B. Kellogg. Compressible Stokes problem on nonconvex polygonal domains. *J. Differential Equations*, 176(1):290–314, 2001.

[83] O. A. Ladyzhenskaya and N. N. Ural′tseva. *Linear and quasilinear elliptic equations*. Translated from the Russian by Scripta Technica, Inc. Translation editor: Leon Ehrenpreis. Academic Press, New York, 1968.

[84] A. M. Lankhorst, B. D. Paarhuis, H. J. M. C. Terhorst, P. J. P. M. Simons, and C. R. Kleijn. Transient ALD simulations for a multi-wafer reactor with trenched wafers. *Surface and Coatings Technology*, 201, 2007.

[85] M. Lenzinger and B. Schweizer. Two-phase flow equations with outflow boundary conditions in the hydrophobic-hydrophilic case. *Nonlinear Anal.*, 73(4):840–853, 2010.

[86] J.-L. Lions and E. Magenes. *Non-homogeneous boundary value problems and applications. Vol. I.* Springer-Verlag, New York, 1972. Translated from the French by P. Kenneth, Die Grundlehren der mathematischen Wissenschaften, Band 181.

[87] P.-L. Lions. On the Schwarz alternating method. I. In *First International Symposium on Domain Decomposition Methods for Partial Differential Equations (Paris, 1987)*, pages 1–42. SIAM, Philadelphia, PA, 1988.

[88] P.-L. Lions. On the Schwarz alternating method. III. A variant for nonoverlapping subdomains. In *Third International Symposium on Domain Decomposition Methods for Partial Differential Equations (Houston, TX, 1989)*, pages 202–223. SIAM, Philadelphia, PA, 1990.

[89] A. Marciniak-Czochra and M. Ptashnyk. Derivation of a macroscopic receptor-based model using homogenization techniques. *SIAM J. Math. Anal.*, 40(1):215–237, 2008.

[90] MATLAB. www.mathworks.com.

[91] I. Metzmacher, F. A. Radu, M. Bause, P. Knabner, and W. Friess. A model describing the effect of enzymatic degradation on drug release from collagen minirods. *European Journal of Pharmaceutics and Biopharmaceutics*, 67(2):349—360, 2007.

[92] A. Mikelić and I. Aganović. Homogenization in a porous media under a nonho-mogeneous boundary condition. *Boll. Un. Mat. Ital. A (7)*, 1(2):171–180, 1987.

[93] A. Mikelić, V. Devigne, and C. J. van Duijn. Rigorous upscaling of the reactive flow through a pore, under dominant Peclet and Damkohler numbers. *SIAM J. Math. Anal.*, 38, 2006.

[94] A. Mikelić and C. J. van Duijn. Rigorous derivation of a hyperbolic model for Taylor dispersion. *M3AS: Mathematical Models and Methods in Applied Sciences*, 21(5):1095–1120, 2011.

[95] A. Mikelić and C. Rosier. Rigorous upscaling of the infinite adsorption rate reactive flow under dominant Peclet number through a pore. *Ann. Univ. Ferrara Sez. VII Sci. Mat.*, 53:333–359, 2007.

[96] K. Mosthaf, K. Baber, B. Flemisch, R. Helmig, A. Leijnse, I. Rybak, and B. Wohlmuth. A coupling concept for two-phase compositional porous-medium and single-phase compositional free flow. *Water Resour. Res.*, 47(W10522), 2011.

[97] P. Moszkowicz, J. Pousin, and F. Sanchez. Diffusion and dissolution in a reactive porous medium: mathematical modelling and numerical simulations. In *Proceedings of the Sixth International Congress on Computational and Applied Mathematics (Leuven, 1994)*, volume 66, pages 377–389, 1996.

[98] A. Muntean and M. Böhm. Interface conditions for fast-reaction fronts in wet porous mineral materials: the case of concrete carbonation. *J. Engrg. Math.*, 65(1):89–100, 2009.

[99] A. Muntean and M. Böhm. A moving-boundary problem for concrete carbonation: global existence and uniqueness of weak solutions. *J. Math. Anal. Appl.*, 350(1):234–251, 2009.

[100] N. Neuss, M. Neuss-Radu, and A. Mikelić. Effective laws for the Poisson equation on domains with curved oscillating boundaries. *Appl. Anal.*, 85(5):479–502, 2006.

[101] M. Neuss-Radu. Some extensions of two-scale convergence. *C. R. Acad. Sci. Paris Sér. I Math.*, 322(9):899–904, 1996.

[102] M. Neuss-Radu and W. Jäger. Effective transmission conditions for reaction-diffusion processes in domains separated by an interface. *SIAM J. Math. Anal.*, 39(3):687–720 (electronic), 2007.

[103] G. Nguetseng. A general convergence result for a functional related to the theory of homogenization. *SIAM J. Math. Anal.*, 20(3):608–623, 1989.

[104] T. L. van Noorden. Crystal precipitation and dissolution in a porous medium: effective equations and numerical experiments. *Multiscale Model. Simul.*, 7(3):1220–1236, 2008.

[105] T. L. van Noorden. Crystal precipitation and dissolution in a thin strip. *European J. Appl. Math.*, 20(1):69–91, 2009.

[106] T. L. van Noorden and I. S. Pop. A Stefan problem modelling dissolution and precipitation. *IMA J. Appl. Math.*, 73:393–411, 2008.

[107] T. L. van Noorden, I. S. Pop, A. Ebigbo, and R. Helmig. An upscaled model for biofilm growth in a thin strip. *Water Resour. Res.*, accepted, 2010.

[108] T. L. van Noorden, I. S. Pop, and M. Röger. Crystal dissolution and precipitation in porous media: L^1-contraction and uniqueness. *Discrete Contin. Dyn. Syst.*, (Dynamical Systems and Differential Equations. Proceedings of the 6th AIMS International Conference, suppl.):1013–1020, 2007.

[109] T. L. van Noorden, I. S. Pop, and M. Röger. Crystal dissolution and precipitation in porous media: L^1-contraction and uniqueness. *Discrete Contin. Dyn. Syst.*, (Dynamical Systems and Differential Equations. Proceedings of the 6th AIMS International Conference, suppl.):1013–1020, 2007.

[110] P. H. L. Notten, F. Roozeboom, R. A. H. Niessen, and L. Baggetto. 3-d integrated all-solid-state rechargeable batteries. *Advanced Materials*, 19(24):4564–4567, 2007.

[111] M. Ohlberger and C. Rohde. Adaptive finite volume approximations for weakly coupled convection dominated parabolic systems. *IMA J. Numer. Anal.*, 22(2):253–280, 2002.

[112] J. F. M. Oudenhoven. *Deposition and characterization of thin films for 3D lithium-ion micro-batteries*. PhD Thesis, Technische Universiteit Eindhoven, 2011.

[113] J. F. M. Oudenhoven, L. Bagetto, and P. H. L. Notten. All-solid-state lithium-ion microbatteries: A review of vaious three-dimensional concepts. *Advanced Energy Materials*, 1(1):10–33, 2011.

[114] J. F. M. Oudenhoven, T. van Dongen, R. A. H. Niessen, M. H. J. M. de Croon, and P. H. L. Notten. Low-pressure chemical vapor deposition of licoo2 thin films: A systematic investigation of the deposition parameters. *Journal of the Electrochemical Society*, 156(5):D159–D174, 2009.

[115] A. Pawell and K.-D. Krannich. Dissolution effects in transport in porous media. *SIAM J. Appl. Math.*, 56(1):89–118, 1996.

[116] I. S. Pop, F. Radu, and P. Knabner. Mixed finite elements for the Richards' equation: linearization procedure. *J. Comput. Appl. Math.*, 168(1-2):365–373, 2004.

[117] J. W. Portegies and M. A. Peletier. Well-posedness of a parabolic moving-boundary problem in the setting of Wasserstein gradient flows. *Interfaces Free Bound.*, 12(2):121–150, 2010.

[118] J. Pousin. Infinitely fast kinetics for dissolution and diffusion in open reactive systems. *Nonlinear Anal.*, 39(3, Ser. A: Theory Methods):261–279, 2000.

[119] A. Quarteroni and A. Valli. *Numerical approximation of partial differential equations*, volume 23 of *Springer Series in Computational Mathematics*. Springer-Verlag, Berlin, 1994.

[120] F. A. Radu and I. S. Pop. Newton method for reactive solute transport with equilibrium sorption in porous media. *J. Comput. Appl. Math.*, 234(7):2118–2127, 2010.

[121] F. A. Radu, I. S. Pop, and S. Attinger. Analysis of an Euler implicit-mixed finite element scheme for reactive solute transport in porous media. *Numer. Methods Partial Differential Equations*, 26(2):320–344, 2010.

[122] F. A. Radu, I. S. Pop, and P. Knabner. Error estimates for a mixed finite element discretization of some degenerate parabolic equations. *Numer. Math.*, 109(2):285–311, 2008.

[123] F. A. Radu and I.S. Pop. Mixed finite element discretization and newton iteration for a reactive contaminant transport model with nonequilibrium sorption: convergence analysis and error estimates. *Comput. Geosci.*, 15, 2011.

[124] A. Raoof and S. M. Hassanizadeh. A new formulation for pore-network modeling of two-phase flow. *Water Resources Research*, 48, W01514:doi:10.1029/2010WR010180, 2012.

[125] A. Raoof and S.M. Hassanizadeh. Upscaling transport of adsorbing solutes in porous media. *J. Porous Media*, 13:395–408, 2010.

[126] A. Rijnks, M. Darwish, and H. Bruining. Computation of the longitudinal dispersion coefficient in an adsorbing porous medium using homogenization. *Proceedings of the COMSOL Conference Milan*, 2009.

[127] B. Rivière and M. F. Wheeler. Non conforming methods for transport with nonlinear reaction. In *Fluid flow and transport in porous media: mathematical and numerical treatment (South Hadley, MA, 2001)*, volume 295 of *Contemp. Math.*, pages 421–432. Amer. Math. Soc., Providence, RI, 2002.

[128] J. Rubin. Transport of reacting solutes in porous media: Relation between mathematical nature of problem formulation and chemical nature of reaction. *Water Resources Research*, 19:1231–1252, 1983.

[129] J. Rubinstein and R. Mauri. Dispersion and convection in periodic porous media. *SIAM J. Appl. Math.*, 46(6):1018–1023, 1986.

[130] E. Sánchez-Palencia. *Nonhomogeneous media and vibration theory*, volume 127 of *Lecture Notes in Physics*. Springer-Verlag, Berlin, 1980.

[131] P.R. Spiesz, M. Ballari, and H.J.H. Brouwers. Rcm: A new model accounting for the non-linear chloride binding isotherm and the non-equilibrium conditions between the free- and bound-chloride concentrations. *Construction and Building Materials*, 27(1):293–304, 2012.

[132] G. I. Taylor. Dispersion of soluble matter in solvent flowing slowly through a tube. *Proc. Royal Soc. A*, 219:186–203, 1953.

[133] R. Temam. *Navier-Stokes equations*, volume 2 of *Studies in Mathematics and its Applications*. North-Holland Publishing Co., Amsterdam, third edition, 1984. Theory and numerical analysis, With an appendix by F. Thomasset.

[134] R. P. Tijburg, J. G. M. Ligthart, H. K. Kuiken, and J. J. Kelly. Centrifugal Etching. *Journal of the Electrochemical Society*, 150(6), 2003.

[135] C. Vuik and C. Cuvelier. Numerical solution of an etching problem. *J. Comput. Physics*, 59:247–263, 1985.

[136] F. Weller. *Modeling, Analysis, and Simulation of Thrombosis and Hemostasis*. PhD thesis, Universität Heidelberg, Institut für Angewandte Mathematik, Heidelberg, 2008.

[137] B. D. Wood, K. Radakovich, and F. Golfier. Effective reaction at a fluidsolid interface: Applications to biotransformation in porous media. *Adv. Water Resour.*, (30):1630–1647, 2007.

Index

Summary

Upscaling of Reactive Flows

The thesis deals with the upscaling of reactive flows in complex geometry. The reactions which may include deposition or dissolution take place at a part of the boundary and depending on the size of the reaction domain, the changes in the pore structure that are due to the deposition process may or may not be neglected. In mathematical terms, the models are defined in a fixed, respectively variable geometry, when the deposition layer generates a free boundary at the pore scale. Specifically, for the chemical vapor deposition (CVD) process on a trenched geometry, we have developed mathematical models for both situations. For the multi-scale computations, numerical methods inspired from domain decomposition ideas have been proposed and the convergence of the scheme has been proved.

Computing the full solution in a domain with oscillating boundary requires a lot of computational effort, as one has to achieve an accuracy that agrees with the scale of oscillations. To approximate these solutions, one defines equations in a simpler domain, where flat boundaries but modified boundary conditions approximate the rough one. The two situations mentioned before were considered: the fixed geometry case, and the time dependent geometry at the microscale (free boundaries). We have derived an approximating (effective) model where a flat boundary is replacing the oscillatory boundary, but defining an effective boundary condition. In the fixed geometry case, we provide rigorous mathematical proofs for the upscaling procedure. The second case, when we take into account the geometry changes at the microscale, is more involved, and we use formal asymptotic methods to derive these boundary conditions. Our contributions in this respect are in dealing with non-Lipschitz reactive terms on the boundary in the fixed geometry case and the formal asymptotic approach for the moving boundary. Both add to the present literature.

Next, to understand the flow in a domain with variable geometry, we have considered

a thin strip with reactions taking place at the lateral boundaries of the strip under dominant transport conditions. Reactions take place at the lateral boundaries of the strip (the walls), where the reaction product can deposit in a layer with a non-negligible thickness compared to the width of the strip. This leads to a free boundary problem, in which the moving interface between the fluid and the deposited (solid) layer is explicitly taken into account. Using asymptotic expansion methods, we derive an upscaled, one-dimensional model by averaging in the transversal direction. The upscaled equations are similar to the Taylor dispersion and we have performed numerical simulations to compare the upscaled equations with other simpler upscaled equations and the transversally averaged, two-dimensional solution. The derivation introduces new terms originating from the changing geometry. The numerical computations also provide an insight into the regimes where such an upscaling is useful.

We have further studied the rigorous homogenization process for the reactive flows for a periodic array of cells and proved the validity of upscaled equations. These reactive flows model the precipitation and dissolution processes in a porous medium. We define a sequence of microscopic solutions u^ε and obtain the upscaled equations as the limit of $\varepsilon \searrow 0$. We adopt the 2-scale framework to achieve this. The challenges are in dealing with the low regularity of microscopic solutions and particular non-linearities in the reaction term. This rigorous derivation closes the gap of the rigorous transition from a given pore scale model to the heuristically proposed macroscopic model.

In addition, numerical methods to compute the solution for an upscaled model have been proposed. The upscaled model describes the reactive flow in a porous medium. The reaction term, especially, the dissolution term has a particular, multi-valued character, which leads to stiff dissolution fronts. We have considered both the conformal and mixed schemes for the analysis including both the semi-discrete (time-discretization) and the fully discrete (both in space and time) cases. The fully discrete schemes correspond to the finite element method and the mixed finite element method for conformal, respectively mixed schemes. The numerical schemes have been analyzed and the convergence to the continuous formulation has been proved. Apart from the proof for the convergence, this also yields an existence proof for the solution of the upscaled model. Numerical experiments are performed to study the convergence behavior. The challenges are in dealing with the specific non-linearities of the reaction term. We deal with them by using the translation estimates which are adapted to the specific numerical scheme.

The applications are in the development of all-solid state rechargeable batteries having a high storage capacity. Such devices have a complex 3D geometry for the electrodes to enhance the surface area. The challenges are in the development of the appropriate technologies for the formation of these electrodes. In particular we focus on chemical vapor deposition processes (CVD), with the aim of getting a deeper understanding of the reactions taking place in a complex geometry. Other applications include flows in porous media, bio-film growth etc.

Acknowledgements

An engineering degree and a brief stint in professional life made me aware of the importance and, in some sense, inevitability of studying applied mathematics. Add to it that there is a certain charm and power of studying it, for example, a single equation describing various phenomena, that it becomes almost imperative to learn it. The charm howsoever seductive it is, in practice, the rigors and tools of it are equally demanding. With this feeling of a bit of adventure combined with apprehensions, I started pursuing my doctoral studies. I use this space to partially reflect on the last four years and acknowledge the contributions of my teachers, colleagues and friends.

If I did have some confidence in the beginning, it was more on my supervisor and first promoter Prof. Sorin Pop. I would like to express my sincere gratitude for his patient and dedicated approach and for his trust on my abilities. His constant encouragements to taking new initiatives have broadened my understanding and given me self-confidence. All through these years, his constant support has been exemplary and an enviable privilege. My profound thanks are also to my second promoter Prof. Mark Peletier, who has always been a source of frank advices and stimulating discussions. He entrusted me with different responsibilities which helped me in both professional and personal developments. He has contributed significantly through his remarks on the papers, and on different topics which he taught me.

I take this opportunity to thank my core committee members Prof. Peter Notten, Prof. Florin Radu, and Prof. Andro Mikelić. With Prof. Notten, who was the project leader, we had several discussions on the exciting subject of 3D batteries. I thank Prof. Florin Radu for his kind invitation to University of Bergen and for the close collaboration on the analysis of numerical schemes for reactive flows. This led to two papers being part of the thesis, next to a conference proceeding. I hope to continue this fruitful collaboration. Special thanks are due to Prof. Mikelić for his insightful comments on the thesis which improved the work. I have been fortunate enough to have discussions with him in several conferences and it has been a great learning experience. The extended committee is completed by two distinguished personalities: Prof. Hans van Duijn and Prof. Willi Jäger. Together with Prof. Notten, Prof. van Duijn was the applicant for the STW

gion. I also thank Jos Oudenhoven and Ilkin Kokal for working together on my project.

Life outside office hours is as important for a successful PhD life as inside. I have considered myself fortunate enough to have engaging leisure activities in the evenings and on the weekends. Valeriu and Maxim, we have made several trips together, have written some papers together and countless sessions of Tennis hours. It has been a privilege to have your company and thanks, in particular to Inga and Kristina for those lovely dinner and movie evenings. Neda, we have shared time, space and ideas together and your provocative, unconventional ideas continue to influence my thought process including, on a lighter note, my poetic skills. Sudhir, I have often turned for help and have never been refused. Niels, your personality inspires me and hopefully, I would learn some of the nice qualities you have. Eric, it has been a pleasure to know you. Jim, you did help me a lot and I remain indebted to you for that.

Last but not the least, I express my deep gratitude to my family. To my brother, Pranav who has always encouraged me and kept me motivated. Finally, my parents have always been a source of inspiration and it is to them that I dedicate this thesis.

Kundan Kumar.
Eindhoven, July 2012.

Curriculum vitae

Kundan Kumar was born on 10-06-1983 in Patna, India. After finishing his schooling from Jawahar Navodaya Vidyalaya, Saran and Science College, Patna, he pursued the Bachelor of Technology in Mechanical Engineering at Indian Institute of Technology, Delhi in New Delhi, India. Subsequent to his Bachelor studies, he was awarded Erasmus Mundus scholarship from the European Commission which allowed him to pursue Double degree program at Eindhoven University of Technology and Technical University of Kaiserslautern, Germany. In 2008 he graduated cum laude within the Department of Mathematics and Computer Sciences on Industrial Mathematics. His masters thesis was carried out at Fraunhofer ITWM, Kaiserslautern under the supervision of Prof. Dr. Oleg Iliev.

From Aug 2008, he started a PhD project at Technical University of Eindhoven, The Netherlands under the supervision of prof. dr. Sorin Pop and prof. dr. Mark Peletier. The results obtained during this period are presented in this dissertation. The PhD position was funded by STW within the project "Second Generation of Integrated Batteries" (07796).